INVESTIGATING EPIDERMOGENESIS IN A HUMAN SKIN EQUIVALENT MODEL

Jacqui Anne McGovern
Bachelor of Applied Science (Hons)

A thesis submitted in fulfilment of the requirements for the degree of
Doctor of Philosophy

School of Biomedical Sciences
Faculty of Health
Queensland University of Technology
December 2012

Statement of Original Authorship

The work contained in this thesis has not been previously submitted to meet requirements for an award at this or any other higher education institution. To the best of my knowledge and belief, the thesis contains no material previously published or written by another person except where due reference is made.

Signature: _____

Date: _____

Keywords

Epidermogenesis

Epidermis

Human skin equivalent

Hyperbaric oxygen

Keratin 1

Keratin 16

Loricrin

p63/proliferative capacity

ki-67/cell cycle

Kallikrein 1

Kallikrein 7

Early growth response 1

CDCP1

Metallothionein

Microarray

Immunohistochemistry

Abstract

Skin is the largest, and arguably, the most important organ of the body. It is a complex and multi-dimensional tissue, thus making it essentially impossible to fully model *in vitro* in conventional 2-dimensional culture systems. In view of this, rodents or pigs are utilised to study wound healing therapeutics or to investigate the biological effects of treatments on skin. However, there are many differences between the wound healing processes in rodents compared to humans (contraction vs. re-epithelialisation) and there are also ethical issues associated with animal testing for scientific research. Therefore, the development of skin equivalent (HSE) models from surgical discard human skin has become an important area of research. The studies in this thesis compare, for the first time, native human skin and the epidermogenesis process in a HSE model. The HSE was reported to be a comparable model for human skin in terms of expression and localisation of key epidermal cell markers. This validated HSE model was utilised to study the potential wound healing therapeutic, hyperbaric oxygen (HBO) therapy.

There is a significant body of evidence suggesting that lack of cutaneous oxygen results in and potentiates the chronic, non-healing wound environment. Although the evidence is anecdotal, HBO therapy has displayed positive effects on re-oxygenation of chronic wounds and the clinical outcomes suggest that HBO treatment may be beneficial. Therefore, the HSE was subjected to a daily clinical HBO regime and assessed in terms of keratinocyte migration, proliferation, differentiation and epidermal thickening. HBO treatment was observed to increase epidermal thickness, in particular stratum corneum thickening, but it did not alter the expression or localisation of standard epidermal cell markers. In order to elucidate the mechanistic changes occurring in response to HBO treatment in the HSE model, gene microarrays were performed, followed by qRT-PCR of select genes which were differentially regulated in response to HBO treatment.

The biological diversity of the HSEs created from individual skin donors, however, overrode the differences in gene expression between treatment groups. Network analysis of functional changes in the HSE model revealed general trends consistent with normal skin growth and maturation. As a more robust and longer

term study of these molecular changes, protein localisation and expression was investigated in sections from the HSEs undergoing epidermogenesis in response to HBO treatment. These proteins were CDCP1, Metallothionein, Kallikrein (KLK) 1 and KLK7 and early growth response 1. While the protein expression within the HSE models exposed to HBO treatment were not consistent in all HSEs derived from all skin donors, this is the first study to detect and compare both KLK1 and CDCP1 protein expression in both a HSE model and native human skin. Furthermore, this is the first study to provide such an in depth analysis of the effect of HBO treatment on a HSE model. The data presented in this thesis, demonstrates high levels of variation between individuals and their response to HBO treatment, consistent with the clinical variation that is currently observed.

Table of Contents

List of Figures

List of Tables

List of Abbreviations

°C	degrees celcius
µl	microlitre
µm	micrometer
2D	two dimensional
3D	three dimensional
ACTH	Adrenocorticotropic hormone
AIHW	Australian Institute of Health and Welfare
ANOVA	Analysis of variance
ATA	atmospheres
ATP	Adenosine triphosphate
AU$	Australian Dollars
AWMA	Australian Wound Management Association
CDCP1	cub-domain containing protein 1
cDNA	complementary deoxyribonucleic acid
CO_2	carbon dioxide
DAB	diaminobenzidine
DED	decellularized de-epidermized dermis
DMEM	Dulbecco's Modified Eagle's Medium
DNA	Deoxyribonucleic acid
dNTPs	deoxynucleotide triphosphates
DTT	Dithiothreitol
ECM	extracellular matrix
EDTA	ethylenediamine tetraacetic acid
EGF	epidermal growth factor
EGR1	Early growth response 1
FBS	Foetal bovine serum
FG	Full Greens media
GC	Glucocorticoid
H&E	haematoxylin and eosin
HBO	Hyperbaric Oxygen
HIF	Hypoxia inducible factor
HRP	Horseradish peroxidase
HSE	human skin equivalent
IPA	Ingenuity pathway analysis
K	keratin
KLK	Kallikrein
L	litre
mm^2	millimeter square
MMP	Matrix metalloproteinase

MT	Metallothionein
MTT	3-(4,5-dimethylthiazol-2-yl)-2,5-diphenyletetrazolium bromide
NEAA	Non-essential amino acids
O_2	Oxygen
O_2.-	Superoxide anion
P1	passage 1
PBS	phosphate buffered saline
PCI	Phenol:chloroform:isoamyl alcohol
PCR	Polymerase chain reaction
pH	Power of Hydrogen
ppO_2	Partial pressure of oxygen
qRT-PCR	Quantitative real time polymerase chain reaction
RNA	ribonucleic acid
ROS	Reactive oxygen species
SC	Stratum corneum
SCCE	Stratum corneum chymotryptic enzyme
SD	standard deviation
SPRR	Small proline rich proteins
TAE	Tris-acetate-EDTA
TEWL	Transepidermal water loss
TIMP	Tissue inhibitors of metalloproteinase
Tm	Melting temperature
UHMS	Undersea and Hyperbaric Medical Society
UV	Ultraviolet
UVB	Ultraviolet-B
v/v	volume per volume calculation
VEGF	Vascular endothelial growth factor
w/v	weight per volume calculation

List of Publications

Publications relating to this thesis:

McGovern J., Heinemann J., Burke L., Dawson R., Parker T., Upton Z., Hooper J. & Manton K. (2012) Stratum basale keratinocyte expression of the cell surface glycoprotein CDCP1 during epidermogenesis and its role in keratinocyte migration. *British Journal of Dermatology* (in press)

Presentations at Scientific Meetings:

- Australasian Wound and Tissue Repair Society (AWTRS) Conference, May, 2012. Sydney, Australia – **Poster Presentation**. *Immunohistochemical characterisation of a developing human skin equivalent model and its comparison to native human skin.* **J. McGovern,** T. Parker, D. Leavesley and Z. Upton.
- Institute of Health and Biomedical Innovation (IHBI) Post-Graduate Student Conference, November 2011. Brisbane, Australia – **Poster Presentation**. *Hyperbaric oxygen therapy increases epidermal thickness and impacts on epidermal generation-related proteins in human skin equivalent models.* **J. McGovern,** T. Parker, D. Leavesley and Z. Upton.
- 21st European Tissue Repair Society Meeting, October, 2011. Amsterdam, The Netherlands – **Poster Presentation**: *Hyperbaric oxygen therapy increases epidermal thickness and Metallothionein, kallikrein and early growth response gene expression in human skin equivalent models.* **J. McGovern,** T. Parker, D. Leavesley and Z. Upton.
- Institute of Health and Biomedical Innovation (IHBI) Post-Graduate Student Conference, November, 2010. Gold Coast, Australia – **Oral Presentation**: *Differential gene expression analysis in human skin equivalent models treated with hyperbaric oxygen therapy*. **J. McGovern,** T. Parker, D. Leavesley and Z. Upton.

- Australian Society for Medical Research (ASMR) Student conference, June, 2010. Brisbane, Australia – **Poster Presentation:** *Hyperbaric oxygen treatment stimulates greater epidermal thickness in human skin equivalent models.* **J. McGovern,** T. Parker, D. Leavesley and Z. Upton.
- Australasian Wound and Tissue Repair Society (AWTRS) Conference, March, 2010. Perth, Australia – **Poster Presentation:** *Hyperbaric oxygen treatment stimulates greater epidermal thickness in human skin equivalent models.* **J. McGovern,** T. Parker, D. Leavesley and Z. Upton.

Australian Society for Medical Research (ASMR) Student conference, May, 2009. Brisbane, Australia – **Poster Presentation:** *Development of an unbiased epidermal thickness measurement technique.* **J. McGovern,** T. Parker, D. Leavesley and Z. Upton

Acknowledgements

Firstly, this research would not have been possible without the financial support from my Australian Postgraduate Award scholarship and the Tissue Repair and Regeneration Program at QUT.

I would like to extend my appreciation and thanks to my Principal Supervisor, Zee Upton for taking me on as an honours and then PhD student and providing me with so many opportunities and support throughout my time at IHBI. Thank you to my Associate Supervisor David Leavesley for the thought-provoking discussions and attention to detail which has helped me immensely throughout my PhD. Last, but not least, I want to thank my other Associate Supervisor, Tony Parker. Tony, thank you so much for all your support over the last few years. You have been more than just a supervisor, you have been my coffee buddy, fellow music festival and concert-goer, at times my crisis counsellor and most importantly, you have been a great friend. I would like to thank all my supervisors for their guidance, encouragement and patience. Without you all, this would have been a truly impossible feat.

I would also like to thank my family, especially my parents, Shane and Janice and my brother, David for their continual support and encouragement throughout the PhD process. I deeply appreciate their belief in my ability, especially during the times when I did not believe in myself. It has been a long and at times arduous process and I cannot even begin to articulate how grateful I am to have such a loving and supportive family.

Next I want to thank my best friend, Matthew Hadaway, who has accompanied me throughout my entire university experience, from undergraduate right through to PhD. Thank you Matt, for being the one constant friend who has supported me unconditionally through both the highs and the lows of this journey.

I will always be grateful to Rebecca Dawson and Yan Xie for teaching me all I know about primary cell culture and human skin equivalent model generation. Without them I would not have been able to perform any of the work in this thesis and they have been invaluable colleagues whenever I needed experimental advice. Furthermore, I want to thank Katia Nones and the microarray facility at UQ for performing the microarray process. Furthermore I want to thank Daniel Haustead,

Brett Hollier and James Broadbent for their assistance with the microarray data analysis, interpretation and presentation. All this would have been impossible without their generous contributions of time and expertise. Lastly, thank you Abrona Bugler and Nicky Gillott for keeping me organised and I would like to thank them especially for their help with the travel forms.

Finally, I want to extend my eternal gratitude to the people who have kept me (mostly) sane; my lunch and coffee buddies and fellow PhD students: Matt, Emily, James, Daniel, Dayle, Helen, Chris, Arnulf and Tony. Thank you for all the good times, ridiculous conversations and laughter.

Chapter 1: Literature Review

1.1 INTRODUCTION

The maintenance of skin integrity is extremely important since the skin provides the first protective barrier for the body. If this natural barrier of defence is compromised through disease or injury, disability and even death can result. Chronic wounds cause a prolonged disruption of the skin barrier and are defined as a wound that fails to heal within 3 months (Wysocki, 1996). In Australia, chronic loss of skin integrity impacts between 200,000-600,000 people, a prevalence of approximately 1-3% of the population (Baker and Stacey, 1994; Gruen *et al.*, 1996). Moreover, Posnett and Franks (2008) determined that up to 3% of the national health care budget in developed countries such as the UK and Australia is spent on chronic wound care. If these data are extrapolated onto Australian figures, where according to the Australian Institute of Health and Welfare (AIHW) in 2005-2006, the national health expenditure was AU$ 86.9 billion, this would suggest up to AU$ 2.6 billion was spent on chronic wound care and management. Thus, the cost of treatment of chronic wounds is a large economic burden.

The treatment and management of wounds is expensive. Furthermore, the above costs do not take into account the financial burden associated with time off work and lost productivity, or the costs of disability payments, etc. This is important as chronic wounds also greatly impact upon the lives of those afflicted with these wounds, their carers, family and friends. According to the Australian Wound Management Association (AWMA), chronic wounds are a major concern in the older population. The AWMA estimates that approximately 60,000 people or ~ 25% of residents in aged care facilities live with chronic wounds which severely impacts the quality of life for a large number of people. Sufferers of chronic wounds typically experience a great deal of pain on a daily basis and have difficulty in terms of mobility and struggle with performing daily activities, including maintaining personal hygiene. They have issues dealing with wound odour and exudate, a general lack of energy and vitality, and restrict themselves from social activities in fear of exacerbating the wound or due to feelings of isolation or embarrassment in relation to their chronic wound (as reviewed by Green and Jester, 2010).

It is clear that the development of improved wound healing therapeutics is needed to alleviate the financial costs associated with wound care and management. However, the development of therapeutics is also important in terms of improving the quality of life of the many people, and those close to them, who are afflicted by chronic wounds. Evidently, further research into the area of wound healing can improve therapeutic options and enhance wound healing outcomes. Moreover, skin and wound healing can be studied using *in vitro* models to understand the underlying biological processes and this technique is routinely used within our research group (Kairuz *et al*., 2007; Topping *et al.*, 2008; Xie *et al*., 2010, Xie *et al.*, 2011). With this is mind, this review will focus on wound healing and epithelialisation in the tissue repair process. In addition, I will elaborate on skin development processes, in particular, the complexity of epithelialisation.

1.2 SKIN AND THE STRUCTURE OF THE EPIDERMIS

1.2.1 Skin biology

Skin covers the entire outer surface of the human body and is also the largest organ. The major function of skin is to maintain internal homeostasis of the organism. It is an efficient, self-repairing and renewing structure that continually tolerates the variable and ever-changing external environment. The thickness of skin in humans varies from 0.5 mm on the eyelid to 6 mm on the soles of the feet, proportional to the amount of chemical and mechanical assaults which skin in these areas would typically be exposed to (Olsen *et al.*, 1995).

The skin is the barrier between the external and internal environments of the human body. It is the first major line of defence in preventing pathogens from entering the body and also in protection against ultraviolet (UV) radiation. In the latter case, this is achieved through the production of melanin within the melanocytes. Melanin absorbs UV light thus preventing damage to cellular DNA and proteins (Miyamura *et al.*, 2007). Furthermore, bone marrow-derived antigen-presenting cells called Langerhan's cells reside in the epidermis and play a key role in the innate immune system of the skin. Antigens are taken up by the Langerhan's cells in the skin, and then the antigens are presented to T cells, acting as a bridge between innate and acquired immunity (Schiller *et al.*, 2006). In addition to protection of the body, skin is involved in the production of vitamin D through a

photochemical reaction in response to UV light (Holick, 1980). This process is essential for facilitating the gastrointestinal absorption of Ca^{2+}, which is vital for the maintenance of bone density (Holick, 1980). It is this diverse, multifaceted nature of skin which makes it such an important organ of the body.

1.2.2 Skin structure

The anatomical structure of the skin consists of three major layers; the epidermis, dermis and the hypodermis. The dermis and the epidermis are separated by a specialised layer known as the basement membrane. Moreover, the epidermis can be further subdivided into a variety of sections and these will be discussed in greater detail below.

The epidermis

The epidermis is the outer-most layer of the skin and is constantly subjected to the external environment. It consists of a variety of cells; predominantly, melanocytes, Langerhan's cells, Merkel cells, lymphocytes and the principal epidermal cell; keratinocytes (Kirfel and Herzog, 2004). The epidermis forms by proliferation and a process of keratinocyte maturation and differentiation, leading to the creation of a stratified epidermis. The stratification process involves proliferative keratinocytes being released from the basal layer, followed by migration and differentiation toward the apical (outer) surface. This usually takes between 15-30 days to complete. Stratification then ends with the fully differentiated keratinocytes sloughing off at the skin surface through a process known as terminal differentiation (reviewed by Candi *et al.,* 2005). Terminal differentiation and the transition of keratinocytes through various stages of maturation lead to the formation of distinct keratinocyte layers in the epidermis. These layers can be distinguished by the production of different types of keratins, the major type of protein produced by keratinocytes (Candi *et al.,* 2005).

The integrity of the epidermis and the process of its normal functioning depend directly on the polarity that keratinocytes exhibit in stratified epithelia. Specifically, keratinocytes near the upper layers (apical surface) differ from basal cells in both structure and function (Devenport and Fuchs, 2008). Keratinocyte polarity is determined by the signals they receive from the surrounding cells (such as keratin expression indicating differentiation status) which facilitate the keratinocyte to

perform its necessary functions at the appropriate time points (Devenport and Fuchs, 2008). Thus in a healthy epidermis, keratinocytes slowly proliferate in the basal layer and move toward the surface through the stages of terminal differentiation, prior to sloughing off at the apical surface (Fuchs, 2007). During the process of terminal differentiation, keratinocytes undergo both biochemical and morphological changes, including keratin expression and loss of their nuclei. The major proteins of the keratinocyte cornified envelope, including loricrin, filaggrin and involucrin, are cross-linked by isodipeptide and disulfide bonds during terminal differentiation (Steven and Steinert, 1994).

Table 1.1 Types of cells found in the epidermis and their functions

Cell Type	Function	Reference
Melanocytes	Production and distribution of melanin; role in pigmentation and UV protection.	Tsatmali *et al.* (2002)
Langerhan's cells	Antigen presenting cells for skin immune system which link with keratinocytes in the epidermis.	Woods *et al*. (2005)
Merkel cells	Mechanoreceptors associated with the sense of light touch and pressure.	Winkelmann and Breathnach (1973)
Lymphocytes	An extensive network of lymphocytes (dendritic cells, T cells, natural killer, mast cells and macrophages) function together to maintain skin integrity by removal of foreign material and monitoring cellular stress signals.	Ebert *el al.* (2006)
Keratinocytes	Make up the bulk of the epidermis. Transit through a terminal differentiation pathway forming a water-impermeable barrier, resulting in the protective nature of the skin.	Kirfel and Herzog (2004)

The epidermis can be subdivided into five distinct layers, which correlate to the different stages of keratinocyte maturation during terminal differentiation (**Figure 1.1**). The specific layers detailed below are described from the outermost layer of the skin to the basal layer adjacent to the underlying dermis.

Stratum corneum

The stratum corneum is the outermost, or most superior, layer of the epidermis and is directly exposed to the external environment. It is characterized by approximately 15 – 30 layers of keratinized, overlapping cells, all of which lack nuclei and are joined tightly by desmosomes. The keratins produced from the terminal differentiation process provide flexibility and strength to the outermost

epidermal layer (Steven and Steinert, 1994). The stratum corneum is also responsible for restricting the release of water from the surface; a phenomenon known as transepidermal water loss (TEWL). This occurs due to the keratinocytes being encased within a lipid envelope which protects the skin from water loss (Proksch *et al*., 2008). Grubauer *et al.* (1989) reported that there was a direct relationship between the amount of lipid present within the stratum corneum and the degree of protection against TEWL. Furthermore, the authors stated that while other lipids such as sterols and fatty acids are important, sphingolipids (e.g. ceramides) may be the principal regulator of barrier function (Grubauer *et al*., 1989). Specifically, these lipids condense in lamellar bodies, specialised secretory organelles within the keratinocyte and increase in quantity during keratinocyte differentiation. The lamellar bodies secrete their stored lipids at the interface of the stratum corneum and stratum granulosum, a necessary process in barrier formation (Menon *et al.*, 1992). By the time keratinocytes reach the upper stratum granulosum, they have lost their nuclei and cytoplasm, thereby completing the terminal differentiation process. These terminally differentiated keratinocytes are no longer able to synthesise additional proteins, therefore no new markers are expressed to characterise this layer.

Stratum lucidum

The stratum lucidum is present in skin found on the palms of the hands or the soles of the feet (palmoplantar skin). This stratum is thought to reflect an abrupt sequence of terminal differentiation and cornification (Compton *et al*., 1998). Its presence is only found in thicker areas of the skin as it helps to reduce friction and shear forces between the stratum corneum and the deeper stratum granulosum. Interestingly, palmoplantar skin is the only site in the body to specifically express keratin 9 (K9; Compton *et al.*, 1998). K9 is localised to the suprabasal epidermal layers, co-localises with skin differentiation marker keratin 1 (K1) and has been found to be induced through interactions with palmoplantar dermal fibroblasts (Yamaguchi *et al.*, 1999). Histologically, the stratum lucidum appears between the stratum corneum and stratum granulosum as a translucent layer of terminally differentiated keratinocytes (Compton *et al*., 1998).

Stratum granulosum

This layer is also known as the granular cell layer, as the keratinocytes produce keratohyaline and keratin granules and these appear as darkly staining granules in haematoxylin and eosin stained sections (Chen *et al.*, 2008). Keratinocytes in the stratum granulosum begin to flatten and lose intracellular organelles and nuclei, therefore adopting the characteristic morphology of this layer. Furthermore, in the stratum granulosum, keratinocytes also express filaggrin, transglutaminase, K1/10/11 and precursors of the cornified envelope; loricrin and involucrin (HogenEsch *et al.*, 1999).

Interestingly, filaggrin has been hypothesised to interact with keratins in order to prevent its proteolytic degradation until it reaches the stratum corneum. Once there, it is then degraded to release free amino acids, assisting in water retention and skin hydration (Rawlings and Hardings, 2004). Moreover, loricrin has been suggested to have an important role in epidermal barrier function during the skin developmental process (Bickenbach *et al.*, 1994). The upper layers of keratinocytes in the stratum granulosum are classified as "dead" once they lose their nuclei. This disintegration causes the cells to dehydrate, resulting in the production of a tough impermeable layer of keratin surrounded by keratohyaline.

Stratum spinosum

The stratum spinosum is formed by newly divided daughter cells which have detached from the basal layer, but remain bound together by desmosomes. These interconnected cells are progressively moved toward the apical surface of the skin by the continual proliferation of the underlying basal cells. The stratum spinosum can be up to approximately 10 cells thick and is also reported to contain Langerhan's cells, which migrate from bone marrow and participate in systemic immunity through association with lymphocytes and keratinocytes (Sugita *et al.*, 2007). No further cell division events occur from this stratum onwards and the cells are now committed to the terminal differentiation pathway. Furthermore, keratinocytes in this stratum begin expressing K1/K2/K10 and K11 as they begin the terminal differentiation process.

Stratum basale

The stratum basale, also known as the basal cell layer, is the deepest, or innermost, layer of the epidermis. It consists mainly of basal cells (undifferentiated keratinocytes, or keratinocyte 'stem cells') that divide to replace superficial

keratinocytes which are then shed at the epithelial surface. The basal cell layer also contains a small proportion of melanocytes which synthesise melanin; these serve to protect basal cells by absorbing the energy of UV radiation and act as a free-radical scavenger (Haake and Scott, 1991). The stratum basale is firmly anchored to the underlying basement membrane via hemidesmosomes, providing structural integrity and strength to the epidermis (Mommaas *et al.*, 1992). This layer also forms rete ridges that extend into the dermis, thus increasing the surface area of contact between the two layers, providing a strong bond between the two skin sections. Additionally, keratinocytes of the stratum basale are characterised by the expression of K5, K14 and K15, and also p63, a member of the p53 transcriptional regulator family, which is a marker of cellular proliferation (Truong and Khavari, 2007).

Layer	**Cellular features**	**Marker expression**	
Stratum corneum	Cells lack nuclei and have thick, lipid matrix envelope. 15-30 cells thick	No new proteins expressed.	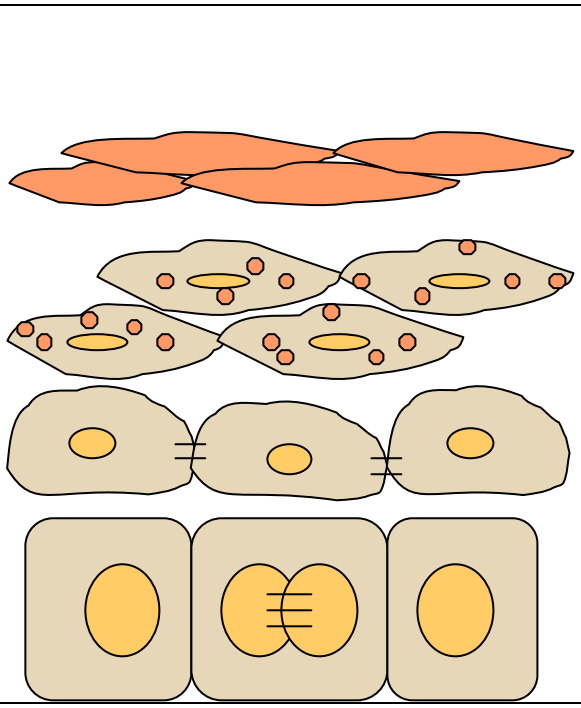
Stratum granulosum	Elongated, 1-2 cells thick, accumulate amorphous keratohyaline granules.	Involucrin, K1/K10, Loricrin, Filaggrin.	
Stratum spinosum	Increased cytoplasm:nuclear ratio, generally 4-6 cells thick, no further cell division occurring	K2, K1/K10, Involucrin, Envoplakin, Periplakin.	
Stratum basale	Cuboidal cells, proliferative, attached to basement membrane, 1-2 cells thick	K5/K14/K15, p63, Ki67.	

Figure 1.1 Morphology of keratinocyte differentiation
Schematic representation of the changes that occur within the keratinocyte as they progress though the stages toward terminal differentiation and associated protein expression and cellular features. Adapted from HogenEsch *et al*. (1999).

The basement membrane

The basement membrane is a specialised zone that separates the epidermis from the dermis, thus is also known as the dermal-epidermal junction or the basal lamina. The stratum basale of the epidermis is also thought to play a key role in influencing keratinocyte function by modulating cell polarity, proliferation, migration and commencement of differentiation (Mommaas *et al.,* 1992). Moreover, this important skin structure is a complex network of interconnecting proteins (such as laminin, nidogen, type IV collagen and heparin sulphate proteoglycans) which lend an intricate architecture to this zone of significant mechanical stability (as reviewed by Burgeson and Christiano, 1997). Histologically, the basement membrane is a structure that stains positively using Periodic acid Schiff (PAS) staining, which is utilised to detect structures with a high proportion of carbohydrates (**Figure 1.2**).

The basement membrane is important in maintaining skin homeostasis; however, it is also important for the epithelialisation process. Ralston *et al.* (1999) found that skin models cultured using a de-cellularised de-epidermized human dermis (DED) with basement membrane proteins removed failed to stratify correctly. Specifically, the epidermis developed with an indistinct basal layer and incomplete differentiation and defined strata. In comparison, the HSE models with the basement membrane intact displayed a distinct cuboidal basal layer and well-defined epidermal strata. Clearly, the basement membrane is an extremely important structure for the normal migration, proliferation, differentiation and stratification of the epidermis.

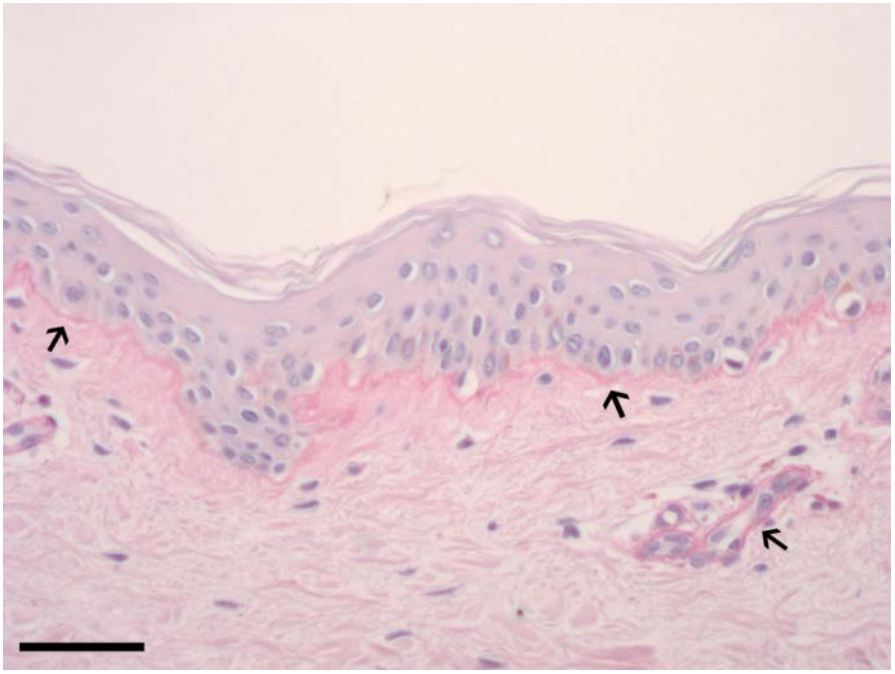

Figure 1.2 Periodic acid-Schiff (PAS) stain to detect basement membrane in human skin
PAS staining of native human skin obtained from a consenting adult undergoing elective abdominoplasty surgery. The black arrows indicate the localisation of carbohydrates which denote the presence of the basement membrane in human skin. Positive staining, as indicated by the dark pink staining, highlights the basement membrane of the epidermal-dermal junction and capillaries present in the skin. The scale bar represents 50 µm.

The dermis

The dermis is made up of a variety of biological components, including vascular structures, hair follicles, sweat glands, cell types such as mast cells, and specialised nerve endings. The most abundant cell type, however, is the fibroblast. Fibroblasts produce the extracellular matrix (ECM) that provides the scaffold for cellular migration and also acts as a reservoir for growth factors (Xu and Clark, 1996).

The primary function of the ECM is to act as a scaffold to hold cells together, thus a majority of the fibroblasts in the dermis are not in direct contact with each other. The main ECM components produced by fibroblasts are collagen, elastin and structural proteoglycans such as glycosaminoglycans (GAGs). GAGs are protein chains bound to branched polysaccharides which bond covalently to form proteoglycans (Iozzo and Murdoch, 1996). The dermis is primarily made up of type I collagen, followed by type III collagen. However, the type V and VI collagens are also found in low amounts. Collagens, in particular type I collagen, are responsible for the tensile strength of the dermis and thus, skin (Garrone *et al.*, 1997).

Furthermore, the dermis is rich in vascular networks that provide direct nutrient supply to the dermis and to the epidermis via diffusion.

The dermis consists of two layers; the superficial papillary layer and the underlying reticular layer, which are outlined below:

Papillary dermis

The papillary layer projects into the epidermis to form structures known as rete ridges. The rete ridges act to increase the surface area contact between the basement membrane and the dermis, thereby increasing the strength of the skin (Mommaas *et al.*, 1992). The papillary dermis contains sensory nerves and capillaries that supply the epidermis with nutrients via diffusion through the superficial cellular layers. Collagen fibres in the papillary dermis are smaller in diameter and form smaller, cable-like structures compared to the reticular dermis (Fleischmajer *et al.*, 1980). This layer also contains small elastic fibres and has a greater proportion of fibroblasts and a greater proportion of ECM (**Figure 1.3**). Furthermore, Harper and Grove (1979) found that papillary fibroblasts possess a greater proliferative capacity than reticular-derived fibroblasts. While both layers of the dermis are rich in type I collagen, the papillary dermis has a higher abundance of type III collagen (Meigel *et al.*, 1977).

Reticular dermis:

The reticular dermis lacks the characteristic rete ridges present in the papillary dermis; however, the strength of this layer can be attributed to the collagen fibres that form denser, 'bundle-like' structures, which function to anchor the reticular layer to the underlying subcutaneous layer (Meigel *et al.*, 1977). In contrast to the papillary dermis, the reticular dermis has substantially less ECM and it contains fewer fibroblasts (**Figure 1.3**).

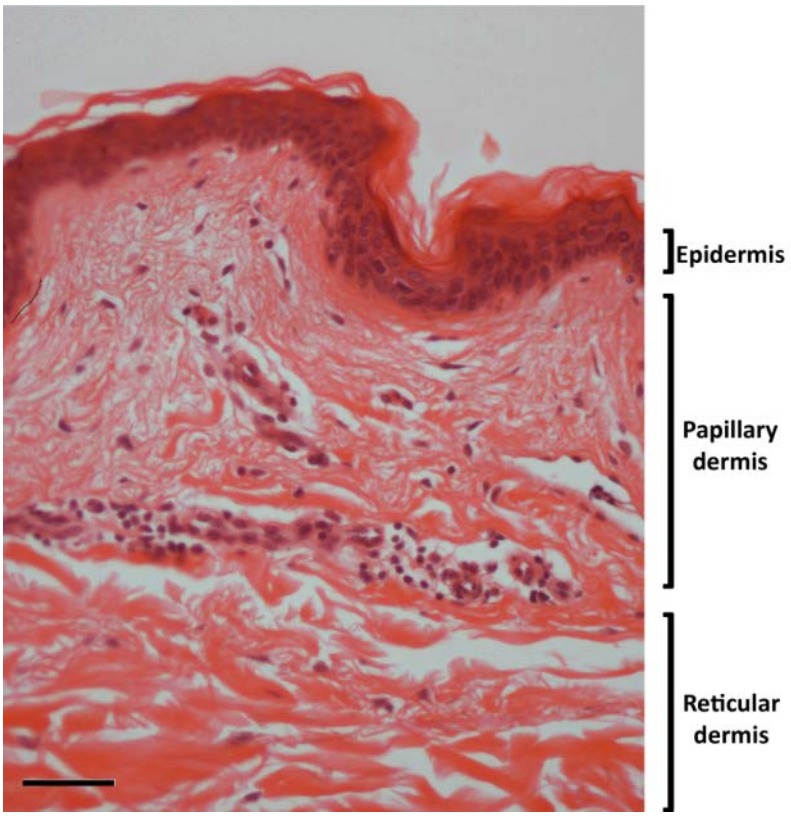

Figure 1.3 Macroscopic structure of the dermis in native human skin
This is a representative image of the organisation of the dermis in native human skin. The papillary dermis is located underneath the epidermis in the skin and is comprised of small-diameter collagen fibres and a larger population of dermal fibroblasts. The reticular dermis is situated below the papillary dermis and contains fewer fibroblasts but thicker collagen-fibre bundles. The scale bar represents 50 µm.

The hypodermis

The hypodermis is essential for internal organ protection, thermal insulation and insulates the upper skin layers from the underlying muscle, tendons and bone. The hypodermis, also known as the subcutaneous layer, is located directly beneath the dermis and consists of loose connective tissue and adipose tissue. Its primary function is to maintain the stability of the skin in relation to its underlying tissues and structures and to also act as a layer of cushioning and insulation. Specifically, the adipose tissue plays a major role in the regulation of heat loss and functions as an energy reserve.

1.3 SKIN HOMEOSTASIS AND TERMINAL DIFFERENTIATION

Maintenance of the skin is imperative for survival and once the skin is formed during embryonic development, it must be maintained for the rest of life. As outlined in section 1.2.2, the epidermis develops via a process of proliferation then a series of biochemical and histological changes (terminal differentiation) in which proliferative basal cells transition into the cornified squames that compose the protective stratum corneum.

Skin homeostasis is thought to be controlled by epithelial – mesenchymal interactions, notably, the cross-talk between epidermal keratinocytes and dermal fibroblasts. Studies performed by Smola *et al.* (1993) found that co-culture of keratinocytes seeded on a collagen matrix containing dermal fibroblasts enhanced proliferation and differentiation of the developing epidermis compared to keratinocyte only controls. These results were supported by work from El Ghalbzouri *et al.* (2002) who further determined that no direct keratinocyte-fibroblast interaction is required; rather, the fibroblasts secreted soluble factors which stimulated keratinocyte proliferation and enhanced the terminal differentiation process. This research clearly demonstrates that the major cell types within the skin communicate with each other to maintain the integrity of the skin.

An important process in epidermal homeostasis is the constant shedding and sloughing off of the stratum corneum at the cellular surface, this stimulates the process of basal cell proliferation and thus epidermal renewal (reviewed by Racila and Bickenbach, 2009). This is supported by Barthel *et al.* (2000) and Potten *et al.* (2000) who demonstrated that adhesive-stripping, which disrupted the stratum corneum only, enhanced the proliferative events of the epidermis in mouse skin, even after the stratum corneum had re-formed. Thus, sloughing off of the surface layers of the stratum corneum is part of a normal event in the skin. This stimulates the renewal of proliferative cells in the basal layer and the reformation of a stratum corneum.

The epidermis is avascular and receives nutrients via diffusion from the vascular system situated in the underlying dermal layer. As keratinocytes move toward the apical surface, they move beyond the diffusive reach of the vascular system and release from the basement membrane, which is an important stimulator of the terminal differentiation process (Watt *et al.*, 1993). Throughout this process, keratinocytes produce different types of keratins based on their level of

differentiation. Thus, keratin expression defines the differentiation status of a keratinocyte (Patel *et al*., 2006). The keratinized cells of the stratum corneum (also known as corneocytes) possess lipids, including free fatty acids, ceramides and cholesterol, covalently bound to their surface. This provides an extracellular lipid matrix to form scale-like sheets known as lamellae. The high lipid composition, in conjunction with the morphological structure, contributes to the low water permeability of the stratum corneum (Potts and Francoeur, 1991).

1.3.1 Keratins

Keratins are the major structural proteins synthesised by keratinocytes and are assembled into a web-like structure throughout the cytoplasm of the cell (Proksch *et al*., 2008). They are classified as a type of intermediate filament and are characterised as fibrous, filamentous polymer structures that extend across the cytoplasm from one cell junction to another, providing mechanical strength to the whole epithelial layer (Proksch *et al*., 2008). Keratins can be broken down into two main subclasses based on charge; Type I keratins are an acidic group of proteins, whereas Type II keratins are neutral to basic (Schweizer *et al.,* 2006). Within the epithelia, keratins are expressed in heterodimeric pairs, generally with one of the members of the pair arising from the Type I group and the other from the Type II group. Keratin expression is histologically significant in that it allows the determination of the differentiation state of a keratinocyte (Dale *et al.,* 1985; **Figure 1.1**).

1.4 WOUND HEALING: SKIN REPAIR AND REGENERATION

Wound healing can be best understood as a cascade of overlapping events, where injury sets into motion a coordinated series of physiological responses which, under normal circumstances, results in tissue repair. Once a wound occurs, one of the body's top priorities is to form a functional epidermis in order to rapidly restore the normal barrier function of the skin (as reviewed by Martin, 1997). To re-epithelialise the wound bed, keratinocytes detach from their region of anchorage and migrate over a provisional matrix deposited by wound repair cells (fibroblasts, macrophages, etc). Subsequent to monolayer formation, hyper-proliferation and migration signals cease and normal proliferation and differentiation can recommence (Patel *et al.,* 2006)

Wound healing generally occurs in four phases (described further in *Table 1.2*). Prolonged time spent in the proliferation phase by fibroblasts is known to lead to abnormal scarring, such as keloid or hypertrophic scars, due to excess ECM production. A prolonged inflammatory phase, however, causes a pathological state and results in a chronic wound (Menke *et al*., 2007).

1.4.1 Acute and chronic wounds

Wounds can be divided into two main categories; acute wounds, which heal in a timely and efficient manner following an injury, and chronic wounds, those which fail to heal even after a long period of time has elapsed (Bowler, 2002; Wysocki, 1996). There is no single factor that results in the development of a chronic wound; however, aspects such as age, nutritional and disease status (e.g. diabetes and Cushing's disease) are all known to be risk factors associated with progression to a chronic wound state. It is difficult to determine at what time a wound can be considered chronic, although it is generally accepted that a wound which fails to initiate the healing process within three months of the initial injury can be classified as a chronic wound (Wysocki, 1996). This is also dependent on the initial size and severity of the wound. Complications of these wounds include functional limitations (e.g. gait changes and difficulty in walking/moving), infections (cellulitis, abscess formation, osteomyelitis, gangrene and even sepsis) and malignant transformation and ultimately, may also result in amputation (Menke *at al*., 2007).

The persistence of the inflammatory phase in chronic wounds has a devastating effect on normal skin physiology. In particular, chronic inflammation is known to disrupt the delicate balance of proteases and their inhibitors, which are crucial for inflammation resolution and regulation of re-epithelialisation. Excessive protease activity causes further tissue damage and rapid degradation of any provisional matrix formation. This was highlighted by Trengove *et al.* (1999) who observed increased levels of matrix metalloproteases (MMPs) and decreased levels of tissue inhibitors of MMPs (TIMPs) in chronic wound fluid as compared to acute wound fluid. Specifically, increased inflammation results in excessive ECM degradation by matrix MMPs, in particular MMP-2 and MMP-9 (Ladwig *et al.*, 2002; Wysocki *et al.*, 1999). Furthermore, it has been previously demonstrated that the level of MMP activity observed in the fluid of chronic wounds can be directly related to the severity of the ulcer (Rayment *et al.*, 2008). It has been suggested that the persistent presence

of neutrophils, which produce MMP-9, may be a potential factor in the persistence of a chronic inflammation state (Yager and Nwomeh, 1999). Furthermore, excessive protease production reduces the concentration of important growth factors and thus the mitogenic activity of cells is suppressed in chronic wounds (Menke *et al*., 2007). In contrast, inflammation is a self-limiting process in acute wounds, and in fact, it is important for the preparation of the wound bed for healing by removal of necrotic tissue, debris and bacterial contamination, as well as recruitment and activation of fibroblasts (Menke *et al*., 2007).

Table 1.2 Summary of the four stages of wound healing

Phase	Action	Biological effects	References
1. Haemostasis	Clot formation and platelet aggregation	Impede blood loss	Martin, 1997
		Release of growth factors/chemical stimuli	Martin, 1997
2. Inflammation	Arrival of neutrophils	Attracted by chemical stimuli released during haemostasis	Martin and Leibovich, 2005
	Monocyte arrival and differentiation to macrophage	Consumption of necrotic material.	Martin and Leibovich, 2005
		Release of growth factors/chemical stimuli	Yager and Nwomeh, 1999.
3. Proliferation	Fibroblasts arrive	Attracted by chemical stimuli released by macrophages	Wilgus, 2008
		Collagen production	Wilgus, 2008
		Release of growth factors/chemical stimuli	Werner *et al*., 2007
	Fibroblast transformation to myofibroblasts	Align with new ECM to contract the wound site	Werner *et al*., 2007
	Keratinocyte migration across the ECM	Attracted by chemical stimuli released by fibroblasts	Wilgus, 2008
		Creation of an epithelial monolayer covering the wound area	Paladini *et al*., 1996
	Release of MMPs from fibroblasts and keratinocytes	Basement membrane digestion	Yager and Nwomeh, 1999.
	New blood vessel formation	Capillary sprouts from pre-existing blood vessels vascularise wound area.	Martin and Leibovich, 2005
4. Remodelling	Vascularised wound area	Elimination of hypoxic environment, leading to reduced vascularisation	Gordillo and Sen, 2003
	Collagen remodelling	Complete wound contraction	Werner *et al*., 2007
		Increased strength of wound	Werner *et al*., 2007

Chronic wounds can be further sub-classified based on their aetiology:

- Diabetic: caused by diabetic neuropathy and/or peripheral vascular disease.
- Venous: caused by malfunctioning of lower extremity circulation (e.g. blood clot or vasculature damage).
- Arterial: as with venous ulcers.
- Pressure: caused by long-term concentrated pressure or friction, particularly at sites where tissue surrounding bone is thin (e.g., hips, heels, coccyx).

It is important to note, however, that although the above ulcer types have differing underlying aetiologies, they all share a common inability to heal correctly.

Bacteria present in wounds consume glucose and oxygen and therefore bacterial contamination of the wound can lead to tissue hypoxia. It is possible for acute wounds to lack bacteria, but most, if not all chronic wounds contain bacteria, which increases the bioburden for the number of metabolically active cells in an area competing for nutrients (Bowler, 2002). However, the presence of bacterial colonisation is distinct from infection and therefore it is important to note that the presence of bacteria in a wound is not the sole contributing factor to the wounds chronicity (Ayello *et al.*, 2004). Moreover, hypoxia is an important signal that drives the process of wound healing in acute wounds (further discussed below). Nevertheless, chronic hypoxia and ischemia are characteristic of many non-healing wounds (Zhang *et al.*, 2008). Thus, there is a delicate balance between wound oxygenation and the hypoxia that is necessary for efficient wound healing

1.4.2 The importance of oxygen

Oxygen (O_2) is a key nutrient for the sustenance of life in complex, multi-cellular organism and also in unicellular aerobic organisms. In particular, O_2 is a key mediator in the tissue repair process with evidence indicating that O_2 plays a role in epithelialisation, collagen synthesis, angiogenesis and prevention of bacterial growth within the wound environment.

Not only is the presence of O_2 at the wound site important, but also the partial pressure of oxygen (ppO_2) needs to be considered. The ppO_2 is dependent upon the arterial oxygen saturation and O_2 diffusion from the capillaries, thus ppO_2 is an

important indicator of superficial skin oxygenation (Gordillo and Sen, 2003). The central region of the wound environment is the most hypoxic, with an increase in the O_2 gradient toward the uninjured tissue at the periphery (Remensnyder and Majno, 1968). The ppO_2 of dermal wounds ranges from 0 to 10 mmHg centrally to 60 mmHg at the periphery, while the ppO_2 in the arterial blood is approximately 100 mmHg (Gordillo and Sen, 2003). It is important to note that adequate O_2 perfusion is needed to continue the wound healing process. Furthermore, it is this gradient of oxygenation in normal tissue to hypoxia in the wound centre that stimulates the wound healing cascade and thus promotes the diffusion of O_2 to the hypoxic tissue (Bishop, 2008).

O_2 is not only essential for gross oxygenation of the skin, but it is also necessary for several post-translational steps in collagen synthesis. The enzymes prolyl hydrolxylase, lysyl hydroxylase and lysyl oxidase all require molecular O_2 as a cofactor in order to perform their biological function in the collagen synthesis and maturation pathway. More specifically, prolyl hydroxylase is required to convert proline residues to hydroxyproline, which allows the procollagen peptide chains to assume their triple helix configuration. Without the presence of O_2, collagen cannot be correctly formed and thus the scaffolding of the wound bed cannot be sufficiently produced since collagen deposition provides an essential matrix for angiogenesis and cellular migration (Sen, 2009).

Bacterial colonisation can result in the continual generation of reactive oxygen species (ROS) as by-products of bacterial metabolism (Bowler, 2002). A portion of the O_2 present in the wound environment is involved in the production of reactive oxygen species (ROS), such as superoxide ions and hydrogen peroxide, in a process known as respiratory burst (Bishop, 2008). It is important to note that the production of ROS by the body is a self-limiting process, as opposed to bacterial ROS production, which is a continual and tissue-destructive process. Moreover, respiratory burst generally occurs by phagocytes and the resulting ROS are important in destroying bacterial membranes and thus, decreasing the bioburden on the wound environment. Interestingly, it has been demonstrated that the stratum corneum can also act to detoxify ROS during wound healing through the formation of disulfide bonds with the cysteine residues of the major stratum corneum proteins (Vermeji and Backendorf, 2010; Vermeji *et al.*, 2011). Specifically, the authors studied the lifetime

of a singlet O_2 molecule in the presence of small proline rich proteins (SPRRs; which contain high levels of proline and cysteine), both with and without cysteine-inhibitors and found that in uninhibited conditions, SPRRs effectively quenched ROS (Vermeji and Backendorf, 2010; Vermeji *et al.*, 2011). However, in a chronic wound environment, when a new epithelium fails to form, this ROS detoxification process cannot be implemented.

1.4.3 The importance of hypoxia

Although it is clear that oxygen is important for the healing of wounds, hypoxia itself plays a crucial role in the initiation of wound healing. When wounding occurs, there is disruption to the vascularisation of the entire wounded area, coinciding with increased nutrient demand due to the reparative processes that must occur. This leads to a decrease in local wound oxygen concentration, thus leading to hypoxia (Malda *et al*., 2007). Furthermore, local hypoxia is inevitable in a wound, and may be crucial in the stimulation of angiogenesis, which enables wound reperfusion (Boraldi *et al.*, 2007).

In a wound environment, initial hypoxia stimulates the wound healing cascade and drives the progression of acute wound healing. This initial hypoxia is also believed to be important in the stimulation of cell proliferation, migration and cellular differentiation via the induction of cytokines and growth factors which stimulate intracellular signalling pathways (Bishop, 2008). It is known that a hypoxic environment stimulates the production of hypoxia inducible factor (HIF), which is involved in the stimulation of processes that enhance the delivery of oxygen to tissues, including red blood cell production and inducement of vascular endothelial growth factor (VEGF), a potent inducer of blood vessel formation (Boraldi *et al.*, 2007; Gordillo *et al*., 2008).

In contrast, hypoxia, in conjunction with ischemia, is also often viewed as the cause and a characteristic of chronic wounds and is related to the inability of such wounds to heal (Sen, 2009). In a chronic wound environment, hypoxia becomes extreme and thus it is important to note that if hypoxia alone is sufficient to heal, all ischemic wounds would have undergone rapid healing. Clinical observations, however, are the exact opposite. Specifically, under hypoxic conditions skin fibroblast-produced collagen cannot be stabilised or cross-linked effectively as O_2 is a required co-factor (Thackham *et al.*, 2008). Several animal studies have

demonstrated that chronic hypoxia results in decreased granulation tissue production and delayed onset of re-epithelialisation (Mustoe *et al.*, 1994; Zhao *et al.*, 1994). Thus, it is clear that in the initial stages of wound healing, hypoxia is unavoidable, but also necessary. Hypoxic conditions only become problematic when re-oxygenation of the wound environment fails to commence and hypoxia prevails, preventing the continuation of the wound healing cascade (Sen, 2009).

1.5 CURRENT CHRONIC WOUND HEALING TREATMENTS AND TECHNIQUES

An important factor in the healing of a chronic wound is proper wound care which focuses on the maintenance of an environment which is optimal for tissue repair and prevents fluid build up and bacterial colonisation. The treatment and management of non-healing wounds generally involves the simple principals of eliminating infection through antibiotic treatment, debridement of necrotic tissue, thorough cleaning and dressings which are designed to maintain a moist environment, yet also draw away excess exudate from the wound bed (Hinchliffe *et al.*, 2008). Currently the gold standard in treating non-healing venous ulcers is pressure bandaging. Pressure bandaging is designed to provide a mechanical means of preventing oedema, an accumulation of fluid in the limb, and also by increasing venous return (Takahashi *et al.*, 2004). By improving circulation, pressure bandaging is also effective at improving oxygenation. Another important therapy that appears to have benefits in stimulating the healing of chronic wounds is hyperbaric oxygen therapy.

1.5.1 Hyperbaric oxygen therapy

Standard hyperbaric oxygen therapy

Hyperbaric oxygen (HBO) therapy can be described, essentially, as a method of administering a higher dose of oxygen at greater-than-normal atmospheric pressures (Wood, 2002). Initially HBO therapy was used in the treatment of decompression sickness (also known as ‘the bends’) in divers. When the body is subjected to high pressures (such as diving conditions) the gases within the body, including nitrogen and oxygen, are forced into solution. Upon return to normal pressure conditions, the gases are able to come out of solution and re-gas. If depressurisation occurs too rapidly for the gas to be exhaled, the nitrogen forms bubbles within the blood stream. This can be extremely painful and in rare cases,

fatal. Oxygen under pressure does not result in the bends as it can be used by tissues; nitrogen on the other hand, is an inert gas that accumulates without being depleted by metabolic needs.

The therapeutic action of HBO treatment is based on the elevation of both the partial pressure of O_2 and hydrostatic pressure. Elevating the hydrostatic pressure increases the partial pressure of gases and causes a reduction in the volume of gas-filled spaces, such as oxygen dissolving in plasma under HBO conditions (Thom, 2009). Currently, a HBO regime is used to treat not only decompression sickness, but aliments such as carbon monoxide poisoning, gas gangrene, crush injuries, anaemia through blood loss, osteomyelitis, radiation injury, compromised skin grafts and flaps, thermal burns and of importance to this project, chronic non-healing wounds (Thom, 2009).

HBO therapy can be administered in either of two types of chambers: monoplace or multiplace (Villanueva 2003). In addition, O_2 can also be administered topically; however, this will be discussed later. Multiplace chambers are designed to house multiple occupants and consist of a large chamber-style room which is pressurised with normal atmospheric air, which allows medical staff to also be present. Pure, 100% O_2 is administered to the patients of a multiplace chamber via masks, head tents (or hoods), endotracheal or nasopharyngeal tubes. Monoplace chambers are generally made with clear walls and are designed for a single person only. Patients can communicate with medical staff through an intercom system installed in the chamber, and rather than breathing O_2 through a mask or tube, the entire chamber is flushed and pressurized with 100% O_2. However, there is an increased fire risk when the entire chamber is pressurised with O_2 rather than air. It is important to note that according to expert clinical opinion, the therapeutic effect is the same regardless of the type of HBO chamber used (Villanueva 2003).

While there is evidence for its efficiency for a variety of ailments, including chronic wound healing applications, HBO therapy is costly. A course of HBO treatment in Australia costs up to $6000, based on $200 per treatment for 6 weeks, 5 times per week (MSAC, 2003). A typical course of HBO therapy involves 100% oxygen at 2.4 atmospheres which is applied in clinical settings such as the Wesley Centre for Hyperbaric Medicine in Brisbane, Australia. Although HBO appears to be a highly efficient mechanism for wound healing purposes, the costs, both financially

and in terms of time, may be too great for some patients. Therefore, further studies need to be conducted in order to elucidate the specific mechanisms of how HBO therapy functions in order to recapitulate these mechanisms via alternative and cheaper therapies to eliminate the need for costly treatments.

Topical hyperbaric oxygen therapy

Topical hyperbaric oxygen therapy is a misleading term, as it suggests that oxygen is administered at greater-than-atmospheric pressures, however, topical oxygen therapy does not reach pressures greater than 1 atmosphere (ATA; the amount of pressure exerted by the atmosphere) and therefore the term 'hyperbaric' should not apply to this application (Feldmeier *et al.,* 2005). None-the-less, topical oxygen therapy differs from traditional monoplace or multiplace methods by a variety of distinguishing factors. Firstly, and as previously stated, traditional HBO chambers reach pressures greater than that of the normal atmosphere, whereas topical oxygen therapy does not exert pressures greater than 1 ATA on the patient. Secondly, topical HBO relies on delivery of oxygen directly to the wound site, whereas, traditional HBO therapy involves systemic oxygen delivery.

A benefit of topical O_2 therapy is the elimination of systemic O_2 toxicity effects since O_2 is not being inhaled. In addition, there is a reduced risk of complications related to increased pressure such as barotrauma and visual refractive changes as pressures greater than ambient atmosphere are not reached. Although there are positive aspects, topical O_2 therapy also has downfalls, such as cellular toxicity due to direct contact between pure O_2 and the skin, which increases the risk of generation of harmful ROS. Moreover, this type of O_2 delivery to a wound site is limited to open wounds. Encrusted ulcers prevent O_2 diffusing through the tissue thus the O_2 fails to reach the ulcerative base. Fries *et al.*, (2005) demonstrated that topical O_2 only penetrates the thickness of the epidermis, thus it may not be optimal for deep tissue wounds. However, the authors also suggested that since re-epithelialisation is the goal of wound healing therapies, this limitation of topical O_2 penetration may be irrelevant (Fries *et al.,* 2005).

There have been reports on successful wound healing using topical O_2 therapy, including Fries *et al.* (2005) who studied the effect of topical O_2 on dermal excisional wounds in pigs and found it increased wound oxygenation, accelerated wound closure and improved wound angiogenesis when compared to untreated controls.

Furthermore, Davis *et al*. (2007) utilised pigs to study the effect of topical O_2 on both burn and partial-thickness wounds using an emulsion of O_2 dissolved in perflurocarbon, which allows the slow-release perfusion of O_2 into the wound over time. The topical O_2 treated pigs had significantly enhanced wound epithelialisation as compared to the untreated controls. However, the perflurocarbon-only treated pigs also demonstrated enhanced epithelialisation at later time points over the untreated control animals. Thus, it is unclear from the literature what the standard method of topical administration is and how the implementation of an O_2 delivery agent affects wound healing outcomes.

Topical O_2 therapy appears to be a promising option for the treatment of wounds. However, it has been theorized, but unsubstantiated, that O_2 presence at the wound surface is not beneficial and may actually be detrimental due to the localised production of reactive O_2 species in the wound bed (Heng and Kloss, 1986). Nevertheless, further studies by the same author revealed that toxic effects of topical O_2 can be avoided by close monitoring of the wound in response to the treatment (Heng, 1993). However, a report was released by the Undersea and Hyperbaric Medical Society (UHMS) indicated that there is a lack of evidence for the benefit of topical HBO based on their review of the available literature (Feldmeier *et al.*, 2005). Hence, while there is emerging evidence that topical O_2 treatment may be a viable alternative to HBO, the benefits and risks associated with topical O_2 therapy have not yet been fully elucidated.

Therapeutic principles and the use of HBO in wound healing

The rationale underlying HBO treatment in remediating chronic wounds is due to the requirement for O_2 in wound healing and the hypoxic nature of chronic wounds (Kulonen and Niinikoski, 1968). Although there are conflicting data in the available literature, there is clear anecdotal and clinical results-based evidence that suggest that HBO therapy is an effective means to remediate wounds (Duzgun *et al.*, 2008; Hammarlund and Sundberg, 1994; May and Hodgson, 2002; Abidia *et al*., 2003 and Kalani *et al*, 2002). The underlying method of action of HBO therapy lies in the theory that it increases systemic oxygenation. At ambient pressure and O_2 concentration, haemoglobin from red blood cells is essentially fully saturated and O_2 does not readily dissolve in plasma, thus maximal oxygenation of blood has occurred. However, under increased pressure and with greater total O_2 present, a

higher level of O_2 can be dissolved in the plasma, therefore a greater amount of O_2 is delivered to all tissues of the body. In this situation, sufficient tissue oxygenation can occur without significant contribution of haemoglobin-bound O_2 (Gill and Bell, 2004; Leach *et al.,* 1998). Although the therapeutic principles underpinning HBO treatment have not yet been fully elucidated, it is clear that further research and clinical trials investigating HBO as a wound healing therapy are required (O'Reilly *et al.,* 2011).

While the conditions (e.g. pressure, O_2 concentration, frequency and duration of administration) for systemic HBO therapy have not been thoroughly optimised on the basis of randomised clinical trials, there is strong evidence for HBOs ability to positively impact wound healing. Indeed, HBO therapy is an FDA-approved therapeutic apparatus used in wound clinics with an encouraging success rate (Gordillo and Sen, 2003). According to Gordillo *et al*. (2008), the most important effects of hyperbaric oxygenation in the treatment of hypoxic and ischaemic wounds, are stimulation of fibroblast proliferation and differentiation, which consequently leads to increased collagen formation and cross-linking. Additionally, HBO is hypothesised to augment neovascularisation (i.e. revascularisation of the wound bed) and stimulate leukocyte-induced microbial killing (Gordillo *et al*. 2008). Furthermore, Hollander *et al.* (2000) investigated HBO treatment on primary human keratinocyte cultures and found that while HBO had no effect on proliferation, it positively influenced keratinocyte differentiation.

Implications of oxygen in HBO treatments

Though the outlook of HBO treatment is quite positive in relation to wound healing, concerns still remain regarding the negative implications that may be associated with HBO (reviewed by Speit *et al.,* 2002). It has been suggested that reactive oxygen species and free radicals would have a detrimental impact on patients undergoing HBO therapy and this will counteract the benefits obtained from HBO therapy (Speit *et al.,* 2002). However, a study by Gröger *et al*. (2009) compared free radical (O_2.-) production and DNA damage and repair levels between combat swimmers and underwater demolition teams (who are constantly exposed to HBO conditions) and normal controls. The authors found that although DNA damage occurs after HBO treatment, this damage is repaired within 1 hour and there appears

to be no difference in damage repair rates between those who experienced long-term HBO exposure and the normal controls (Gröger *et al*., 2009).

It is also a commonly accepted view that biological oxidants primarily incite oxidative damage in body tissues (Sen, 2003). Generally, reactive oxygen species have been extensively studied as damaging by-products accidentally "leaked" from the mitochondrial respiratory chain, thus it has been difficult for some authors to conceive that these species may be beneficial to the body, and in fact may act as signalling messengers and regulators of gene transcription within the cell (Sen, 2000; Sen, 2003). A key factor tightly controlled by O_2 and hypoxia is hypoxia-inducible factor-1 (HIF-1). HIF-1 plays a central role in oxygen homeostasis through a redox-dependent mechanism (Zhang 2008). These authors believe that modulation of prolonged over-expression of HIF-1α and its target gene signal axis plays an important role in this response. The authors hypothesise that this occurs via HBO treatment and that HIF-1α expression is regulated through an increase in free-radical O_2 species production. Moreover, Zhang *et al*. (2008) found decreased VEGF expression in HBO-treated ischemic wound rat models along with decreased HIF-1α expression.

1.6 INVESTIGATING THE IMPACT OF HBO ON EPIDERMOGENESIS USING A HUMAN SKIN EQUIVALENT MODEL

The complex and multi-dimensional nature of human skin renders it impossible to fully model in standard 2D culture systems. In addition, there are inherent differences between human skin and animal skin. This means that animal models do not fully represent the biological and physiological processes that occur in humans. This is markedly obvious in the way rodents heal (by contraction), as opposed to humans (by re-epithelialisation, with minimal contraction). Human skin equivalent (HSE) models are a common substitute for animals when studying factors which may impact on skin and wound healing (Topping *et al.,* 2006; Kairuz *et al.,* 2007; Upton *et al.,* 2008; Xie *et al*., 2010; Xie *et al.,* 2011; Ponec *et al*., 2002)

HSE models have been extensively utilised to study skin biology, however, only two studies have been conducted in which HSE models have been utilised to study the effectiveness of HBO as a wound healing therapeutic. Initially,

Dimitrijevich *et al.* (1999) constructed a HSE from a fibroblast-containing collagen scaffold cultured at the air-liquid interface following keratinocyte seeding. HBO treatment on these HSEs was performed with 100% O_2 at 2 ATA. The results from these studies demonstrated that HBO increased epidermal thickness after a 10 day treatment period in comparison to HSEs treated with 100% O_2 at 1 ATA or air at 1 ATA (Dimitrijevich *et al.,* 1999). The other study conducted on HBO treatment on HSE models was performed within our research group by Kairuz *et al*. (2007). In this study, the HSE models were constructed by seeding keratinocytes onto a de-epidermised dermis (DED) followed by culture at the air-liquid interface. The authors found that HBO significantly increased the thickness of the cellular layer and stratum corneum following 3 and 5 days of culture when compared to controls (air, 1 ATA). Furthermore, immunohistochemical analysis demonstrated that HBO enhanced p63 expression and markers of epidermal differentiation. However, these images were not quantitatively analysed.

1.7 CONCLUDING REMARKS

From the literature review, it can be determined that the skin is a highly sophisticated organ of the body and when injured, induces a complex and multifaceted series of events to ensure the survival of the organism. However, there are occurrences when the normal wound healing processes fail and a chronic wound develops. Currently there are a range of wound healing techniques available and commonly implemented, including HBO treatment. HBO is based on the premise that a chronic wound is a perpetually hypoxic environment and that there is a lack in the resident vascular structure available to re-oxygenate the wound environment (Sen 2009). Furthermore, wound healing is a difficult area of study due to the lack of effective models available which effectively and accurately recapitulate human skin. This has led to the creation and implementation of HSE models as a laboratory practice utilised to investigate a plethora of skin-related areas. These include UV irradiation and melanoma, drug delivery and cutaneous permeation, and of pertinence to my project, HBO therapy.

1.8 PROJECT OUTLINE

The HSE model has widely been used within our laboratory as a biologically relevant tool to study skin (Topping *et al.,* 2006; Kairuz *et al.,* 2007; Upton *et al.,*

2008; Xie *et al.*, 2010; Xie *et al.*, 2011). To date, however, no studies have been conducted to compare the DED-HSE model to native human skin at both the transcriptional and translational level. Therefore, the first part of this thesis was directed at comparative studies to investigate the phenotypic similarities between the HSE model and native skin. After this gene microarray analysis was employed to investigate the global changes in gene expression that occur as the HSE model develops. Together these data validated the use of HSE as an appropriate model of human skin epidermogenesis.

Furthermore, based on this analysis of the literature it would appear that HBO may induce fundamental changes within the skin that stimulate the wound healing response. I proposed that this can be quantitatively measured via changes in relevant gene, and thus protein, expression levels. This is based on the premise that HBO therapy has a beneficial impact on wound healing. However, the evidence supporting HBO as a wound healing therapeutic is primarily anecdotal and the exact mechanisms of HBO treatment are yet to be elucidated. Since HSE models had previously been shown to be an effective tool for studying the effect of HBO therapy on the epidermal layer, I adopted this approach (Kairuz *et al.*, 2007). The second part of my PhD studies therefore were directed at building on the work conducted by Kairuz *et al.* (2007), by extending the length of the experiments to 9 days. In addition, I also investigated the effect that HBO treatment had at the molecular level, by investigating gene expression changes in the HSE model and validated the correlating protein expression levels.

1.8.1 Hypothesis

The two underlying hypotheses of this PhD project were that:

1. The HSE model currently employed in our laboratory is an appropriate model of native human skin and can therefore be used to characterise the epidermogenesis process.
2. HBO induces changes to the epidermal cell phenotype and morphology via alterations in expression of genes at the transcriptional and proteins at the translational levels.

1.8.2 Aims

These hypotheses were addressed through the following aims:

1. To generate HSE models and investigate the immunoreactivity and localisation of key epidermal markers in comparison to native human skin.
2. To examine the gene expression profile of the HSE model during epidermogenesis using gene microarray analysis.
3. To generate and subject human skin equivalent models to a daily clinical HBO treatment regime and investigate the immunoreactivity and localisation of key epidermal makers.
4. To examine the effect of HBO treatment on gene and protein expression in HSE models using gene microarrays, quantitative real time PCR and immunohistochemistry.

Chapter 2: Methods and Materials

2.1 INTRODUCTION

All general reagents and chemicals were of the highest quality and were obtained from reputable distributors. Suppliers of method-specific reagents are detailed in the appropriate methods sections that follow.

2.2 CULTURE OF 3T3 FIBROBLASTS

Murine 3T3 feeder cells (CCL-92; ATCC, Manasses, CA, USA) were expanded and maintained in Dulbecco's Modified Eagles Medium (DMEM; Invitrogen, Mulgrave, VIC, Australia) supplemented with 5 % foetal calf serum (FCS; Hyclone, Logan, UT, USA), 2 mM L - glutamine (Invitrogen) and 1% (*v/v*) Penicillin / Streptomycin (Invitrogen). The 3T3 fibroblasts were mitotically inactivated by gamma-irradiation (50 Grays) at the Australian Red Cross Blood Services (Brisbane, QLD, Australia) and seeded into T 75 culture flasks (Thermo Fisher Scientific, Rochester, NY, USA) at a density of 2.0×10^6 cells per flask for use as a feeder layer for primary keratinocyte expansion and culture at 37 °C in a 5% CO_2 atmosphere (standard conditions).

2.3 CULTURE OF PRIMARY HUMAN KERATINOCYTES

Keratinocytes were cultured in Full Greens (FG) medium which was comprised of a 3:1 mixture of DMEM (Invitrogen) and Hams F12 medium (Invitrogen) supplemented with 10% FCS (Hyclone), 1 μg / mL insulin (Sigma-Aldrich, Castle Hill, NSW, Australia), 10 ng / mL recombinant human epidermal growth factor (EGF; Invitrogen), 180 μM adenine (Sigma-Aldrich), 0.1 μg / mL cholera toxin (Sigma-Aldrich), 2 mM L-glutamine (Invitrogen), 0.4 μg / mL hydrocortisone (Sigma-Aldrich), 0.01% (*v/v*) Non Essential Amino Acids solution (NEAA; Invitrogen), 5 μg / mL transferrin (Sigma-Aldrich), 0.2 M triiodothyronine (Sigma-Aldrich) and 1% (*v/v*) penicillin / streptomycin solution (Invitrogen). During keratinocyte expansion, the culture medium was replaced every two to three days.

2.4 ISOLATION OF PRIMARY HUMAN KERATINOCYTE

Human skin was obtained from consenting adult donors undergoing elective cosmetic breast reduction or abdominoplasty surgeries conducted at the Princess Alexandra, St Andrews and Brisbane Private hospitals. Human ethics approval was obtained from each hospital, as well as the Institute of Health and Biomedical Innovation and the Queensland University of Technology (St Andrews Hospital; approval # 200 4/46, Princess Alexandra Hospital and Brisbane Private Hospital; approval # QUT 3865H).

Primary human keratinocytes were isolated and cultured using a modification of Rheinwald and Greens method (Rheinwald and Green, 1975). Briefly, small pieces of donor skin were incubated in an excess of 0.125% trypsin (Invitrogen) overnight at 4 °C to promote separation of the epidermis from the dermis. The epidermal layer was peeled off and discarded. The keratinocytes were collected by gentle scraping of the newly exposed dermal layer only, into an excess volume of FG medium. This was to select for cells closer to the basal, proliferative layer of the epidermis. The freshly isolated keratinocytes were then cultured in FG medium over approximately seven days on a feeder layer of lethally irradiated 3T3 fibroblasts, under standard conditions. Cultured primary human keratinocytes were harvested before reaching confluency through two incubation and collection steps using 0.05% trypsin / EDTA (Invitrogen), to lift the keratinocytes in multiple stages. The detached keratinocytes were collected into an excess of FG medium and pelleted via a centrifugation at 106 × *g* for 5 minutes. The cells were counted then resuspended at a dilution of 2×10^5 cells / mL.

2.5 PREPARATION OF THE DERMAL EQUIVALENT (DEEPIDERMIZED DERMIS)

The dermal equivalent was prepared following an adaptation of the protocol of Chakrabarty *et al.* (1999) as described by Dawson *et al.* (2006). In brief, donor skin was cut into approximately 1.4 cm^2 pieces and incubated in 1 M sodium chloride at 37 °C for 18 - 24 hours. The epidermis was removed using forceps, leaving behind the de-cellularized, de-epidermized dermis (DED). The DED underwent at least three subsequent washes in DMEM containing 1% (*v/v*) penicillin / streptomycin (Invitrogen) at 4 °C before being transferred into FG medium and incubated at 37 °C under standard conditions at least four hours before use.

2.6 GENERATION AND CULTURE OF HUMAN SKIN EQUIVALENT MODELS

The human skin equivalent models were prepared following the method of Topping *et al.*, (2006). Briefly, the DED pieces were placed papillary side up in a 24-well culture plate (Thermo Fischer Scientific, Waltham, MA, USA). Sterile, stainless-steel rings (6.7 mm diameter; Aix Scientifics, Aachen, Germany) with a silicone washer base were placed on top of the DED. Each ring received, 2.0×10^4 keratinocytes (P1), suspended in 100 µL of FG medium prior to the DEDs being incubated at 37 °C under standard conditions. After 48 hours of incubation, the rings were removed and the human skin equivalents (HSEs; defined as DED plus keratinocytes) were elevated to the air - liquid interface by transferring the composite to a stainless - steel grid in a 6-well culture plate (Thermo Fischer Scientific). The HSEs were maintained in FG medium under standard conditions for up to nine days, with daily replenishment of the culture medium (**Figure 2.1**). Furthermore, the culture medium was completely replaced once per week.

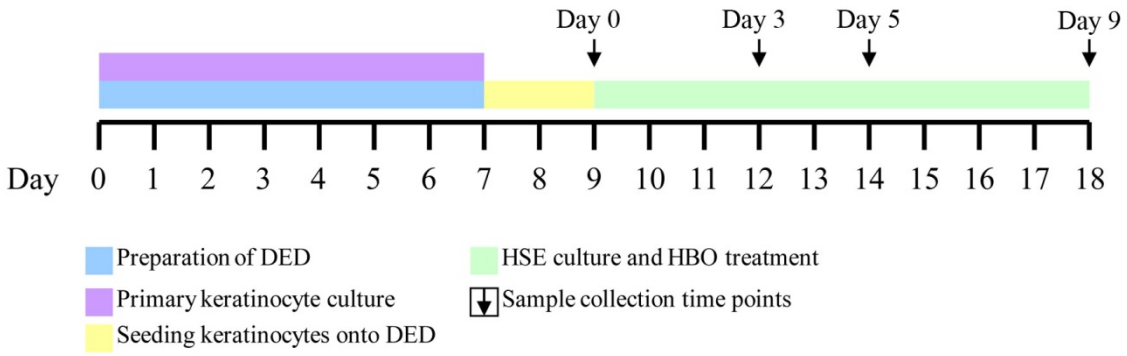

Figure 2.1 Timeline of HSE production and treatment
The experimental workflow of HSE model generation demonstrating that it takes at least 18 days from skin collection until the end of an experiment.

2.7 HYPERBARIC OXYGEN TREATMENT

HSEs were treated daily for nine consecutive days, in a temperature and humidity-controlled, custom-made, 7 L capacity, hyperbaric oxygen (HBO) chamber (Fink Engineering, Cheltenham, VIC, Australia). After placing the HSE samples in the HBO chamber, it was sealed and flushed for 90 seconds with 100% O_2 and subsequently pressurised to 2.4 atmospheres (ATA) over a period of 5 minutes. The pressure of the chamber was maintained for 90 minutes at 37 °C, after which the chamber was slowly depressurised over a further 5 minute period. Controls were concurrently treated for 90 minutes in a humidified box at 37 °C without injected CO_2. This was designed to act as a comparison between HBO treatment and non-treated (i.e. normobaric air) responses.

2.8 GROUPING OF HSE MODEL DATA

HSE models generated from eight individual skin donors were analysed throughout this Chapter. The skin samples were divided into two groups; group A which contained 3 skin samples and group B which contained 5 skin samples. Quantitative image analysis data generated from group A were pooled, for the reason that RNA were isolated and pooled from this group for the microarray gene analysis studies performed in section 2.12. The image data generated from group B were expressed as individual skin samples since RNA from these samples were not used for the microarray studies and therefore sufficient quantities were available without pooling. Furthermore, donor-matched native skin samples were collected for group B, whereas native skin controls from unrelated donors were used in group A. The breakdown of how the skin samples were sorted into groups A and B and which experiments were performed on each of the groups is outline in **Figure 2.2**.

2.9 MEASUREMENT OF THE PH OF HSE CULTURE MEDIUM

Duplicate pH measurements were taken of freshly prepared Full Greens medium and also of culture media before treatment and within 5 minutes after treatment protocols. In addition, the pH of culture media with or without the presence of the HSE was also measured.

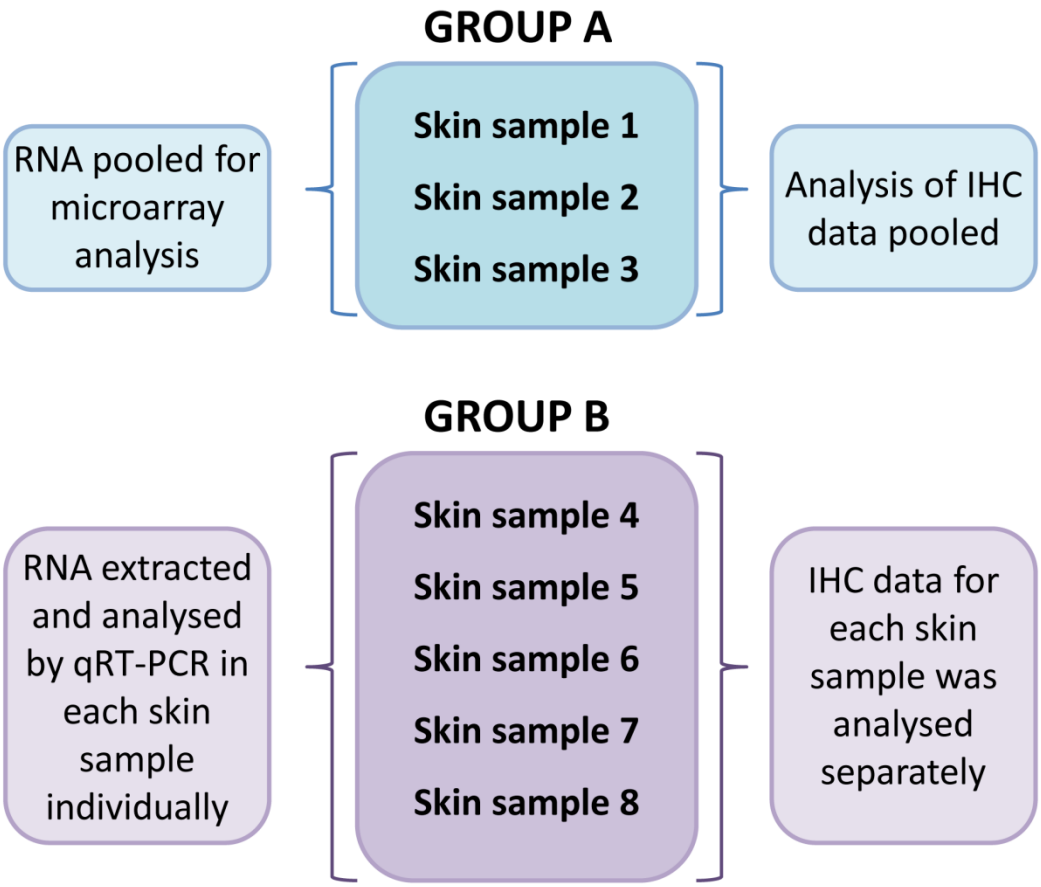

Figure 2.2 Grouping of the HSE models generated from skin samples 1 – 8
Within group A: n = 2 HSEs per time point and treatment group for each skin sample. Pooled data is obtained from duplicate HSE models for each of the three skin samples resulting in a total of n = 6 HSEs for each time point and treatment group. Within group B: n = 2 HSEs per time point and treatment group for each skin sample. Since the data is not pooled in group B, it remains n = 2 HSEs.

2.10 QUANTIFYING KERATINOCYTE OUTGROWTH OVER THE DED

Keratinocyte outgrowth was examined by measuring the increase in the surface area of the reconstructed epidermis. Samples were harvested after 0, 3, 5 and 9 days of culture at the air-liquid interface (n = 2 per time point, per skin sample) and stained with 3-(4,5-dimethylthiazol-2-yl)-2,5-diphenyltetraoliumbromide (MTT; Sigma-Aldrich) to visualise the epidermis macroscopically. This involved submerging the samples in a sufficient volume of 0.5 mg / mL MTT reagent and incubating the samples at 37 °C for 90 minutes. The stained, reconstructed epidermis was subsequently photographed (Nikon Coolpix 4500, Maxwell Optical, Lidcombe, NSW, Australia) and the mean area (mm^2) of lateral outgrowth was quantified (from two independent measurements per skin sample) using ImageJ software.

2.11 GENERAL HISTOLOGY

Following MTT analysis, the samples were trimmed down to remove excess unstained DED (**Figure 2.3**). The HSEs were then fixed in 10% formalin and dehydrated in a graded ethanol series, consisting of 100%, 90% and 70% ethanol. The samples were subsequently embedded in paraffin wax and cut using a microtome (Leica Microsystems, North Ryde, Australia) to yield 5 µm-thick cross sections. The sections were then stained with haematoxylin and eosin (H&E) for analysis of general morphology and also quantitation of epidermal thickness as described in section 2.11.2.

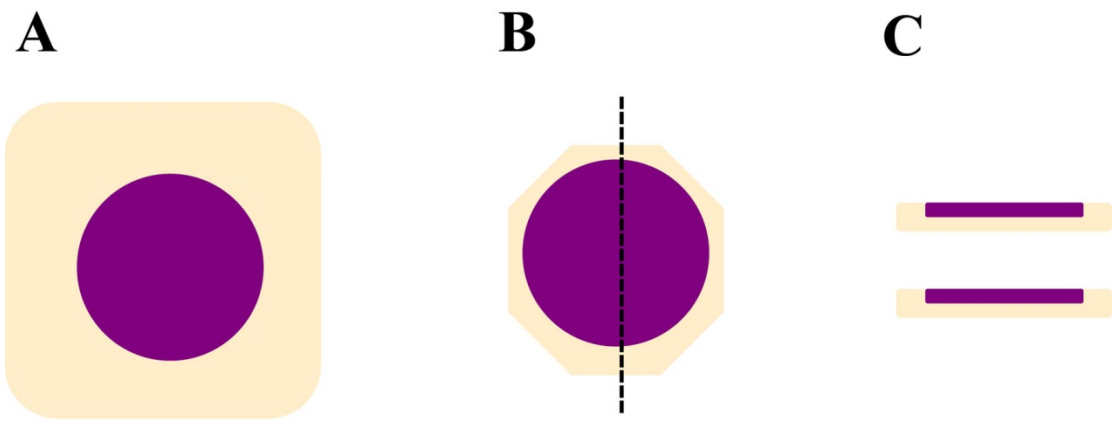

Figure 2.3 Preparing MTT-HSEs for histology
Schematic overview depicting (**A**) the MTT stained HSE, with the purple area representing the cell-containing region. (**B**) The HSE is trimmed to remove excess DED and then sectioned through the middle to create two equivalent halves. (**C**) A side-view of the HSE representing how the HSE will be embedded for further histological analysis.

2.11.1 Immunohistochemistry analysis

Additional 5 µm thick sections of the paraffin wax embedded HSEs were cut for further immunohistochemical analysis to validate keratinocyte marker expression. The sections were deparaffinised in Xylene and rehydrated in a graded ethanol series (2 × 100% ethanol, followed by 90% and 70% ethanol) in preparation for the analysis. The sections were then pre-treated using heat-mediated antigen retrieval methods specific for each antibody. Antigen retrieval was performed in a decloaking chamber (Biocare Medical, Pike Lane, USA) by heating the sections at a specified temperature and duration (also outlined in *Table 2.1* and *Table 2.2*) then allowing

them to cool to room temperature for 20 minutes in fresh phosphate buffered saline (PBS).

After antigen retrieval, the sections were blocked with peroxidazed 1 (Biocare Medical), a hydrogen peroxide-based reagent used to quench background peroxidase activity, and blocked using the background sniper (Biocare Medical), a serum-free, recombinant protein-based universal blocking reagent. The sections were then incubated with primary antibody diluted in da vinci green diluent (Biocare Medical) as indicated in *Table 2.1* and *Table 2.2*. This was followed by 15 minutes incubation at room temperature with a mouse probe, a mouse-specific secondary antibody, then 15 minutes incubation at room temperature with horseradish peroxidise (HRP) polymer, both from the Mach 4 Universal-Polymer kit (Biocare Medical). Rabbit primary antibodies were incubated only with the HRP polymer for 45 minutes at room temperature. Peroxidase activity was detected with diaminobenzidine (DAB) from either the DAKO Envision kit (Dakocytomation, Botany, NSW, Australia) or the Betazoid DAB detection kit (Biocare Medical) according to the manufacturer's instructions, with equivalent results obtained from both kits. All sections were counterstained with haematoxylin and Scotts Bluing reagent (Kinetic, Nambour, Australia) and examined by light microscopy. Immunostaining in the absence of the primary antibody was used as a negative control, while native skin, with an exception for keratin 16, acted as a positive control. The thickness of the DAB-positive regions in each section was determined using the same method described in section 2.11.2.

Table 2.1 Details of primary antibodies used for immunohistochemical analysis: characterisation

Antibody	Source	Antigen Retrieval Method	Incubation proto	Dilution
Keratin 1[c]	Novus biologicals, Littleton, USA	97 ℃ / 15 minutes - EDTA Buffer, pH=9.0	1 hour, 37 ℃	1:500
Keratin16[c]	Novus biologicals,	90 ℃ / 45 minutes - EDTA Buffer, pH=9.0	overnight, 4 ℃	1:100
Loricrin[a]	Abcam, Cambridge, USA	97 ℃ / 15 minutes - EDTA Buffer, pH=9.0	1 hour, 37 ℃	1:1000
p63[c]	RDI, Research Diagnostics, Concord, USA	94 ℃ / 4 minutes - Sodium Citrate Buffer, pH=6.0	1 hour, 37 ℃	1:2000
Ki-67[c]	Dako, Botany, NSW, Australia	90 ℃ / 45 minutes - EDTA Buffer, pH=9.0	1 hour, 37 ℃	1:100

List of antibodies (IgG) used for immunohistochemistry staining of HSE tissue sections. [a]Rabbit polyclonal antibody. [b]Mouse polyclonal antibody, [c] mouse monoclonal antibody.

Table 2.2 Details of primary antibodies used for immunohistochemical analysis: validation

Antibody	Source	Antigen Retrieval Method	Incubation Protocol	Dilution
Metallothionein [c]	Invitrogen, Mulgrave, VIC, Australia	90 ℃ / 45 minutes - EDTA Buffer, pH=9.0	1 hour, 37 ℃	1:200
Kallikrein 1 [b]	Novus biologicals, Littleton, USA	90 ℃ / 45 minutes - EDTA Buffer, pH=9.0?	overnight, 4 ℃	1:500
Kallikrein 7 [a]	Novus biologicals, Littleton, USA	90 ℃ / 45 minutes - Sodium Citrate Buffer, pH=6.0	75 minutes, 37 ℃	1:400
Early Growth Response 1 [a]	Cell Signaling Technology, Danvers, USA	90 ℃ / 45 minutes - EDTA Buffer, pH=9.0	1 hour, 37 ℃	1:300
CDCP1 [a]	Cell Signaling Technology, Danvers, USA	90 ℃ / 35 minutes - EDTA Buffer, pH=9.0	75 minutes, 37 ℃	1:300

List of antibodies (IgG) used for immunohistochemistry staining of HSE tissue sections. [a]Rabbit polyclonal antibody. [b]Mouse polyclonal antibody, [c] mouse monoclonal antibody.

2.11.2 Image data analysis

Image data analysis was performed on images obtained from both haematoxylin and eosin (H&E) and immunohistochemistry experimental results. For all samples, image analysis was determined from four consecutive images per section (for the group A skin samples: 1 section per HSE, therefore 4 images per individual HSE replicate and for the group B skin samples and native skin: 2 sections per HSE, therefore 8 images per individual HSE replicate) acquired in the centre of the HSE at 200 X magnification using an Olympus BX41 microscope (Olympus, Q-Imaging) with a mounted digital camera (MicroPublisher 3.3 RTV, Olympus, Q-Imaging). Refer to **Figure 2.4** for a visual representation. All image data analysis was performed using open source ImageJ software (available at: http://rsbweb.nih.gov/ij/) with the MacBiophotonics Plugins (available at: http://www.macbiophotonics.ca/imagej/).

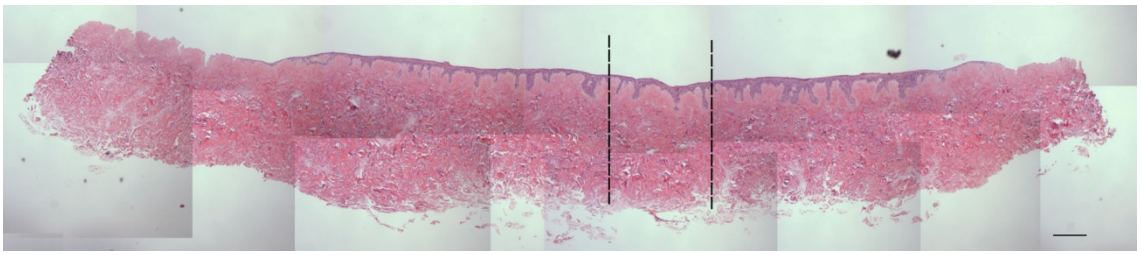

Figure 2.4 Acquisition of consecutive images for epidermal thickness quantification
Demonstration of an entire H&E stained HSE section and the approximate middle region of the HSE in which the four consecutive images are captured for subsequent epidermal thickness quantification. The selected region represents a region approximately 1420 µm - wide, equivalent to four consecutive images. The scale bar represents 500 µm.

Quantifying the epidermal thickness

The average thicknesses (µm) of both the cellular layer and stratum corneum of the HSEs were measured from H&E sections. Images were opened in ImageJ and either the colour deconvolution tool or manual separation of the image was used to create two additional files to the original, containing only the stratum corneum or cellular layer for each image. From this point, both images were treated the same. The separated H&E image was converted to 8 - bit colour (grey-scale), the threshold tool was then used to convert the image to binary (black and white), with the black pixels representative of the HSE structure (**Figure 2.5**). To determine a complete picture of the HSE architecture, the histogram tool was used to determine the total

number of black pixels present within the binary image. This value was then imported into an Excel spreadsheet for conversion to the epidermal thickness data. Each image obtained from the Olympus microscope was captured and saved as a standard .TIFF file with a width of 2048 pixels and a height of 1536 pixels, in which the image scaling was at 5.7866 pixels per µm. Therefore, the total number of pixels obtained from the above method was divided by 2048 (the width of the image in pixels) to obtain the average number of pixels per single pixel - wide column within the image. To convert this value into a measurable amount (µm) the value was then divided by 5.7866, resulting in the average thickness of either the cellular layer or the stratum corneum for each image.

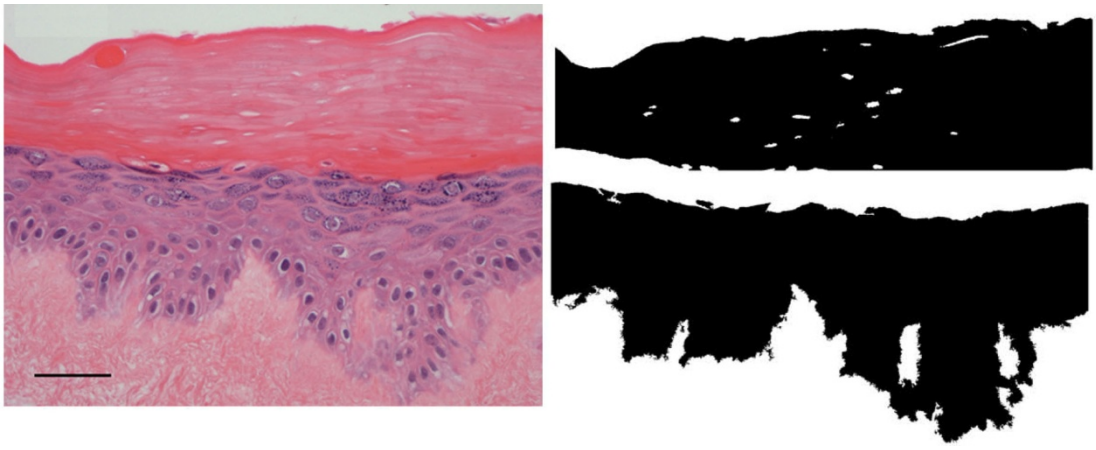

Figure 2.5 Creating a binary image from a H&E section
The image is opened in ImageJ and the stratum corneum (dark pink region) and the cellular layer (purple region) are converted to binary respectively. This figure is a representative image depicting how the pixel data results are obtained. The scale bar represents 50 µm.

Immunohistochemistry image data analysis

The thickness of Keratin 1, Keratin 16, Loricrin, Kallikrein 7, Kallikrein 1, Metallothionein and CDCP1 layers in the sections were determined using the same method described in section 2.11.2, with slight modifications. In addition, only one additional image analysis file was created per original immunohistochemistry image. The immunohistochemistry image file was opened in ImageJ and the colour balance tool was used to remove all other colour from the image, leaving only the DAB - stained sections visible. The DAB areas were then converted to 8 - bit, then binary and the total numbers of black pixels were measured. Again, the data were imported into an Excel sheet and converted to µm as described above. The correlating value was indicative of the thickness of each particular proteins expression within the HSE model.

In addition, the numbers of p63, ki-67 and early growth response 1 - positive nuclei were determined using ImageJ software. The immunohistochemical image was opened and the cell counter tool was used to manually determine the number of positively-stained nuclei within each image. The data was then imported into an excel sheet and the values averaged to determine the mean number of positive nuclei per 353.92 μm histological section within the centre of the HSE.

Final data analysis and statistics

As outlined in section 2.8 and visualised in **Figure 2.2**, the HSE models were separated into either group A or group B. All data generated from the group A skin samples was pooled, whereas data generated from the group B skin samples remained separate. All image analysis data is expressed as mean ± standard deviation. Tukey's post hoc analysis following a one-way ANOVA was performed with a p value < 0.05 accepted as significant on all data presented in this thesis.

2.12 MICROARRAY ANALYSIS OF DIFFERENTIAL GENE EXPRESSION

2.12.1 Extraction of total RNA from HSE models

Total RNA was isolated from the epithelial layer of HSE models after exposure to either HBO or control treatment as described in section 2.7. This was achieved following completion of each time point by immediately placing the HSE model in a petri dish with 1 mL Trizol (Invitrogen) and scraping the epidermal layer off the DED using a scalpel blade. The excised epidermal sheet was then homogenised in the Trizol solution by repeated passing through a 26 -, 21 -, and subsequently a 19 - gauge needle with a 1 mL syringe. Once homogenised, the HSE epidermal samples were stored in the Trizol at -80 °C until further analysis could be performed. To obtain replicate samples, the whole HBO and control treatment protocol and RNA extraction were repeated in three separate skin samples. The RNA from each skin sample was extracted and purified separately as described below.

Total RNA isolation - Part 1 (RNA separation and precipitation)

RNA extraction from Trizol involved the addition of 200 μL of chloroform (Sigma-Aldrich) to induce the separation of the solution into an upper aqueous phase containing RNA and a lower organic phase containing protein, both of which were separated by a DNA-containing interphase. The solution was centrifuged at 12,000 × *g* for 15 minutes at 4 °C to enhance phase separation and the upper aqueous layer

was transferred to a fresh eppendorf tube. RNA was precipitated by the addition of 500 µL isopropanol (Sigma-Aldrich) containing 7.5 M ammonium acetate and 1 µg / mL linear acrylamide (Applied Biosystems, Scoresby, VIC, Australia) at room temperature for 15 minutes. The precipitated RNA was pelleted by centrifugation for 15 minutes at 4 °C prior to a final 70% ethanol wash step to enhance RNA yield. The resulting RNA pellet was air dried and then resuspended in RNase - free water.

To assess the quality of the extracted RNA, 300 ng of each sample was separated on a 1.5% agarose / tris-acetate-EDTA (TAE) gel and electrophoresed for 30 minutes at 120 Volts. The quality of the RNA was determined with gel analysis by the presence of two distinct 28S rRNA and 18S rRNA bands, with the former at least twice as intense as the latter. To quantify the RNA, a NanoDrop spectrophotometer (Thermo Scientific, Wilmington, DE, USA) was employed. Absorbance ratio measurements of A_{260} / A_{280} and A_{260} / A_{230} were also recorded to analyse the level of purity, as A_{260} / A_{280} and A_{260} / A_{230} ratios of at least 1.8 were necessary for downstream applications.

Total RNA isolation – Part 2 (DNase treatment and clean-up)

To ensure the RNA samples were pure, any residual contaminating DNA was removed by DNase treatment. The RNA samples describe above were treated with 10 U / mL rDNase (Ambion) in a final volume of 200 µL and incubated at 37 °C for 30 minutes. DNase was then inactivated by the addition of an equal volume of phenol:chloroform:isoamyl alcohol (PCI; ratio 25 : 24 : 1), mixed by inversion and allowed to stand at room temperature until phase separation occurred (~ 5 minutes). The tubes were then centrifuged at room temperature for 5 minutes (~ 18,000 × g) and the aqueous phase containing the RNA was transferred to new tubes. Additionally, 200 µL volume of chloroform was then added to each tube and centrifuged at 18,000 × g for 5 minutes at room temperature. The aqueous phase was then transferred into a new tube and the RNA was precipitated with 1 mL isopropanol and 50 µL of 7.5 M ammonium acetate at room temperature for 15 minutes, followed by centrifugation for 15 minutes at 4 °C. The supernatant was carefully poured off and the pellet was washed briefly with ice cold 70% Ethanol. The RNA samples were then centrifuged at ~ 10,000 × g) at 4 °C for 10 minutes, after which the ethanol was aspirated off and the pellets were allowed to air dry. The RNA pellets were then resuspended in 20 µL of sterile, RNase - free H_2O and 2 µL

of the resulting solution was used to assess RNA quality and quantity as described in Part-1.

One microgram of total RNA was necessary for the gene microarray analysis, however, in RNA samples from early time points (days 0 and 3), insufficient amounts of RNA could be extracted from the HSE model. At this point, I decided to pool the RNA from the three separate skin samples to obtain sufficient amounts. The extracted RNA was diluted to 50 ng / µL. To form a total concentration of 1 µg in a total volume of approximately 20 µL, 6.7 µL of diluted RNA from each of the group A skin samples was combined. The pooled RNA from the three skin samples was sent to the microarray facility at the Institute for Molecular Biosciences at the University of Queensland. The gene microarray procedure and data collection was performed by Dr Katia Nones.

2.12.2 Microarray analysis

To determine the gene expression profiles of the HSE models with and without HBO treatment, the Illumina whole genome (HT-12 v 3.0) BeadChip system (Illumina Inc., San Diego, CA, USA) was utilised. The microarray analysis was performed by Dr Katia Nones at the Special Research Facility Microarray Service at the University of Queensland Institute for Molecular Biosciences. The outcomes were read using the Illumina Beadstation 500, with the resulting data processed using Illumina Genome Analyser system software, which converted the raw data into intensity scores for downstream analysis. At this point, the data were returned to me for analysis. It is important to note that since the RNA was pooled from three separate skin samples the below outlines procedures differ from standard microarray analysis.

2.12.3 Data analysis

All microarray data analysis was performed at the University of Western Australia with generous help and guidance received from Daniel Haustead.

The Genespring formatted files containing the raw array data were imported into GeneSpring GX 10.0 and a quantile normalisation was used. Since these data were obtained using pooled samples, there were no biological replicates present, and therefore it was not necessary to average over replicates as would usually be required

for microarray data analysis. The data were pre-processed using the baseline to median baseline transformation tool. Standard filtering options were selected in which an upper cut off of 100 and lower cut off of 20 were selected when analysing raw data. This process filtered out approximately 600 raw data points from the results.

The data were run through a flag cell check. The stringency was set to a value of 1 out of 7, which is less stringent than general microarray analysis, but it was incorporated due to the initial sample pooling. Data signal strength is tagged by GeneSpring as either 'present', 'marginal' or 'absent'. For data to be deemed 'present', on the array it must come up as positive, significant, uniform, above background, not saturated and not an outlier of the general population. The flag cell check filtered out data that was tagged as 'absent' (no signal for that array above the background level), but data that was tagged as 'marginal' was likely to be included due to the low stringency. Furthermore, no false discovery testing or analysis was performed because there were no p values associated with this data. In addition, statistical analysis could not be performed since there were no biological replicates. To determine changes that occurred between sample pairs, the fold-change was manually investigated on a gene-to-gene basis, rather than filtering the data by a set fold-change threshold cut off. The resulting data were exported, all in one document, into an Excel spreadsheet. The resulting list of genes and their fold-change values were used as the basis of further investigation. Rather than performing hierarchical clustering of the data, it was decided to manually sort through the list and select genes on the basis of their relevance to wound healing and epidermogenesis and investigate their expression profile over the days, comparing between HBO- and control-treated samples. This is further discussed in Chapter 6.

2.12.4 Visualisation of IPA Ontology Analysis Results

IPA ontology analysis results were visualised using Cytoscape® v2.8.2 (Smoot, *et al.*, 2011). Tabulated IPA data were manually formatted into tab-delimited binary interactions and imported into Cytoscape® using the 'Network from table' import option. Node attributes, including ontology over-representation *p*-values, ontology gene frequency, gene / ontology identity and gene regulation were imported in a single tab-delimited file for each network. These attribute data were visually mapped onto networks as node colour, node size, node shape and node boarder

colour (genes only), respectively. Nodes were arranged using the JGraph radial tree layout and exported as jpeg images.

2.13 VALIDATION OF DIFFERENTIAL GENE EXPRESSION USING QUANTITATIVE REAL-TIME RT-PCR (QRT-PCR)

2.13.1 Standard PCR conditions

All PCR reactions were performed using the Platinum Taq PCR kit (Invitrogen). The standard reaction conditions included: 1U Platinum Taq, 1.5 mM $MgCl_2$, 0.2 mM dNTPs, 0.2 µM each of forward and reverse primers and 1 µL cDNA template in a total volume of 25 µL. PCR reactions were then run on a MJ Research Thermocycler (Geneworks, Hindmarsh, SA, Australia) with the following cycling conditions: 94 °C for an initial 5 minutes, followed by 35 cycles of 94 °C for 45 seconds, 60 °C for 1 minute and 72 °C for 90 seconds. Amplification of PCR products of the correct size were then confirmed by agarose gel electrophoresis and ethidium bromide / UV visualisation.

2.13.2 Primer Design

All primers, unless otherwise specified, were designed using a combination of Primer-BLAST (available at: http://www.ncbi.nlm.nih.gov/tools/primer-blast/) and OligoPerfect™ designer (Invitrogen). The primer design parameters were adjusted to define acceptable primer sets which included: minimum primer melting temperature (T_m) of 57 °C, maximum of 63 °C and optimal T_m of 60 °C, with no more than 2 °C difference in T_m between primers; GC content of approximately 50%; primer length between 18 - 22 bases; minimum amplicon T_m of 75 °C and maximum of 85 °C; with an amplicon length between 80 - 200 base pairs.

2.13.3 Reverse transcription (RT) for qRT-PCR

cDNA synthesis

First strand cDNA synthesis was performed with the Superscript III first - strand cDNA synthesis kit (Invitrogen) to reverse-transcribe total RNA in 20 µL reactions. Each reaction mixture contained 700 ng of total RNA, 50 ng random hexamers and 10 mM dNTP mix and was then diluted to 10 µL with water. This was then incubated at 65° C for 5 minutes, followed by incubation at room temperature for 5 minutes before proceeding. First strand synthesis was carried out using 200 U SuperScript III reverse transcriptase (Invitrogen), 10 mM dithiothreitol (DTT), 0.5

mM dNTPs, 1 X first strand buffer (250 mM Tris - Cl pH 8.3, 375 mM KCl, 15 mM $MgCl_2$) to a final volume of 20 µL. Each reaction was incubated at 25° C for 10 minutes, 50 °C for 50 minutes and 85 °C for 5 minutes to inactivate the SuperScript III enzyme. The resulting cDNA samples were then either stored at -80 °C or diluted to either 2 ng / µL or 20 ng / µL (as indicated in *Table 2.3*) with sterile nuclease free water for qRT - PCR analysis.

PCR and amplicon purification

PCR was performed as described in section 2.12.1 using Platinum Taq High Fidelity DNA Polymerase PCR kit (Invitrogen). The standard reaction conditions utilised 50 mM $MgSO_4$, 1 U Platinum Taq, 10 mM dNTPs and sequence specific primers at a concentration of 1.25 µM for each transcript to be analysed by qRT-PCR. PCR reactions were run on a MT Research Thermocycler (Geneworks) with the following conditions: 94 °C for 5 min, followed by 35 cycles of 94 °C for 45 seconds, 60 °C for 1 minute, 72 °C for 90 seconds, followed by 72 °C for 10 minutes before samples were finally held at 4 °C. Note, some primers required the 60 °C step to be increased to 62 °C and this is indicated in *Table 2.3*.

The resulting PCR amplicons were electrophoresed on 1.5% agarose gels and visualized with ethidium bromide staining under UV illumination. The resulting band for each amplicon was excised from the agarose gel using a sterile scalpel blade and was subsequently purified from the agarose using a MinElute gel extraction kit (Qiagen, Doncaster, Vic, Australia). The PCR products were then quantified by UV Spectrophotometry at 260 nm and the yields converted to absolute cDNA copy numbers. cDNA copy numbers were determined based on 1 DNA base pair having a molecular mass of 660 g / n and calculated per µL of cDNA sample.

qRT-PCR

qRT - PCR was used to validate microarray expression data by measuring absolute expression levels of selected genes of interest. Primer - BLAST and OligoPerfect™ were used to design all primers used in qRT - PCR as outlined in section 2.13.2. Absolute quantification was carried out using standard curves covering eight logs of amplicon copy number, generated by 10-fold serial dilutions of purified target PCR amplicons. All reactions were performed in triplicate in 20 µL volumes in a 96-well format, using SYBR green (Applied Biosystems) and an ABI Prism 7300 Sequence Detection System (Applied Biosystems). Reactions contained

1 X SYBR - green PCR mix, 0.25 μM of each forward and reverse primers and either 10 ng or 100 ng of the cDNA dilutions (as indicated in *Table 2.3*). PCR amplification followed a two - step cycling protocol with an initial 10 minute denaturation at 95 °C, with 40 cycles of 95 °C for 15 seconds and 60 °C for 1 minute. All RT-PCR reactions included a post - amplification melt curve analysis to determine the melting temperature (Tm) of the amplified PCR product, indicating amplification of the correct sequence. Real - time curves were analysed with ABI Sequence Detection System software version 1.2 (Applied Biosystems) using the automatic option for baseline and threshold values. The software determines the PCR cycle at which each reaction reached its log - linear phase and is directly proportional to the amount of starting cDNA transcript. The cDNA copy number for each reaction was then calculated by direct comparison to the known standards for each gene, which are run concomitantly. Target gene expression for each sample was then normalised to 18S rRNA, in addition to normalisation to the day 0 time point.

2.14 STATISTICAL ANALYSIS

The real time PCR data was pooled from multiple experiments with each treatment in triplicate wells in each experiment. Tukey's post hoc analysis following a one-way ANOVA was performed with a p value < 0.05 accepted as significant on all data, unless otherwise specified.

Table 2.3 Summary of primers used for qRT-PCR gene expression analysis

Gene	Symbol	Primer	
Metallothionein 1G[b]	KLK7	F	CTTCTCGCTTGGGAACTCTA
		R	AGGGGTCAAGATTGTAGCAAA
Metallothionein 2A	MT2A	F	CGCGTGCAACCTGTCCCGA
		R	GCAGCAGCTTTTCTTGCAGGAGGT
S100A8	S100A8	F	TCAGAAGACCTGGTGGGGCAAGTC
		R	TCTTCAGGTCATCCCTGTAGACGGC
Kallikrein-related peptidase 7	KLK7	F	CGCCCCATGTGCAAGAGGCT
		R	TTGCAGTGGGCGGCAGTGAG
Kallikrein-related peptidase 1	KLK1	F	AGACACCTGTGTGGGTGATTCAGGG
		R	GGGGTGCCACAAGGGACGTAGC
Integrin alpha v	ITGAV	F	GTGGAAGGAGGGCAGGTCCTCA
		R	GGTACAATGGGGCACAGGCCAAAA
Grainyhead-like 3	GRHL3	F	GATGACCCACAGGAGTCGAT
		R	GAGCCCAGGGTGTATTCAAA
CDCP1	CDCP1	F	GTTCAAGCTGGAGGACAAGC
		R	CATGGCTCGCTCATTACTCA
Early Growth response 1	EGR1	F	GACCGCAGAGTCTTTTCCTG
		R	AGCGGCCAGTATAGGTGATG
Early Growth response 3	EGR3	F	CAATCTGTACCCCGAGGAGA
		R	GGAAGGAGCCGGAGTAAGAG
18S rRNA [a]	RN18S1	F	TTCGGAACTGAGGCCATGAT
		R	CGAACCTCCGACTTTCGTTC

[a] – 0.1ng cDNA used. [b] – 100ng cDNA used. For all others, 10 ng of cDNA was used per well for qRT-PCR.

Chapter 3: Histological characterisation of the HSE model and its comparison to native human skin

3.1 INTRODUCTION

Skin is a complex and multi-dimensional tissue which is impossible to fully model in conventional 2D culture settings. Currently, rodents (mice and rats) or pigs are used to study wound healing therapeutics or to investigate the biological effects of treatments on skin (Amendt *et al.,* 2002; Davis *et al.,* 2007; Fries *et al.,* 2005). However, rodents heal by a process of wound contraction and their skin is covered by fur. Furthermore, rodents are loose-skinned whereas humans have "fixed" skin that is attached to the underlying musculature. In addition, rodents have a much thinner epidermis compared to humans. Considering the sparse distribution of hair on human skin and the fact that humans heal by re-epithelialisation rather than contraction, rodents are a suboptimal model for studying wound healing. Conversely, pigs are more similar to humans in regards to their dermal-epidermal composition ratio (the thickness of the epidermis in relation to the dermis is similar in pigs and humans) and the presence of rete ridges in the skin. Furthermore, the presence of subcutaneous adipose tissue, the distribution of blood vessels within the skin and also the rate of epidermal turnover and stratum corneum composition is similar between humans and pigs (Sullivan *et al.,* 2001; Vardaxis *et al.,* 1997).

Although pigs are a relevant model for studying human wound healing, they are notoriously difficult to handle, expensive and require specialised housing and infrastructure. In addition, there are ethical issues concerning the use of animals for scientific research as many of these experiments cause pain to the animal and decrease their quality of life. Indeed, as of 2009 the European Union has implemented a ban on testing of products for cosmetic or consumer use on animals, including product's constituents (76/768/EEC, February, 2003). The development of skin equivalent models from donated, surgical discarded human skin therefore, has become an important area of research in terms of developing alternatives to animal testing.

3.1.1 Human skin equivalent models available

There is a vast array of human skin equivalent (HSE) models available for use in research, including models grown on de-epidermized dermis (DED; Chakrabarty *et al.*, 1999), models utilising collagen matrices as dermal substrates (Topol *et al.*, 1986) or commercially available, acellular dermal substitutes such as Alloderm® (LifeCell Corporation, NJ, USA) or Integra® (Integra Life Sciences Holding Co., NJ, USA) to name a few (Bannasch *et al.*, 2007 and Kremer *et al.*, 2000). The basic models either contain keratinocytes only, or incorporate both keratinocytes and fibroblasts. However, more complex HSE models have been developed as discussed below.

3.1.2 Complex HSE models

Pigmentation: incorporating melanocytes into HSE

HSE models that incorporate melanocytes have long been utilised to study the effects of UV irradiation on melanin production (Topol *et al.*, 1986 and Archambrault *et al.*, 1995). This began when Topol *et al.* (1986) created a HSE model containing fibroblasts, keratinocytes and melanocytes and observed transfer of pigmentation from the melanocytes to the surrounding keratinocytes. Furthermore, it was demonstrated that UV irradiation increased the size and number of melanosomes within the keratinocytes (Topol *et al.*, 1986). In addition to increased melanin expression following UV-irradiation, Archambrault *et al.* (1995) demonstrated that melanocytes in a pigmented HSE model had increased survival as compared to monolayer melanocyte culture. Moreover, Liu *et al.* (2011) created an epidermis-only HSE by co-culturing melanocytes and keratinocytes on a membrane prior to implantation onto the back of a mouse and found that the pigment was retained following tissue integration. The authors hypothesised that a pigmented HSE could be used for tissue engineering of pigmented skin in the future (Liu *et al.*, 2011).

Incorporating endothelial cells

A HSE model containing endothelial cells would be necessary to determine the effects of angiogenic and angiostatic effectors on the skin microvasculature. A dermal-only model was created by Hudon *et al.* (2003), in which human umbilical vein-isolated endothelial cells were seeded into a fibroblast-populated collagen sponge. Capillary-like tube formation was observed throughout the dermal model and the authors hypothesised that fibroblast-endothelial cell interactions are key for tube

formation (Hudon *et al.*, 2003). Given it has been demonstrated that interactions between ECM and endothelial cells are necessary for tube formation (Berthod *et al.*, 2006), the authors supplemented the culture media with ascorbic acid (vitamin c), a known stimulator of fibroblast derived ECM production (Hata and Senoo, 1989). This supplementation may have enhanced ECM production and facilitated tube formation.

Incorporating immune cells

The skin contains an innate immune system in the form of immunogenic Langerhan's cells which can stimulate an inflammatory response. Previously, immune-stimulating effects within the skin could not be investigated due to a lack of a relevant model. However, Bechetoille *et al*. (2007) created a HSE model using a fibroblast-populated dermal substrate seeded with keratinocytes and immune cells (Langerhan's and dendritic cells) which were isolated and differentiated from blood-derived monocytes. The immunocompetent HSEs were UV-treated which induced increased secretion of pro-inflammatory cytokines and migration of Langerhan's and dendritic cells (Bechetoille *et al*., 2007). A similar approach was taken by Laubach *et al.* (2011), who created a fibroblast-keratinocyte HSE model, also incorporating a skin immune system. To create the immune cells, the monocytic human acute myeloid leukemia cell line, MUTZ-3, was differentiated into Langerhan's-like cells (Laubach *et al.*, 2011). However, the authors did not test the effectiveness of the Langerhan's cells in response to immunogenic stimuli.

Inclusion of hair follicles

Hair follicles affect the permeability of skin, therefore development of a HSE model containing hair follicles is important for investigating the absorption of topical agents. In general, there are two main routes of skin permeation, trans-epidermal (where the agent must cross through the stratum corneum) or trans-follicular (where the agent bypasses the stratum corneum and penetrates skin through the hair follicle, directly to the dermis). This was highlighted by Hueber *et al.* (1994) who demonstrated that topically applied steroids absorbed more quickly in normal skin (via trans-follicular penetration) as compared to scarred skin, which lacks hair follicles (via trans-epidermal penetration). Thus, a HSE model which incorporated hair follicles, in addition to a fibroblast-populated, scaffold-free (fibroblasts self generated) dermis and keratinocyte epidermis, was developed (Michel *et al.*, 1999). They then demonstrated increased hydrocortisone absorption in the follicle-containing

HSE than was observed in a HSE without follicles; thus demonstrating the importance of utilising a biologically relevant HSE model for the type of skin analysis to be performed.

The DED skin model

A human skin equivalent model is currently used within our laboratory to investigate novel wound healing therapeutics in a 3D environment which mimics native skin. This HSE model is created utilising components obtained from human skin donated by individuals undergoing elective cosmetic surgeries using a method adapted from Chakrabarty *et al.* (1999). The model is generated by isolating primary human keratinocytes from the donor skin, and expanding the cells for a week in two-dimensional tissue culture. The keratinocytes are subsequently grown at the air-liquid interface on a DED, encouraging the normal stratification and differentiation of the epidermis to form a structure that is histologically similar to native skin.

This construct allows the study of epidermal generation alone, in the absence of cross-talk between epidermal keratinocytes and dermal fibroblasts. Within our research group, the HSE model has been utilised to investigate epidermal healing following burn injury (Topping *et al.*, 2006), the effect of HBO on epidermal generation (Kairuz *et al.*, 2007), and also the effect of vitronectin:growth factor interactions on partial thickness, full thickness and burn wounds (Upton *et al.*, 2008; Xie *et al.*, 2010 and Xie *et al.*, 2011). Furthermore, the HSE model has been used to examine keratinocyte epidermal-formation abilities following expansion on microcarriers (Borg *et al.*, 2008) and also to evaluate whether chemically defined, serum-free growth media sustains epithelial formation (Mujaj *et al.*, 2010).

The aims of the studies reported in this Chapter were to histologically characterise the keratinocyte-only HSE model over a 9 day period and compare it to native human skin. This will enable assessment of the biological relevance of this HSE model for further studies.

3.2 METHODS AND MATERIALS

A complete explanation of both the materials and methods and the experimental procedures used in the generation of data presented in this Chapter have been described in Chapter 2. The following is a brief summary of the experimental protocols used to generate the data presented in section 3.3.

3.2.1 Generation of the human skin equivalent (HSE) model

HSE models were generated using skin obtained from individuals undergoing elective cosmetic breast reduction or abdominoplasty surgeries as fully described in sections 2.4 - 2.6. Following generation of the HSE model, they were cultured at the air-liquid interface and maintained in Full Greens (FG) culture media. The media was replenished daily to maintain the HSE cultures at the air-liquid interface and was fully replaced once per week.

3.2.2 Keratinocyte lateral migration within the HSE model

For full details of determining the epidermal outgrowth of newly formed epidermis over the DED using 4,5-dimethylthiazol-2-yl)-2,5-diphenyltetraoliumbromide (MTT), please refer to section 2.9.

3.2.3 Assessment of the epidermal generation process of the HSEs

Following MTT analysis, HSE models were formalin-fixed and paraffin embedded for histological analysis as described in section 2.10.1. Following this, sections of skin were cut using a microtome (Leica) to 5 µm thick and transferred to a glass microscope slide (HD scientific, Willawong, QLD). Sections were either used for haematoxylin and eosin (H&E) staining to determine epidermal morphology and thickness, or used for immunohistological analysis.

To determine the expression of specific skin developmental markers, slides containing sections from each time point for each HSE model were incubated with each the following primary antibodies: p63 (1:2000 dilution), ki-67 (1:100 dilution), keratin 1 (K1; 1:500 dilution), loricrin (1:1000 dilution) or keratin 16 (K16; 1:100 dilution). Immunoreactivity was determined using the Dako Envision kit (Dakocytomation) following the manufacturer's instructions. The resulting H&E or immunohistochemistry slides were observed using an Olympus BX41 microscope (Olympus) with a mounted digital camera (Olympus).

3.2.4 Image data analysis

Image analysis was performed on consecutive images taken from the centre of each HSE. All image data analysis was performed using open source ImageJ software (available at: http://rsbweb.nih.gov/ij/) with the MacBiophotonics Plugins (available at: http://www.macbiophotonics.ca/imagej/). For full details on the image data analysis protocol, please refer to section 2.10.2.

3.2.5 Statistical analysis

Skin samples generated from eight individual donors were analysed throughout this Chapter. The skin samples were divided into two groups, group A which contained 3 skin samples and group B, which contained 5 skin samples. Image analysis data generated from group A were pooled, for the reason that RNA were isolated and pooled from this group for microarray analysis in future studies (Chapter 5). The image data generated from group B were expressed as individual skin samples since RNA from these samples were not used for microarray studies and were therefore not pooled. Furthermore, donor-matched native skin samples were only collected for group B, whereas native skin controls were from unrelated donors in group A. All data is expressed as mean ± standard deviation. Tukey's post hoc analysis following a one-way ANOVA was performed with a p value < 0.05 deemed significant on all data presented in this Chapter.

3.3 RESULTS

3.3.1 Analysis of keratinocyte outgrowth in the developing HSE model

The epidermal outgrowth of keratinocytes over a DED can be measured through the visualisation of metabolically active cells using the MTT assay (Kairuz *et al.*, 2007). In the study reported herein, the HSE model was cultured at the air-liquid interface for nine consecutive days, prior to detection with MTT. The areas positive for MTT staining revealed an outgrowth of keratinocytes from the centre seeding region to the outer edges of the HSE models as time progressed (**Figure 3.1 A**).

3.3.2 The epidermis continually expands over the DED in a time dependent manner

The 3D HSE model was employed to investigate the expansion of the developing epidermis. The HSEs were harvested after 0, 3, 5 and 9 days culture at the air-liquid interface and stained with MTT to visualise the viable epidermal surface area. Images were captured and used to quantify the lateral migration of the keratinocytes over the DED using ImageJ software (Appendix Table A1 and Table A2).

The surface area of DED covered by newly formed epidermis was determined using ImageJ software. Analysis of this data revealed that all samples followed the same trend. As expected, the epidermal surface area was almost identical between all samples at day 0, since all keratinocytes were seeded into identical rings of a defined size (**Figure 3.1**). The surface area covered by newly formed epidermis continued to increase as the experiment progressed and this increase in outgrowth was significant in most samples at day 9, when compared to the surface area at day 5 (41.03 mm^2 ±11.10 mm^2 to 76.21 mm^2 ± 16.66 mm^2 in the group A samples, 42.54 mm^2 ± 0.48 mm^2 to 74.26 mm^2 ± 12.21 mm^2 in sample 4, 44.66 mm^2 ± 3.37 mm^2 to 77.54 mm^2 ± 12.16 mm^2 in sample 5 and 48.79 mm^2 ± 6.69 mm^2 to 104.30 mm^2 ± 1.06 mm^2 in sample 8; $p < 0.05$; **Figure 3.1 B – D** and **G**)

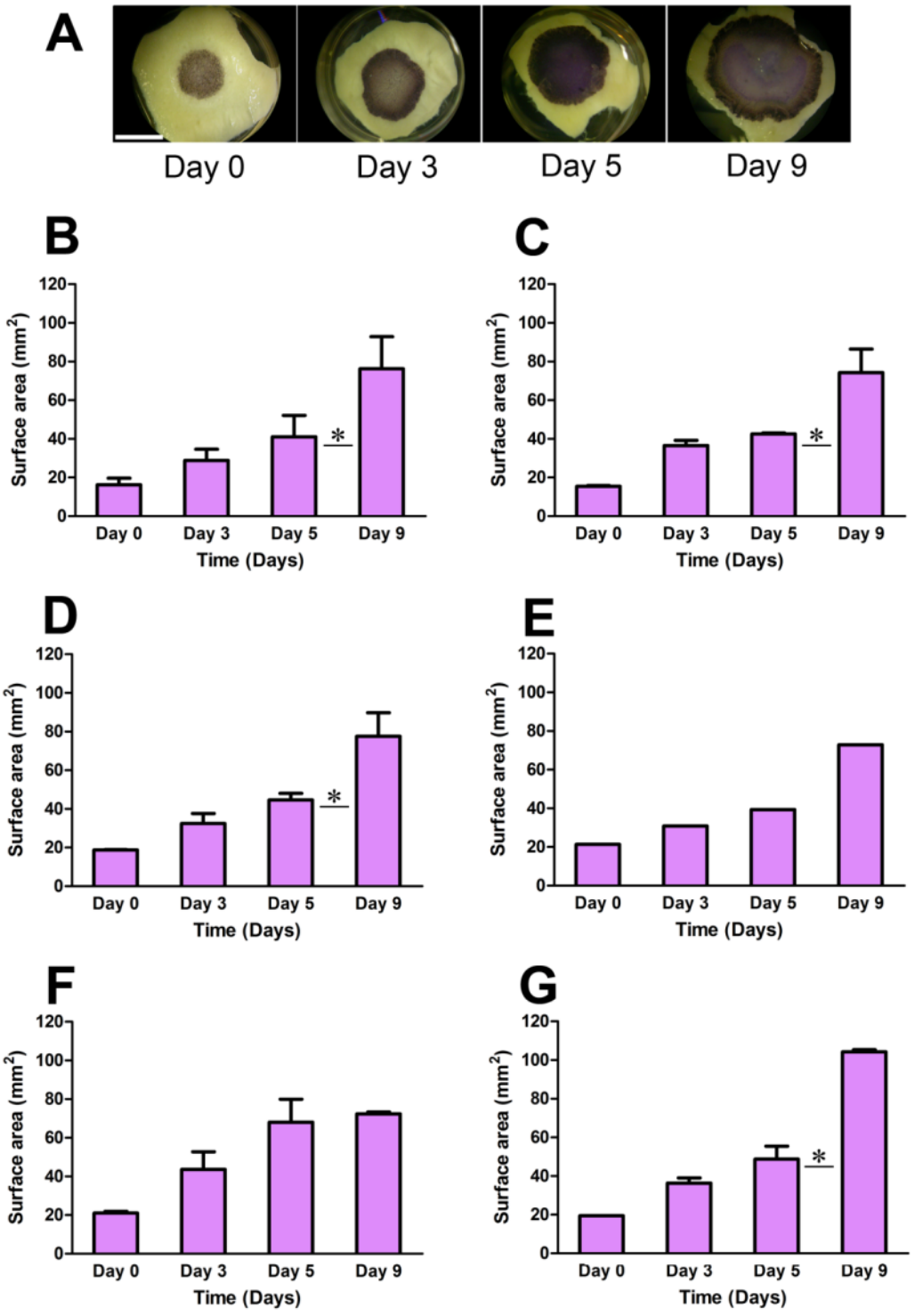

Figure 3.1 Keratinocyte outgrowth in the HSE model
Reconstructed HSE models were cultured at the air-liquid interface for up to 9 days. Outgrowth of metabolically active keratinocytes over the DED was visualised via MTT staining after 0, 3, 5 and 9 days culture at the air-liquid interface (**A**). The surface area of viable epidermis (stained purple) covering the HSE was determined at each time point and differences in outgrowth were determined between days in skin samples from group A (**B**), and group B (**C - G**). No error bars are present for sample 6 (**E**), as n=1 HSE model for each time point. Significant differences between time points are indicated by the asterisk (*; $p < 0.05$). The scale bar represents 5 mm.

3.3.3 The HSE model most closely resembles native skin at day 5

In order to evaluate the developing epidermis in the HSE model, histological analysis on the samples collected for MTT staining in section 3.2.1 was performed. Specifically, epidermal generation and morphology of the HSE model in comparison to native, intact human skin was investigated. The formation of the epidermis and its architecture was assessed by haematoxylin and eosin (H&E) staining of sections from HSEs collected after 0, 3, 5 and 9 days culture at the air-liquid interface.

Examination of sections from day 0 samples revealed that the epidermis was comprised of morphologically undifferentiated keratinocytes that did not form a continuous epithelium. In particular, the keratinocytes had migrated into the rete ridge structures of the DED, forming pockets of cuboidal cells. These pockets of cells were dispersed between regions in which keratinocytes were either absent, or squamous in morphology, reminiscent of the initiation of stratum corneum formation or of keratinocytes in a migratory phenotype (**Figure 3.2 A**; Savagner *et al.*, 2005).

By 3 days of growth in the HSE model, a corneum layer was apparent. In addition, a cellular layer which resembled a stratified epithelium had formed, yet was still immature in appearance. There was a lack of clear distinction between the cuboidal, proliferative cells of the basal layers and the squamous, differentiating cells of the upper stratified layers. However, a complete stratified and well differentiated epithelium had developed by day 5. Specifically, sections from the 5 day post – elevation HSE models were comprised of distinguished basal layers, flattened keratinocytes of the spinosum layer, squamous cells containing keratohyaline granules in the granulosum layer and finally the cornified stratum corneum. By day 9, however, there was an observable decrease in the total viable epidermal thickness and a vast increase in the thickness of the cornified layer (**Figure 3.2 A**). This indicates that differentiation was predominating over proliferation in the HSE model as time progressed.

3.3.4 Quantitative image analysis of epidermal thickness in the developing HSE

From observation of the H&E stained HSE sections, it became apparent that there was a need to develop a method to accurately quantify the thickness of the epidermis which could take into consideration the ridge – like structure of human skin. The development and subsequent stratification of the HSE models as represented in the H&E sections were quantified via image analysis to accurately determine the average thicknesses of the epidermis (**Figure 3.2**). ImageJ was employed to evaluate the thickness of the cellular and stratum corneum layers at each time point (Appendix Table A3 – Table A6).

Investigation of the epidermal thickness of the HSE models revealed that most HSE models followed the same general trend. Initially, there was an increase in the thickness of the cellular layer between days 0 and 3, a peak at day 5, followed by a decrease in thickness by day 9 (**Figure 3.2**). However, sample 7 varied from this trend in that the cellular layer thickness peaked at day 3 then progressively decreased over the course of the experiment (**Figure 3.2 F**). Concurrently, the stratum corneum progressively increased in thickness from day 0 until day 9 in all samples. Interestingly, the stratum corneum was thicker than the cellular layer in the HSE models from samples 5, 6 and 7 at day 9 (**Figure 3.2 D - F**). Furthermore, it was observed that most samples contained stratum corneum and cellular layer proportions in the day 5 HSEs that were similar to those present in the native skin (**Figure 3.2**). Overall, these results demonstrate that a viable epidermis can be created and maintained in an *ex vivo* environment. Furthermore, the analysis of the HSE models reveals that proportionally, the day 5 samples most closely resemble native skin (**Figure 3.2**).

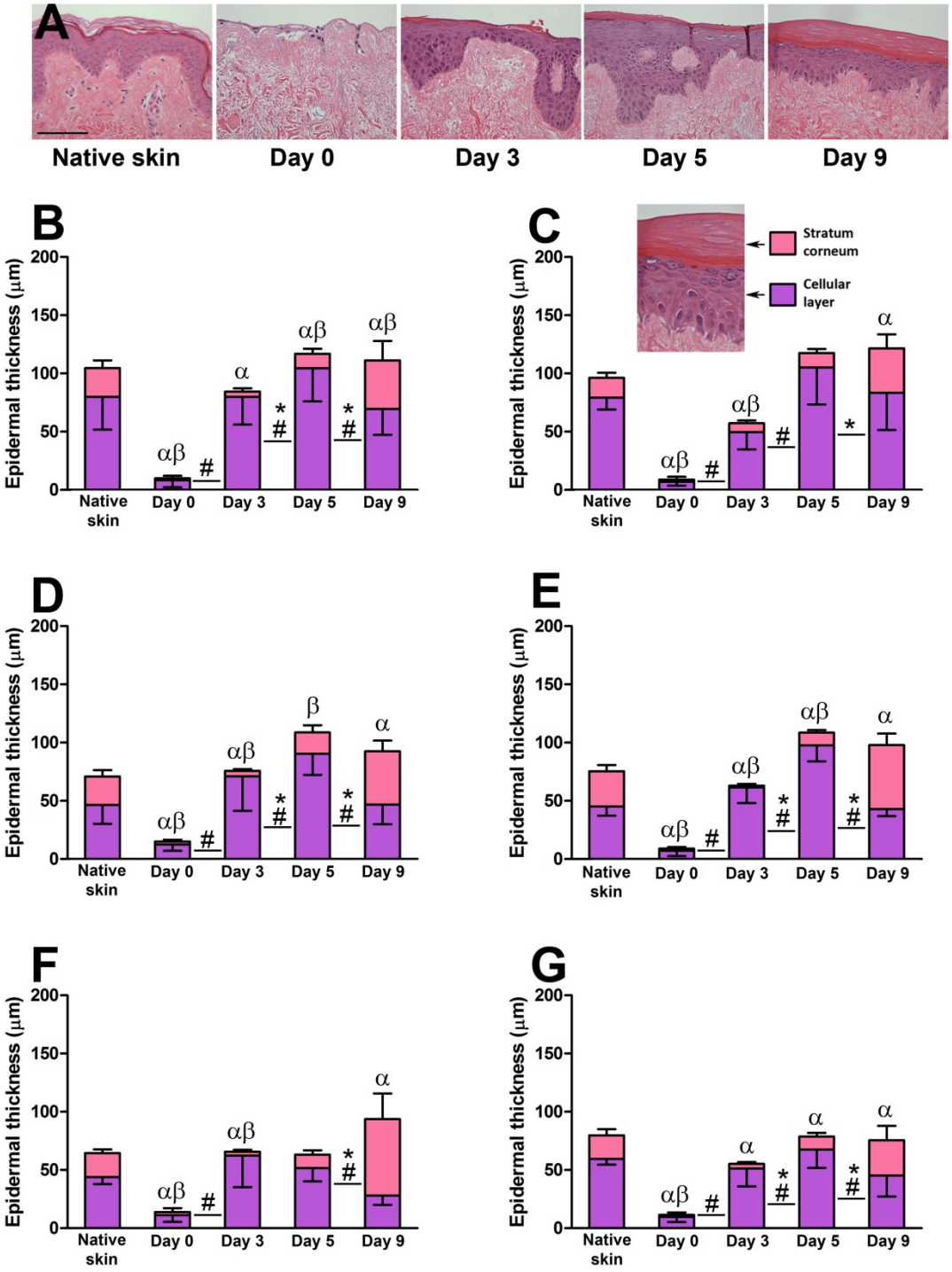

Figure 3.2 Epidermal thickness of the HSE over 9 days of culture
Image analysis was performed on H&E images of both native skin and the HSE models captured from each sample over time (**A**). The graphs represent the data obtained from (**B**) sample group A, (**C**) epidermal thickness data for sample 4, (**D**) sample 5, (**E**) sample 6, (**F**) sample 7 and (**G**) sample 8. The graphs represent the histological sections, therefore the viable cellular region is indicated by the purple and the stratum corneum of the epidermis is indicated by the pink. Data obtained from n = 2 HSEs per time point, except sample 6, where n = 1 per time point. There were a total of 8 histological sections analysed per HSE model, therefore, 16 images for each sample, except sample 6. Graphs represent mean epidermal thickness (µm) ± standard deviation. α - significant difference between native skin and the HSE ($p < 0.05$; SC only), β - significant difference between native skin and HSE ($p < 0.05$; Cellular only), αβ - significant difference between native skin and HSE ($p < 0.05$; Cellular and SC), * - significant difference between days ($p < 0.05$; SC only), # - significant difference between days ($p < 0.05$; Cellular only).

3.3.5 The HSE model expresses established markers of epidermal proliferation and differentiation

Immunohistochemical analysis was performed on HSE models to determine differences in general markers of skin proliferation and differentiation status, in order to define the HSE model and its development over time. To assess the rate of proliferation, sections generated after 0, 3, 5 and 9 days of culture at the air-liquid interface were probed with antibodies specific to p63 and ki-67. Furthermore, to determine the degree of differentiation occurring within the HSE, sections generated from the same experiments were probed with antibodies to keratin 1 (K1), loricrin and keratin 16 (K16; **Figure 3.3**). The images captured from these experiments are discussed further in sections 3.3.6 - 3.3.15.

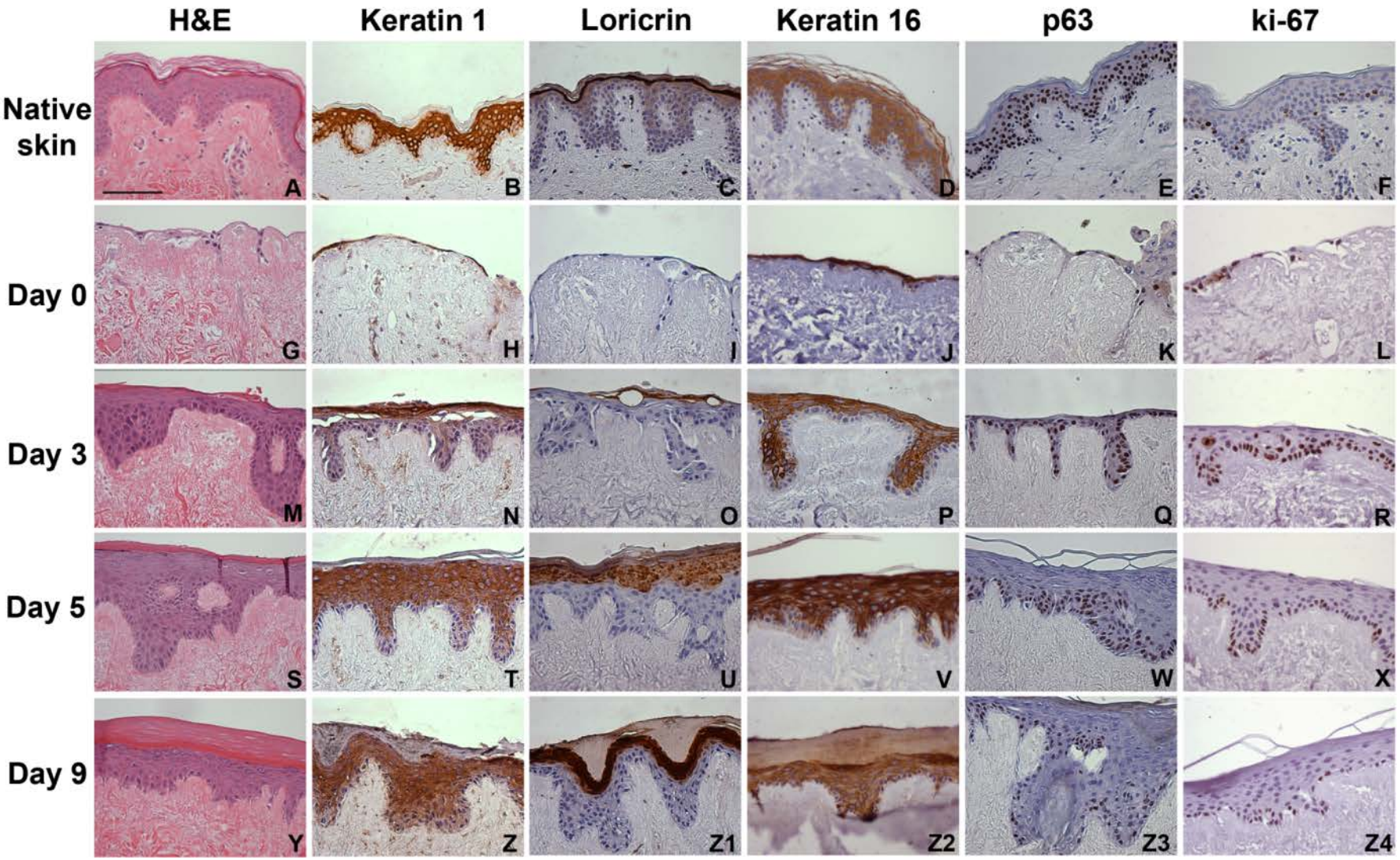
H&E
Keratin 1
Loricrin
Keratin 16
p63
ki-67
Native skin
Day 0
Day 3
Day 5
Day 9
A
B
C
D
E
F
G
H
I
J
K
L
M
N
O
P
Q
R
S
T
U
V
W
X
Y
Z
Z1
Z2
Z3
Z4

Figure 3.3 Histological detection of keratinocyte developmental markers during epidermogenesis in the HSE model
Sections of native skin (**A-F**) and HSE models cultured at the air-liquid interface for 0 days (**G-L**), 3 days (**M-R**), 5 days (**S-X**) and 9 days (**Y-Z4**) were probed with antibodies to K1 (**B, H, N, T** and **Z**), loricrin (**C, I, O, U**, and **Z1**), K16 (**D, J, P, V, Z2**), p63 (**E, K, Q, W, Z3**) and ki-67 (**F, L, R, X, Z4**). Presence of the antigens is represented by brown immunoreactivity and the nuclei were counter-stained blue with haematoxylin. General tissue morphology was visualised through haematoxylin and eosin saining of skin and HSE sections (**A, G, M, S, Y**). The scale bar represents 100 μm. These are representative images from both the group A and group B samples.

3.3.6 Expression and localisation of p63 in native skin and the HSE model

The transcription factor p63 is highly expressed in basal and/or progenitor cells in epithelial tissues, such as skin, and is an indicator of the proliferative capacity of that cell (Parsa *et al.*, 1999). Importantly, p63 is not necessarily expressed in actively proliferating cells. The expression of p63 therefore was analysed to determine the proliferative capacity of the HSE model, and also to determine if culturing skin *in vivo* alters the proliferative ability of the epidermis.

In sections of native skin, there was a very high level of p63 expression. It appeared that all nuclei throughout native skin were p63 positive, including keratinocytes from the basal layer, through to the suprabasal layers (**Figure 3.4 A**). In the HSE model, p63 was expressed in isolated patches of keratinocytes in the day 0 epidermis. Sections from day 3 HSE models expressed p63 in almost all nuclei, as was found in the native skin sections. At day 5, p63 was evident in only the basal layer of the epithelium. This trend continued in the day 9 samples, where p63 expression appeared to have diminished, even in the basal layers of the epidermis. Overall, the expression of p63 appeared to be much lower in the HSEs than in native skin (**Figure 3.4 A**). In order to quantify the difference in p63 expression, the images were analysed using ImageJ.

3.3.7 The HSE model has a lower proliferative capacity than native skin

Images captured of the immunoreactivity described above were analysed using ImageJ. The p63 positive nuclei were counted to determine the temporal expression levels of this proliferation marker in native skin and the HSE model (Appendix Table A7 and Table A8). In most skin samples p63 levels initially increased significantly between days 0 and 3 (from 8.71 ± 4.34 to 86.88 ± 44.45 in the group A samples, from 9.75 ± 7.37 to 79.00 ± 20.04 in samples 4, from 14.94 ± 6.24 to 47.31 ± 13.28 in sample 5, from 4.13 ± 1.36 to 69.13 ± 15.26 in sample 6, from 12.63 ± 9.51 to 64.31 ± 23.98 in sample 7 and from 12.25 ± 3.32 to 68.75 ± 17.38 in sample 8; $p < 0.05$), remained relatively stable into day 5, before decreasing by day 9 (**Figure 3.4 B - G**). Sample 4 deviated from this trend, however, as the expression of p63 significantly increased between days 3 (79.00 ± 20.04 p63 nuclei) and 5 (105.88 ± 26.43 p63 nuclei; $p< 0.05$);**Figure 3.4 C**). Interestingly, the number of p63-positive nuclei was consistently and significantly higher in native skin than was found in any

of the HSE models (192.95 ± 52.25, 154.75 ± 22.91, 169.25 ± 36.21, 169.50 ± 40.30, 104.50 ± 26.61 and 127.88 ± 27.65 p63 nuclei in the group A samples and samples 4 – 8 respectively; $p < 0.05$; **Figure 3.4**). This suggests that the HSE models are not retaining their proliferative potential over time and also, have a lower proliferative capacity than native human skin.

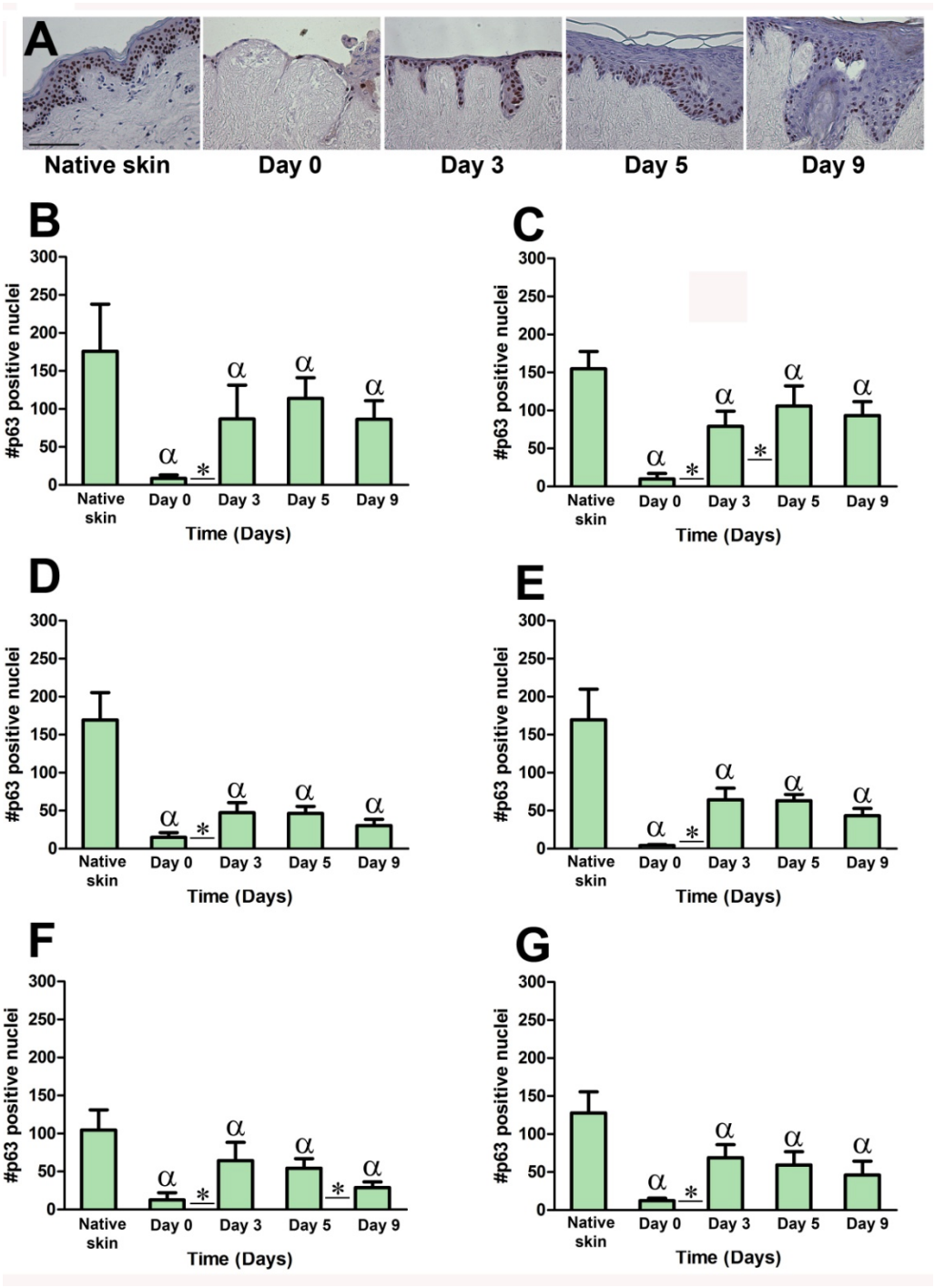

Figure 3.4 The expression of p63 in the HSE model over 9 days of treatment
Histological sections of native skin and the HSE model were probed for p63 expression to determine the proliferative capacity of the epidermis after 0, 3, 5 and 9 days growth at the air-liquid interface. Presence of the p63 antigen is represented by brown immunoreactivity, whereas all other nuclei are counter-stained blue with haematoxylin. The scale bar represents 100 µm. These are representative figures using images captured from sample 4 (**A**). Additionally, the number of p63 positive nuclei were counted using ImageJ in sequential histology sections to determine the average number of positive nuclei per section. The graphs represent the p63 data obtained from (**B**) group A samples, and (**C**) p63 data from sample 4, (**D**) sample 5, (**E**) sample 6, (**F**) sample 7 and (**G**) sample 8. Data obtained from n = 2 HSEs per time point, except sample 6, where n = 1 per time point. There were a total of 8 histological sections analysed per HSE model, therefore, 16 images for all samples, except sample 6. Data represents mean numbers of positive nuclei ± standard deviation. * indicates significance between days ($p < 0.05$), where as α indicates significant differences to native skin ($p < 0.05$).

3.3.8 Expression and localisation of ki-67 in native skin and the HSE model

The cell cycle marker ki-67 is expressed in the nuclei of all cells that are not in the G_0 resting phase of the cell cycle. Hence ki-67 was investigated in order to more accurately discern the proliferative status of both the native skin and the developing HSE model (Noszczyk and Majewski, 2001). In sections from the HSE model at day 0, ki-67 was expressed in almost all keratinocytes in the newly forming epidermis. By day 3, the HSE still expressed ki-67 in most nuclei. At day 5, ki-67 immunoreactivity was isolated to only the basal layer of the epithelium and the positive nuclei were intermittently spaced. This trend continued into day 9, wherein ki-67 expression appeared to have diminished, even in the basal layers of the epidermis (**Figure 3.5 A**). Examination of the images captured of ki-67 in native skin revealed that the expression of ki-67 was low and that the positive nuclei appeared to be restricted to the basal layer of the epidermis (**Figure 3.5 A**).

3.3.9 The number of actively proliferating keratinocytes peaks after 3 days of epidermogenesis in the HSE model

Images captured of the immunoreactivity described above were analysed using ImageJ. The nuclei expressing ki-67 were individually counted to determine the temporal expression of this proliferation marker during epidermogenesis in the HSE model (Appendix Table A9 and Table A10). Generally, ki-67 expression followed the same trend in all HSE models. The numbers of ki-67 positive nuclei were low at day 0, increased significantly by day 3 (from 9.83 ± 3.69 to 65.50 ± 13.56 in the group A samples, from 15.50 ± 10.12 to 78.81 ± 11.44 in sample 4, from 17.44 ± 7.28 to 46.56 to 10.46 in sample 5, from 9.13 ± 2.42 to 66.00 ± 13.43 in sample 6, from 25.31 ± 6.96 to 61.25 ± 23.29 in sample 7 and from 14.00 ± 4.98 to 68.75 ± 23.17 in sample 8; $p < 0.05$). After day 3, ki-67 levels significantly decreased at both days 5 (to 47.54 ± 8.90 in the group A samples and to 42.19 ±8.60, 23.25 ± 7.61, 20.25 ± 15.69, 24.06 ± 11.85 and 42.94 ± 13.73 in samples 4 – 8 respectively; $p < 0.05$) and 9 (to 22.67 ± 7.87 in the group A samples and to 20.75 ± 6.03, 13.50 ± 2.93, 8.69 ± 4.47 and 20.88 ± 8.10 in samples 4, 5, 7 and 8 respectively; $p < 0.05$, **Figure 3.5 B – D, F – G**). Additionally, the level of ki-67 in native skin was low and most similar to the day 9 HSE models (**Figure 3.5 B – G**). This suggests that the HSE models are highly proliferative until day 3, thereafter differentiation predominates over proliferation.

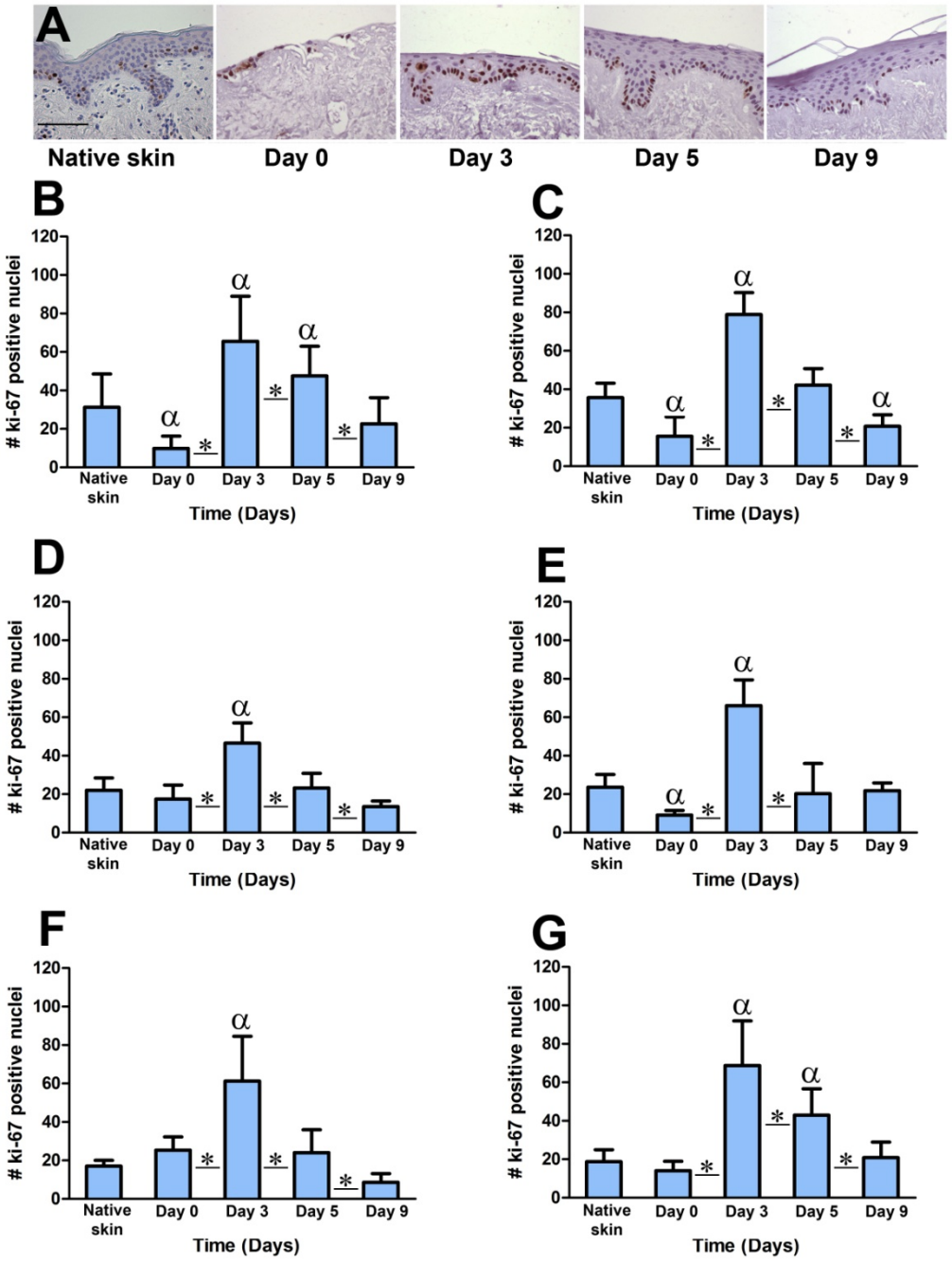

Figure 3.5 Expression of ki-67 in the HSE model of 9 days of treatment
Histological sections of native skin and the HSE model were probed for ki-67 expression to determine the number of actively proliferating keratinocytes in the epidermis after 0, 3, 5 and 9 days growth at the air-liquid interface. Presence of the ki-67 antigen is represented by brown immunoreactivity, whereas all other nuclei are counter-stained blue with haematoxylin. The scale bar represents 100 µm. These are representative figures using images captured from group A (**A**). Additionally, the number of ki-67 positive nuclei were counted using ImageJ in sequential histology sections to determine the average number of positive nuclei per section. The graphs represent the ki-67data obtained from (**B**) the group A skin samples and (**C**) ki-67 data from sample 4, (**D**) sample 5, (**E**) sample 6, (**F**) sample 7 and (**G**) sample 8. Data obtained from n = 2 HSEs per time point, except sample 6, where n = 1 per time point. There were a total of 8 histological sections analysed per HSE model, therefore, 16 images for all samples, except sample 6. Data represents mean numbers of positive nuclei ± standard deviation. * indicates significance between days ($p < 0.05$), where as α indicates significant differences to native skin ($p < 0.05$).

3.3.10 Expression and localisation of K1 in native skin and the HSE model

Proliferation and differentiation processes both occur during re-epithelialisation and the formation of a stratum corneum is evidence of the latter. Evaluation of differentiation in the HSE models and the effect of culture on K1 expression were therefore conducted. K1 is a marker of early differentiation and is expressed in keratinocytes as the differentiation process commences (Leigh *et al.*, 1993). It is one of the first markers to appear during the epidermogenesis process in HSE models (Kairuz *et al.*, 2007). Qualitative analysis of K1 in native skin revealed that it was expressed in all supra-basal layers of the epidermis and was absent from the stratum corneum (**Figure 3.6 A**). The K1-positive immunoreactivity was difficult to determine in the day 0 samples since a continuous and stratified epithelium had not yet established, however, expression was observed in sparse regions within the HSE. In images from days 3, 5 and 9, K1 was expressed in all supra-basal epidermal layers but was absent from the stratum corneum (**Figure 3.6 A**). In order to quantify these observations, the thickness of K1 expressed in each sample was analysed as described in section 2.11.2.

3.3.11 Early differentiation in the HSE model is most similar to native skin after 5 days culture at the air-liquid interface

Images captured of the immunoreactivity described in section 3.3.11 were analysed using ImageJ. The thickness of the epidermis expressing K1 was determined using image analysis techniques to examine the expression of this marker over time (Appendix Table A11 and Table A12). The image data was analysed and a common trend of K1 expression was evident within the developing HSE models. In all but sample 4, the thickness of K1 significantly increased between days 0 and 3 (from 2.57 µm ± 2.76 µm to 18.96 µm ± 18.15 in the group A samples and from 6.05 µm ± 4.20 µm to 15.00 µm ± 4.30 µm in sample 5, from 2.73 µm ± 1.10 µm to 17.42 µm ± 4.26 µm in sample 6, from 1.74 µm ± 2.04 µm to 11.90 µm ± 7.20 µm in sample 7 and from 3.21 µm ± 2.18 µm to 17.16 µm ± 12.43 µm in sample 8; $p < 0.05$), after which the levels peaked at day 5 (67.78 µm ± 19.31 µm, 76.04 µm ± 17.74 µm, 36.65 µm ± 10.66 µm, 37.97 µm ± 5.15 µm, 36.79 µm ± 12.31 µm and 40.11 µm ± 10.21 µm in the group A samples – sample 8 respectively ;$p < 0.05$; **Figure 3.6 B - G**) and began to decrease by day 9 ($p < 0.05$; **Figure 3.6 B, D – F**). Furthermore, at day 5, most skin samples expressed a K1 level similar to that found

in native skin (**Figure 3.6 B, D – G**). This suggests that, at day 5, the early differentiation status of the HSE model is most similar to native skin.

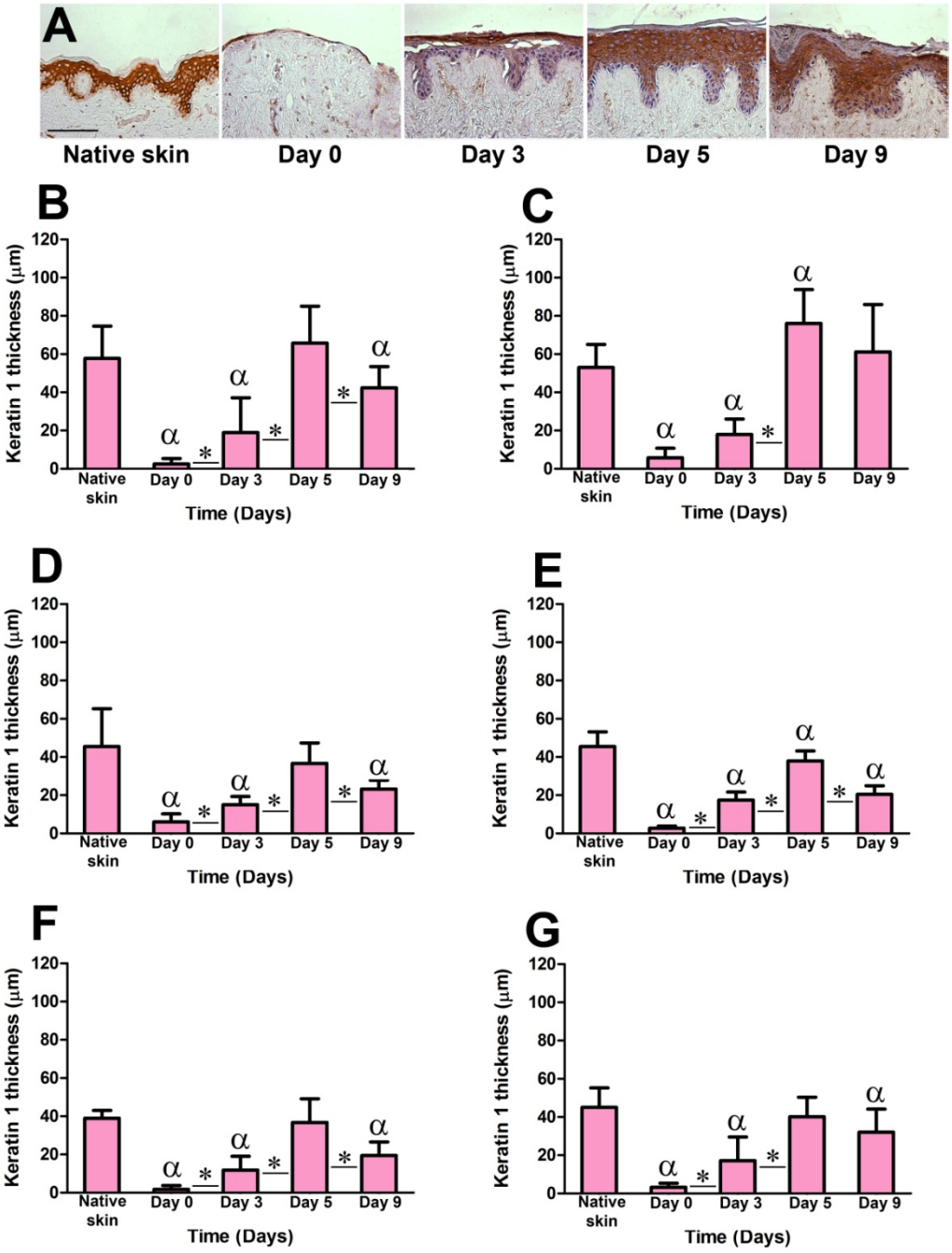

Figure 3.6 K1 immunoreactivity in the HSE model over 9 days of treatment
Histological sections of native skin and the HSE model were probed for K1 expression to determine the early differentiating keratinocytes of the epidermis after 0, 3, 5 and 9 days growth at the air-liquid interface. Presence of the K1 antigen is represented by brown immunoreactivity, and all nuclei are counter-stained blue with haematoxylin. The scale bar represents 100 μm. These are representative figures using images captured from sample 4 (**A**). Additionally, the thickness of K1-positive epidermis was calculated using ImageJ in sequential histology sections to determine the average thickness of K1 per section. The graphs represent K1 data obtained from (**B**) group A samples and (**C**) K1 data from sample 4, (**D**) sample 5, (**E**) sample 6, (**F**) sample 7 and (**G**) sample 8. Data obtained from n = 2 HSEs per time point, except sample 6, where n = 1 per time point. There were a total of 8 histological sections analysed per HSE model, therefore, 16 images for all samples, except sample 6. Data represents the mean numbers of positive nuclei ± standard deviation. * indicates significance between days ($p < 0.05$), where as α indicates significant differences to native skin ($p < 0.05$).

3.3.12 Expression and localisation of loricrin in native skin and the HSE model

The terminal differentiation marker, loricrin, is expressed in keratinocytes of the upper stratum granulosum and the stratum corneum (Gibbs and Ponec, 2000). It is a major protein present in the cornified layer and all epidermal cells that express it are committed to becoming part of the stratum corneum. Initial investigation into the expression of loricrin in native skin revealed that it was expressed in the upper-most layer of the viable cellular epidermis, just below the stratum corneum (**Figure 3.7 A**). In some images, loricrin immunoreactivity was also present in the stratum corneum. In the sections from the day 0 HSEs, there was no apparent loricrin expression, most likely due to the immaturity of the epidermis. In all images of sections from the days 3, 5 and 9, loricrin was detected in the upper-most layers of the epidermis but was absent from the stratum corneum (**Figure 3.7 A**). To establish if there were any quantitative differences in loricrin expression, the thickness of loricrin-positive epidermis quantified using ImageJ analysis as described in section 2.11.2.

3.3.13 Terminal differentiation is greatly enhanced in the HSE model in comparison to native skin

Images captured of the immunoreactivity described above were analysed using ImageJ. The thickness of the epidermis expressing loricrin was determined using image analysis techniques to examine the expression of this marker over time (Appendix Table A13 and Table A14). Analysis of the data obtained from the immunohistological images from the HSEs revealed that all samples followed the same trend of loricrin expression over time (**Figure 3.7 B - G**). Initially, there was either absence or very low expression of loricrin at day 0. Loricrin expression increased significantly by day 3 in all but sample 4 (to 5.81 µm ± 5.25 µm in the group A samples and 10.73 µm ± 4.33 µm, 5.70 µm ± 3.19 µm, 12.15 µm ± 3.10 µm and 17.25 µm ± 5.30 µm in samples 5 – 8 respectively; $p < 0.05$). Furthermore, the expression of loricrin increased significantly between days 3 and 5 in all samples (to 32.96 µm ± 9.84 µm, 39.14 µm ± 10.29 µm, 30.10 µm ± 6.69 µm, 28.76 µm ± 6.06 µm, 21.88 µm ± 5.13 µm and 26.21 µm ± 7.82 µm in the group A samples to sample 8 respectively; $p < 0.05$), before significantly decreasing by day 9 (to 22.09 µm ± 5.72 µm, 28.31 µm ± 8.13 µm, 22.56 µm ± 3.17 µm and 14.25 µm ± 1.96 µm in samples group A – 6 respectively; $p < 0.05$). Native skin expressed relatively low

levels of loricrin, approximately equivalent to the levels present in the HSEs at day 3 (**Figure 3.7 B – E**). This suggests that the HSE model enters into an enhanced terminal differentiation program in comparison to native skin. The HSE model, therefore, forms a stratum corneum at a greater rate than native skin.

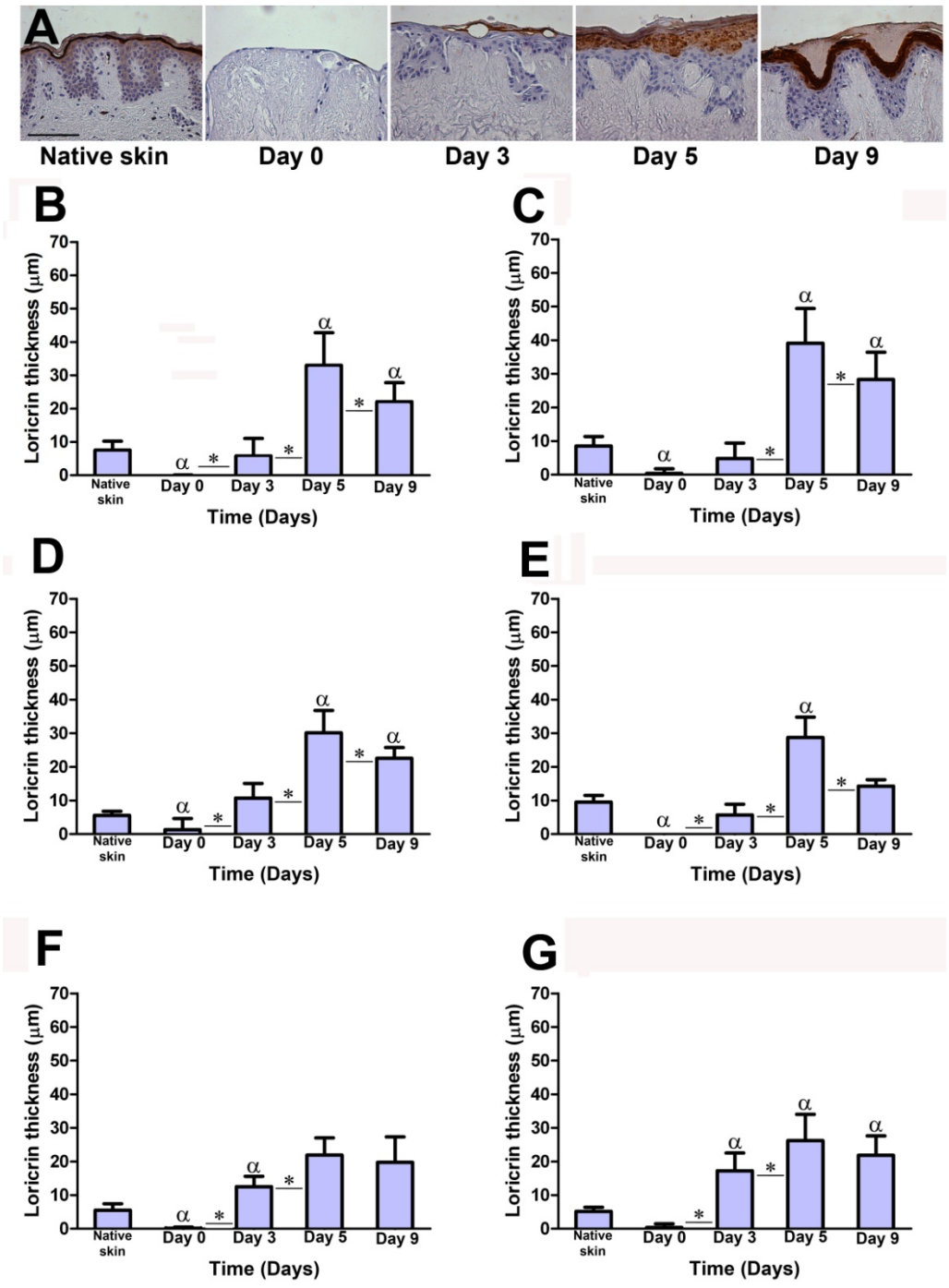

Figure 3.7 Loricrin immunoreactivity in the HSE model over 9 days of treatment
Histological sections of native skin and the HSE model were probed for loricrin expression to determine the early differentiating keratinocytes of the epidermis after 0, 3, 5 and 9 days growth at the air-liquid interface. Presence of the loricrin antigen is represented by brown immunoreactivity, and all nuclei are counter-stained blue with haematoxylin. The scale bar represents 100 μm. These are representative figures using images captured from sample 4 (**A**). Additionally, the thickness of loricrin-positive epidermis was calculated using ImageJ in sequential histology sections to determine the average thickness of loricrin per section. The graphs represent the data obtained from (**B**) Group A samples and (**C**) loricrin data from sample 4, (**D**) sample 5, (**E**) sample 6, (**F**) sample 7 and (**G**) sample 8. Data obtained from n = 2 HSEs per time point, except sample 6, where n = 1 per time point. There were a total of 8 histological sections analysed per HSE model, therefore, 16 images for all samples, except sample 6. Data represents the mean numbers of positive nuclei ± standard deviation. * indicates significance between days ($p < 0.05$), where as α indicates significant differences to native skin ($p < 0.05$).

3.3.14 Expression and localisation of K16 in native skin and the HSE model

K16 is a marker of stress and is also known as a hyper-proliferation marker (Paladini *et al.,* 1995). Generally, K16 is expressed in areas of high cellular turnover, such as in wound healing, psoriasis and some carcinomas (Paladini *et al.,* 1995). Interestingly, in the native skin samples, K16 was expressed in the supra-basal layers of the epidermis (**Figure 3.8 A**). Investigations into the K16 expression patterns in the HSE sections revealed that K16 was expressed in all supra-basal epidermal layers but was absent from the stratum corneum, irrespective of sample treatment. This was observed in all images from days 3, 5 and 9 (**Figure 3.8 A**). To determine if these observations were accurate, the thickness of K16-positive epidermis in each sample was quantified using acquired images, as described in section 2.11.2.

3.3.15 Quantitative image analysis of K16 expression in native skin and the HSE model

Images captured of the immunoreactivity described above were analysed using ImageJ. The thickness of the epidermis expressing K16 was determined using image analysis techniques to calculate the expression of this marker over time (Appendix Table A15 and Table A16). The level of K16 present in HSE sections from day 0 was quite low. However, K16 presence significantly increased between day 0 and day 3 (from 6.23 µm ± 3.88 µm to 46.07 µm ± 16.96 µm in the group A samples and in samples 4 – 8 respectively from 5.37 µm ± 4.28 µm to 44.95 µm ± 15.07 µm, 12.09 µm ± 10.18 µm to 44.56 µm ± 14.76 µm , 7.49 µm ± 6.57 µm to 35.91 µm ± 5.27 µm, 8.45 µm ± 3.24 µm to 49.55 µm ± 10.93 µm and 6.05 µm ±3.55 µm to 55.65 µm ± 18.42 µm; $p < 0.05$). K16 levels then peaked at day 5 significant in samples group A, 4 and 6; 84.25 µm ± 17.78 µm, 97.69 µm ± 21.02 µm, 64.39 µm ± 7.10 µm; $p < 0.05$) and began to decrease by day 9 (significant in the group A samples and sample 6 and 8; 51.35 µm ± 18.78 µm, 43.07 µm ± 3.64 µm and 46.11 µm ± 16.08 µm, $p < 0.05$, **Figure 3.8 B**, **C, E** and **G**). Samples 5 and 7, however, differed in that they exhibited an initial increase in the level of K16 between day 0 and day 3, but then the level of K16 remained consistent over days 3, 5 and 9 (**Figure 3.8 D** and **F**). When the level of K16 in native skin was compared to HSE models, the day 3 and day 9 HSE models were most similar to native skin (**Figure 3.8**). This suggests that both the HSE models and native human skin are in a "stressed" or hyper-proliferative state.

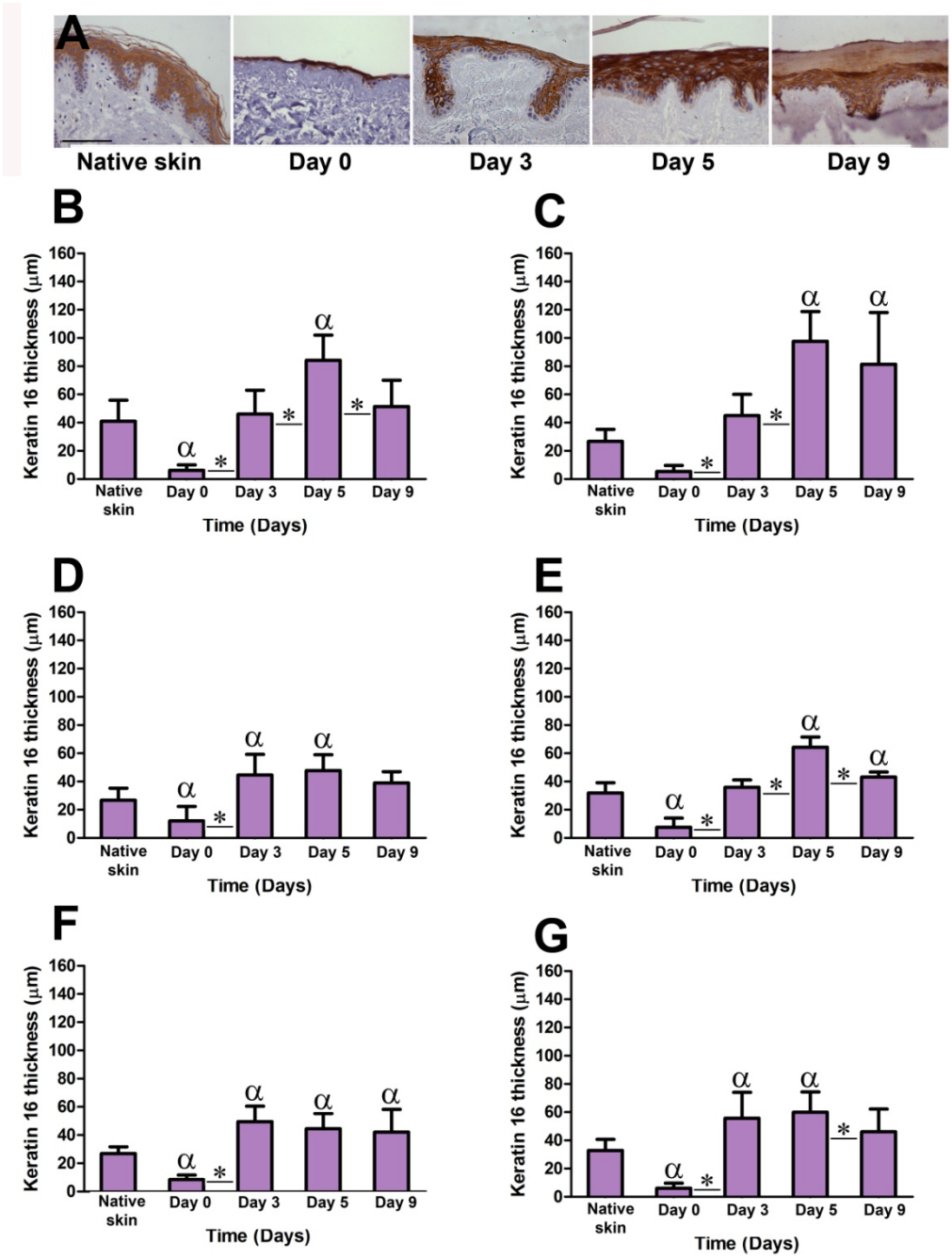

Figure 3.8 K16 immunoreactivity in the HSE model over 9 days of treatment
Histological sections of native skin and the HSE model were probed for K16 expression to determine the early differentiating keratinocytes of the epidermis after 0, 3, 5 and 9 days growth at the air-liquid interface. Presence of the K16 antigen is represented by brown immunoreactivity, and all nuclei are counter-stained blue with haematoxylin. The scale bar represents 100 µm. These are representative figures using images captured from group A samples (**A**). Additionally, the thickness of K16-positive epidermis was calculated using ImageJ in sequential histology sections to determine the average thickness of K16 per section. The graphs represent the data obtained from (**B**) the group A samples and (**C**) K16 data from sample 4, (**D**) sample 5, (**E**) sample 6, (**F**) sample 7 and (**G**) sample 8. Data was obtained from n = 2 HSEs per time point, except sample 6, where n = 1 per time point. There were a total of 8 histological sections analysed per HSE model, therefore, 16 images for all samples, except sample 6. Data represents the mean numbers of positive nuclei ± standard deviation. * indicates significance between days ($p < 0.05$), where as α indicates significant differences to native skin ($p < 0.05$).

3.4 DISCUSSION

This Chapter focused on investigating the phenotype and morphology of a developing epidermis using a novel 3D approach. Importantly, this is the first work to histologically characterise the HSE model over a nine day period. A crucial benefit of this model is that it allows keratinocyte migration, proliferation and differentiation to be studied simultaneously. As reported herein, the HSE models were cultured at the air-liquid interface for 9 days. Samples were harvested and analysed at days 0, 3, 5 and 9 using MTT, histology and immunohistochemistry. These techniques were used to investigate the HSE model as it undergoes epidermogenesis, including keratinocyte outgrowth over a DED substrate, epidermal development and stratification. In addition, the expression of histologically relevant markers of keratinocyte proliferation and differentiation were investigated. Whilst a wound healing environment would have been more comparable to the epidermogenesis process, native human skin was chosen as a comparison for the HSE model in order to determine if the HSE will develop into a model which is comparable to native tissue. The HSE model was observed to have similar morphology, structure and function to *in vivo* skin (**Figure 3.3**).

The analysis of epidermal outgrowth, as measured by MTT, revealed that the epidermis of most HSEs continually expanded over the DED throughout the experiment (**Figure 3.1**). It was interesting to note, however, that sample 7 stopped expanding between days 5 and 9 (**Figure 3.1 F**). This correlated to the epidermal thickness data, in which the viable cellular layer of the HSE from sample 7 had decreased in thickness and had an increased stratum corneum thickness by day 9. This suggests that the HSE was going through accelerated differentiation (**Figure 3.2 F**). Indeed, all of the HSE models demonstrated evidence of a decreasing viable cell layer and thickening of the stratum corneum by day 9 (**Figure 3.2**). Taken together, these results infer that our HSE model may have a limited lifespan in culture.

The limited lifespan of the cultures may be due to the lack of stratum corneum sloughing in the HSE models, thereby disrupting the skin renewal cycle. Importantly, skin homeostasis is maintained by continual stratum corneum sloughing, as this process stimulates basal cell proliferation and thus epidermal renewal (reviewed by Racila and Bickenbach, 2009). Ponec *et al.* (2002) also reported that excessive stratum corneum thickening occurred in their HSE model cultures over time.

Furthermore, the authors concluded that mechanical sloughing of the upper stratum corneum using a glass microscope slide was effective in both maintaining the stratum corneum and cellular layer at thicknesses equivalent to native skin, whereas chemical sloughing did not have any effect (Ponec *et al.*, 2002). Therefore, a future study incorporating a sloughing protocol as standard HSE culture may both extend the lifespan of the model and maintain the HSE at equivalent proportions to native skin for a longer period of time.

While epidermal sloughing is an important physical process in epidermal homeostasis, the expression of the transcription factor p63 is also thought to be involved in epidermal maintenance (Senoo *et al.*, 2007). In fact research has been conducted into the expression of p63 in the skin since it was determined by Mills *et al.* (1999) and Yang *et al.* (1999) to be essential for epithelial stratification and limb development. McKeon (2004) has previously reviewed the literature available on p63 function and summarised the two main trains of thought regarding its functions. Firstly, p63 is hypothesised to be a differentiation marker as it is essential in the commitment from ectoderm to epidermal lineage development (Mills *et al.*, 1999; Yang *et al*, 1999), while the other argument is that p63 is not a commitment marker, but rather, an indicator of the proliferative potential of epithelial stem cells (Senoo *et al*., 2007). Furthermore, the idea of p63 being a marker of proliferative potential, rather than actively proliferating cells, is also supported by Parsa *et al.* (1999), who detected p63 expression in all basal epidermal keratinocytes and in supra-basal keratinocytes that had not yet entered into terminal differentiation.

Interestingly, Noszczyk and Majewski (2001) demonstrated that p63 is expressed in all nucleated layers of the epidermis during wound healing, which reflects the results obtained in this Chapter (**Figure 3.4**). Of particular interest, I observed that native human skin appeared to have greater regenerative potential than the HSE model and that the same level of p63 expression was maintained in the HSE for most of the experimental time frame (**Figure 3.4**).

Since p63 is an indicator of proliferative potential only, a more specific marker of epidermal proliferation activity was necessary to develop a clearer picture of HSE growth characteristics over the 9 days of culture. Therefore I investigated the expression of ki-67 in both native skin sections and sections of the HSE model (**Figure 3.5**). Ki-67 is a cell cycle marker and its expression is analysed to determine

the proliferative state of a tissue (Noszczyk and Majewski, 2001). Many others have found an increase in basal layer ki-67 expression during wound healing (Mirastschijski *et al.,* 2006; Patel *et al.,* 2006; Usui *et al.,* 2008). The results presented in this Chapter indicate that ki-67 was also expressed in the basal layer of the epidermis, as expected from the results of previous studies (**Figure 3.5 A**; Mirastschikski *et al.,* 2006; Noszczyk and Majewski, 2001; Patel *et al.,* 2006; Usui *et al*., 2008). Of particular interest, the day 3 HSE models expressed significantly more ki-67 than was present in native skin (**Figure 3.5 B – G**). After this time point, however, the number of ki-67 positive nuclei declined. These results are similar to previously published reports, in which ki-67 initially increases during post-wounding re-epithelialisation, before declining to quiescent levels similar to native skin once stratification and maturation have occurred (Betz *et al.,* 1993; Usui *et al.,* 2005).

When the results from the p63 and ki-67 immunohistochemistry are considered together, it appears that the process of culturing the HSE fundamentally changes its proliferation profile from that of native skin (**Figure 3.4** and **Figure 3.5**). Specifically, it appears that the HSE has a higher number of cells actively proliferating (ki-67 positive), even though the number of keratinocytes with proliferative potential (p63 positive) is lower than in native skin. This suggests that the keratinocytes are working to their full capacity to restore the DED with a continuous epithelium.

In addition to the markers of proliferation, the expression of K1 and loricrin as standard indicators of differentiation in both native skin and the HSE model were also investigated. Specifically, K1 is a marker of early differentiation and loricrin is a marker of keratinocytes committed to terminal differentiation (Leigh *et al.,* 1993; Gibbs and Ponec, 2000). Interestingly, the time point when the HSE most resembled native skin in terms of stratum corneum and viable cellular layer thickness ratio (day 5, **Figure 3.2 B – G**) was also the same time point when the K1 expression was most similar between the HSE and native skin (day 5, **Figure 3.6**). This is supported by previously published work from Ponec *et al*. (1991) who described K1 and K10 expression in HSE models as similar to that in native skin. However, the authors also reported that their HSE models had greater immunoreactivity for the terminal differentiation markers, involucrin and filaggrin, which are expressed in the same epidermal region as loricrin (Ponec *et al.,* 1991). It appears therefore that the

transition of keratinocytes from a proliferating to a differentiating phenotype is similar between HSE models and native skin. There does, however, appear to be an enhanced commitment to terminal differentiation in the HSE model, indicated by loricrin expression, in comparison to native skin.

As noted above, K1 expression in the HSE was most similar to native skin at day 5. This was, however, the time point in which loricrin expression in the HSE was most different to native skin (**Figure 3.7**). Loricrin is expressed in keratinocytes which are committed to becoming a part of the stratum corneum (Gibbs and Ponec, 2000). More diffuse immunoreactivity of loricrin was observed in the HSE model than in native skin (**Figure 3.7**). Conincidentally, proliferation was also enhanced in the HSE (**Figure 3.5**). This could thereby encourage terminal differentiation, resulting in excessive thickening of the stratum corneum (**Figure 3.2**).

As discussed previously, Ponec *et al.* (2002) demonstrated that mechanical sloughing of the epidermis resulted in maintenance of the viable cellular layer and reduced excessive stratum corneum thickening. This may also affect expression of loricrin and other terminal differentiation markers. Interestingly, Gibbs *et al*. (1998) found that HSE models grown at 33° C (the temperature of human skin) as opposed to 37° C (cell culture temperature) had decreased levels of loricrin expression which more closely mimicked native skin. Furthermore, Gibbs *et al.* (1998) demonstrated that the presence of fibroblasts in the HSE model affected differentiation marker immunoreactivity. In addition, it has previously been reported that incorporating fibroblasts into the DED increased the lateral migration of keratinocytes across the DED, increased the number of ki-67 positive keratinocytes and decreased the expression of K16 in the epidermis. Thus, it is clear the multiple HSE culture factors can influence the development of the epidermis.

The final standard immunohistological marker I analysed and found to be expressed in the HSE model was K16. This was expected as the epidermogenesis process results from hyper-proliferation activity. Furthermore, K6, which co-expresses with K16, has been detected in HSE models within our research group and had been previously reported (Borg *et al.,* 2009; Kairuz *et al.,* 2007; Topping *et al.,* 2006). However, it was an unexpected finding to observe K16 immunoreactivity in the native skin sections (**Figure 3.8**). A review of the literature revealed that K16 should only be present during hyper-proliferation events, such as wound healing,

epithelialisation and disease states such as psoriasis and certain cancers (Gibbs and Ponec, 2000; Paladini *et al.*, 1995, Patel *et al.*, 2006; Usui *et al*, 2009).

Due to the discrepancy in expected K16 expression, the skin collection process was re-examined and I noted that native skin was transferred into a fixing solution (formalin) three hours post-surgery, at the very earliest. In studies on mouse skin, Bernot *et al.* (2002) reported that K16 was detectable in the skin histology sections 6 hours post-injury. Myers *et al.* (2007) created suction blister wounds in volunteers, analysed wound-area biopsies and found K16 was expressed in the skin sections 6 hours after the initial injury event, which was the earliest time point analysed. Castelijns *et al*. (1999) reported K16 present in normal human skin 24 and 48 hours post tape-stripping, a mild form of skin aggravation which removes the outer layers of the stratum corneum with general-use adhesive tape. It should also be noted that Castelijns *et al.* (1999) detected K16 expression using the same antibody clone as I used in my studies. Therefore, it is possible that the skin collection process, or even the use of general anaesthesia, induces a trauma response within the donor and/or their skin. Furthermore, it is also possible that 3 hours is sufficient time for the induction of K16 expression, thereby explaining the K16-positive immunoreactivity in native skin samples which were not expected to express K16 (**Figure 3.8**). At the moment, it is not known if K16 expression is induced in the native skin pre-surgery or post-surgery, during the skin removal and transportation process. The examination of K16 expression in sections of native skin fixed immediately after removal from the skin donor are currently underway in our laboratory and should provide more information on when K16 is expressed.

In conclusion, our HSE model does not incorporate sloughing, an important factor in skin homeostasis. Additionally, the HSE model utilised for this study did not contain fibroblasts, which have recently been demonstrated as crucial for epidermal-dermal cross-talk (Tara Fernandez, unpublished data). Nonetheless, the keratinocyte only HSE is similar to native skin and while variability exists between models, it appears to be an effective tool to study skin *in vivo*. Furthermore, K16 is important in terms of wound healing and is expressed in this model, thus the HSE may also be an effective model to study wound healing.

Chapter 4: Analysis of molecular changes during epidermogenesis of the HSE model

4.1 INTRODUCTION

Gene microarrays are an invaluable tool for the investigation of the global gene expression profile in biological samples. They are commonly employed to help determine the molecular changes that occur within a sample in response to various treatments or disease states. Currently there are a limited number of studies investigating human skin equivalent (HSE) models using gene microarrays (Holland *et al.,* 2009; Hu *et al.,* 2010; Koria and Andreadis, 2006; Kurata *et al.,* 2010; Mazar *et al.,* 2010). Previously published HSE-microarray studies include investigation of the innate skin immune response in reaction to commensal and pathogenic bacteria colonisation (Holland *et al*., 2009). In addition, gene microarrays have been used to determine the metabolic pathways of a HSE model in comparison to native skin, comparing commercially available EpiDerm™ HSE model with human skin biopsies (Hu *et al*., 2010). Genes involved in keratinocyte differentiation in HSE models have also been analysed by comparing submerged HSE models to HSEs cultured at the air-liquid interface (Koria and Andreadis, 2006; Mazar *et al.,* 2010). Similarly, UVB-induced inflammatory processes involved in pigmentation and erythema (Kurata *et al*., 2010) have been investigated using gene microarray approaches. The changes that occur at the transcriptional level have not, however, been investigated in a HSE model undergoing epidermogenesis.

In order to more completely understand the capabilities of the HSE as a model to study skin in response to specific treatments or applications, an analysis of the transcriptional processes that occur in the HSE model during epidermogenesis is an important step. As reported in Chapter 3, the HSE model was demonstrated to be histologically comparable to native human skin. In this Chapter I report my investigations into the molecular changes during epidermogenesis of the HSE model through the use of gene microarrays and functional ontology analysis of the differentially regulated genes.

4.2 METHODS AND MATERIALS

Full details of the materials and methods used in the experimental procedures for this Chapter are fully described in Chapter 2. Herein is a brief summary of the procedures used to generate the data presented in section 4.3.

4.2.1 Generation and culture of human skin equivalent models

HSE models were generated using skin obtained from three individuals undergoing elective cosmetic breast reduction or abdominoplasty surgeries as fully described in sections 2.4 - 2.6. Following generation of the HSE models, they were cultured at the air-liquid interface and maintained in Full Greens (FG) culture media. The media was replenished daily to maintain the HSE culture at the air-liquid interface and was fully replaced once per week.

4.2.2 Extraction of RNA from the HSE model epidermis

HSE models were harvested at days 0, 3, 5 and 9. At each of these time points RNA extraction was performed by isolating the epidermis in Trizol. For specific details of the RNA extraction protocol, please refer to section 2.12.1.

4.2.3 Microarray analysis of differential gene expression

To perform the gene microarray analysis, 1 µg of total RNA was required. Due to the low amounts of RNA which could be isolated from the HSEs, it was necessary to pool the RNA from these three individuals. To maintain consistency with further experimentation (immunohistochemistry analysis), all subsequent data from these three individuals was pooled and they were denoted as the group A samples. The pooled RNA was sent to the microarray facility at the Institute for Molecular Biosciences at the University of Queensland and the gene microarray procedure and data collection was performed by Dr Katia Nones. The Illumina Human HT-12 v3 Expression BeadChip microarray (Illumina) was utilised to determine genes which were differentially expressed during epidermogenesis. For full details of this process, please refer to section 2.12

4.2.4 Microarray data analysis

The microarray data was analysed in GeneSpring GX 10.0.2 (Agilent Technologies) and this was performed at the University of Western Australia with

generous help and guidance received from Daniel Haustead. Full details of the microarray data analysis methods can be found in section 2.12.2

4.2.5 Gene Ontology and Functional Network Analysis

IPA tools (Ingenuity Systems) were utilised to examine Gene Ontology and Functional Network Analysis of the microarray data. Please refer to section 2.12.3 for the full details of this process.

4.3 RESULTS

4.3.1 General data observations

Analysis of the gene microarray data was performed to investigate the temporal changes in the gene expression profile as the HSE model underwent epidermogenesis. Following analysis, pre-processing and normalisation of the microarray data in GeneSpring, a list of 2,611 genes that were differentially expressed in the HSE model throughout the course of the experiment was generated.

Heat map analysis of the gene microarray data revealed a large temporal variation in gene expression within the developing HSE model (**Figure 4.1**). Furthermore, the gene expression 'signature' of the day 0 samples is clearly different to any other time point, indicating that all other time points are more similar to each other than they are to day 0 (**Figure 4.1**).

4.3.2 Differential gene expression

The number of genes differentially expressed during epidermogenesis was analysed using Venn diagrams and sorted based on up- or down-regulation status (**Figure 4.2**). All gene expression levels were normalised to the expression levels present at day 0. Venn diagrams were also produced to determine the overlap of genes differentially expressed during epidermogenesis. This revealed that the number of genes differentially regulated during epidermogenesis increased over time and that some genes were either up- or down-regulated at all three time points (**Figure 4.2**). Therefore, epidermogenesis clearly involves a large amount of differential gene regulation over time.

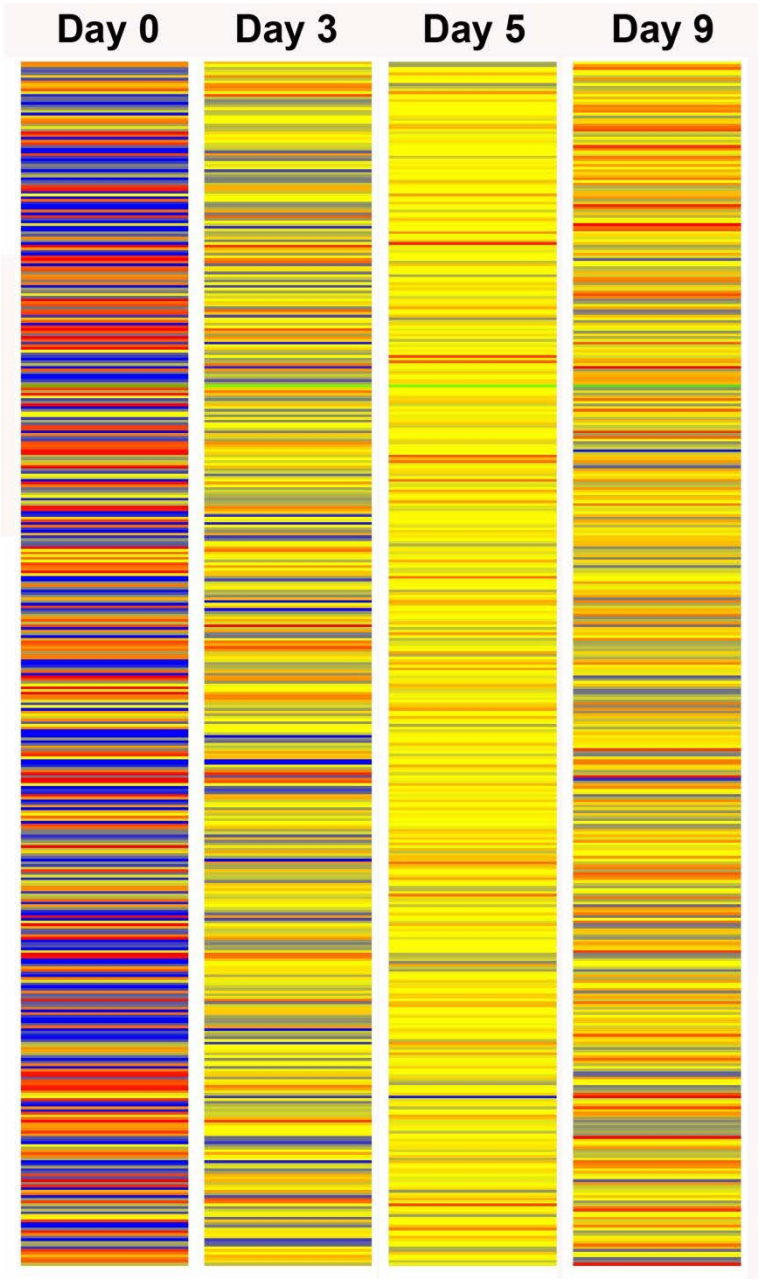

Figure 4.1 Heat-map of genes differentially expressed in the HSE as determined by microarray analysis
The heat-map provides visual representation of all genes differentially regulated during epidermogenesis as determined by the microarray analysis. The colour scale indicates the normalised gene expression intensity; low gene expression is blue and high gene expression is red. Unchanged gene expression is yellow.

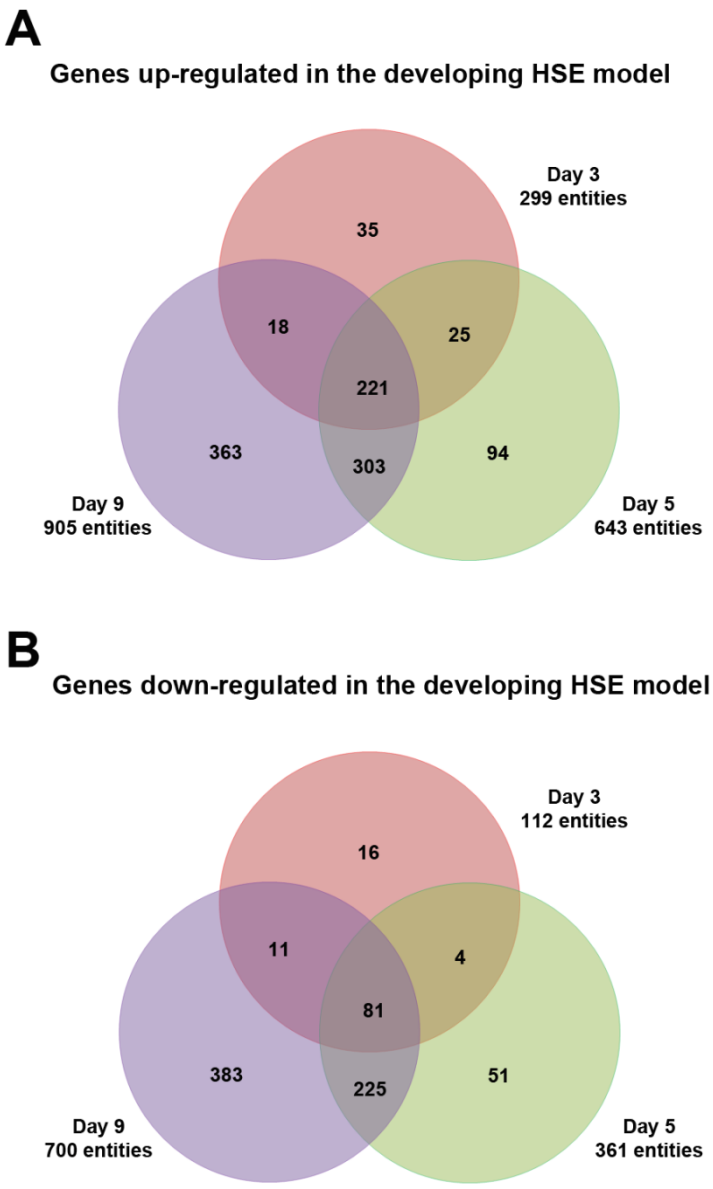

Figure 4.2 Genes differentially expressed by during epidermogenesis of the HSE model as determined by microarray analysis
The Venn diagram visually represents the number of genes commonly or uniquely expressed at each time point. The Venn diagram is separated by either (**A**) genes down-regulated during epidermogenesis, or (**B**) genes up-regulated during epidermogenesis. Only genes > 1.5 fold differentially regulated were included.

4.3.3 Gene Ontology and Functional Analysis of Microarray data

4.3.4 Genes relating to molecular and cellular functions

The gene microarray analysis in sections 4.3.1 and 4.3.2 reported the number of genes differentially regulated in HSEs undergoing epidermogenesis. In order to elucidate the relationships between these differentially regulated genes, the IPA knowledge base was employed. The gene expression data was normalised to the day 0 sample and genes which were at least ± 1.5 fold differentially regulated in the HSE model were uploaded into the IPA software. This resulted in the generation of a list of functional groups under the umbrella of molecular and cellular functions which were affected during epidermogenesis (*Table 4.1* - *Table 4.3*). IPA software-driven functional analysis of the microarray data utilises the information about the genes to assign biological functions which are differentially regulated during HSE model development. The data generated from IPA analysis (*Table 4.1* - *Table 4.3*) was uploaded into Cytoscape®, an open-source network visualisation tool, to view the temporal changes in the functional data over time (**Figure 4.3**).

Interestingly, the number of genes associated with many of the functions which exhibited significant change during epidermogenesis progressively increased from days 3 until 9 (**Figure 4.4**). These included functions such as 'cellular growth and proliferation' and 'DNA replication, recombination and repair', suggesting that these functions are important and are altered in the HSE model undergoing epidermogenesis. Other noteworthy functional ontologies were 'drug metabolism' and 'vitamin and mineral metabolism', which remained fairly constant in terms of the number of associated genes which exhibited altered expression throughout the course of the experiment (**Figure 4.4**). This suggests that these metabolism-related functions may not be greatly altered, or may not be particularly important, to the overall epidermogenesis process in the HSE model.

Table 4.1 Ontology of differentially expressed genes at day 3

Molecular and Cellular Functions	**Significance P-value**	**# genes**
Lipid Metabolism	3.29E-09 – 1.27E-02	78
Molecular Transport	3.29E-09 – 1.30E-02	67
Small Molecule Biochemistry	3.29E-09 – 1.30E-02	93
Cellular Movement	2.33E-07 – 1.30E-02	70
Vitamin and Mineral Metabolism	1.46E-06 – 1.20E-02	29

Table 4.2 Ontology of differentially expressed genes at day 5

Molecular and Cellular Functions	**Significance P-value**	**# genes**
Cell Cycle	1.57E-14 – 9.91E-03	142
Cellular Assembly and Organization	1.57E-14 – 7.63E-03	78
DNA Replication, Recombination, and Repair	1.57E-14 – 9.45E-03	94
Lipid Metabolism	2.50E-09 – 8.47E-03	131
Small Molecule Biochemistry	2.50E-09 – 8.47E-03	163

Table 4.3 Ontology of differentially expressed genes at day 9

Molecular and Cellular Functions	**Significance P-value**	**# genes**
Cell Cycle	1.39E-17 – 3.07E-03	244
Cellular Assembly and Organization	1.39E-17 – 2.93E-03	210
DNA Replication, Recombination, and Repair	1.39E-17 – 1.82E-03	181
Cellular Development	2.40E-13 – 2.93E-03	326
Cellular Growth and Proliferation	2.40E-13 – 2.93E-03	402

Data presented in these tables contains a range of p-values as each molecular and cellular functions category contains multiple sub-groups and each sub-group has a p-value assigned to it.

.

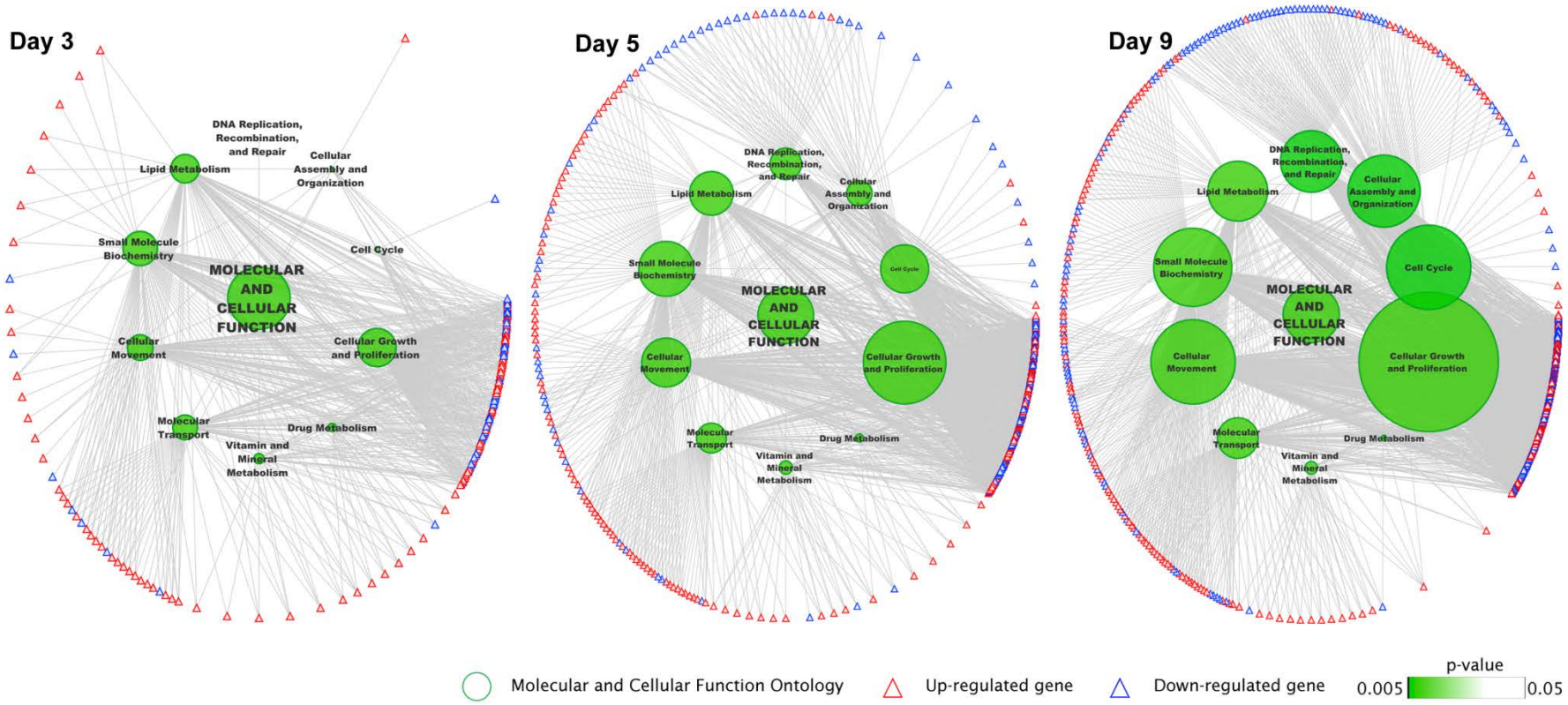

Figure 4.3 Visual representations of the temporal changes in molecular and cellular functions ontology during epidermogenesis in the HSE model
Genes with p - values < 0.05 and more than 1.5 fold change in expression in the HSE model were imported to IPA to generate functional gene associations. This functional data was then up-loaded into the open source software, Cytoscape®, to visually represent the data. Down-regulated genes are represented by the blue triangles, whereas up-regulated genes are represented by the red triangles. The intensity of the green colour indicates p-value and the size of the function ontology circle represents the relative number of genes associated with it.

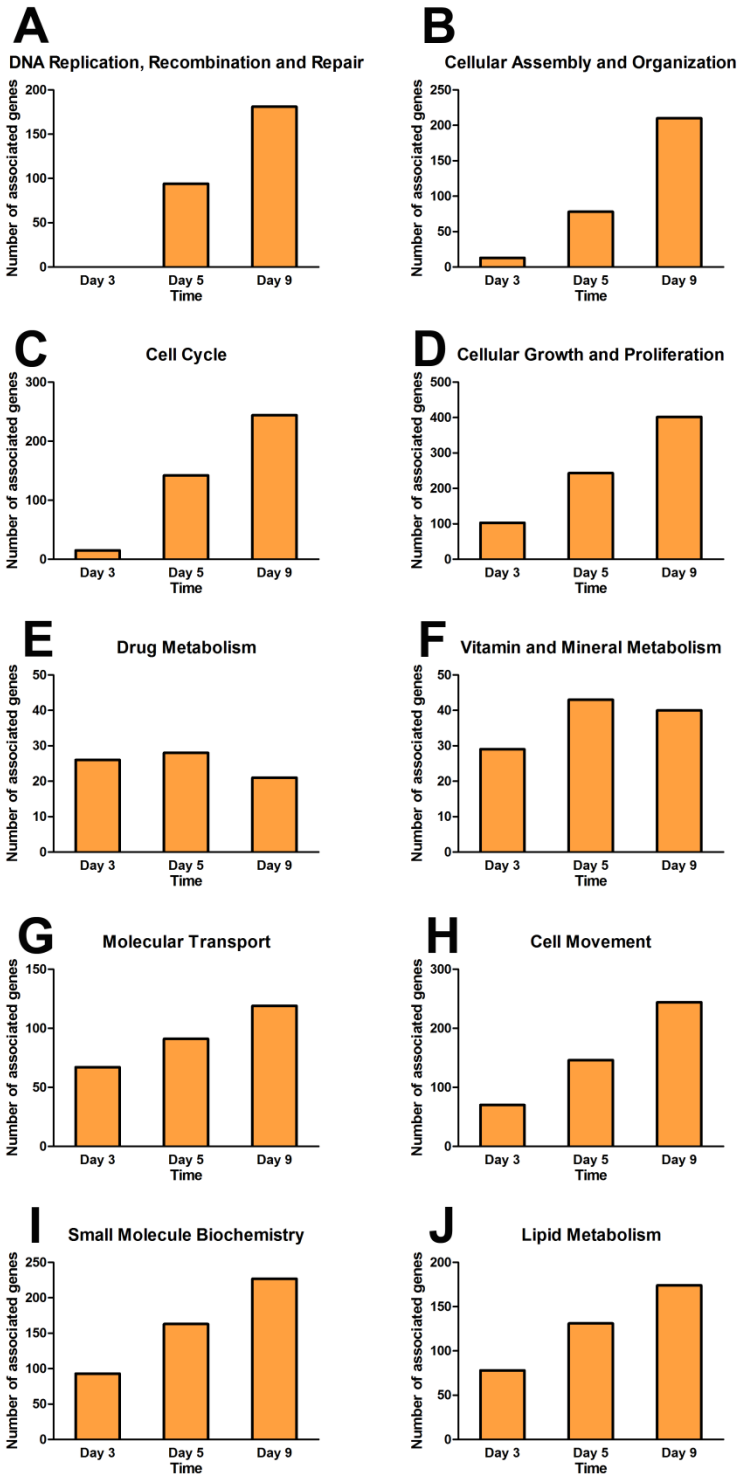

Figure 4.4 Graphical representations of the temporal changes in molecular and cellular functions ontology during epidermogenesis in the HSE model
Graphical representation of ontologies significantly influenced by epidermogenesis in the HSE model over time. The bars represent the number of genes relating to the ontologies (**A**) DNA replication, recombination and repair, (**B**) cellular assembly and organization, (**C**) cell cycle, (**D**) cellular growth and proliferation, (**E**) drug metabolism, (**F**) vitamin and mineral metabolism, (**G**) molecular transport, (**H**) cell movement, (**I**) small molecule biochemistry and (**J**) lipid metabolism.

4.3.5 Functional network analysis

Functional network diagrams were created in IPA tools and were generated from the microarray data input from each time point. The program determines functional network pathways based on the genes up- or down-regulated in the HSE model during epidermogenesis. Furthermore, the data generated is different from previous functional analyses reported in this Chapter as it creates networks based on individual genes, rather than on functional ontology. Analysis of the networks generated at days 3, 5 and 9 revealed the consistent association of the following networks: 'dermatological diseases and conditions, 'cellular assembly and organization', 'cell cycle' and 'DNA replication, recombination and repair'. The top 5 molecular and cellular functional networks for each time point are listed in Appendix Table A17 – Table A19 and the interactions of the genes within these networks are presented in Appendix Figures A1 – A9. These relevant networks were further investigated in sections 4.3.6 - 4.3.10.

4.3.6 Comparison of gene microarray data to molecules of interest investigated in Chapter 3

In Chapter 3, standard markers of skin morphology, namely p63, ki-67, keratin 1 (K1), loricrin and K16, were investigated using immunohistochemistry. Significant increases in the expression of these proteins between time points were described in section 3.3. The list of genes deemed to be significantly differentially regulated in the top 10 functional ontologies (visualised in **Figure 4.3**) were examined to determine if the genes correlating to the previously investigated markers of skin morphology were also differentially regulated.

Interestingly, only the K1 gene (*KRT1*) was observed to be significantly differentially regulated. *KRT1* was associated with two of the functional ontology groups; 'small molecule biochemistry' (*Table 4.4*) and 'vitamin and mineral metabolism' (*Table 4.5*). As expected, *KRT1* was up-regulated at all three time points when normalised to day 0. However, none of the other genes corresponding to the other protein markers of skin morphology were significantly differentially regulated at any of the time points analysed.

Table 4.4 Focus genes differentially expressed in the HSE during epidermogenesis within the 'Small molecule biochemistry' data set

Time	Focus Genes
Day 3	ABCG1, ACER1, ACPP, ACSL1, ACSS2, AKR1B10, AKR1C1/AKR1C2, AKR1C3, AKR1C4, ALDH1A1, ALDH3A1, ALOX12B, ALOX15B, ANGPTL4, ARG1, ASS1, ATF3, BLMH, CD36, CFD, CGA, CLDN7, CPE (includes EG:12876), CPT1A, CRABP2, CXCL1, CXCL14, CYB5A (includes EG:109672), CYP2C18, CYP3A5, DEFB4A/DEFB4B, DHCR24, DHRS9, DLK1, EDN1, EEF1A2, ELOVL7, FABP5, FDPS, FOXA1, GAL, GJB2, GK, GM2A, GSN, GSTA4, IDE, IGFBP3, IGFBP5, IL24, IL8, **KRT1**, LPIN1, MMP7, MMP9, MSMO1, NCEH1, NMU, PCCA, PCSK6, PDGFA, PDK4, PHGDH, PLA2G3, PLA2G4F, PLAUR, PLIN2, PTGES, PTGS1, PYCARD, RBP1, RDH12, RGS2 (includes EG:19735), RORA, RRM2, SC5DL, SCD, SCG5, SCNN1A, SCNN1B, SLC7A2, SLC7A5, SNTB1, SPTSSB, SREBF1 (includes EG:176574), SRM, STC1, THBS1, THRSP, TIMP1, TNFSF10, TYMS, VSNL1
Day 5	AADAC, ABCA12, ABCG1, ABCG4, ACER1, ACOT9, ACPP, ACSBG1, ACSL1, ACSS2, ADRB2, AK1, AKR1B10, AKR1C1/AKR1C2, AKR1C3, AKR1C4, ALDH1A1, ALDH1A3, ALDH2, ALDH3A1, ALDH5A1, ALOX12, ALOX12B, ALOX15B, ANGPTL4, APOD, AQP9, ARG1, ASS1, ATP11B, ATP7A, BCL6, BID, BLM, BLMH, BMP6, BRE, CAV1, CCNB1, CD36, CDK1, CEBPA, CEBPB (includes EG:1051), CERK, CERS4, CES1, CFD, CGA, CHPT1, CIDEA, CLDN7, CPE (includes EG:12876), CRABP2, CROT, CTPS, CTSD, CXCL1, CXCL14, CYB5A (includes EG:109672), CYP2C18, CYP3A5, CYP4F12, CYP4F2, CYP4F3, DEGS2, DGAT2, DHCR24, DHRS4, DHRS9, DKK1, DLK1, EDN1, EEF1A2, ELOVL1, ELOVL3, ELOVL4, ELOVL7, ENTPD3, ERBB2, ETNK2, FABP5, FASN, FDPS, FGFR3, FOXA1, G6PD, GBA, GK, GM2A, GSN, GSTA4, HMGCL, HOMER2, HSPD1, IDE, IGFBP7, IL8, KITLG, **KRT1**, LPIN1, LRP10, MAPK3, MITF, MMP9, MVD, NCEH1, NMU, NRG1 (includes EG:112400), NT5E, OAT, OGDH, PANK1, PCCA, PDGFA, PFAS, PGD, PHGDH, PIK3C2B, PKM2, PLA2G3, PLA2G4F, PLAUR, PLCD1, PLSCR1, POR, PRDX3, PTGER4, PTGES, PTGS1, PTH2R, PTTG1, PYCARD, RBP1, RDH12, RFC3, ROCK2, RORA, RRM2, RRM2B, RUNDC3A, SCD, SCNN1A, SCNN1B, SDR16C5, SMOX, SMPD3, SOX9, SPTSSB, SQLE, SREBF1 (includes EG:176574), SRM, STC1, SULT2B1, TBX21, TECR, THBS1, THRSP, TIMP1, TNFSF10, TNNT2 (includes EG:21956), TYMS, VIPR1, YWHAH
Day 9	AADAC, ABCA1, ABCA12, ABCG1, ABCG4, ACADVL, ACAT1, ACER1, ACOT9, ACPP, ACSBG1, ACSL1, ADORA2B, ADRB2, ADSL, AGPS, AHCY, AKR1B10, AKR1C1/AKR1C2, AKR1C4, AKT1, ALDH1A1, ALDH1A3, ALDH2, ALDH3A1, ALDH3A2, ALDH5A1, ALOX12, ALOX12B, ALOX15B, ANGPTL4, AQP3, AQP9, ARG1, ASS1, ATP11B, ATP7A, BAX, BID, BLM, BRCA1, C1QBP, CASP3, CAV1, CBS, CCNB1, CD36, CDK1, CDK4, CEBPA,

	CEBPB (includes EG:1051), CERS2, CERS3, CERS4, CES1, CGA, CH25H, CHPT1, CLDN7, CLN8, CPE (includes EG:12876), CPT2, CTPS, CTSD, CXCL1, CXCL14, CYP2C18, CYP2J2, CYP2R1, CYP3A5, CYP4F12, CYP4F3, DAGLB, DCTPP1, DECR1, DEFB4A/DEFB4B, DEGS2, DGAT2, DHCR24, DHRS4, DHRS9, DKK1, DKK3, DLK1, DNMT1, DUSP1, EDN1, EEF1A2, ELOVL1, ELOVL3, ELOVL4, ELOVL7, ENTPD3, ERBB2, ETNK2, FA2H, FABP5, FGFR3, FOS, FOXA1, FOXO3, GAL, GART, GBA, GGH, GGPS1, GJA1, GK, GNA11, GNAI1, GPX1 (includes EG:14775), GRHL3, GSN, GSTA4, HMGCL, HMGCR, HMOX1, HOMER2, HPGD, HPRT1, HSPD1, IDE, IFRD1, IGFBP7, IL33, IL8, KDM3A, KIF20B, KITLG, **KRT1**, LGALS8, LRP10, MAP3K8, MAPK14, MAPK9, ME1, MET, MID1IP1, MMP9, MSH6, MSMO1, MTHFD1L, MTHFS, NAMPT, NCEH1, NCOA1, NME2, NMNAT3, NMU, NPR2 (includes EG:116564), NRF1, NRG1 (includes EG:112400), NT5E, NUDT15, OAS1, OAT, OSBPL2, PANK1, PARP1, PCCA, PDGFA, PDPN (includes EG:10630), PFAS, PHGDH, PIK3C2B, PKM2, PLA2G3, PLA2G4F, PLAUR, PLD1, PLSCR1, PNPLA8, POR, PPAP2A, PRDX3, PRPS1, PTGER3, PTGER4, PTGES, PTGES2, PTGS1, PTGS2, PTHLH, PTTG1, PYCARD, RBP1, RDH12, RDH16, RFC3, RGS17, RORA, RRM2, RUNDC3A, RXRA, SC5DL, SCD, SCG5, SCNN1A, SCNN1B, SDR16C5, SLC1A3, SLC25A19, SLC25A4, SMPD3, SNTB1, SPHK1, SPTSSB, SQLE, SREBF1 (includes EG:176574), STC1, SULT2B1, TAP1, TFAM, THRSP, TIMP2 (includes EG:21858), TK1, TMEM97, TNFRSF12A, TNFSF10, TNNT2 (includes EG:21956), TXNIP, TYMS, UGCG, VIPR1, VLDLR, YWHAH, ZBTB16

Genes of interest are presented in **bold underlined** type. Up-regulated genes are highlighted in red, whereas down-regulated genes are highlighted in blue.

Table 4.5 Focus genes differentially expressed in the HSE during epidermogenesis within the 'Vitamin and mineral metabolism' data set

Time	Focus Genes
Day 3	ABCG1, AKR1B10, AKR1C1/AKR1C2, AKR1C3, AKR1C4, ALDH1A1, CD36, CGA, CRABP2, CYP3A5, DHCR24, DHRS9, EDN1, ELOVL7, FDPS, FOXA1, **KRT1**, MMP9, MSMO1, NCEH1, PLAUR, PLIN2, RBP1, RDH12, SC5DL, SCD, SREBF1 (includes EG:176574), STC1, TNFSF10
Day 5	ABCG1, AKR1B10, AKR1C1/AKR1C2, AKR1C3, AKR1C4, ALDH1A1, ALDH1A3, ALOX12, BMP6, BRE, CAV1, CEBPA, CGA, CRABP2, CYP3A5, CYP4F2, DHCR24, DHRS4, DHRS9, EDN1, ELOVL7, FDPS, FOXA1, G6PD, GGH, IGFBP7, KITLG, **KRT1**, MMP9, MTHFD1L, MVD, PLAUR, POR, RBP1, RDH12, SCD, SDR16C5, SQLE, SREBF1 (includes EG:176574), STC1, SULT2B1, TNFSF10, YWHAH
Day 9	ABCA1, ABCG1, AKR1B10, AKR1C1/AKR1C2, AKR1C4, ALDH1A1, ALDH1A3, C1QBP, CAV1, CEBPA, CGA, CH25H, CLN8, CYP2J2, CYP2R1, CYP3A5, DHCR24, DHRS4, DHRS9, DKK3, EDN1, FOXA1, GGPS1, HMGCR, **KRT1**, MMP9, MSMO1, PLAUR, POR, RBP1, RDH12, RDH16, SDR16C5, SQLE, SREBF1 (includes EG:176574), STC1, SULT2B1, TNFRSF12A, TNFSF10, YWHAH

Genes of interest are presented in **bold underlined** type. Up-regulated genes are highlighted in red, whereas down-regulated genes are highlighted in blue.

4.3.7 Investigation of genes relating to physiological system development and function

As noted earlier, the focus of this Chapter was to investigate changes in gene expression during epidermogenesis in a HSE model. With this in mind, functional groups of genes (as determined by IPA) associated with epidermal development were further investigated. The 'hair and skin development and function' data set was determined to be particularly relevant to epidermogenesis in a HSE model and was further investigated (*Table 4.6*). The number of focus genes in this particular data set increased as the HSE model developed (*Table 4.6*). Similarly, 'tissue development' was considered to be another highly relevant functional category since the epidermis is a highly complex tissue which forms through a process of proliferation, stratification and differentiation. Similarly, the number of focus genes in the 'tissue development' category continually increased as the experiment progressed (*Table 4.6*).

4.3.8 Investigation of genes from the 'hair and skin development and function' data set

The genes of interest correlating to the proteins investigated in Chapter 3 were analysed in the list of 'hair and skin development and function' focus genes. The proteins from Chapter 3 were p63, ki-67, K1, loricrin and K16 and correlate to the genes *TP63*, *MKI67*, *KRT1*, *LOR*, and *KRT16*. The gene *KRT1* was found to be significantly up-regulated at all three time points as described previously in section 4.3.6. Interestingly, genes correlating to other standard markers of skin development outlined in **Figure 1.1**, namely K15 (*KRT15*), K10 (*KRT10*), filaggrin (*FLG*) and envoplakin (*EVPL*) were found to be differentially regulated within the microarray data (*Table 4.7*). As expected, basal cell marker, *KRT15* was down-regulated at day 9, whereas terminal differentiation makers (*FLG* and *EVPL*) were up-regulated at days 3, 5 and 9. This suggests that the gene expression of some of the standard markers of skin development changes over time in the developing HSE model as expected.

Table 4.6 Ontology of differentially expressed genes in the HSE that are involved in 'hair and skin development and function'

	Time	P-value range	Focus Genes
Hair and Skin Development and Function	Day 3	1.74E-05 – 1.20E-02	28
	Day 5	2.02E-06 – 9.34E-03	57
	Day 9	1.39E-08 – 4.60E-04	69
Tissue Development	Day 3	1.74E-05 – 1.20E-02	56
	Day 5	2.02E-06 – 9.34E-03	108
	Day 9	1.39E-08 – 3.07E-03	154

Table 4.7 Focus genes differentially expressed in the HSE during epidermogenesis within the 'hair and skin development and function' data set

Time	Focus Genes
Day 3	ALOX12B, CASP14, CD36, CRABP2, CSTA, CTGF, CXCL1, CYR61, DHCR24, DSC1, FABP5, FLG, FOXM1, IGFBP5, IL8, KLK5, **KRT1**, KRT10, KRT2, KRT9, MMP9, PDGFA, PTGS1, SPINK5, TGM3, THBS1, TIMP1, TNFSF10
Day 5	ABCA12, ADRB2, ALOX12B, ASPRV1, ATP7A, AURKB, CALML5, CASP14, CD36, CDC25A, CDC25B, CDSN, CKAP2, CRABP2, CSTA, CTGF, CXCL1, DHCR24, DKK1, DLX3, DSC1, ELOVL3, ELOVL4, EMP1, ERBB2, EVPL, FABP5, FLG, FOXM1, FST, HPSE, ID1, IL8, KITLG, KLK6, **KRT1**, KRT10, KRT2, KRT34, KRT9, MITF, MMP1 (includes EG:300339), MMP9, PBK, PDGFA, PLCD1, PRSS8, PTGS1, PTTG1, ROCK2, SOX9, SPINK5, TGM3, TGM5, THBS1, TIMP1, TNFSF10
Day 9	ABCA12, ACVR1B, AKT1, ALOX12B, AQP3, ASPRV1, ATP7A, AURKB, CALML5, CASP14, CASP3, CBS, CCND3, CDC25A, CDC25B, CDSN, CERS3, CKAP2, CSTA, CTGF, DHCR24, DKK1, DLX3, DSC1, ELOVL3, ELOVL4, EMP1, EVPL, FABP5, FLG, FOXM1, FST, GRHL3, HBP1, HPSE, ID1, JUP, KLF4, KLF5, **KRT1**, KRT10, KRT13, KRT15, KRT2, KRT34, KRT9, LAMC2, MAPK9, NME2, OVOL1, PBK, PDGFA, PLOD3, PRDM1, PRSS8, PTGS1, PTGS2, PTHLH, PTTG1, RBM38, RXRA, SPHK1, SPINK5, TGM1, TGM3, TGM5, TNFSF10, TXNIP, UGCG

Genes of interest are presented in **bold underlined** type whereas genes used as standard markers of skin development are presented in underlined type. Up-regulated genes are highlighted in red, whereas down-regulated genes are highlighted in blue.

4.3.9 Investigation of genes from the 'tissue development' data set

Similar to the 'hair and skin development and function' data set, only *KRT1* from the Chapter 3 targets of interest was present in the list of focus genes relating to 'tissue development' (*Table 4.8*). Other genes relating to skin development, however, were found to be significantly differentially regulated during the course of the experiment under this functional ontology. These genes were *KRT15*, *KRT9*, *KRT10*, *FLG* and *EVPL* (*Table 4.8*) and the trend in expression levels were as described in section 4.3.8. Once more, this highlights the expected differential gene expression of other standard markers of epidermogenesis over time in the developing HSE model.

Table 4.8 Focus genes differentially expressed in the HSE during epidermogenesis within the 'tissue development' data set

Time	Focus Genes
Day 3	ADAMTS1, ALDH1A1, ALOX12B, ANGPTL4, ARG1, CA2, CASP14, CD36, CD97, CRABP2, CTGF, CXCL1, CXCL14, CYR61, DHCR24, DSC1, EDN1, F3, FABP5, FLG, FOXA1, FOXM1, GCNT3, GJB2, GSN, ID3 (includes EG:15903), IDE, IGFBP3, IGFBP5, IL8, KLK3, KLK5, **KRT1**, KRT10, KRT2, KRT8, KRT9, LPIN1, MMP9, PDGFA, PITX1, PLAUR, QPCT, SEMA3F, SERPINA3, SPINK5, SREBF1 (includes EG:176574), STC1, TGM3, THBS1, TIMP1, TM7SF2, TNFSF10, TNNC1, TNNT2 (includes EG:21956), VSNL1
Day 5	ABCA12, ACP5, ADAM8, ADAMTS1, ALDH1A1, ALDH1A3, ALOX12B, ANGPTL4, ANXA9, ARG1, ASPRV1, ATP7A, BCAR3, BCL6, BMP6, CALML5, CASP14, CAV1, CD36, CDC25B, CDSN, CEACAM1 (includes others), CEBPA, CEBPB (includes EG:1051), CITED2, CLIP3, CRABP2, CRNN, CTGF, CXCL1, CYBA, CYFIP2, CYR61, DHCR24, DKK1, DLGAP5, DLX3, ECT2, EDN1, EMP1, EPCAM, ERBB2, EVPL, F3, FABP5, FASN, FBXO5, FEN1, FGFR3, FLG, FOXA1, FOXM1, FST, G6PD, GCNT3, GJB2, GSN, HAS3, HPSE, ID1, ID3 (includes EG:15903), IL8, ISL1, ITGAM (includes EG:16409), KITLG, KLK3, KLK6, **KRT1**, KRT10, KRT2, KRT34, KRT8, KRT9, LPIN1, MAP2, MAPK3, MFGE8, MITF, MMP9, MPZL2, NCAPG2, NRG1 (includes EG:112400), NUSAP1, PDGFA, PIM1, PITX1, PLAUR, POLD4, PRSS8, PTGES, SEMA4D, SKP2 (includes EG:27401), SLC11A2, SMPD3, SOX9, SPINK5, SREBF1 (includes EG:176574), STC1, STMN1, TGM3, TGM5, THBS1, TIMP1, TM7SF2, TNFSF10, TNNC1, TNNT2 (includes EG:21956), WNT5A,
Day 9	ABCA1, ABCA12, ACP5, ACVR1B, ADAMTS1, AKT1, ALOX12B, ANGPTL4, ARG1, ARHGAP24, ASPRV1, ATP7A, AXL, BID, BIRC5, CALML5, CASP14, CASP3, CAV1, CBS, CCM2, CCND3, CD36, CDC25B, CDK2, CDK4, CDSN, CEACAM1 (includes others), CEBPA, CENPF, CERS3, CITED2, CLCN3, CLIP3, CTGF, CTSH, CXCL1, CYBA, CYR61, DHCR24, DKK1, DLGAP5, DLX3, DLX5, DUSP1, ECT2, EDN1, EFEMP1, EGR3, ELOVL4, EMP1, EPHB3, ERBB2, ERBB3 (includes EG:13867), EVPL, F3, FABP5, FBXO5, FGFR3, FLG, FOXA1, FOXM1, FOXO3, FST, FSTL1, GDA, GJB2, GPX1 (includes EG:14775), GRHL3, HAS3, HELLS, HMGB2, HMOX1, HOPX, HPSE, ID1, ID3 (includes EG:15903), IL8, ISL1, JUN, JUP, KITLG, KLF4, KLF5, KLK3, **KRT1**, KRT10, KRT13, KRT15, KRT2, KRT34, KRT9, LAMC2, LMNB1, LMNB2, LY6E, MAP2, MAPK7, MAPK9, MET, MMP9, MYCN, NFIB, NME2, NRG1 (includes EG:112400), NRP1 (includes EG:18186), NUSAP1, OVOL1, PCSK6, PDGFA, PDPN (includes EG:10630), PIM1, PITX1, PLAUR, PLOD3, POR, PRDM1, PRSS8, PSRC1, PTGER4, PTGES, PTGS2, PTHLH, RBP1, ROBO1, RXRA, SC5DL, SEMA4D, SERPINH1, SKP2 (includes EG:27401), SLC39A14, SMPD3, SPINK5, SREBF1 (includes EG:176574), STC1, STMN1, TGFBR2, TGM1, TGM3, TGM5, THBS1, TIMELESS, TIMP2 (includes EG:21858), TK1, TNFRSF12A, TNFRSF6B, TNFSF10, TNNC1, TNNT2 (includes EG:21956), TUBB, UGCG, VLDLR, WNT5A, ZBTB16

Genes of interest are presented in **bold underlined** type whereas genes used as standard markers of skin development are presented in underlined type. Up-regulated genes are highlighted in red, whereas down-regulated genes are highlighted in blue.

4.3.10 Genes relating to diseases and disorders

The epidermis of the HSE model undergoes rapid proliferation and differentiation, both of which are key processes in epidermal development. In addition to normal tissue formation, these processes are also involved in some disease states relating to the skin, such as psoriasis (Benoit *et al.*, 2006). Therefore, gene data sets deemed to be related to epidermal diseases and conditions were also investigated (*Table 4.9*). The sub-groups of disorders within the 'dermatological diseases and disorders' functional category that were common between all three time points included diffuse palmoplantar keratoderma, hyperkeratosis and ichtyosis. It was noted that some of the focus genes present within the 'dermatological diseases and disorders' data set were also present in the 'hair and skin development' and 'tissue development' data sets (*Table 4.7* and *Table 4.8*). This includes genes such as *KRT1, FLG, KRT15, KRT9* and *KRT10 (Table 4.10)*. However, this is unsurprising as many genes associated with skin development and functions have their gene expression disrupted in disease states.

Table 4.9 Ontology of differentially expressed genes in HSEs involved 'dermatological diseases and conditions'

Time	P-value range	Focus Genes
Day 3	1.28E-25 – 1.14E-02	97
Day 5	1.88E-22 – 6.70E-03	139
Day 9	1.66E-24 – 1.66E-03	214

Table 4.10 Focus genes differentially expressed in HSE during epidermogenesis within the 'dermatological diseases and conditions' data set

Time	Focus Genes
Day 3	ACPP, AKR1B10, ALOX12B, ALOX15B, ANGPTL4, ARG1, ARHGDIB, ATP12A, AURKB, BLMH, C10orf99, CALML3, CCNA2, CD207, CD36, CD97, CDC25A, CFD, CLCA2, CPT1A, CRABP2, CSTA, CXCL1, CYP3A5, DEFB4A/DEFB4B, DSC1, DSG1, EDN1, FABP5, FLG, GAL, GBP2 (includes EG:14469), GJB2, GK, GM2A, GSN, HLA-B, HRNR, IDE, IFI27, IGFBP3, IGFBP5, IL24, IL36B, IL36G, IL8, KLK1 (includes EG:24523), KLK13, KLK4, KLK5, KLK9, **KRT1**, KRT10, KRT2, KRT6B, KRT79, KRT9, LAMP3, LCE3C, MMP7, MMP9, MSMB, MUCL1, PDGFA, PDK4, PDZK1IP1, PHGDH, PITX1, PLAUR, PSORS1C2, PTGS1, RARRES1, RRM2, S100A12, S100A7A, SC5DL, SCD, SCG5, SERPINB13, SERPINB3, SERPINB4, SLURP1, SPINK5, SPRR2A (includes others), SPRR2C, SRM, TAGLN, TGM3, THBS1, THRSP, TIMP1, TNFAIP3, TNFSF10, TUBA3C/TUBA3D, TYMS, WFDC12, ZNF91
Day 5	ABCA12, ACPP, ACSBG1, AKR1B10, ALDH1A3, ALOX12B, ALOX15B, ALOXE3, APOD, AQP9, ARG1, ARHGDIB, ATP12A, ATP7A, AURKB, BLMH, C10orf99, CALML5, CAMK2N1, CAV1, CCNA2, CD36, CDC25A, CDC25B, CDK2, CDSN, CEBPA, CEBPB (includes EG:1051), CFD, CIDEA, CLCA2, CRABP2, CSTA, CTNNBIP1, CXCL1, CXCL6, CYP3A5, CYP4F22, DDX39A, DGAT2, DLX3, DSC1, DSG1, EIF5A, ELOVL3, EPHB6, ERBB2, FABP5, FAM153A/FAM153B, FASN, FEN1, FGFR3, FLG, FST, G6PD, GBA, GBP2 (includes EG:14469), GJB2, GJB6, GK, GLRX, GM2A, GSN, HAL, HLA-DRB5, HNMT, HNRNPR, HPSE, HRNR, ID1, IDE, IGFBP7, IL22RA1, IL36B, IL36G, IL8, KIAA0101, KIF11, KITLG, KLK1 (includes EG:24523), KLK4, KLK6, KLK9, KPNA2, **KRT1**, KRT10, KRT2, KRT6B, KRT79, KRT9, LAMP3, LCE2B (includes others), LCE3C, LCE3E, MAD2L1, MITF, MMP1 includes EG:300339), MMP9, OASL, PDCD4, PDZK1IP1, PGD, PHGDH, PITX1, PKM2, PLAUR, PLSCR1, POR, PSORS1C2, PTGS1, RARRES1, S100A12, S100A7A, SAMD9, SCD, SERPINB2, SERPINB3, SERPINB4, SLURP1, SOX9, SPC25 (includes EG:100144563), SPINK5, SPRR2A (includes others), SPRR2C, SQLE, SRM, SULT2B1, TAGLN, TGM3, THBS1, THRSP, TIMP1, TNFSF10, TUBA3C/TUBA3D, TYMS, VWF, WFDC12, WNT5A, ZNF91
Day 9	ABCA1, ABCA12, ACADVL, ACPP, ACSBG1, AHCY, AKT1, ALDH1A3, ALDH3A2, ALOX12, ALOX12B, ALOX15B, ALOXE3, ANGPTL4, ANXA8/ANXA8L1, AQP3, AQP9, ARG1, ARHGDIB, ATP12A, ATP1B1, AURKB, BIRC5, BLMH, C10orf99, C1QBP, CALML5, CAMK2N1, CAV1, CBS, CCL20, CCNA2, CCND3, CCNF, CD36, CD97, CDC25A, CDC25B, CDK2, CDK4, CDSN, CEBPA, CEBPB (includes EG:1051), CERS3, CLCA2, CSE1L, CSNK1A1, CSTA, CXCL1, CYP3A5, CYP4F22, DDX39A, DEFB4A/DEFB4B, DGAT2, DLX3, DSC1, DSG1, DUSP1, DUSP2, EDN1, EIF2AK2, ELOVL3,

	EPHB6, ERBB2, FA2H, FABP5, FEN1, FGFR3, FLG, FMO5, FOS, FOXO3, FST, GAL, GAPDH, GARS, GBA, GBP2 (includes EG:14469), GJA1, GJB2, GK, GLRX, GNA11, GPR56, GPX1 (includes EG:14775), GRHL3, GSN, GSTM1, H2AFZ, HAL, HELLS, HERC6, HMGCR, HMGCS2, HMOX1, HNMT, HPSE, HRNR, HSP90AB1, HSPE1, ID1, IDE, IFI27, IGFBP7, IL22RA1, IL33, IL36B, IL36G, IL8, JUN, JUP, KIAA0101, KIF23, KITLG, KLK1 (includes EG:24523), KLK8, KLK9, KPNA2, **KRT1**, KRT10, KRT13, KRT15, KRT2, KRT6B, KRT79, KRT9, LAMP3, LCE2B (includes others), LCE3C, LCE3E, LIG1, MAD2L1, MAPK9, MCM4, MCM7, ME1, MET, MMP1 (includes EG:300339), MMP9, MSMB, MT1X, NAMPT, NCOA1, NFKBIZ, NRP1 (includes EG:18186), NT5E, NUSAP1, OAS1, OASL, PCNA, PDCD4, PDZK1IP1, PHGDH, PITX1, PKM2, PLK1, PLSCR1, POR, PSMB10, PSORS1C2, PTGS1, PTGS2, PTPN22, RANBP1, RASGRP1, RBBP6, RRM2, RUVBL1, RXRA, S100A12, S100A7A, SAMD9, SCD, SCG5, SERPINB13, SERPINB2, SERPINB3, SERPINB4, SERPINB8, SKP2 (includes EG:27401), SLURP1, SPC25 (includes EG:100144563), SPINK5, SPRR2A (includes others), SPRR2C, SQLE, SRM, SULT2B1, TAGLN, TAOK1, TGFBR2, TGM1, TGM3, THBS1, THRSP, TIMP2 (includes EG:21858), TNFRSF12A, TNFSF10, TOP2A, TUBA3C/TUBA3D, TUBB, TUBB2A, TXNIP, TYMS, UBIAD1, VNN3, WF, WFDC12, WNK1, WNT5A, XRCC3, XRCC6, ZBTB16, ZNF91

Genes of interest are presented in **bold underlined** type whereas genes used as standard markers of skin development are presented in underlined type. Up-regulated genes are highlighted in red, whereas down-regulated genes are highlighted in blue.

4.4 DISCUSSION

The data presented in this Chapter are novel in that this is the first study to investigate gene expression using microarray approaches in HSE models undergoing epidermogenesis. However, pooling of the RNA from HSE models constructed from three individual skin donors may not have been optimal overall. The pooling was advantageous in that it allowed gene microarray analysis to be performed on the HSE models within the confines of limited sample availability. It also negated any inter-individual variability and revealed the commonly differentially regulated genes within the HSE model. On the other hand, pooling of RNA from multiple individuals concealed the differences in inter-individual gene expression, thus the extent of variability between samples is unknown. Nonetheless, the results from this experiment can be viewed as a general screen to evaluate global changes in gene expression patterns in a developing HSE model. Interestingly, the data reported in this chapter demonstrate that a large cohort of genes is differentially expressed during epidermogenesis (**Figure 4.2**) and that the expression profile of these genes varies greatly between time points (**Figure 4.1**). Furthermore, when the genes are examined at a functional ontology level, the top functions relating to epidermogenesis become more significantly differentially regulated over time (**Figure 4.3**). Together, these data suggest that many important functional and biochemical changes are occurring within the skin during epidermogenesis and that these can be investigated through microarray analysis techniques. Furthermore, the results presented in this Chapter supports the use of the developing HSE as an appropriate model of skin development.

Interestingly, a study recently reported by Mazar *et al.* (2010) employed microarray analysis to investigate gene expression changes related to keratinocyte differentiation in a HSE model. Importantly, the HSEs used in this study were commercially available HSEs grown on a collagen scaffold, rather than a DED. Mazar *et al*. (2010) investigated this by comparing the gene expression profile of a submerged HSE model to one cultured at the air-liquid interface. The authors reported genes such as *TGM2*, *STAT2*, *FGFR2* and *IGFBP4* were differentially regulated in a differentiated versus undifferentiated HSE epidermis (Mazar *et al.*, 2010). Interestingly, the above mentioned genes were not differentially regulated in the microarray studies reported herein.

Another study by Koria and Andreadis (2006) used microarray analysis to investigate the changes in gene expression during epidermal development and stratification. Similar to Mazar *et al.* (2010), Koria and Andreadis (2006) compared submerged HSE models to those cultured at the air-liquid interface. Importantly, however, in this study the HSE model was generated from primary human keratinocytes grown on a DED (Koira and Andreadis, 2006). In accordance with the results described in this Chapter, Koria and Andreadis (2006) found many genes related to cellular growth and proliferation were differentially regulated. Specifcally, these included the genes of the retinoic acid receptor responder (*RARRES1*), insulin-like growth factor binding protein 7 (*IGFBP7*), cyclins A2 and B1 (*CCNA2* and *CCNB1*) and *CDC20* (Koira and Andreadis, 2006). When the results of this Chapter, Koira and Andreadis (2006) and Mazar *et al.* (2010) are considered, it can be suggested that epidermogenesis of HSE models grown on a collagen scaffold elicits differential regulation in a separate subset of focus genes than HSEs cultured on a DED. This is highlighted in the similarities of differential gene expression between this Chapter and the genes reported in Koira and Andreadis (2006) and the differences between this Chapter and those reported in Mazar *et al*. (2010).

Genes relating to the proteins investigated in Chapter 3, namely *TP63*, *MKI67*, *KRT1*, *LOR*, *KRT16*, were analysed in the microarray data as a form of internal validation to determine if gene expression changes were occurring in an appropriate manner. Surprisingly, only *KRT1* was significantly differentially regulated during epidermogenesis in the HSE model (*Table 4.7*, *Table 4.8* and *Table 4.10*). Examination of the original microarray data, prior to GeneSpring analysis, revealed that the genes *LOR*, *MKI67*, *KRT16* and *TP63* were present, however, they were removed during GeneSpring analysis as their signal intensities were lower than the background 'noise' of the data. Based on these findings, the proteins investigated in Chapter 3 may not have been the best representatives to select, in order to examine keratinocyte proliferation and differentiation in the HSE model. The correlating genes of other proteins which are also routinely used as markers of skin proliferation and differentiation were investigated in the gene microarray data. These included basal/progenitor cell marker K15 (*KRT15*; Porter *et al.*, 2000) and differentiation makers filaggrin (*FLG*; Rawlings and Hardings, 1994) and envoplakin (*EVPL*; Ruhrberg *et al.*, 1996).

While detection of p63 and ki-67 are commonly used to examine the proliferation and proliferative potential of the epidermis (Noszczyk and Majewski, 2001; Parsa *et al.*, 1999), K15 is also a marker of the basal epidermal keratinocyte population and has also been used to investigate the self-renewing potential of skin models (Pontiggia *et al.*, 2009; Truong and Khavari, 2007). Interestingly, K5 and K14, which have previously been employed as markers of basal/proliferative epidermal keratinocytes, were also not differentially regulated in this system according to gene microarray analysis (Alam *et al.*, 2011). Furthermore, Alam *et al.* (2011) reported that knockdown of K14, at the gene and protein level, affected cell cycle progression and enhanced differentiation. However, this was performed using keratinocyte cell lines and 2D cell culture, which does not accurately represent the native environment of keratinocytes *in vivo*. Therefore, K15 may be a useful marker of basal/proliferative keratinocytes in future investigations of epidermal development in HSE models.

In the data reported herein, the gene *LOR* whose protein expression was investigated in Chapter 3 was not differentially regulated in this experiment. However, the differentiation markers filaggrin and envoplakin were up-regulated during epidermogenesis of the HSE model when analysed via gene microarrays (*Table 4.7*, *Table 4.8* and *Table 4.10*). Filaggrin is specifically expressed in differentiating keratinocytes in the epidermis and is degraded in the stratum corneum to release free amino acids which assist water retention and therefore skin hydration (Rawlings and Hardings, 2004; Ruhrberg *et al.*, 1996). In addition, envoplakin is a corneocyte precursor protein which provides structural integrity to the stratum corneum and assists with skin barrier function (DiColandrea *et al.*, 2000; Määttä *et al.*, 2001). Importantly, filaggrin and envoplakin have both previously been investigated as markers of differentiation in a HSE model (Biedermann *et al.*, 2010). In this study, Biedermann *et al.* (2010) generated HSE models by seeding human-derived keratinocytes onto a human fibroblast-populated collagen gel and compared the end-point HSE models to native human skin. The authors found that filaggrin and envoplakin proteins were expressed earlier in the stratum granulosum layers of the HSE model than in native skin, which is consistent with the pattern of loricrin protein expression observed in **Figure 3.7**. Together, this suggests that filaggrin and envoplakin may be useful markers to assess epidermogenesis in future studies.

The loss-of-function mutation of the *FLG* gene is associated with ichthyosis, one of the 'dermatological diseases and conditions' determined to be altered in section 4.3.10. Ichthyosis is a skin disorder characterised by dry and scaly skin (Gruber *et al.,* 2011). A deficiency in *FLG*, leading to a lack of filaggrin protein, has been reported to impair keratin organisation and disrupt epidermal architecture, resulting in impaired epidermal barrier function (Gruber *et al.,* 2011). This highlights the importance of the *FLG* gene in the epidermogenesis process. Interestingly, another one of the 'dermatological diseases and conditions' was diffuse palmoplantar keratoderma, which is proposed to be due to mutation of the *KRT9* gene (Rugg *et al.,* 2002). The disease is characterised by diffuse and even thickening of plamoplantar skin (Rugg *et al.,* 2002). Enhanced thickening of the stratum corneum was observed in **Figure 3.2** after the HSE model was cultured for 9 days, however, the skin used for generating the HSE model is from non-palmoplantar areas. In general, while the genes commonly associated with these diseases were differentially regulated in the HSE model it does not necessarily mean that these skin samples were affected by these disease states.

Curiously, *KRT9* was present in the microarray data and was up-regulated at all three time points (*Table 4.7*, *Table 4.8* and *Table 4.10*). The protein keratin 9 (K9) and its correlating gene, *KRT9*, are widely reported to be specifically expressed in palmoplantar skin (palms of hands and soles of feet; Compton *et al.*, 1998). In most previous microarray studies investigating HSE models, the presence of K9 has not been reported (Holland *et al.*, 2009; Hu *et al.*, 2010; Kurata *et al.*, 2010; Mazar *et al.*, 2010). However, Koira and Andreadis (2006) reported an up-regulation of *KRT9* in their stratified HSE model, when compared to the cubmerged HSE. In addition, Yamaguchi *et al.* (1999) reported that K9 expression could be induced in non-palmoplantar keratinocytes by co-culture with palmoplantar fibroblasts through epithelial-mesenchymal interactions. Since this is a single cell type model, induction of *KRT9* gene expression through this mechanism is not likely the case. Interestingly, Moll *et al.* (1987) reported the presence of K9 protein in acrosyringia (eccrine sweat glands) keratinocytes in non-palmoplantar skin. Therefore, the expression of *KRT9* may simply be an artefact of the gene microarray or culturing HSE models on a DED substrate, or it could possibly be that K9-positive acrosyringia keratinocytes were

also cultured and expanded with the standard K9-negative epidermal keratinocytes from the donor skin samples.

The results presented in this chapter highlighted that the standard protein markers of gene expression, namely p63, ki-67, loricrin and K16, may not be the most appropriate representatives for the investigation of differential gene expression during epidermogenesis. This does not, however, negate their validity as protein markers of proliferation, maturation and differentiation as was previously presented in Chapter 3. The post-transcriptionl mechanisms involved in the generation of protein from mRNA are not fully understood. As described by de Sousa Abreu *et al*. (2008), the discrepancies between mRNA and protein levels can be due to lack of sensitivity or specificity in gene or protein measurements, inability to detect target proteins due to post-translational modifications and also gene specific regulation of protein degradation. Furthermore, protein levels are controlled at both the transcriptional and translational level and the relative abundance of a protein influences further mRNA translation (Glickman and Ciechanour, 2002; Greenbaum *et al.,* 2003). Interestingly, discrepancies between gene and protein levels have been described previously. Gry *et al* (2009) and Pascal *et al*. (2008) analysed the correlation between gene (via microarray analysis) and protein (via immunohistochemistry) analysis and reported that correlation only existed between gene and protein expression at a rate of ~ 30% (Gry *et al.,* 2009) or had a Pearson's correlation score between 0 and 0.63 (1.0 is perfect correlation; Pascal *et al.,* 2008). Therefore, there are many possible reasons for a lack of correlation between the microarraydata presented in this data and the immunohistochemistry data from Chapter 3.

In general, the data presented in this Chapter, in addition to the data presented in Chapter 3, demonstrate that the HSE is a biologically relevant model to study epidermogenesis. Furthermore, the studies conducted throughout this Chapter have shed light on other possible gene and protein markers for future investigations and raised important issues involved in correlating gene and protein expression levels.

Chapter 5: Histological characterisation of the HSE model in response to HBO treatment

5.1 INTRODUCTION

Epidermal regeneration is a critical factor in the wound healing response and is characterised by the migration of epithelial cells to the wound site after the formation of a fibrin clot. The re-epithelialisation process must occur rapidly after the onset of the initial injury event in order to restore the barrier function of the skin. Usui *et al.* (2005) proposed the theory of the "rolling" method of wound re-epithelialisation, which proposes that all keratinocytes, both basal and supra-basal, are involved in migration and proliferation into the wound area (**Figure 5.1**). To complete the epithelialisation process, the epidermal keratinocytes transition through four specific and highly regulated epithelialisation events, namely migration, proliferation, stratification and differentiation.

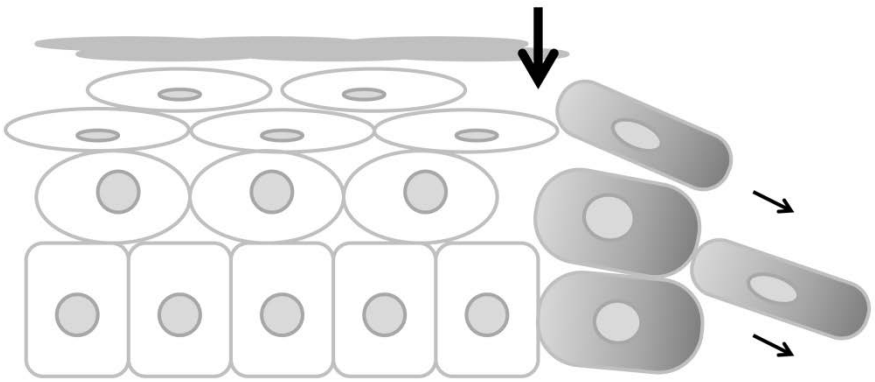

Figure 5.1 "Rolling" method of wound re-epithelialisation
This image adapted from Usui *et al.,* 2005 depicts a hypothesis of wound re-epithelialisation in which keratinocytes from both basal and supra-basal layers migrate into the wound bed from the leading edge of the wound in order to form a new epidermis.

Migration is thought to be the earliest physical event in the wound healing process. In addition, it must closely coincide with proliferation to be effective at repopulating the cells that migrate out from the wound edge. Usui *et al.* (2005) found that keratinocyte migration preceded proliferation events and concluded that keratinocyte movement into the wound bed is caused by migratory cells as opposed to keratinocytes proliferating at the wound front. Importantly, in normal, unwounded skin, keratinocytes are not migratory (Nickoloff *et al.*, 1988). In order to migrate in response to a wound, keratinocytes in the epidermis must restructure their cytoskeleton and cell junctions, enabling them to transition from the stationary to the motile state (Kirfel and Herzog, 2004).

In addition to a lack of keratinocyte migration within the normal, unwounded epidermal tissue environment, it is also thought that there is a limited population of proliferative cells (Gibbs and Ponec, 2000). Proliferation, however, is an important event that is stimulated in the wound healing environment and coincides with migration to repopulate the wound bed with cells (Odland and Ross, 1968). Paladini *et al.* (1996) proposed that induction of keratin 16 (K16) enables differentiating keratinocytes to become involved in proliferation events by allowing keratin intermediate filament remodelling. However, this situation is limited to keratinocytes that have not yet committed to terminal differentiation. The authors propose that cells from the basal and spinosum layer are able to become proliferative by the presence of K16, while cells from the stratum granulosum and corneum are excluded (Paladini *et al.*, 1996). Other important markers within the skin are p63, a marker of cells with a proliferative capacity (Parsa *et al.*, 1999), and ki-67, a cell cycle marker expressed in all cells except those in G_0 (resting phase; Noszczyk and Majewski, 2001).

The process of differentiation and subsequent transition through the various stages of maturation leads to the formation of distinct keratinocyte layers in the epidermis (Watt and Green, 1982). This stratification process is imperative to the normal functioning and integrity of the epidermis (Watt and Green, 1982), while the differentiation process coincides with tightly regulated keratin expression (Patel *et al.*, 2006). Thus, the differentiation of the epidermis can be distinguished via detection of markers such as keratin 10 (K10), an early differentiation marker (HogenEsch *et al.*, 1999), and loricrin, a late differentiation marker. Indeed, cells that express loricrin are committed to terminal differentiation (Yoneda and Steinert,

1993). The end result of both stratification and differentiation is the sloughing off of cells at the skin surface once the epithelium is fully formed and functional.

5.1.1 Oxygen in skin and re-epithelialisation

Oxygen is an important factor in the re-epithelialisation process. While initial tissue hypoxia is thought to stimulate migration and proliferation of keratinocytes into the wound bed (O'Toole, 1997), oxygen is a critical component of oxidative phosphorylation occurring within the mitochondria, resulting in the generation of adenosine triphosphate (ATP), which is critical for cellular activity (as reviewed by Gordillo and Sen, 2003; Rodriguez *et al.*, 2008, Tandara and Mustoe, 2004).

The lack of oxygenation in chronic wound tissue is the rationale behind the implementation of hyperbaric oxygen therapy (HBO). It is generally hypothesised that HBO acts to increase wound oxygenation, thereby stimulating the wound healing process (as reviewed by Kulikovsky *et al.*, 2009). Many studies have shown that there appears to be a beneficial impact from the use of HBO as a wound healing therapy. Specifically, it was found that HBO seemed to improve functional recovery and blood flow in mouse ischemic hind limb models (Asano *et al.*, 2007). Additionally, research from Duzgun *et al.* (2008) concluded that HBO increased foot ulcer healing and decreased the severity of amputation if it was required. HBO therapy has been shown to significantly increase healing in non-diabetic wounds (Hammarlund and Sundberg, 1994) and to augment neovascularisation and decrease oedema in burn wounds in rats (Türkaslan *et al.*, 2010). Significantly, none of these studies identified the mechanism of action through which HBO was able to induce these changes. In view of this, this Chapter attempts to investigate these mechanisms in order to further our understanding of the functional responses of skin to HBO treatment.

5.1.2 Human skin equivalent models

Studying wound healing and the use of potential therapeutics on humans is not always practical and is ethically challenging; therefore it is often necessary to study wound healing in a model system. The limitations of animal models have previously been discussed (Chapter 3). Furthermore, two-dimensional, monolayer culture does not reflect the complexity of skin cell biology, hence is not a model that can be appropriately used to investigate and extrapolate wound healing therapies directly to

native human skin. In view of the similarities between native skin and the three dimensional (3D) human skin equivalent (HSE) model observed in Chapter 3, the HSE was used as a somewhat more biologically relevant tool for examination of the mechanistic and functional effects of HBO treatment on skin cells.

Other members of our research program have previously used HSE models to investigate serum-free cell culture (Mujaj *et al.*, 2010) and various wound healing models (Topping *et al.*, 2006; Upton *et al.*, 2008; Xie *et al.*, 2010). Of particular relevance to this research, the HSE model has previously been used to investigate the effects of HBO on epidermal generation (Kairuz *et al.*, 2007). Kairuz *et al.* (2007) found that HBO increased epidermal thickness after 3 and 5 days of culture at the air-liquid interface and also increased the migration of keratinocytes within the HSE model. The thesis Chapter reported here expands on this previous work by extending the period of analysis from 5 days to 9 days and by pursuing additional structural and functional characterisation of the HSE model in both the presence and absence of HBO treatment.

Previous research by other investigators examining the effects of HBO treatment on HSE models found that HBO inhibited keratinocyte proliferation (Dimitrijevich *et al.*, 1999), whereas others found that HBO treatment increased proliferation of keratinocyte cultures (Hollander *et al.*, 2000). In addition, there have been differences in the results obtained from 2D monolayer studies in comparison to 3D HSE models. Thus it was found that HBO treatment significantly enhanced cellular proliferation and epidermal generation in the HSE model, whereas HBO treatment appeared to inhibit keratinocyte proliferation in 2D culture (Dimitrijevich *et al.*, 1999).

In this Chapter the phenotypic responses of the HSE model to HBO treatment have been investigated through the analysis of keratinocyte differentiation using immunohistological analysis of key epidermal markers. Furthermore, the functional characteristics of the HSE model were investigated through analysis of epidermal expansion using the MTT stain and by measuring the epidermal thickness of the model via image analysis of standard haematoxylin and eosin (H&E) images.

5.2 METHODS AND MATERIALS

A complete explanation of both the materials and methods and the experimental procedures used in the generation of data presented in this Chapter have been described in Chapter 2. The following is a brief summary of the experimental protocols used to generate the data presented in section 5.3.

5.2.1 Generation of the human skin equivalent (HSE) model

HSE models were generated using skin obtained from individuals undergoing elective cosmetic breast reduction or abdominoplasty surgeries as fully described in sections 2.4 - 2.6. Following generation, HSE models were cultured at the air-liquid interface and maintained in Full Greens (FG) culture media. The media was replenished daily to maintain cultures at the air-liquid interface and was fully replaced once per week.

5.2.2 Hyperbaric oxygen treatment

HSE models cultured at the air-liquid interface were treated with 100% oxygen at 2.4 atmospheres for 90 minutes daily. Correlating control HSEs were placed in a humidified box without the presence of CO_2 for an equivalent period of time. For full details on HBO and control treatment protocols, please refer to section 2.7. The HSE generation and HBO treatment experiments were performed using skin obtained from a total of eight donors.

5.2.3 Measurement of the pH of HSE culture medium

Duplicate pH measurements were taken of freshly prepared FG medium and also of culture media before treatment and within 5 minutes after completion of the treatment protocols. In addition, the pH of the culture media without the presence of the HSE was also measured in order to evaluate the effect of HSE metabolism on culture media pH.

5.2.4 Keratinocyte lateral migration within the HSE model

For full details of the method used to determine the effect of HBO or control treatment on the epidermal outgrowth of newly formed epidermis over the DED using 4,5-dimethylthiazol-2-yl)-2,5-diphenyltetraoliumbromide (MTT) please refer to section 2.10.

5.2.5 Assessment of the epidermal generation process of the HSEs

Following MTT analysis the HSE models were formalin-fixed and paraffin embedded for histological analysis as described in section 2.11. Following this, sections of the HSE were cut using a microtome (5 µm; Leica) and transferred to a slide (HD scientific). Sections were either used for haematoxylin and eosin (H&E) staining to determine epidermal morphology and thickness or used for immunohistological analysis.

To determine the expression of specific skin developmental markers, slides containing sections from each time point for each sample were incubated separately with the following primary antibodies: p63 (1:2000 dilution), ki-67 (1:100 dilution), keratin 1 (K1; 1:500 dilution), loricrin (1:1000 dilution) or keratin 16 (K16; 1:100 dilution). For full details on the antibodies, refer to *Table 2.1*. Immunoreactivity was determined using the Dako Envision kit (Dakocytomation) following the manufacturer's instructions. The resulting H&E or immunohistochemistry slides were observed using an Olympus BX41 microscope (Olympus) with a mounted digital camera (Olympus).

5.2.6 Image data analysis

Image data analysis was performed on images obtained from both H&E and immunohistochemistry experimental results. For all samples, image analysis was performed on consecutive images taken from the centre of each HSE. All image data analysis was performed using open source ImageJ software (available at: http://rsbweb.nih.gov/ij/) with the MacBiophotonics Plugins (available at: http://www.macbiophotonics.ca/imagej/). For full details on the image data analysis protocol, please refer to section 2.11.2.

5.3 RESULTS

5.3.1 HBO treatment does not affect culture media pH

The pH of the FG media was measured over 9 consecutive days in both control- and HBO-treated samples, using media sampled from wells both with and without the HSEs. These measurements were performed to determine if HBO treatment had an impact on the pH of the culture medium and also to determine if the presence of the HSE model in the culture medium influenced the pH of the media supporting its growth. Interestingly, the media supporting the growth of the HSE models were less basic (lower pH) than media without the HSEs (**Figure 5.2**). However, there were no differences between the samples taken from control and HBO-treated media that did not contain HSEs (**Figure 5.2**)

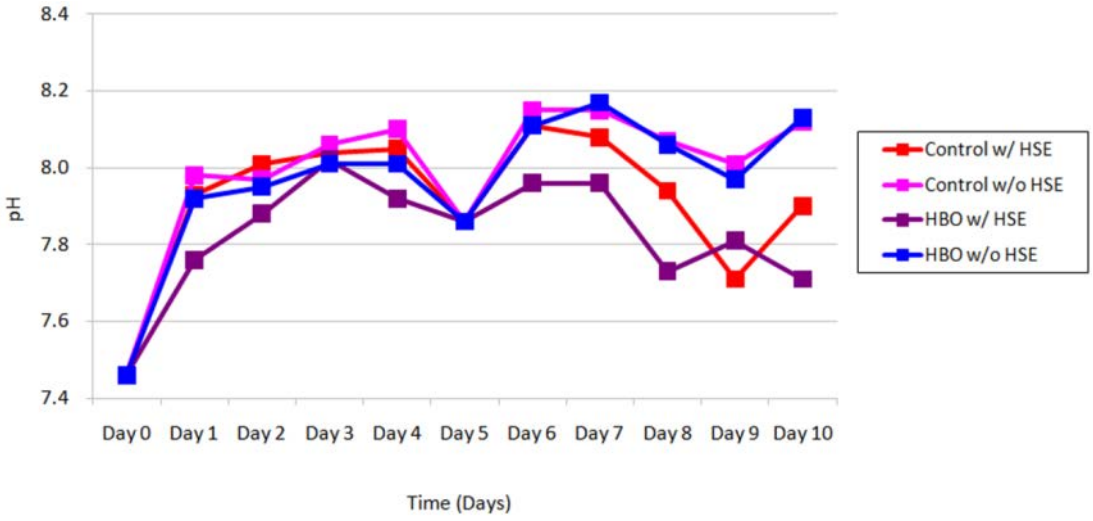

Figure 5.2 HBO treatment does not affect cell culture media pH
The pH of FG media in cultures with and without the HSE models was measured daily after HBO or control treatment to determine if pH was affected. The drop in pH level at day 5 is due to the complete replacement of the existing FG media with fresh media.

5.3.2 Analysis of keratinocyte outgrowth in the HBO treated HSE model

The HSE model was utilised to investigate the influence of HBO treatment on epidermal expansion over the DED. This was performed by exposing the HSE models to a daily HBO regime, over nine consecutive days, prior to detection of epidermal outgrowth with MTT (**Figure 5.3**). Interestingly, some day 9 HBO samples had no purple staining in the centre of the HSE (white arrow in **Figure 5.3 G**), suggesting a reduction in metabolic activity in the centre of the HSE. In these same samples, the outer edges remain purple suggesting that most of the metabolic activity was still occurring at the advancing front of the HSE. Furthermore, the darker the purple staining indicates higher metabolic activity as compared to the lighter purple staining, which is evident in **Figure 5.3 D** and **E**. In general, HBO treatment did not appear to impart any significant effects on epidermal expansion over the DED as similar responses in keratinocyte outgrowth were obtained from both HBO-treated and control samples (**Figure 5.3**).

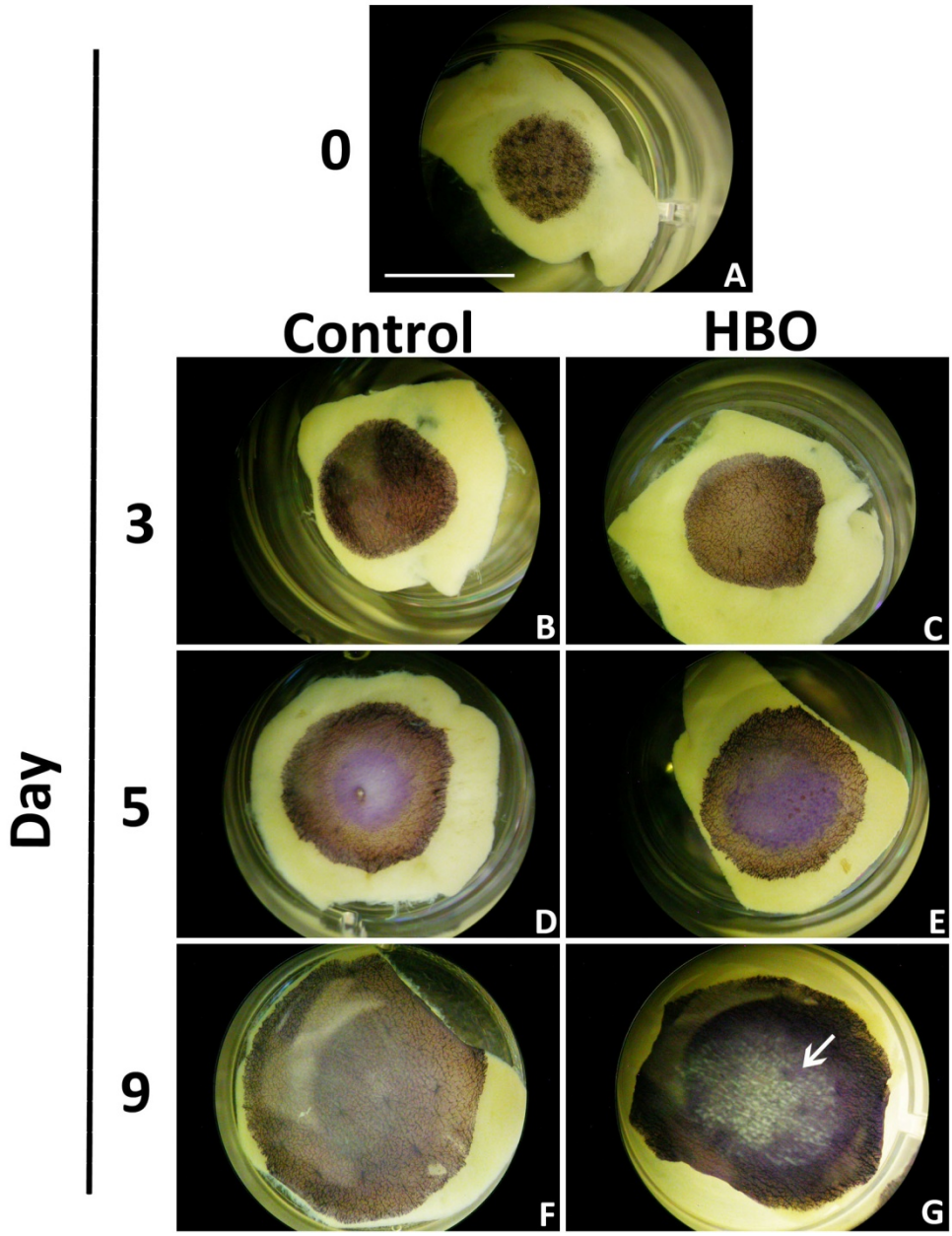

Figure 5.3 Keratinocyte outgrowth in the HBO-treated HSE model
Reconstructed HSE models were cultured at the air-liquid interface and treated with HBO for up to 9 days. Outgrowth of metabolically active keratinocytes over the DED was visualised via the MTT assay. The surface area of viable epidermis covering the HSE was determined after (**A**) 0 days, (**B, C**) 3 days, (**D, E**) 5 days and (**F, G**) 9 days of culture at the air-liquid interface. Representative images of control-treated (**B, D, F**) and HBO-treated (**C, E, G**) MTT-stained HSE models for each treatment and time point are presented. The arrow indicates where no MTT-positive staining was present in the centre of the day 9 HSE model. The scale bar represents 5 mm.

5.3.3 HBO treatment does not influence lateral epidermal expansion over the DED

The MTT-stained HSE images were analysed using ImageJ to quantify lateral epidermal expansion in response to HBO treatment (Appendix Table A20 and Table A21). This revealed that the surface area covered by newly formed epidermis increased over time, irrespective of treatment (**Figure 5.4**); hence HBO does not appear to have a significant impact on lateral epidermal expansion over the DED.

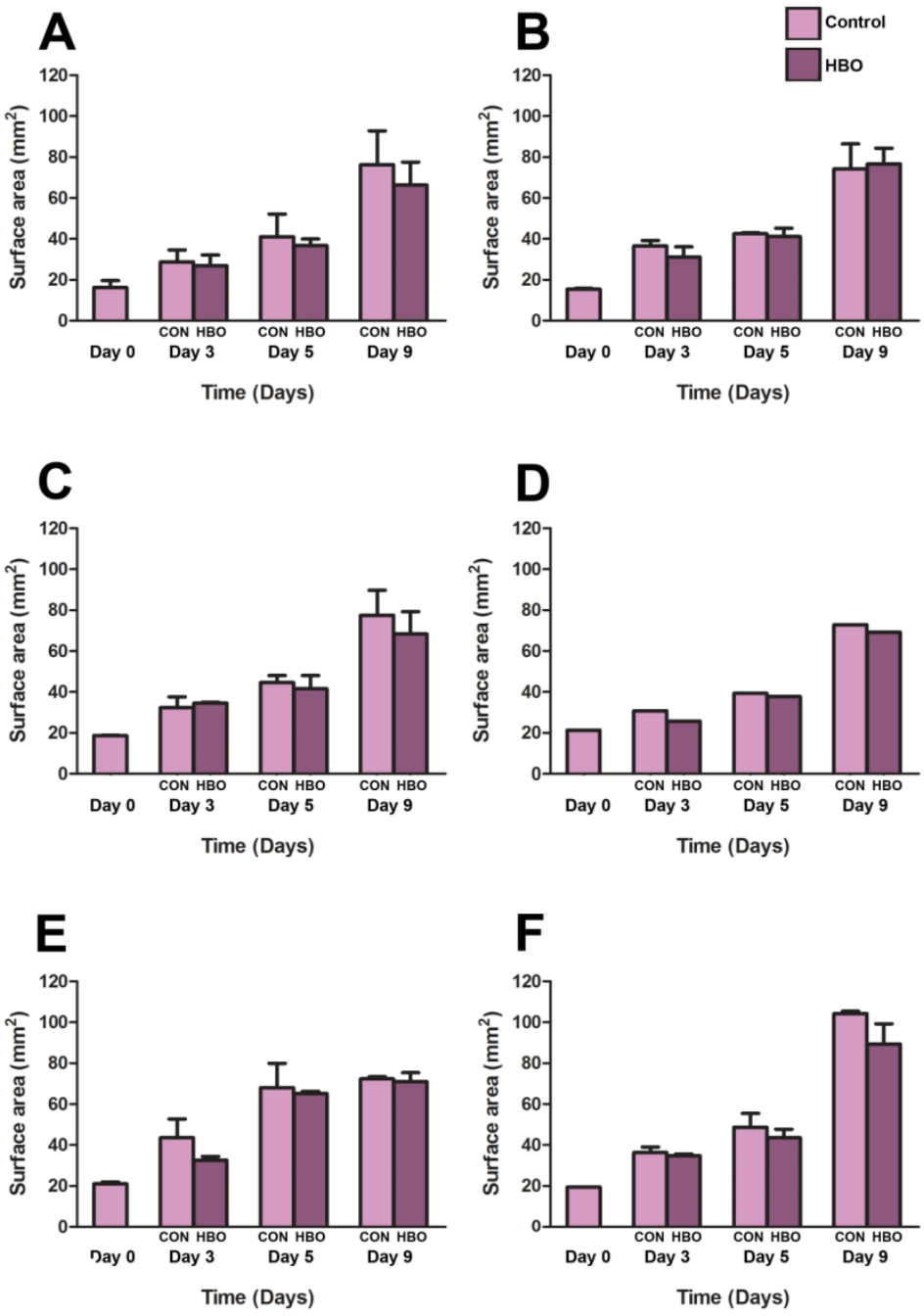

Figure 5.4 Lateral epidermal expansion in the HSE model increases with time irrespective of treatment method

Lateral epidermal expansion was quantified in the images of MTT-stained HSE models to determine the total surface area of the DED covered by metabolically active keratinocytes. The graphs show (**A**) pooled surface area data from the group A skin samples, (**B**) surface area data from sample 4, (**C**) sample 5, (**D**) sample 6, (**E**) sample 7 and (**F**) sample 8. Data were obtained from n = 2 HSEs per time point, except sample 6, where n = 1 per time point. Graphs represent mean surface area ± standard deviation. No significant differences were observed.

5.3.4 Morphology of the HSE model in response to HBO treatment

In order to evaluate the influence of HBO on epidermal generation and morphology in the HSE model, the MTT-stained samples (section 5.2.4) were subjected to haematoxylin and eosin (H&E) staining. Subsequently, images of the H&E sections were captured to qualitatively assess epidermogenesis of the HSE model in response to HBO treatment. This analysis revealed that epidermal development in the HBO-treated HSE paralleled the development of the control HSE, as was previously described in section 3.3.3. This suggests that HBO treatment does not influence epidermal generation or morphology (**Figure 5.5**).

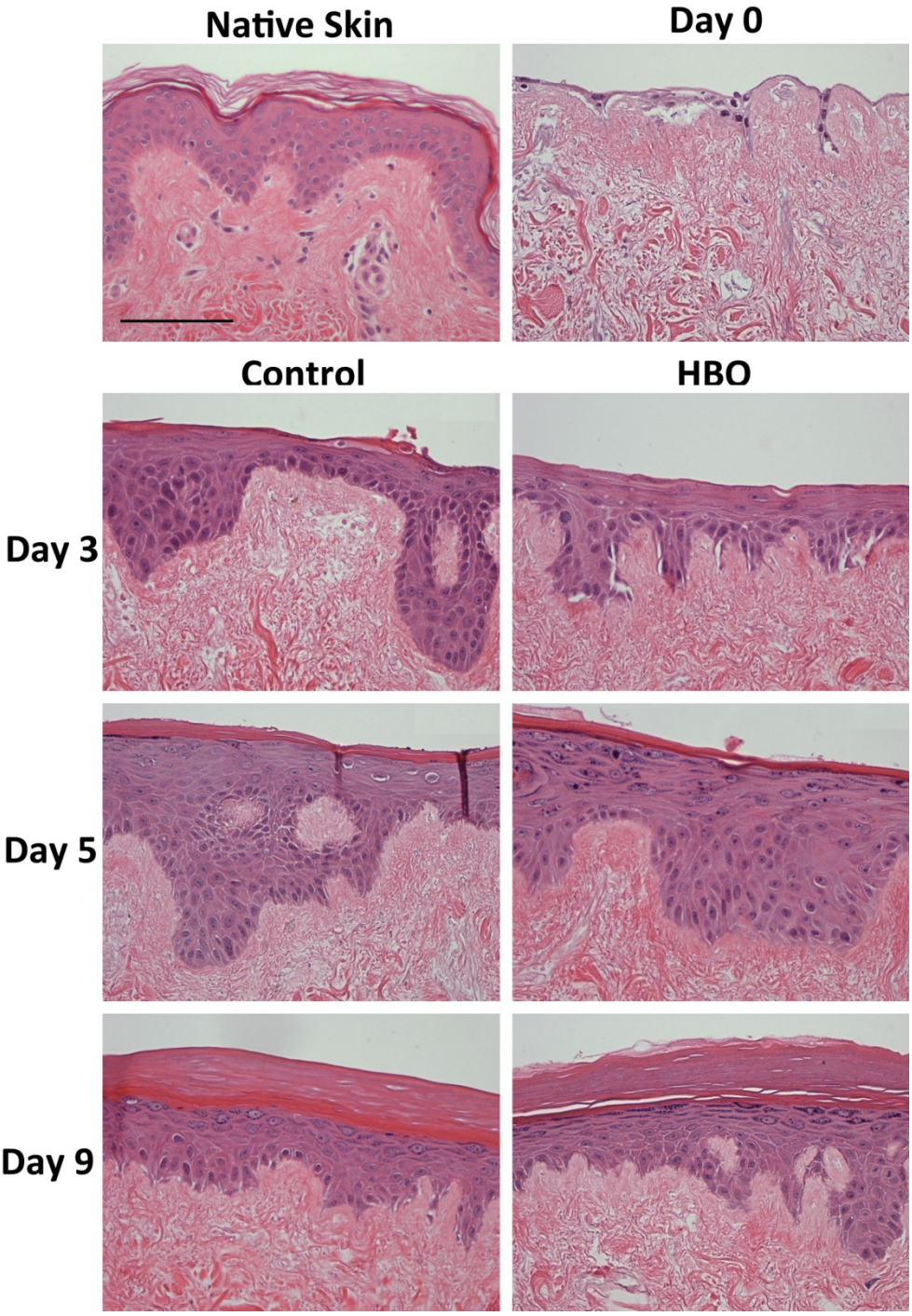

Figure 5.5 Morphology of the HSE model in response to HBO treatment during epidermogenesis

Histological sections of the HSE models were stained using H&E to investigate epidermogenesis after 0, 3, 5 and 9 days growth at the air-liquid interface. At each time point the HSE model was compared to native skin. The cellular region of the epidermis is stained with purple, while the stratum corneum stains pink. These images are representative of typical H & E stained sections taken from the group A skin samples. The scale bar represents 100 µm.

5.3.5 HBO treatment stimulates thickening of the stratum corneum over a 9 day period

The H&E images captured of the HSE model were quantified using ImageJ to evaluate the thickness of the cellular and stratum corneum layers in response to HBO treatment (**Figure 5.6**). Group A skin samples were analysed and the resulting data were pooled (Appendix Table A22 and Table A23), whereas the group B skin samples were also analysed but the data expressed separately (Appendix Table A24 and Table A25).

At each time point the stratum corneum and cellular layer thickness of the HSEs appeared to be similar between control and HBO treatment. However, sample 8 had a significantly thicker cellular layer at days 3 (68.55 µm ± 12.32 µm in HBO compared to 51.32 µm ± 15.33 µm in control; $p < 0.01$), 5 (81.87 µm ± 13.18 µm in HBO compared to 67.54 µm ± 15.74 µm in HBO; $p < 0.05$) and 9 (64.35 µm ±14.57 µm in control compared to 45.29 µm ±18.04 µm in HBO; $p < 0.001$), and a thicker stratum corneum at day 9 in response to HBO treatment (50.23 µm ± 13.36 µm in control compared to 30.26 µm ± 12.32 µm in HBO; $p < 0.05$; **Figure 5.6 F**). Conversely, the cellular layer was significantly less thick in response to HBO treatment, as compared to the control in the group A skin samples at day 3 (59.97 µm ± 23.05 µm in HBO compared to 79.86 µm ± 23.70 µm in the control; $p < 0.001$; **Figure 5.6 A**) and in sample 6 at day 5 (79.85 µm ± 6.46 µm in HBO compared to 97.65 µm ± 13.78 µm in the control; $p < 0.05$; **Figure 5.6D**). In addition, the stratum corneum was significantly thicker in response to HBO treatment at day 9 in the group A samples (55.50 µm ± 22.51 µm in HBO compared to 41.55 µm ± 16.70 µm in the control;$p < 0.05$; **Figure 5.6 A**), in sample 5 (88.44 µm ± 48.01 µm in HBO compared to 45.84 µm ± 9.15 µm in the control; $p < 0.001$; **Figure 5.6 C**) and in sample 6 (83.21 µm ± 18.03 µm in HBO compared to 54.88 µm ± 9.93 µm in the control; $p < 0.001$; **Figure 5.6 D**). Overall, these results demonstrate that a significantly thicker stratum corneum was observed in day 9 HBO treated samples in four of six the individual HSE models analysed (**Figure 5.6 A, C, D** and **F**).

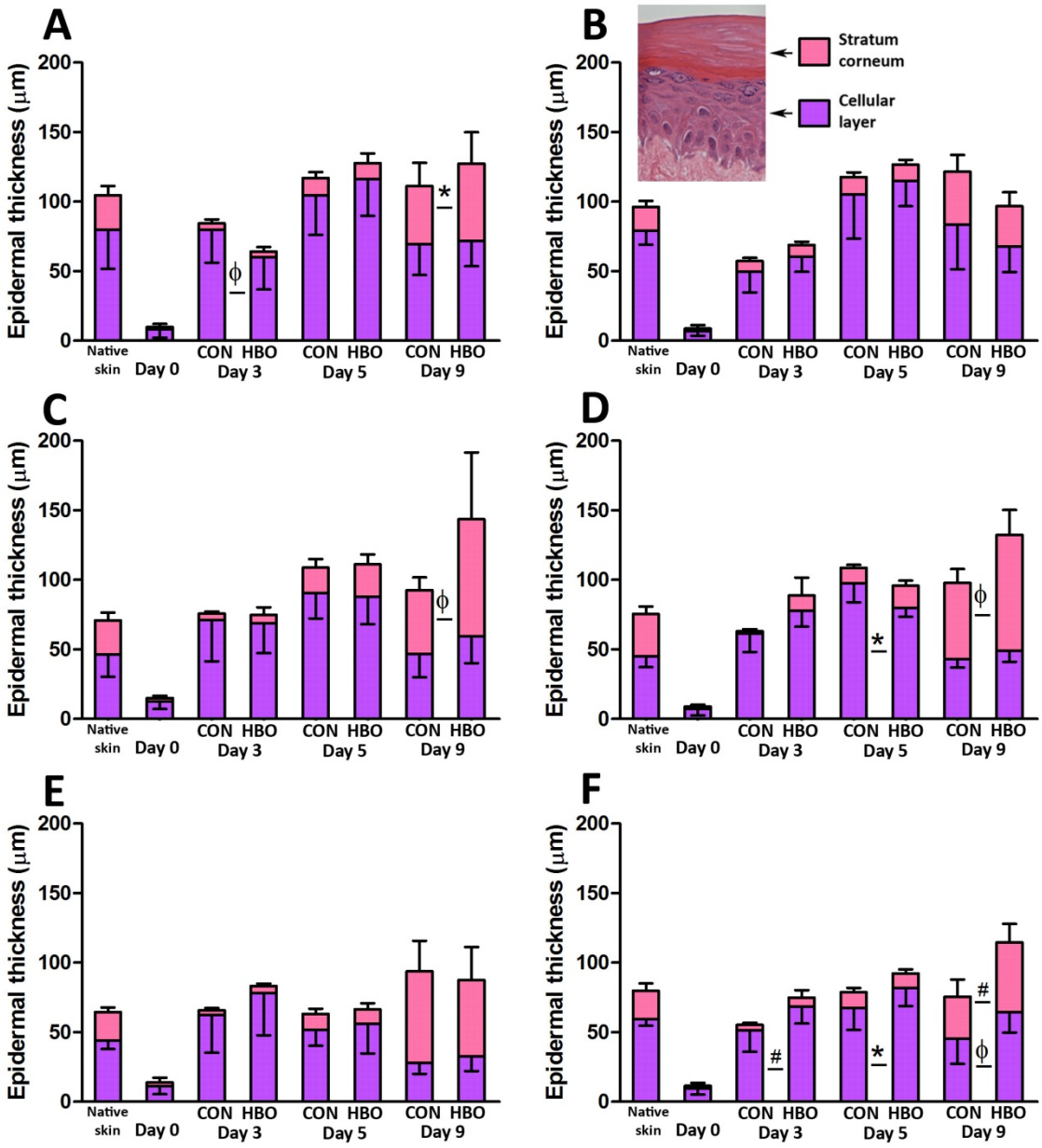

Figure 5.6 The effect of HBO treatment on epidermogenesis in the HSE model
Image analysis was performed on H&E images of both native skin and the HSE models captured from each sample over time. The graphs represent the data obtained from (**A**) pooled epidermal thickness data from the group A skin samples, (**B**) epidermal thickness data for sample 4, (**C**) sample 5, (**D**) sample 6, (**E**) sample 7 and (**F**) sample 8. The thickness of viable cellular region is indicated by the purple bars and the stratum corneum is indicated by the pink bars. Data obtained from n = 2 HSEs per time point, except sample 6, where n = 1 per time point. There were a total of 8 histological sections analysed per HSE model, therefore, 16 images for all samples, except sample 6. The data is expressed as the mean epidermal thickness ± standard deviation (* represents $p < 0.05$, # represents $p < 0.01$ and φ represents $p < 0.001$).

5.3.6 Immunohistochemical analysis of the HSE models over time.

After 9 days of treatment the HSE models developed a thicker stratum corneum in response to HBO (**Figure 5.6**). This suggests that HBO treatment may enhance the development and maturation of the HSE model. In view of this immunohistochemical analysis was performed using markers of skin proliferation and differentiation status to determine if differences in response to HBO treatment were apparent. As was previously described in section 3.3.6, keratinocyte proliferation was investigated using antibodies specific to p63 and ki-67, whereas differentiation was analysed using antibodies to keratin 1 (K1), loricrin and keratin 16 (K16).

5.3.7 Expression and localisation of p63 in the HSE model in response to HBO treatment

The expression of p63 was analysed to determine if HBO treatment influenced the proliferative capacity of the epidermis in the HSE model. Immunoreactivity and localisation of p63 in the developing HSE and native skin was previously described in section 3.3.6 - 3.3.7. From qualitative analysis of the images captured from both control and HBO-treated HSE models, it does not appear that HBO treatment affected the presence or localisation of p63 (**Figure 5.7**). To quantitatively determine if HBO affected p63 immunoreactivity, the images were analysed using ImageJ.

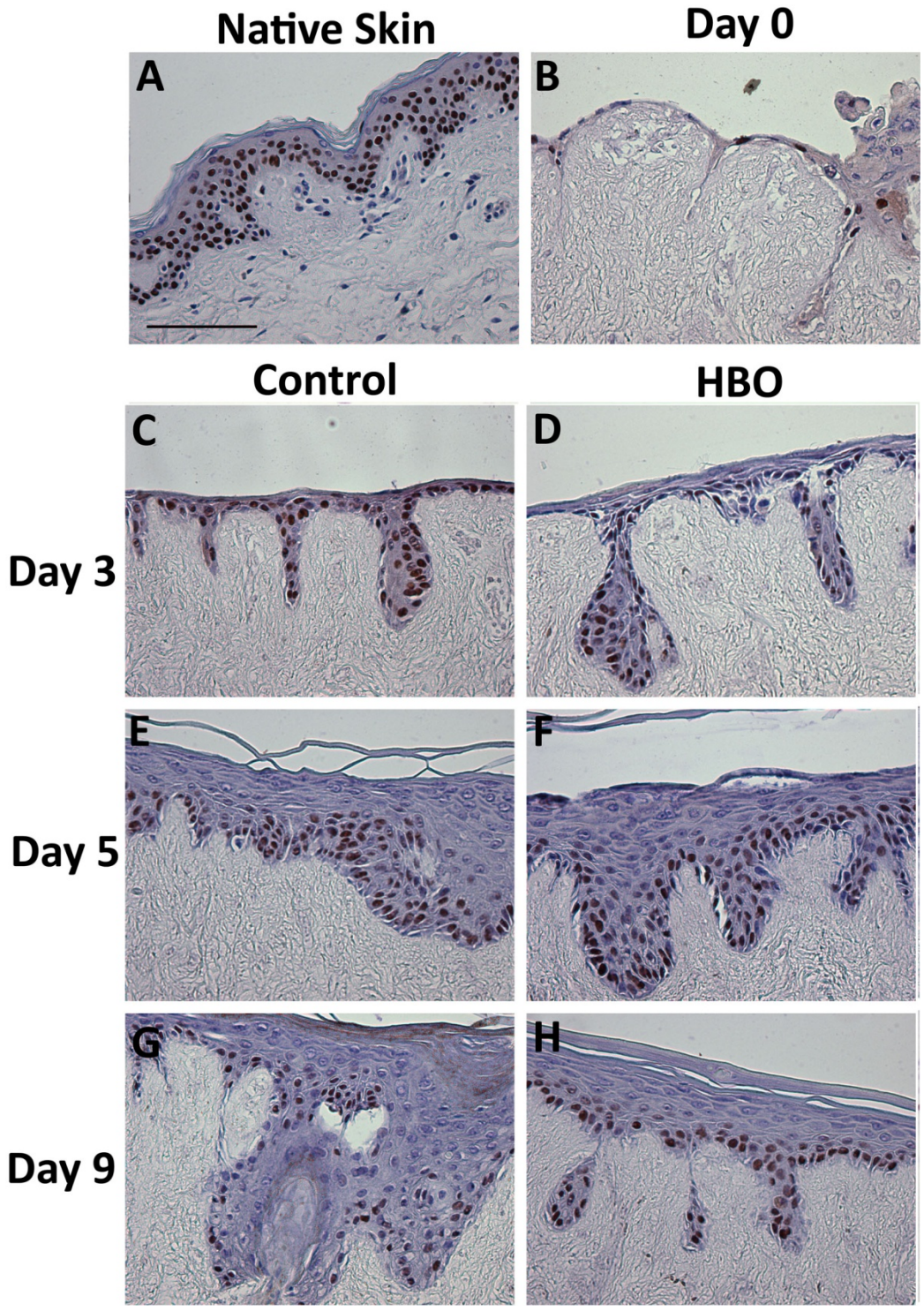

Figure 5.7 The effect of HBO treatment on p63 expression in the HSE model
The HSE models were treated either with or without HBO for nine consecutive days and harvested at each time point. The expression of p63 was detected in (**A**) native skin and in HSE models at (**B**) day 0, (**C, D**) day 3, (**E, F**) day 5 and (**G, H**) day 9. HBO-treated samples are represented in images **D, F** and **H**, whereas control samples are in images **C, E** and **G**. Presence of the p63 antigen is represented by brown immunoreactivity, whereas nuclei are counter-stained blue with haematoxylin. The scale bar represents 100 µm. This is a representative figure using images captured from skin sample 4.

5.3.8 HBO treatment does not consistently influence p63 expression in HSE models

Images captured of the p63 immunoreactivity described above (section 5.3.7) were analysed using ImageJ. The numbers of p63 positive nuclei were counted to determine the temporal expression of this proliferation marker in response to HBO treatment. The group A skin samples were analysed by image analysis techniques and the resulting data was pooled (Appendix Table A26). The group B skin samples were analysed and the data expressed separately (Appendix Table A27). In three out of the six skin HSE groups analysed, there was a significantly greater number of p63-positive nuclei at day 5 in response to HBO treatment than was present in the control (138.88 ± 37.61in HBO compared to 105.88 ± 26.43 in control in sample 4 and 61.94 ± 19.96 in HBO compared to 46.25 ± 9.46 in control in sample 5; $p < 0.05$; **Figure 5.8 B** and **C**) and (88.94 ± 21.62 in HBO compared to 59.31 ± 17.45 in the control in sample 8; < 0.001; **Figure 5.8 F**). In contrast, sample 7 had significantly less p63-positive nuclei at day 5 in response to HBO treatment as compared to the correlating control (62.38 ± 6.99 in HBO compared to 63.00 ± 6.99 in control in sample 6; $p < 0.05$; **Figure 5.8 E**). Therefore, it appears that HBO only impacts the expression of p63 in the HSE model after 5 days of treatment and this is not constant between each HSE model. This suggests that HBO does not consistently affect epidermal proliferative capacity.

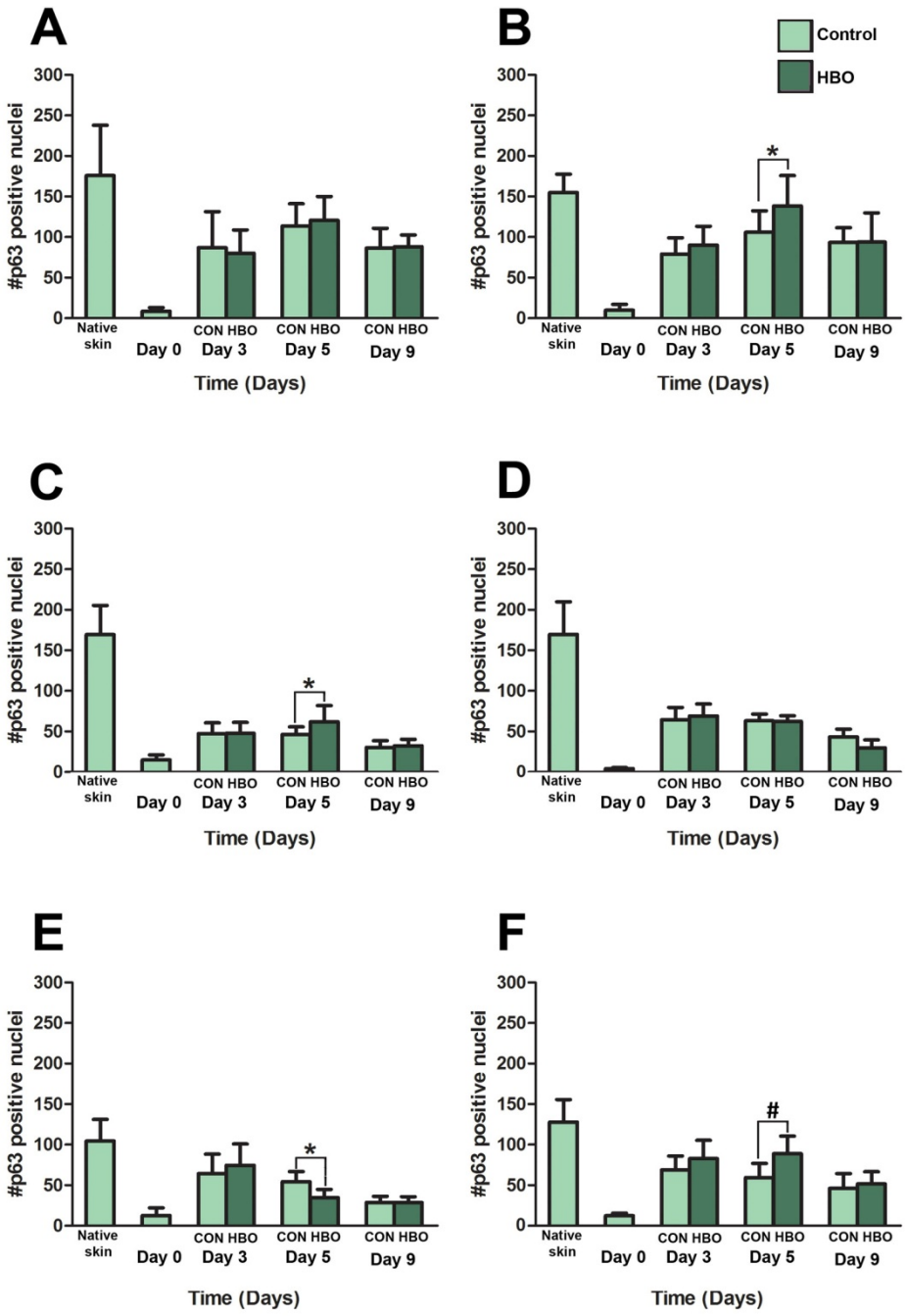

Figure 5.8 The effect of HBO treatment on p63 expression in the HSE model
The number of p63 positive nuclei were counted using ImageJ in sequential histology sections to determine the average number of positive nuclei per section. The graphs represent the data obtained from (**A**) pooled p63 data from the group A skin samples, (**B**) p63 data from sample 4, (**C**) sample 5, (**D**) sample 6, (**E**) sample 7 and (**F**) sample 8. Data obtained from n = 2 HSEs per time point, except sample 6, where n = 1 per time point. There were a total of 8 histological sections analysed per HSE model, therefore 16 images for all samples, except sample 6. Data represents mean numbers of positive nuclei ± standard deviation. * indicates $p < 0.05$ and # indicates $p < 0.001$.

5.3.9 Expression and localisation of ki-67 in the HSE model in response to HBO treatment

Immunoreactivity for the cell cycle marker ki-67 was examined to determine if HBO influenced the proliferative status of the HSE model. Previously, in sections 3.3.8 - 3.3.9, the temporal immunoreactivity and localisation of ki-67 in native skin and the HSE model was reported. Qualitative analysis of the immunohistochemical images revealed that ki-67 was localised to the basal layer of the epidermis in all samples. However, it appeared that the number of ki-67 positive nuclei may be lower in HBO-treated HSEs at days 3 and 5, compared to the correlating control-treated HSEs (**Figure 5.9 C - F**). In order to quantitatively determine ki-67 positive cell numbers, the images were analysed using ImageJ.

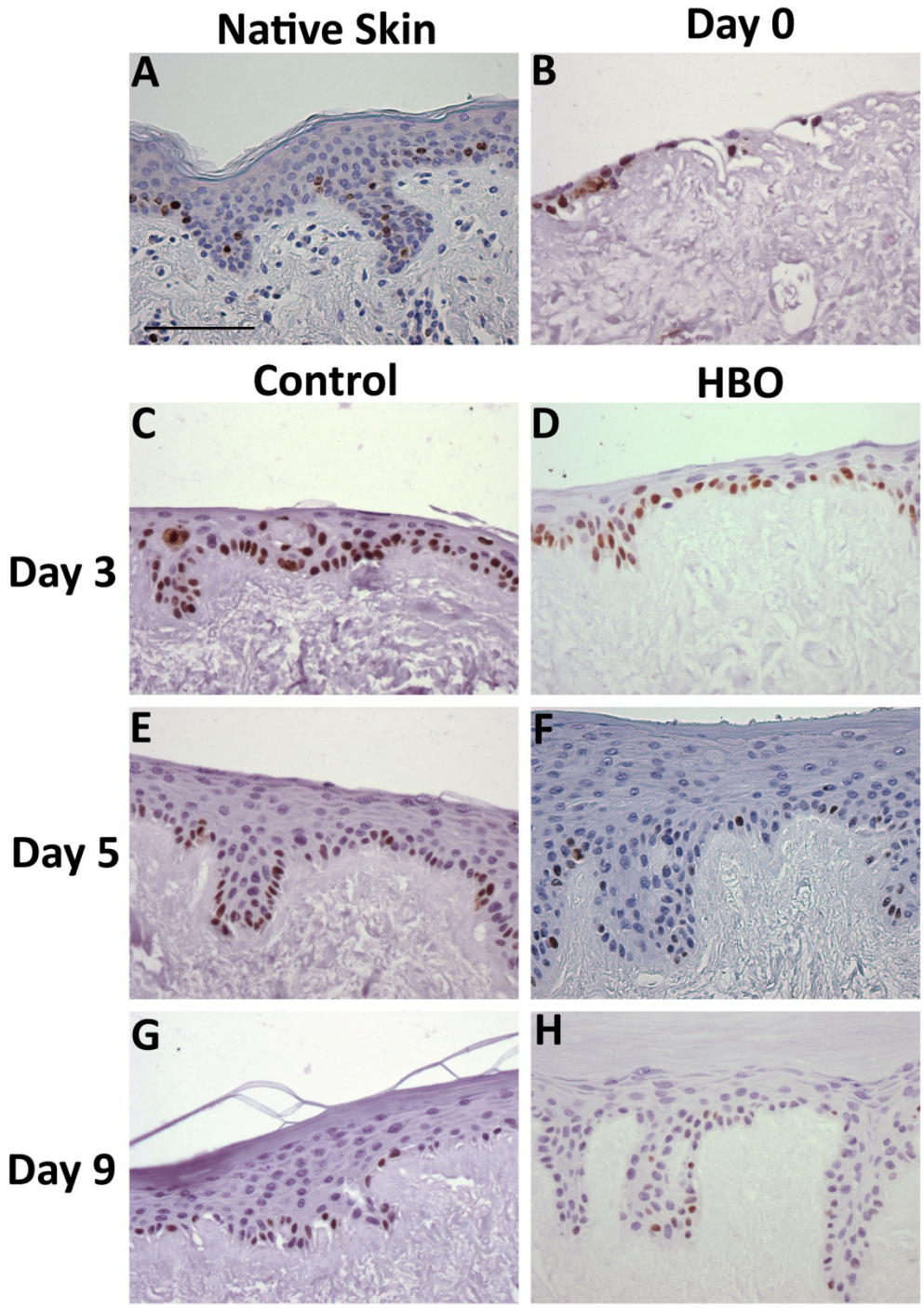

Figure 5.9 The effect of HBO treatment on ki-67 expression in the HSE model
The HSE models were treated either with or without HBO for nine consecutive days and harvested at time points. The expression of ki-67 in keratinocytes was detected in (**A**) native skin and in HSE models at (**B**) day 0, (**C, D**) day 3, (**E, F**) day 5 and (**G, H**) day 9. HBO-treated samples are represented by figures **D, F** and **H**, whereas control samples were in figures **C, E** and **G**. The presence of the ki-67 antigen is represented by brown immunoreactivity, whereas nuclei were counter-stained blue with haematoxylin. The scale bar represents 100 µm. These are representative images from the group A skin samples.

5.3.10 HBO treatment does not consistently influence ki-67 expression in HSE models

Images captured of ki-67 immunoreactivity described above (section 5.3.9) were analysed using ImageJ. The numbers of ki-67 positive nuclei were counted to determine the temporal expression levels of this proliferation marker, in response to HBO treatment. The group A skin samples were analysed by image analysis techniques and the resulting data was pooled (Appendix Table A28). The group B skin samples were analysed and the data expressed separately (Appendix Table A29). At day 3, HSEs from the group A samples had a significantly lower number of ki-67 positive nuclei in response to HBO treatment when compared to the day 3 control (50.83 ± 9.60 in HBO compared to 65.50 ± 13.56 in HBO; $p < 0.05$; **Figure 5.10 A**). In contrast, at day 3 in sample 4, there were a significantly higher number of ki-67 positive nuclei in response to HBO treatment. (90.69 ± 13.30 in HBO compared to 78.81 ± 11.44 in the control; $p < 0.05$; **Figure 5.10 B**). In sample 8, a significantly lower number of ki-67 positive nuclei at day 5 in response to HBO treatment were observed as compared to the day 5 control (70.50 ± 16.84 in HBO compared to 68.75 ± 23.17 in control; $p < 0.05$; **Figure 5.10 F**). In general there were no consistent trends in response to HBO treatment in the HSE models at any time point.

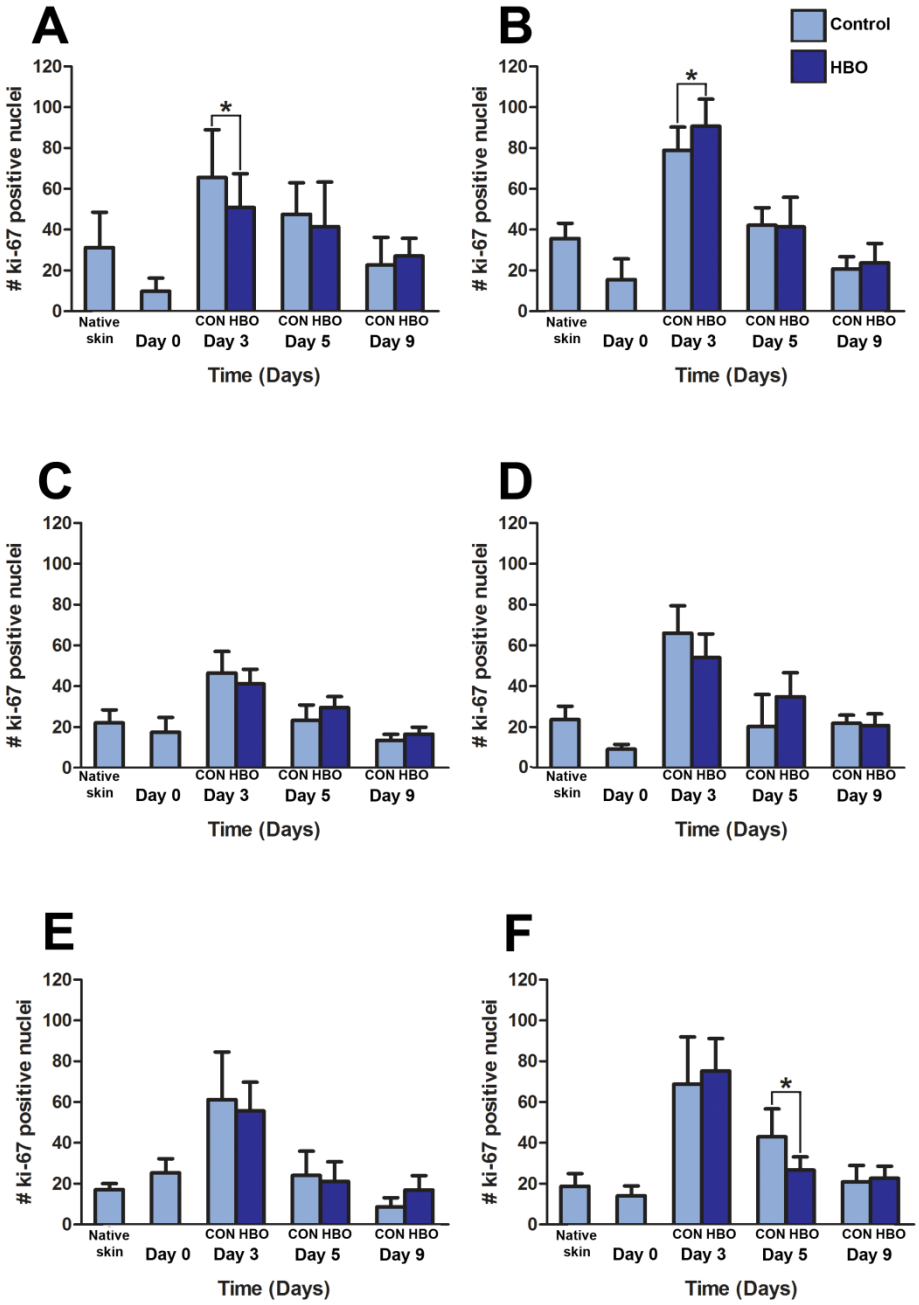

Figure 5.10 The effect of HBO treatment on ki-67 expression in HSE models
The number of ki-67 positive nuclei were counted using ImageJ in sequential histology sections to determine the average number of actively proliferating cells per section. Data from (**A**) the group A skin samples, (**B**) from sample 4, (**C**) sample 5, (**D**) sample 6, (**E**) sample 7 and (**F**) sample 8 are presented. Data was obtained from n = 2 HSEs per time point, except sample 6, where n = 1 per time point. There were a total of 8 histological sections analysed per HSE model, therefore, 16 images for all samples, except sample 6, where n = 8. Graphs represent mean number of ki-67 positive nuclei ± standard deviation. Statistical significance $p < 0.05$ is indicated by *.

5.3.11 Expression and localisation of K1 in the HSE model in response to HBO treatment

Since HBO treatment did not appear to have any major effects on epidermal proliferation, the early differentiation marker, K1, was investigated to determine if HBO treatment influenced HSE maturation. The immunoreactivity and localisation of K1 in native skin and the HSE model over time was previously reported in sections 3.3.10 - 3.3.11, the focus of the studies reported here was to analyse the impact of HBO treatment on K1 expression in the HSE model. From the immunohistochemistry images, it appears that K1 was expressed to a greater extent in the control samples, specifically at days 5 and 9 (**Figure 5.11 E** and **G**). In particular, at day 5 K1 was expressed in all supra-basal layers, while K1 was expressed in the upper supra basal layers in HBO-treated HSEs (**Figure 5.11 E** and **F**). To quantify the thickness of K1 expressed in each sample the images were analysed using ImageJ.

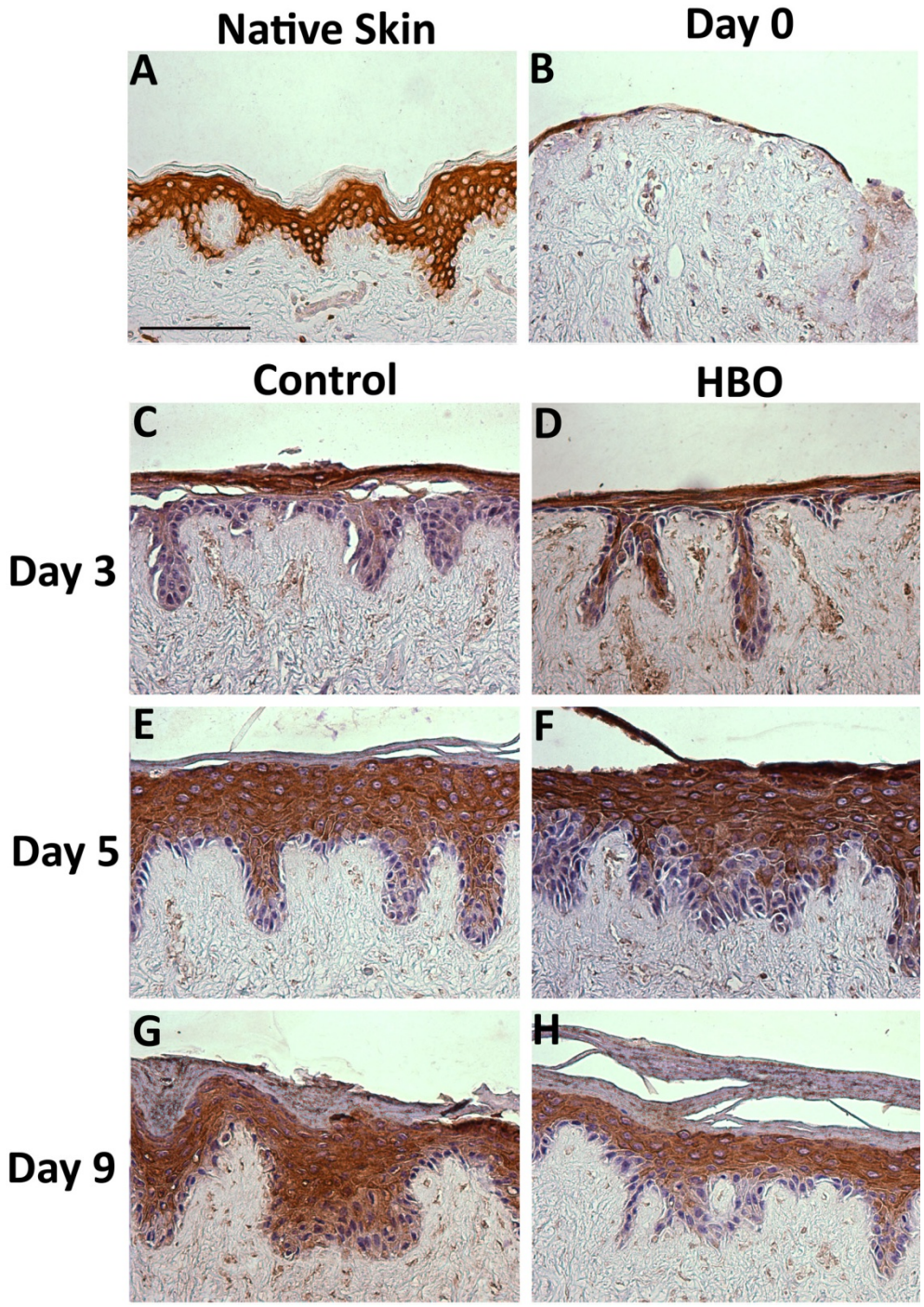

Figure 5.11 The effect of HBO treatment on K1 expression in HSE models
The HSE models were treated either with or without HBO for nine consecutive days and harvested at various time points. The expression of K1 in the epidermis was detected in (**A**) native skin and in HSE models at (**B**) day 0, (**C ,D**) day 3, (**E, F**) day 5 and (**G, H**) day 9. HBO-treated samples are represented in images **D, F** and **H**, whereas control samples are in images **C, E** and **G**. Presence of the K1 antigen is represented by brown immunoreactivity. The nuclei are counter-stained blue by haematoxylin. The scale bar represents 100 µm. These are representative images using images captured from sample 4.

5.3.12 HBO treatment does not consistently influence K1 expression in HSE models

Images captured of the K1 immunoreactivity described above were analysed using ImageJ and the thickness of the epidermis expressing K1 in response to HBO treatment was determined. The group A skin samples were analysed by image analysis techniques and the resulting data were pooled (Appendix Table A30). The group B skin samples were analysed and the data expressed separately (Appendix Table A31). Statistical analysis was performed on the data to determine if control or HBO treatment had an impact on the thickness of K1 in the HSE models over time. Significantly lower amounts of K1 immunoreactivity were present in the day 5 epidermis in HBO HSEs from the group A samples (45.74 µm ± 25.06 µm in HBO compared to 65.78 µm ± 19.31 µm in control; $p < 0.001$; **Figure 5.12 A**) and sample 6 (25.50 µm ± 3.29 µm in HBO compared to 37.97 µm ± 5.15 µm in control; $p < 0.001$; **Figure 5.12 D**) when compared to the correlating controls. HBO treatment also induced significantly enhanced K1 at day 5 in sample 5 (47.23 µm ± 14.13 µm in HBO compared to 36.65 µm ± 10.66 µm in control; $p < 0.05$; **Figure 5.12 C**). At day 9, there was also significantly less K1 present in response to the HBO treatment in both sample 4 (61.17 µm ± 24.82 µm in HBO compared to 76.25 µm ± 20.11 µm in the control; $p < 0.01$; **Figure 5.12 B**) and sample 6 (20.40 µm ± 4.59 µm in HBO compared to 25.50 µm ± 3.29 µm in the control; $p < 0.001$; **Figure 5.12 D**) compared to the control samples. Taken together, these data indicate there were no consistent trends in response to HBO treatment in the HSE models at any time point.

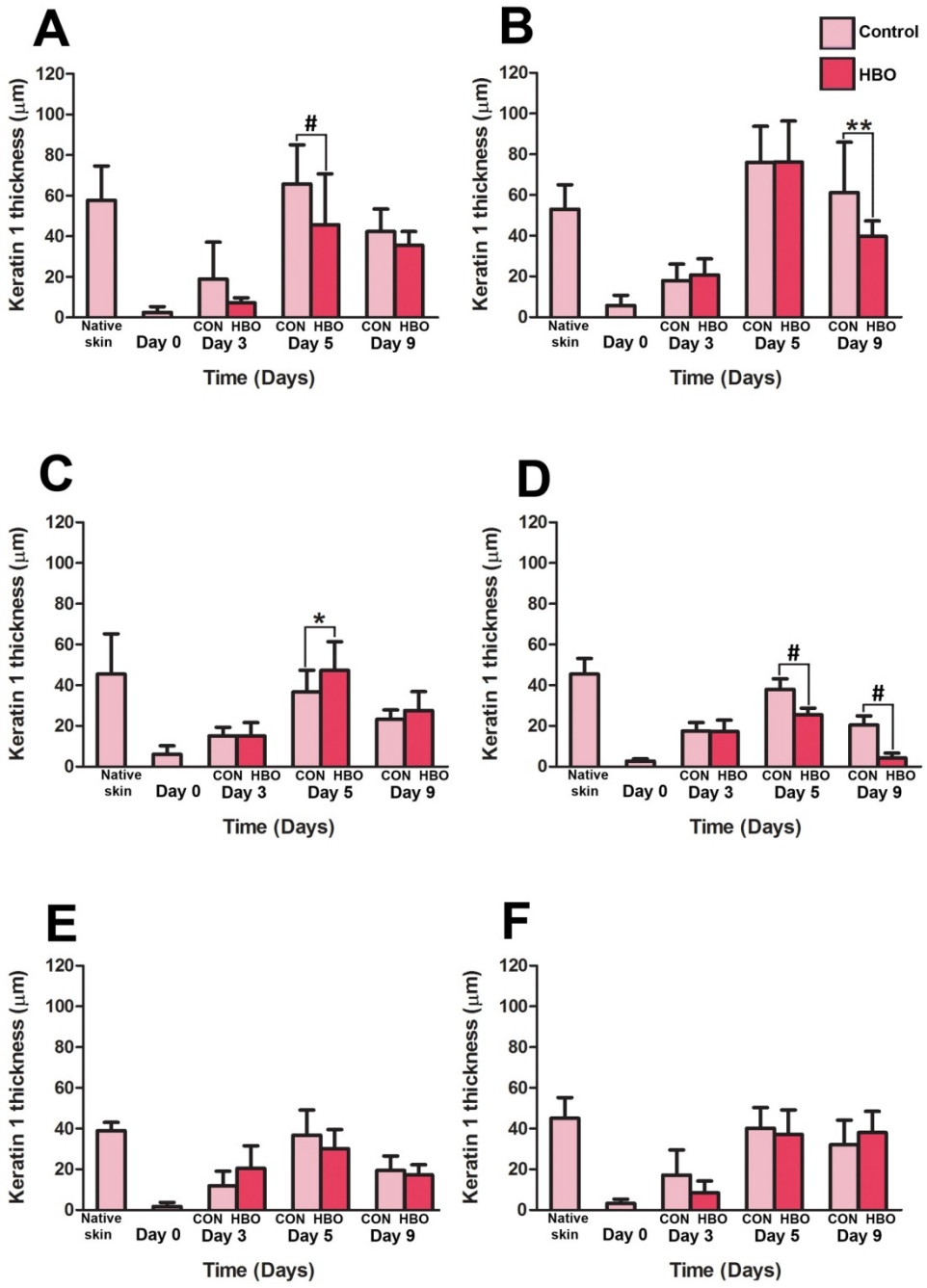

Figure 5.12 The effect of HBO treatment on K1 expression in HSE models
The thickness of K1 – positive epidermis was determined using ImageJ in sequential histology sections. Data from (**A**) the group A skin samples, (**B**) from sample 4, (**C**) sample 5, (**D**) sample 6, (**E**) sample 7 and (**F**) sample 8 are presented. Data was obtained from n = 2 HSEs per time point, except sample 6, where n = 1 per time point. There were a total of 8 histological sections analysed per HSE model, therefore, 16 images for all samples, except sample 6, where n = 8. Graphs represent mean thickness of K1-positive epidermis ± standard deviation. Statistical significance $p < 0.05$ is indicated by *, $p < 0.01$ is indicated by **, and $p < 0.001$ is indicated by #.

5.3.13 Expression and localisation of loricrin in the HSE model in response to HBO treatment

To more closely examine the potential effect of HBO on epidermal differentiation, the presence of loricrin was examined. Loricrin is a terminal differentiation marker and was investigated to determine if HBO treatment influenced epidermal cornification in the HSE model. The immunoreactivity and localisation of loricrin in native skin and the HSE model over time was previously reported in sections 3.3.12 - 3.3.13, therefore, the focus of these new studies was to analyse the impact of HBO treatment on loricrin expression in the HSE model. Loricrin was expressed to a greater extent in the control samples, particularly at days 5 and 9 (**Figure 5.13 E** and **G**). Overall, it was observed in all experimental samples that loricrin was expressed in the upper stratum granulosum and there did not appear to be any striking differences in loricrin expression between control and HBO-treated HSE models. To establish if there were any differences in the expression that were not immediately obvious from the immunohistochemistry images, the thickness of loricrin-positive epidermis quantified using ImageJ analysis as described in section 2.11.2.

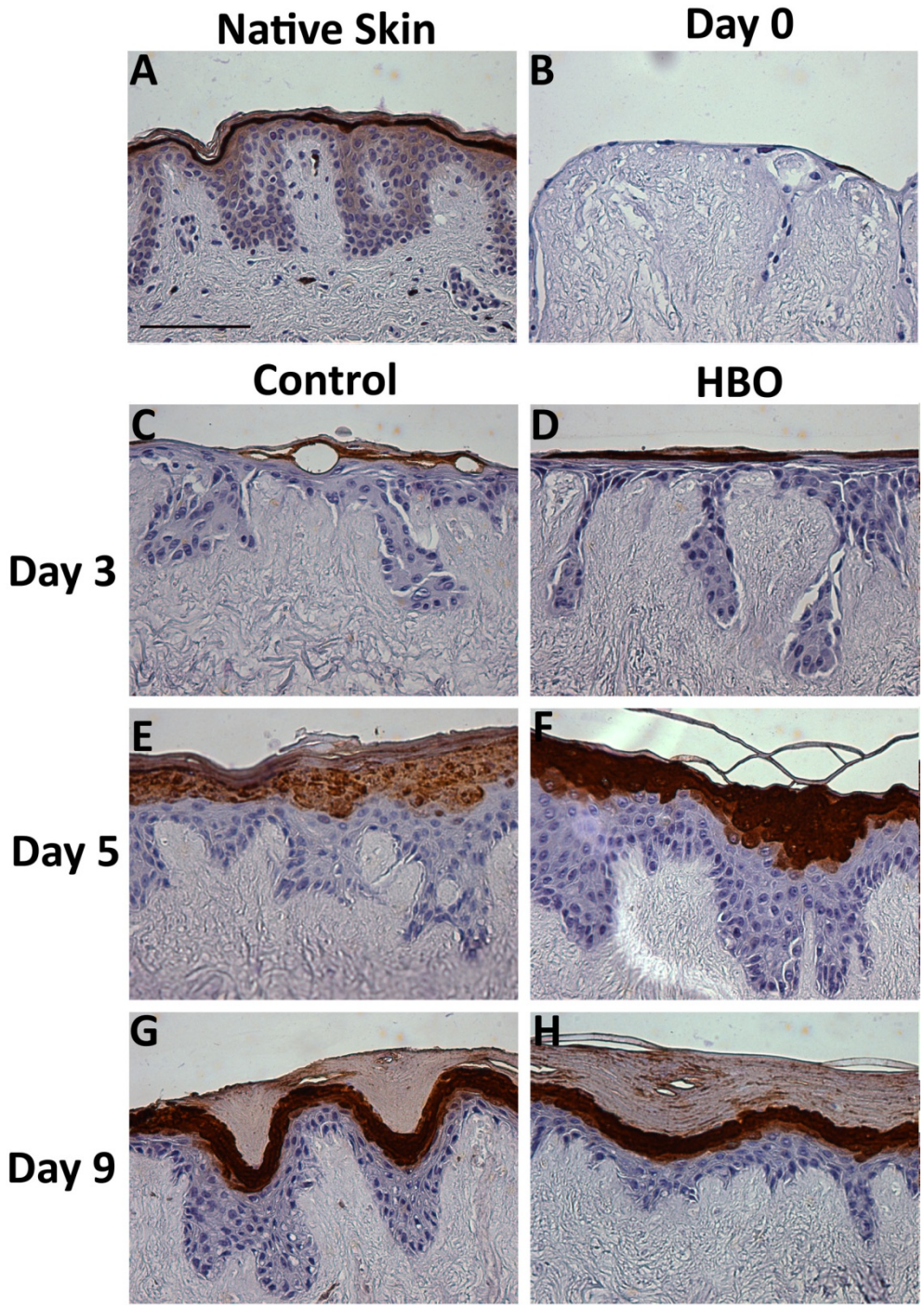

Figure 5.13 The effect of HBO treatment on loricrin expression in HSE models
The HSE models were treated either with or without HBO for nine consecutive days and harvested at the indicated time points. The expression of loricrin in keratinocytes was detected in (**A**) native skin and in HSE models at (**B**) day 0, (**C ,D**) day 3, (**E, F**) day 5 and (**G, H**) day 9. HBO-treated samples are represented in images **D, F** and **H**, whereas control samples are in images **C, E** and **G**. Presence of the loricrin antigen is represented by brown immunoreactivity. The nuclei are counter-stained blue with haematoxylin. The scale bar represents 100 µm. This is a representative figure using images captured from sample 4.

5.3.14 HBO treatment does not consistently influence loricrin expression in HSE models

Images captured from immunoreactivity results described above were analysed using ImageJ. The thickness of the epidermis expressing loricrin was determined using image analysis techniques to determine the expression of this marker over time in response to HBO treatment. The group A skin samples were analysed by image analysis techniques and the resulting data were pooled (Appendix Table A32). The group B skin samples were analysed and the data expressed separately (Appendix Table A33). Statistical analysis was performed on the image analysis data to determine if HBO treatment induced changes in loricrin expression levels. Of the six data sets analysed, only two demonstrated any significant changes in response to control or HBO treatment. HBO treatment induced significantly less loricrin immunoreactivity at days 5 (18.97 µm ± 2.69 µm in HBO compared to 28.76 µm ± 6.06 µm in control; $p < 0.001$) and 9 (4.03 µm ± 2.95 µm in HBO compared to 14.25 µm ± 1.96 µm in the control; $p < 0.001$) in sample 6 and day 9 in sample 7 (9.52 µm ± 4.46 µm in HBO compared to 19.73 µm ± 7.60 µm in the control; $p < 0.001$) than was present in the control samples (**Figure 5.14 D** and **E**). In addition, there was a significant increase in loricrin expression at day 5 in response to HBO treatment in sample 7 (29.33 µm ± 6.79 µm in HBO compared to 21.88 µm ± 5.13 µm in the control; $p < 0.01$; **Figure 5.14 E**). In general, loricrin appeared to be differentially expressed in response to HBO treatment at later time points (day 5 or 9), but this was not consistent between HSE models.

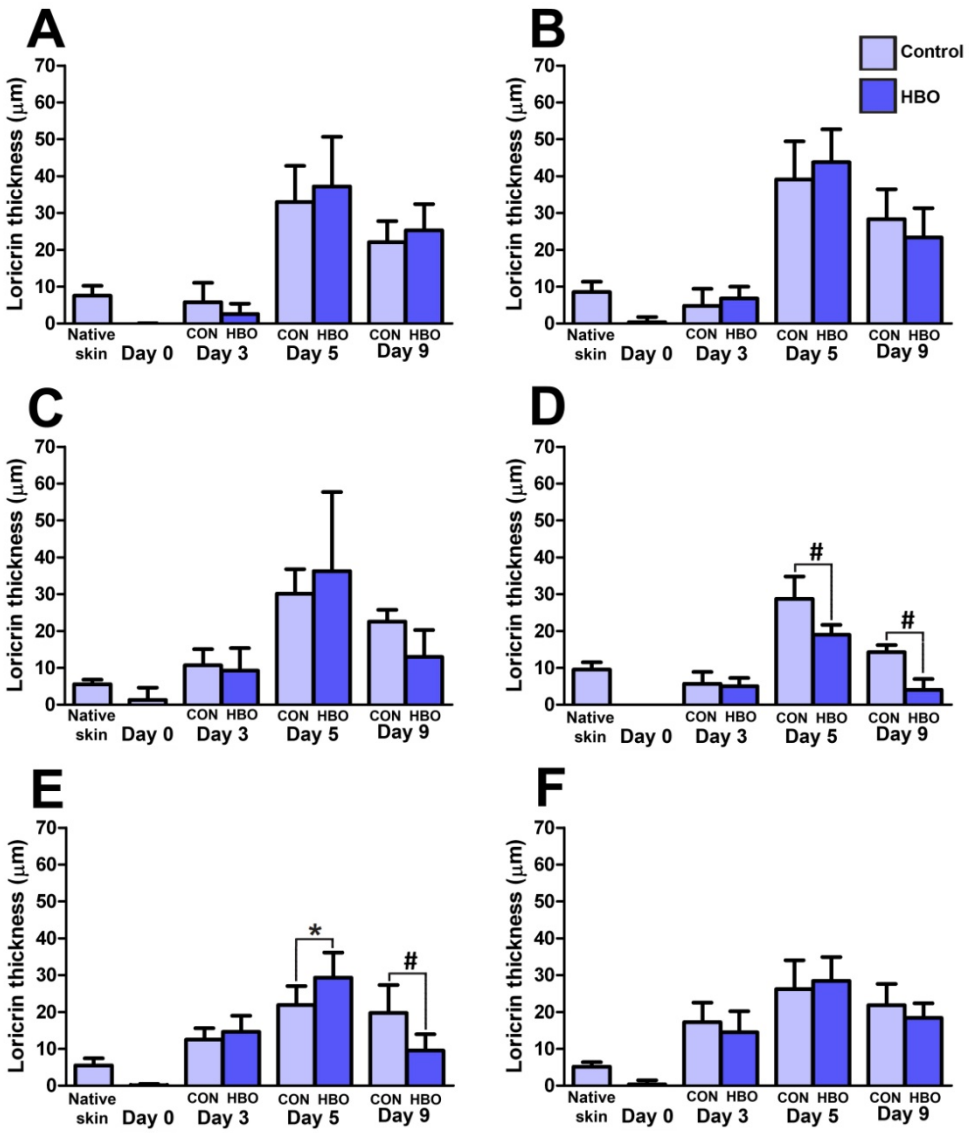

Figure 5.14 The effect of HBO treatment on loricrin expression in HSE models
The thickness of the loricrin-positive epidermis in the HSE models was quantified using ImageJ in sequential histological sections. The thickness of loricrin immunoreactivity in the epidermis was obtained from (**A)** the group A skin samples, (**B**) sample 4, (**C**) sample 5, (**D**) sample 6, (**E**) sample 7 and (**F**) sample 8. Data obtained from n = 2 HSEs per time point, except sample 6, where n = 1 per time point. There were a total of 8 histological sections analysed per HSE model, therefore, 16 images for each sample, except sample 6. The data represents the mean thickness of loricrin-positive epidermis ± standard deviation. Statistical significance $p < 0.01$ is indicated by *, and $p < 0.001$ is indicated by #.

5.3.15 Expression and localisation of K16 in the HSE model in response to HBO treatment

The hyper-proliferation marker, K16, was analysed to determine if HBO treatment influenced epidermal turnover in the HSE model. The immunoreactivity and localisation of K16 in native skin and the HSE model over time was previously reported in sections 3.3.14 - 3.3.15. The focus of this section was to analyse the impact of HBO treatment on K16 expression in the HSE model. From the immunohistochemistry images, it appeared that K16 was expressed in the supra-basal layers of the epidermis, irrespective of treatment method (**Figure 5.15**). Furthermore, there were no visible differences in the immunoreactivity and localisation of K16 in any of the HSE models (**Figure 5.15**). To quantify the thickness of the K16-positive epidermis, the images were analysed using ImageJ.

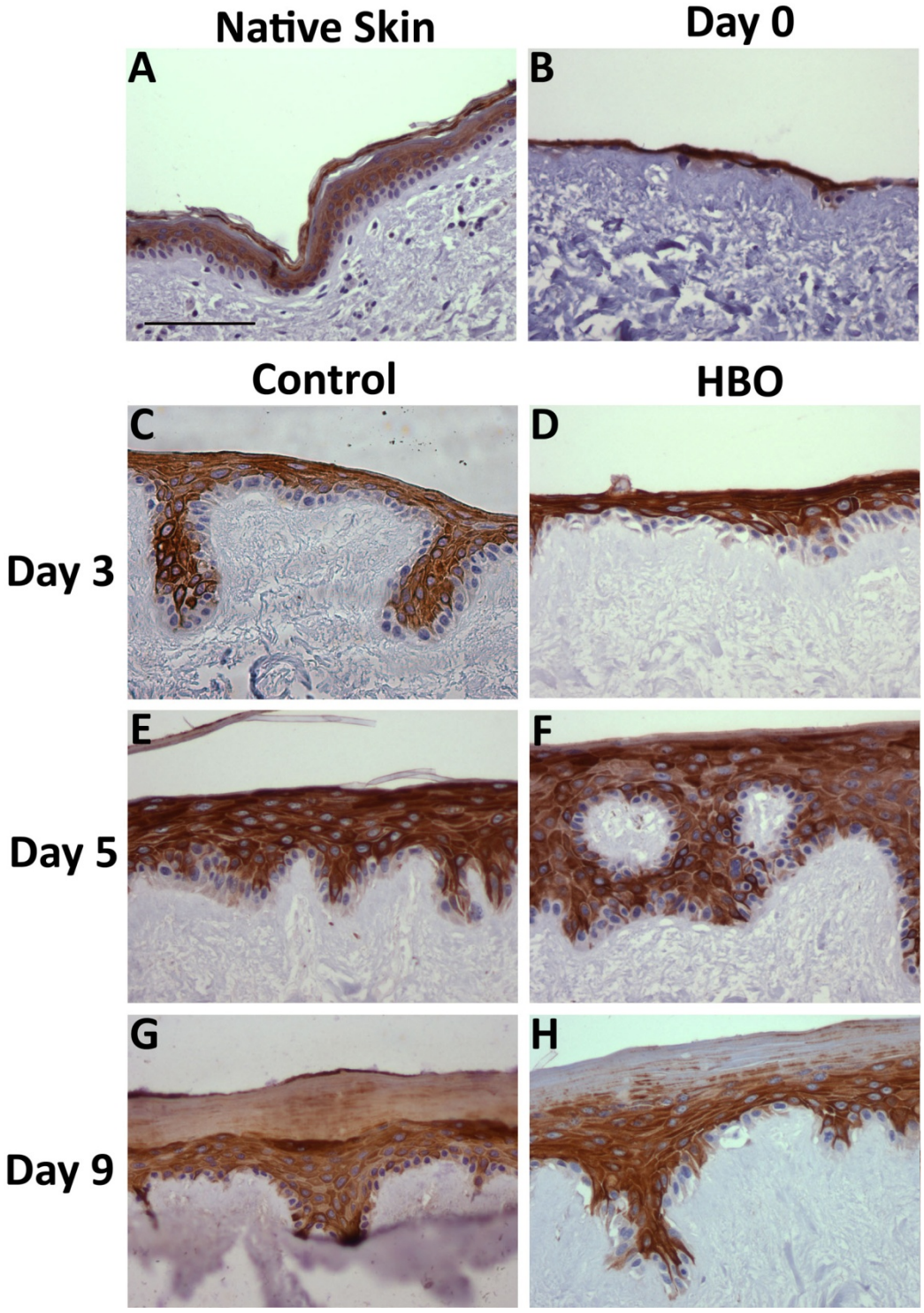

Figure 5.15 The effect of HBO treatment on K16 expression in HSE models
The HSE models were treated either with or without HBO for nine consecutive days and harvested at the indicated time points. The expression of K16 in keratinocytes was detected in (**A**) native skin and in HSE models at (**B**) day 0, (**C ,D**) day 3, (**E, F**) day 5 and (**G, H**) day 9. HBO-treated samples are represented in figures **D, F** and **H**, whereas control samples are in figures **C, E** and **G**. Presence of the K16 antigen is represented by brown immunoreactivity. The nuclei are counter-stained blue with haematoxylin. The scale bar represents 100 µm. This is a representative figure using images captured from the group A skin samples.

5.3.16 HBO treatment does not consistently influence K16 expression in HSE models

The thickness of the epidermis expressing K16 was determined using image analysis techniques to quantify the expression of this marker over time, in response to HBO treatment. The group A skin samples were analysed by image analysis techniques and the resulting data were pooled (Appendix Table A34). The group B skin samples were analysed and the data expressed separately (Appendix Table A35). Statistically significant differences between control and HBO treatment were observed in two out of the six data sets. Specifically, at day 5 there was an increased level of K16 in sample 5 in response to HBO treatment (64.65 µm ± 16.32 µm in HBO compared to 47.77 µm ± 11.20 µm in the control; $p < 0.01$; **Figure 5.16 C**). In addition, there was a lower level of K16 in sample 6 at day 5 and day 9 in response to HBO treatment, than was present in the controls at day 5 and 9 (49.45 µm ± 9.82 µm in HBO compared to 64.39 µm ± 7.10 µm in the control at day 5 and 28.87 µm ± 6.17 in HBO compared to 43.07 µm ± 3.64 µm in the control at day 9; $p < 0.01$; **Figure 5.16 D**). Apart from these exceptions, the level of K16 was essentially similar in the control and HBO-treated HSEs at each time point in all samples (**Figure 5.16**). This suggests that K16 is not influenced by HBO treatment in the HSE model.

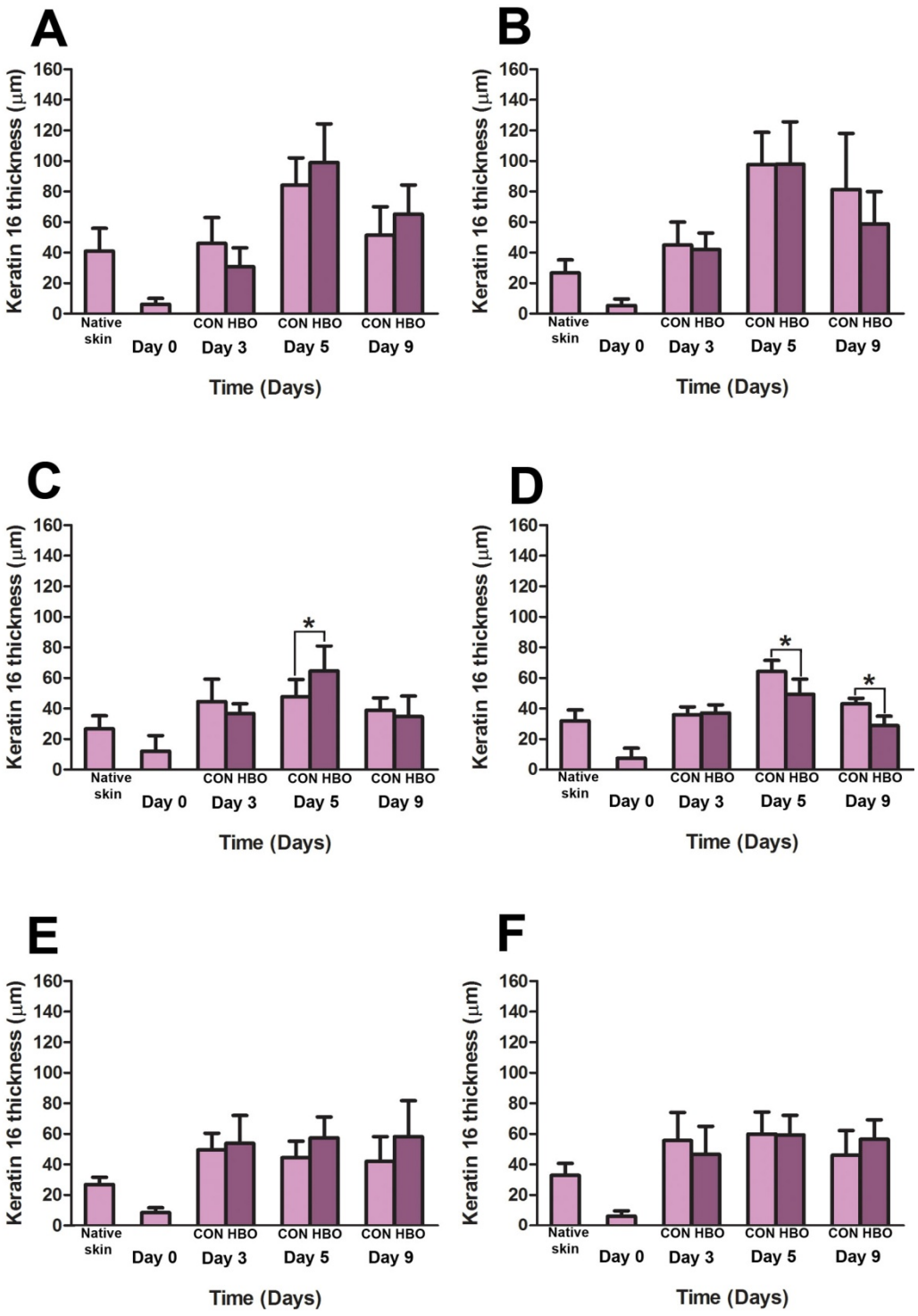

Figure 5.16 The effect of HBO treatment on K16 expression in HSE models
The thickness of K16 immunoreactivity in the HSE epidermis was quantified using ImageJ in sequential histological sections. The graphs show the data obtained from (**A**) the group A skin samples, (**B**) K16 data from sample 4, (**C**) sample 5, (**D**) sample 6, (**E**) sample 7 and (**F**) sample 8. Data obtained from n = 2 HSEs per time point, except sample 6, where n = 1 per time point. There was a total of 8 histological sections analysed per HSE model, therefore, 16 images for all samples, except sample 6 (n = 8 images). Data represent mean thickness of K16 immunoreactivity in µm ± standard deviation. Statistical significance $p < 0.01$ is indicated by *.

5.4 DISCUSSION

In Chapter 3 the validity of the keratinocyte-only HSE as a model of human skin was investigated. The focus of this Chapter on the other hand was to evaluate the influence of HBO treatment on epidermal outgrowth, epidermogenesis and the temporal expression of relevant cell markers. Firstly, the effect of HBO treatment on the pH of the culture medium used in the HSE culture system was examined. The buffering system in the HSE culture medium requires elevated CO_2 levels to maintain a stable pH. Over the course of the experiment, both control and HBO-treated HSE models were exposed to a CO_2-free atmosphere for 90 minutes/day. Previously, Ceccarini and Eagle (1971) reported that fluctuations in culture media pH (between pH 6.7 and pH 8.4) altered normal cellular growth by encouraging continued protein synthesis in the absence of cell division. The results reported herein however, indicate that neither treatment nor the presence of the HSE affected the pH of the culture media for the first 5 days of the experiment (**Figure 5.2**). This indicates that the subsequent results reported in this Chapter were due to the effect of HBO treatment itself upon the skin model and not caused by alterations to the pH environment of the composite.

Based on previous results by Kairuz *et al*. (2007), the studies which prompted the experiments in this Chapter, it was anticipated that HBO treatment would enhance keratinocyte migration and epidermal thickness. Interestingly, no significant differences were observed between HBO and control-treated HSE models in respect to migration and standard immunohistochemistry analysis (**Figure 5.3 - Figure 5.16**). However, an increase in epidermal thickness in response to HBO treatment was observed at day 9; this time period was longer than the scope of the Kairuz *et al*. (2007) study. The differences in results between this Chapter and Kairuz *et al*. (2007) most likely stem from the greater depth and more quantitative measuring techniques of the histology and immunohistochemistry analysis adopted in the studies reported herein. Moreover, this increase in epidermal thickness was obvious in a subset of the HSE models analysed (**Figure 5.5** and **Figure 5.6**). This increase in epidermal thickness of the HSE in response to HBO treatment reflects results previously reported by Dimitrijevich *et al*. (1999) who found after 10 days of HBO treatment, greater oxygen tension also resulted in greater epidermal thickness.

The results obtained and HSEs generated from skin from sample 5 were particularly interesting; the stratum corneum was almost twice as thick in the HBO-treated sample compared to the control at day 9 (**Figure 5.6C**). In addition, the stratum corneum of the HBO-treated samples was visibly thicker than the control at day 9 in HSEs from the group A samples and samples 6 and 8 (**Figure 5.6 A, D** and **F**). Further investigation into what made the HSEs generated from skin sample 5 so unique from the others revealed that this individual suffered from Cushing syndrome. This disease is known to have an impact on wound healing responses in people with this condition (Bitar *et al.,* 1999).

Cushing syndrome is a disease of the pituitary gland which involves hyper-secretion of adrenocorticotropic hormone (ACTH) and chronic excess of glucocorticoids (GC) and is characterised by persistent hyperglycaemia, which is caused by steroid-induced diabetes (Afandi *et al.,* 2003). These physiological changes result in dramatic losses in muscle and bone protein, and water and salt retention, leading to hypertension and oedema (Fernandez-Rodriguez *et al.,* 2009). Furthermore, other physical symptoms include a swollen "moon" face, redistribution of fat to the abdomen and the posterior neck ("buffalo hump"), a tendency to bruise, and of pertinent to the results of this study, poor wound healing. A review of pituitary gland diseases by Davidovici *et al.* (2008) summarised that the disruption of hormones in Cushing syndrome results in inhibited epidermal cell division and impairment of collagen synthesis, in turn affecting wound healing.

The effect of Cushing's syndrome has previously been studied in a 3D skin model in order to determine the effect of GC excess on the epidermis. Specifically, Zöller *et al.* (2008) isolated foreskin fibroblasts and keratinocytes to create a HSE model using type 1 bovine collagen scaffold as the dermal matrix. Once a stratified epidermis was formed, the HSEs were treated with GCs either 'systemically' (GCs introduced into the culture medium) or topically. The authors found similar results between both treatment methods with up to 50% and 54% reduction in the number of epidermal layers as compared to the untreated controls in the 'systemic' and topical groups respectively. Furthermore, the authors demonstrated a decrease, although not statistically significant, in the number of ki-67 positive nuclei in the GC-treated groups (Zöller *et al.,* 2008). Furthermore, Kao *et al.* (2003) topically applied GCs to the skin of healthy human volunteers and determined the trans-epithelia water loss of

the stratum corneum, as a measure of skin integrity. They found that topical GC application had adverse effects on epidermal permeability barrier function (Kao *et al.*, 2003). Therefore, it is clear that GC excess has detrimental effects on skin, which leads to impaired wound healing. There is, however, no clear evidence as to the specific molecular mechanisms that cause this. Interestingly, based on the results of the experiments reported in this Chapter, it is possible that HBO treatment is not the optimal therapy for healthy individuals, as skin donors 1 – 4 and 6 – 8 appeared to be. HBO treatment may, however, prove to be a useful wound healing tool in patients that have impaired wound healing. Further studies could investigate the effects of HBO on HSE models derived from individuals with afflictions that impair wound healing such as diabetes or other vascular conditions.

The results presented in section 5.3 suggest that HBO treatment increases epidermal thickness in some of the HSEs (**Figure 5.6**). Immunohistological markers of p63, ki-67, K1, loricrin and K16 were therefore investigated to determine if these were altered by HBO treatment and provide insight into the observed HBO-induced phenotypic responses. A marker of cellular proliferative capacity, p63, was examined in the HSE model. Previous reports by Kairuz *et al.* (2007) found enhanced p63 immunoreactivity in day 3 HBO-treated HSEs as compared to the control using qualitative analysis. Similarly, in the studies reported herein, the HSE models from 3 skin samples had significantly greater p63 immunoreactivity in response to HBO treatment at day 3 (**Figure 5.8 B, C** and **F**). While this result was not found in HSEs generated from all skin samples, it suggests that HBO treatment may enhance the proliferative capacity of the HSE model in the early stages of epidermogenesis.

The cell cycle marker ki-67 is indicative of the proliferative state of a tissue (Noszczyk and Majewski, 2001). Specifically, ki-67 is expressed in the nuclei of all cells that are not in the G_0 resting phase of the cell cycle, hence accurately discerns a cell's proliferative status (Noszczyk and Majewski, 2001). Importantly, Gill *et al.* (2010) generated HSE models to study the effect of chronic ischemia of human skin. The authors reported that oxygen deprivation led to a decrease in proliferation as indicated by a lack of ki-67 immunoreactivity in basal keratinocytes after only 48 hours of treatment (Gill *et al.*, 2010). Thus, if hypoxia inhibits proliferation as indicated by ki-67 expression, HBO may enhance it. The results presented in this Chapter, however, suggest that ki-67 was not differentially regulated in the HSE

model in response to HBO treatment (**Figure 5.10**). Furthermore, the significantly higher number of ki-67 positive nuclei measured in the HBO-treated HSEs from skin sample 3 at day 3 (**Figure 5.10 B**) did not correlate with an increase in epidermal thickness in the HSE from skin sample 3 (**Figure 5.6 B**). Similar lack of correlation between ki-67 expression and epidermal thickness was observed in each of the HSEs, regardless of the donor skin used. However, the expression of ki-67 in HSEs from both treatment groups was similar to the expression of ki-67 reported by others for a wound environment (Usui *et al.,* 2005). In a post wounding environment, when the keratinocytes have just migrated across the wound bed to form a single layer epidermis (similar to the day 0 HSE; Betz *et al.,* 1993), all keratinocytes express ki-67 and this trend continues at day 3. This increase in ki-67 expression remained elevated until the epithelium had stratified and began to resemble native skin, at which time the level of ki-67 expression greatly decreases (Betz *et al.,* 1993; Usui *et al.,* 2005).

In light of these results, the differences in epidermal thickness and maturation observed in response to HBO-treatment would therefore appear to be the product of factors other than an increase in standard proliferation markers. Thus standard markers of differentiation and their expression in the HSE model undergoing epidermogenesis were investigated. The immunoreactivity patterns for the early differentiation marker, K1, and the late differentiation marker, loricrin, were very similar in both the HBO- and control-treated HSE models (**Figure 5.11 - Figure 5.14**). These results differ from those reported by Kairuz *et al.* (2007) who previously found that HBO treatment enhanced the differentiation process in the skin models. However, as previously noted in section 1.6, Kairuz *et al.* (2007) did not utilise quantitative image analysis techniques, therefore the results reported here may well more accurately represent the biological processes that occurred at each time point within the HSE model.

Finally, K16 expression in the developing HSE model was examined and reported in Chapter 3, revealing that epidermogenesis resulted from hyper-proliferative activity of keratinocytes. Interestingly, the effect of oxygen on the expression of K16 has not been widely investigated. Wruck *et al.* (2011), however, reported that transcription factor nrf2 (nuclear factor E2-related factor 2) was up-regulated in response to oxidative stress and reactive oxygen species (ROS)

generation. Importantly, the authors also determined that K16 gene and protein expression was regulated by nrf2 in the presence of increased oxygen (Wruck *et al.*, 2011). Furthermore, Schäfer *et al*. (2012) have correlated increased epidermal thickening and impaired desquamation with oxidative stress-induced nrf2 expression. Therefore, HBO may induce oxidative stress in the HSE models, thereby inducing nrf2 and later K16 expression in this model system. From the results reported herein, there were no consistent differences in response to HBO treatment in the HSE model in terms of K16 expression.

Taken together, the results of the experiments reported in this Chapter indicate that in some cases, HBO clearly and in a temporal manner increases the thickness of the epidermis and its protective component, the stratum corneum. However, these results cannot be fully explained by standard histological markers of proliferation, p63, ki-67 and K16, or by differentiation-specific markers such as K1 and loricrin. Thus, it is clear that investigation of standard markers of skin proliferation and differentiation alone are not sufficient to elucidate the mechanisms of HBO action; investigation of the molecular changes that occur in response to HBO treatment may shed further light. In the next Chapter a detailed investigation into the changes that occur in gene and correlating protein expression in response to HBO is performed in a further attempt to determine molecular modifications that may result from this treatment.

Chapter 6: Analysis of genes and proteins involved in the response of the HSE model to HBO treatment

6.1 INTRODUCTION

While previous research has been conducted into the effect of hyperbaric oxygen (HBO) on skin cells and HSE models, no studies have been conducted investigating the effect of HBO treatment on a HSE model at the molecular level. Investigations of the effects of HBO on keratinocytes cultured in 2D systems demonstrated that HBO induced accelerated differentiation as determined through analysis of immunohistological markers (Hollander *et al.*, 2000). Dimitrijevich *et al*. (1999) and Kairuz *et al.* (2007) previously demonstrated that HBO treatment of HSE models led to an increase in epidermal thickness in comparison to control, non-HBO-treated samples. Additionally, Kairuz *et al.* (2007) found that HBO treatment enhanced keratinocyte proliferation and accelerated epidermal maturation in comparison to control samples. Thus, these studies suggest that HBO treatment impacts upon the basic physiology of the HSE model, enhancing the formation and maturation of the epidermis. These effects have, however, only been analysed at the basic phenotypic level (Kairuz *et al.*, 2007).

The data presented in this Chapter arise from investigation of the effects of HBO on global gene expression within the epidermis of the HSE model. This was pursued since no previous studies have been published examining the changes in gene expression that occur in response to HBO treatment in a HSE model. As detailed in Chapter 5, changes in the fundamental architecture of the HSE model in response to HBO treatment is unable to be explained by simple immunohistochemical analysis of basic epidermal markers. Therefore, these changes were further investigated via gene microarray studies and quantitative real time PCR, and with immunohistochemistry for correlating protein expression. These were performed in order to better understand what molecular events underpin these HBO-induced physiological changes in the epidermis.

6.2 METHODS AND MATERIALS

Full details of the materials and methods used in the experimental procedures for this Chapter are fully described in Chapter 2. Herein is a brief summary of the procedures used to generate the data presented in section 6.3.

6.2.1 Generation and culture of human skin equivalent models

HSE models were generated using skin obtained from individuals undergoing elective cosmetic breast reduction or abdominoplasty surgeries as fully described in sections 2.4 - 2.6. Following generation of the HSE models, they were cultured at the air-liquid interface and maintained in Full Greens (FG) culture media. The media was replenished daily to maintain the HSE culture at the air-liquid interface and was fully replaced once per week.

6.2.2 Hyperbaric oxygen treatment

HSE models cultured at the air-liquid interface were treated with 100% oxygen at 2.4 atmospheres for 90 minutes daily. Correlating control HSEs were placed in a humidified box without the presence of CO_2 for an equivalent time period. For full details on HBO and control treatment protocols, please refer to section 2.7. For microarray analysis, the HSE generation and HBO treatment experiments were performed using the group A skin samples.

6.2.3 Extraction of RNA from the HSE model epidermis

HSE models were treated with either HBO or control conditions for 90 minutes daily, prior to harvesting samples at days 0, 3, 5 and 9. At each of these time points RNA extraction was performed by isolating the epidermis in Trizol. For specific details of the RNA extraction protocol, please refer to section 2.12.1.

6.2.4 Microarray analysis of differential gene expression

To perform the gene microarray analysis, 1 µg of total RNA was required. Due to the low amounts of RNA which could be isolated from the HSEs, it was necessary to pool the RNA from the group A HSE models. The pooled RNA was sent to the microarray facility at the Institute for Molecular Biosciences at the University of Queensland and the gene microarray procedure and data collection was performed by Dr Katia Nones. The Illumina Human HT-12 v3 Expression BeadChip microarray (Illumina) was utilised to determine genes which were differentially expressed in

response to HBO treatment. For full details of this process, please refer to section 2.12

6.2.5 Microarray data analysis

The microarray data was analysed in GeneSpring GX 10.0.2 (Agilent Technologies) and this was performed at the University of Western Australia with generous help and guidance received from Daniel Haustead. Full details of the microarray data analysis methods can be found in section 2.12.2

6.2.6 Gene Ontology and Functional Network Analysis

IPA tools (Ingenuity Systems) were utilised to examine Gene Ontology and Functional Network Analysis of the microarray data with the generous help and guidance of Dr Brett Hollier. Please refer to section 2.12.3 for the full details of this process.

6.2.7 Confirmation of differential gene expression using quantitative real-time PCR (qRT-PCR)

Standard PCR conditions

All PCR reactions were performed using the Platinum® *Taq* DNA Polymerase High Fidelity kit (Invitrogen). Refer to section 2.13 for specific details on the PCR reactions, temperature cycling conditions and amplicon validation.

qRT-PCR validation of differentially expressed genes

Analysis of the gene microarray data led to the identification of target genes which were differentially regulated by HBO treatment. A short-list of genes deemed biologically interesting due to their apparent HBO-induced differential expression was selected for further examination by qRT-PCR. Briefly, the primers used for qRT-PCR were designed using Primer-BLAST (NCBI) and OligoPerfect™ designer (Invitrogen) and are outlined in *Table 2.3*. In addition, the specific qRT-PCR methods are detailed in section 2.13.3. Standard curves were generated for each target gene using purified target PCR amplicon product. Each standard curve covered 8 logs of copy number. All gene expression data was normalised to 18S rRNA and then fold change expression compared to the day 0 time point.

6.2.8 Confirmation of differential protein expression in response to HBO in the HSE model using immunohistochemistry

Cultured HSE models were formalin-fixed and paraffin embedded for immunohistological analysis as described in section 2.11.1. Following this, 5 µm thick sections were cut from the blocks of embedded HSEs using a microtome (Leica) and transferred to glass microscope slides (HD Scientific). Immunohistochemistry was then used to detect the presence of kallikrein (KLK) 1 and KLK7, metallothioneins 1 and 2 (MT1/2), cub-domain containing protein 1(CDCP1) and early growth response 1 (EGR1) antigens (Full details listed in *Table 2.2*). Immunoreactivity was visualised with diaminobenzidin (DAB), while the absence of primary antibody served as a negative control and native skin as a positive control.

6.2.9 Image data analysis

The thickness of the epidermis immunoreacting positively for KLK1, KLK7, MT1/2 and CDCP1, as well as the number of EGR1 positive nuclei in each section, was determined using ImageJ software. Full details on the image analysis technique are outlined in section 2.11.2.

6.2.10 Statistical analysis

HSE models generated from eight individual skin donors were analysed throughout this Chapter. The skin samples were divided into two groups; group A which contained 3 skin samples and group B which contained 5 skin samples. Quantitative image analysis data generated from group A were pooled, for the reason that RNA were isolated and pooled from this group for the microarray gene analysis studies performed in section 6.2.4. The image data generated from group B were expressed as individual skin samples since RNA from these samples were not used for the microarray studies and therefore sufficient quantities were available for analysis without the need to pool samples to meet minimal assay requirements. Furthermore, donor-matched native skin samples were collected for group B, whereas native skin controls from unrelated donors were used in group A. All image analysis data was expressed as mean ± standard deviation. The qRT-PCR data for HSEs from the group B skin samples were expressed as mean gene fold change ± standard deviation for each skin sample. Tukey's post hoc analysis following a one-

way ANOVA was performed with a p value < 0.05 accepted as significant on all data presented in this Chapter.

6.3 RESULTS

6.3.1 General data observations

Following analysis, pre-processing and normalisation of the microarray data in GeneSpring, a list of 2,611 genes in total that were differentially expressed in the HSE model throughout the course of the experiment was generated. The gene expression profile of the developing HSE model in the absence of HBO treatment (control HSEs) was previously reported in Chapter 4, but has been included in this Chapter for comparison to the HBO-treated HSEs (**Figure 4.1**). Gene microarray data analysis revealed only subtle differences in gene expression between control- and HBO-treated HSEs at each time point, whereas the differences in temporal gene expression were distinct (**Figure 6.1**). Therefore, the gene expression changes that occur in response to HBO treatment of the HSE model are subtle.

6.3.2 Differential gene expression

Venn diagrams were also produced to determine the overlap of genes differentially expressed in response to HBO treatment. This revealed that the variation between HBO and control-treated HSEs was caused by a unique set of genes at each time point (**Figure 6.2**). Therefore, it appears the HBO treatment does alter the temporal gene expression profile in the HSEs.

The number of genes differentially expressed in response to HBO treatment at each time point was analysed using Venn diagrams (**Figure 6.2**). The data was sorted based on which genes were down-regulated and up-regulated in response to HBO treatment. All gene expression levels were normalised to the expression levels present at day 0 and the fold change of the genes from the microarray data ranged from -2.82 to 3.38. Additionally, Venn diagram analysis was used to determine overlap in HBO-induced gene regulation (**Figure 6.2**). At all three days, no genes were consistently up- or down-regulated in HBO-treated HSEs as compared to control-treated HSEs (**Figure 6.2**). Importantly, as time progressed, the number of genes down-regulated in response to HBO treatment increased. In contrast to the down-regulated genes, the number of up-regulated genes peaked at day 5, but was similar between days 3 and 9.

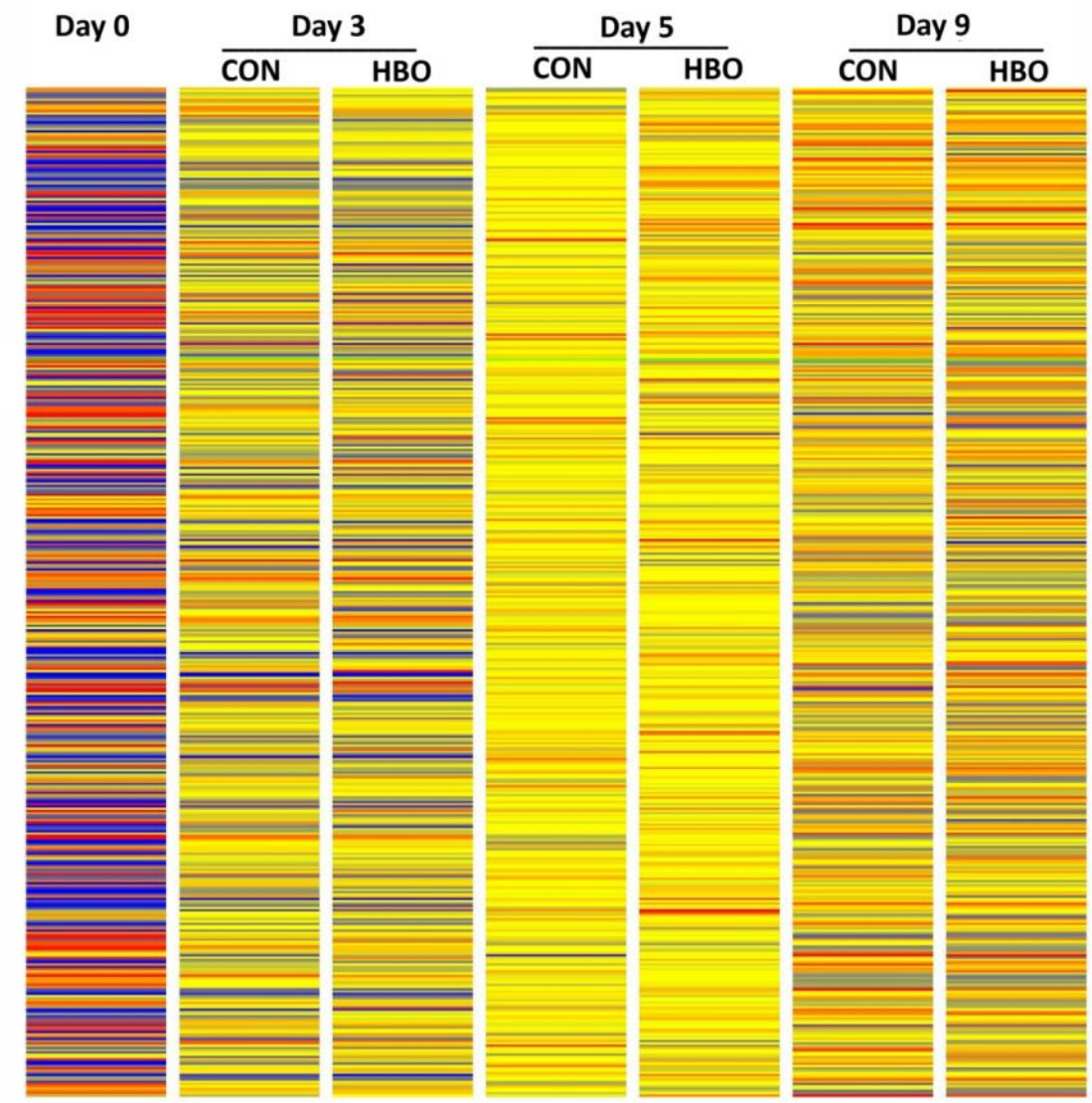

Figure 6.1 Heat-map of genes differentially expressed by HBO treatment of HSE models as determined by microarray analysis

The heat-map provides visual representation of all genes differentially regulated in response to HBO treatment as determined by the microarray analysis. The two treatment groups were more similar to each other at each time point compared to the change observed within treatment groups over time. The colour scale indicates the normalised gene expression intensity; low gene expression is blue and high gene expression is red. Unchanged gene expression is yellow.

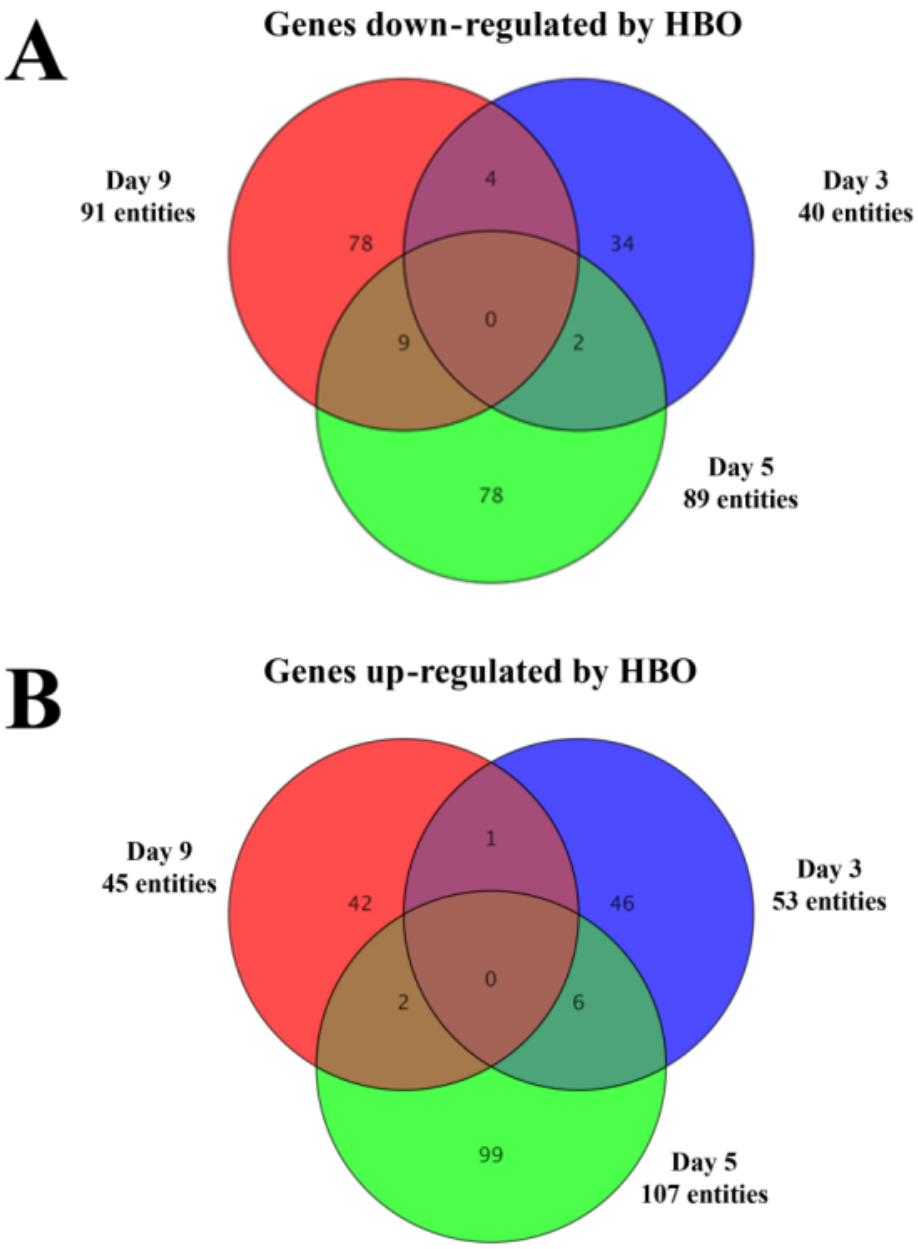

Figure 6.2 Genes differentially expressed by HBO treatment of HSEs as determined by microarray analysis
The Venn diagram visually represents the number of genes commonly or uniquely expressed, at each time point. The Venn diagram is separated by either (**A**) genes down-regulated in response to HBO treatment, or (**B**) genes up-regulated in response to HBO treatment. Only genes > 1.5 fold differentially regulated were included.

6.3.3 Gene Ontology and Functional Analysis of Microarray data

Genes relating to molecular and cellular functions

The gene expression analysis in sections 6.3.1 and 6.3.2 reported the number of genes differentially regulated in HSEs in response to HBO and the breakdown of the number of genes differentially expressed at each time point. However, in order to elucidate the possible relationships between the differentially regulated genes in the HSE model in response to HBO treatment, the ingenuity pathway (IPA) knowledge base was employed. Genes in HSEs which were at least ± 1.5 fold differentially regulated in response to HBO treatment were normalised to the day 0 sample before being uploaded into the IPA software. This functional analysis of the microarray data utilises the gene data to assign biological functions which are differentially regulated in response to HBO treatment, which generates of a list of molecular and cellular functional ontologies which were affected by HBO treatment (Appendix: Table A36 – A38).

To visually analyse the changes that occur in the functional ontologies over time in response to HBO treatment of the HSE models, the IPA-generated data was uploaded into Cytoscape®. This tool is a network analysis program specifically designed to visualise largescale data sets such a gene microarray data (**Figure 6.3**). Interestingly, the number of genes associated with 'cellular growth and proliferation', increased between days 3 and 5, before slightly decreasing by day 9 (**Figure 6.3**). This suggests that 'cellular growth and proliferation' is an important function altered in response to HBO treatment in the HSE model undergoing epidermogenesis.

Another noteworthy functional ontology was 'DNA replication, recombination and repair'. The number of genes associated with this ontology progressively decreased over time (**Figure 6.4 A**). This suggests that the number of genes associated with 'DNA replication, recombination and repair' was not only influenced by HBO treatment, but also became less important to the HSE model as a continuous epithelium was created. Moreover, the number of genes associated with 'cellular movement' increased in a temporal manner (**Figure 6.4 H**). This does not necessarily suggest that keratinocyte migration was increased both temporally and in response to HBO treatment. It may, however, suggest that genes associated with 'cellular movement' were down-regulated as the epidermis matured.

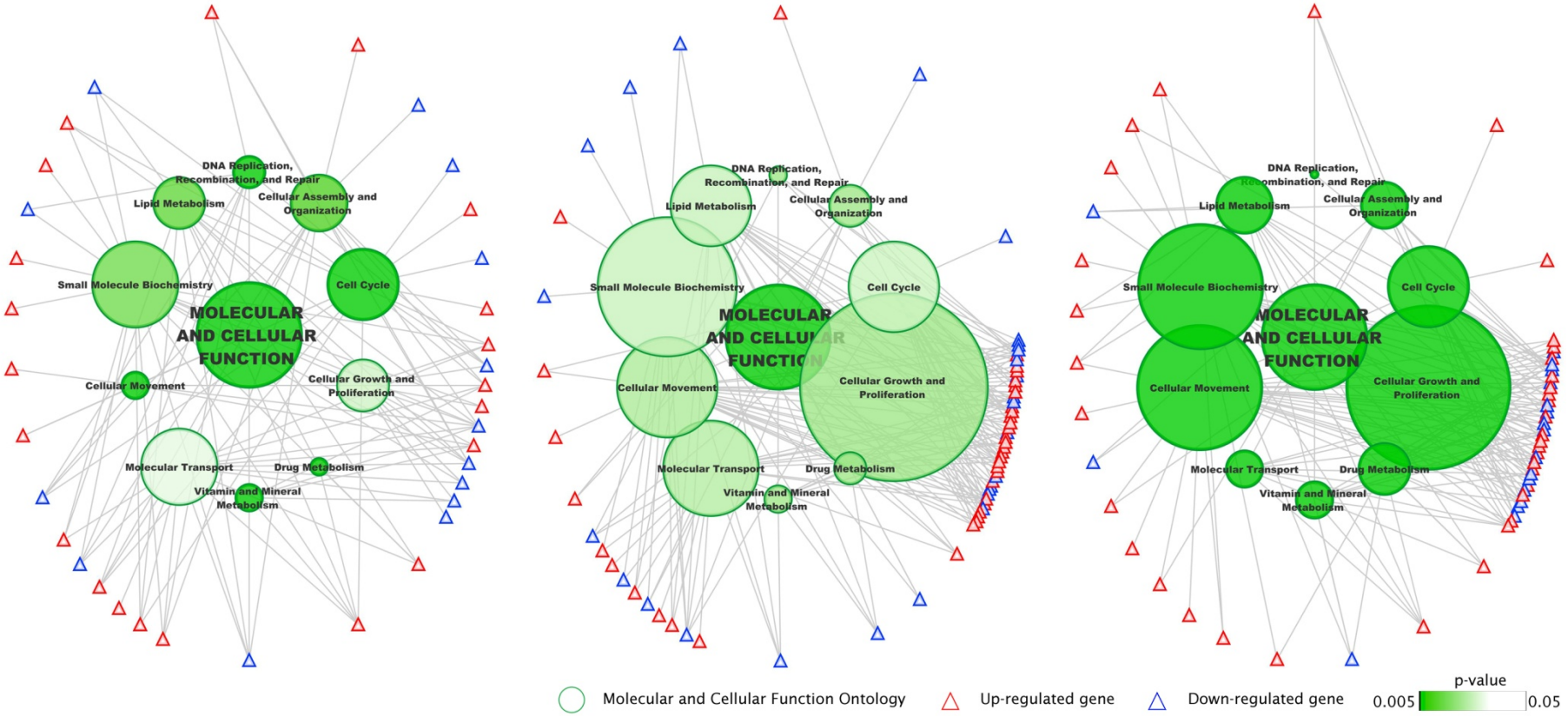

Figure 6.3 Visual representations of the temporal changes in molecular and cellular functions ontology in response to HBO treatment
Genes with p - values < 0.05 and more than 1.5 fold change in expression in response to HBO or control treatment were imported to IPA to generate functional gene associations. This functional data was then up-loaded into open source software, Cytoscape®, to visually represent the data. Down-regulated genes are represented by the blue triangles, whereas up-regulated genes are represented by the red triangles. The intensity of the green colour indicates p-value and the size of the function ontology circle represents the relative number of genes associated with it. The IPA analysis and Cytoscape® graph generation was kindly performed by Dr James Broadbent for inclusion in this thesis.

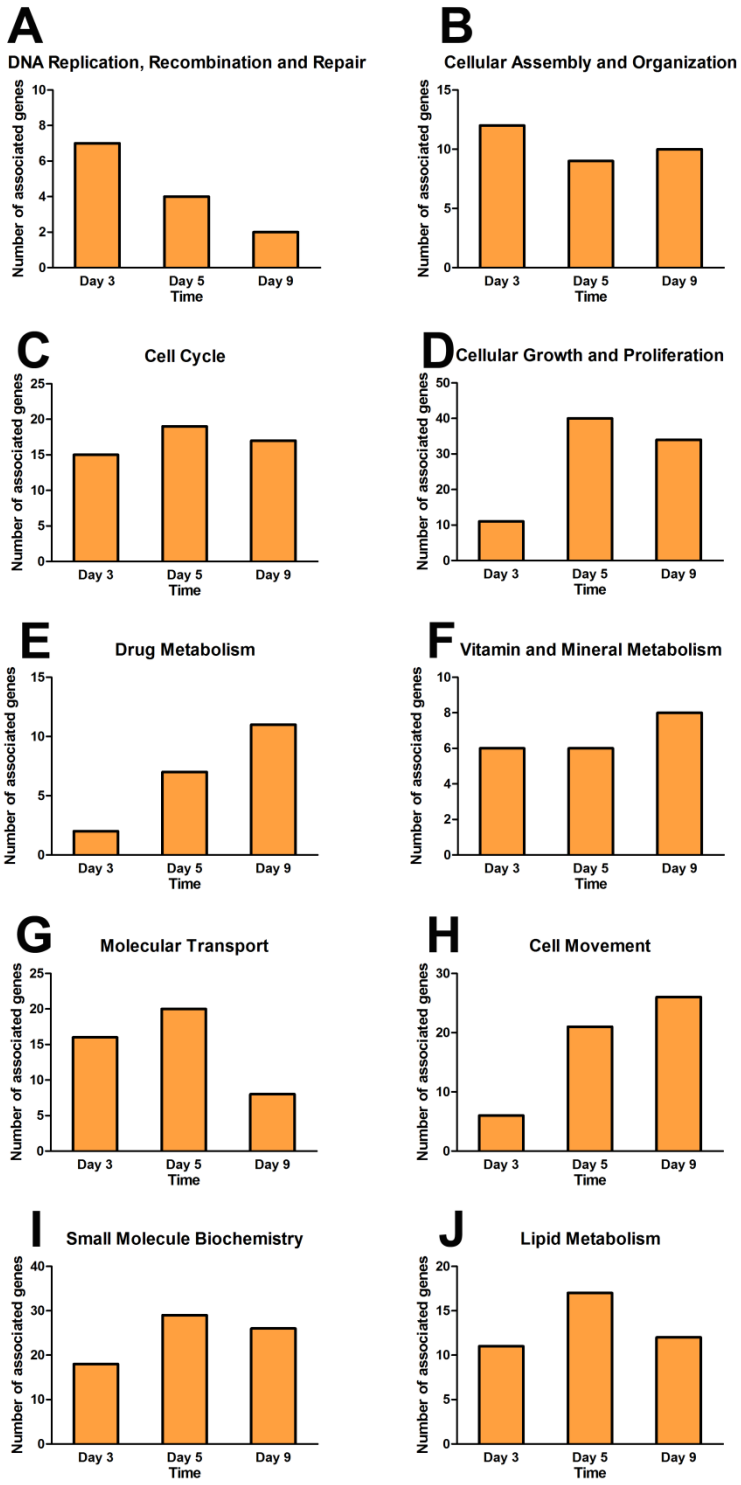

Figure 6.4 The temporal changes in molecular and cellular functions ontology during HBO treatment of the HSE model

The functional ontologies significantly influenced by HBO treatment of the HSE model over time. The bars represent the number of genes relating to the ontologies (**A**) DNA replication, recombination and repair, (**B**) cellular assembly and organization, (**C**) cell cycle, (**D**) cellular growth and proliferation, (**E**) drug metabolism, (**F**) vitamin and mineral metabolism, (**G**) molecular transport, (**H**) cell movement, (**I**) small molecule biochemistry and (**J**) lipid metabolism.

Genes relating to 'Cellular Growth and Proliferation'

'Cellular growth and proliferation' was a statistically significant data set ($p < 0.05$); thus the number of focus genes (i.e. genes associated with the data set which were greater than 1.5 fold differentially regulated) found to be differentially regulated increased between days 3 and 5, after which the level of differentially regulated genes decreased only slightly (**Figure 6.4 D**). However, the focus genes within this data set varied with each time point (*Table 6.1*). Specifically, genes associated with epithelial cell adhesion, such as *CDCP1* and *ITGAV* which are expressed in fully stratified epithelium (Alvares *et al.*, 2008 and Cavani *et al.*, 1993), were present at day 9, but were not differentially expressed at the earlier time points.

Table 6.1 Focus genes differentially expressed in response to HBO treatment within the cellular growth and proliferation data set

Time	Focus Genes
Day 3	CREB1, IL28A, TNFRSF9, DLK1, RORA, SMPD1, **S100A1**, IDO1, ORM1/ORM2, MAD2L1
Day 5	ADAMTS1, ALDH3A1, ARID5B, BNIPL, BTC, CA9, CCL20, CCNA1, CD36, FBLN1, FKBP1A, GAL, GCAT, GCNT1, HMOX1, HPGD, IGFBP3, IL28A, KLF4, KRT4, MCPH1, MTTP, MVD, NDRG1, NDRG2, NFE2, PLAC1, PNPT1, RAN, RARRES1, RORA, **S100P**, SERPINA1, SLC9A1, TIMP2, TNFRSF9, TSPAN5, TXNRD1, VIM
Day 9	ALDH1A1, ARRDC3, CCL20, **CDCP1**, CEACAM1 (includes others), CREB1, CYP1B1, DCBLD2, DKK3, E2F1, E2F7, **EGR1**, GAL, GCNT1, GSTM1, HAS3, HLA-DRB1, IL6ST, **ITGAV**, **KLK3**, KRT2, MAFF, NAMPT, NDUFAF4, PTGES, RARRES1, **S100A4**, SDR16C5, SLC3A2, SPINK7, TCP1, TFPI2, XRCC2, ZBTB16

Genes in **bold** type were deemed as genes of interest and gene expression levels were validated in sections 6.3.6 -6.3.11. Up-regulated genes are highlighted in red, whereas down-regulated genes are highlighted in blue.

Genes relating to physiological system development and function

In order to further investigate the effect of HBO treatment on the HSE model, functional groups of genes (as determined by IPA) associated with epidermal development were investigated. Two gene data sets were particularly relevant to epithelial development within the HSE: 'hair and skin development and function'; and 'tissue development' and the general observations of these ontological groups are outlined in *Table 6.2*.

Many of the phenotypical changes observed within the HBO-treated HSE (Chapter 5) are likely due to alterations to epidermal growth and development, hence the functional group 'hair and skin development and function' was likely to be relevant. The number of focus genes in this particular data set was relatively similar between all three time points (*Table 6.3*). Similarly, 'tissue development' was considered to be another highly relevant functional category since it includes epidermal development. Interestingly, the number of focus genes in the 'tissue development' category was stable at days 3 and 5, but was followed by a doubling of focus genes differentially regulated by HBO treatment at day 9 (*Table 6.4*).

Through combined analysis of the 'hair and skin development and function' and 'tissue development' functional groups, key genes which were differentially regulated in response to HBO treatment were identified. These specific genes, such as *KLK7*, *ITGAV* and *EGR1*, were also found to be differentially regulated genes under the 'cellular growth and proliferation' ontology (*Table 6.1*). Thus, the expression of these genes warrants further examination in an additional cohort of skin samples.

Table 6.2 Ontology of differentially expressed genes in the HSE that are involved in physiological system development and function

	Time	P-value range	Focus Genes
Hair and Skin Development and Function	Day 3	6.05E-04 – 2.06E-02	8
	Day 5	9.30E-05 – 2.87E-02	10
	Day 9	2.11E-04 – 1.16E-02	9
Tissue Development	Day 3	8.30E-03 – 1.00E-02	9
	Day 5	1.57E-02 – 7.89 E-03	9
	Day 9	5.58E-05 – 2.31E-02	19

Table 6.3 Focus genes differentially expressed in the HSEs in response to HBO treatment within the 'hair and skin development and function' data set

Time	Focus Genes
Day 3	CASP14, **KLK7,** KRT10, KRT13, RORA, DSC1, MAD2L1, SYTL1
Day 5	CASP14, KLF4, KRT13, KRT15, TGM3, TGM5, RORA, ROCK2, ALDH3A1, TRIM16
Day 9	CASP14, **GRHL3**, KRT13, KRT2, LAMC2, E2F1, **EGR1, ITGAV,** PTGES

Table 6.4 Focus genes differentially expressed in the HSEs in response to HBO treatment within the 'tissue development' data set

Time	Focus Genes
Day 3	DLK1, F2RL3, PTGS1, RORA, SMPD1, TNFRSF9, FKBP1A, MAL, NDEL1
Day 5	F2RL3, NDRG1, IFRD1, PCSK5, HMOX1,TIMP2, CCL20, TNFRSF9, NPR2
Day 9	ALDH1A1, ALDH1A3, CCL20, CCNC, **CDCP1**, CEACAM1 (includes others), CYFIP2, DKK3, E2F1, **EGR1**, HAS3, IFRD1, IL6ST, **ITGAV,** KLK3, LAMC2, PHC2, PTGES, SLC3A2

Genes in **bold** type were deemed as genes of interest and gene expression levels were validated in sections 6.3.6 -6.3.11. Up-regulated genes are highlighted in red, whereas down-regulated genes are highlighted in blue.

Genes relating to diseases and disorders

The 'diseases and disorders' category contains functional ontological groups which are highly relevant to skin and the developing HSE model. In particular, this included the 'dermatological diseases and conditions' functional category (*Table 6.5* and *Table 6.6*). Importantly, some of the focus genes present in the 'dermatological disease' data set were also present in the 'hair and skin development' and 'tissue development' data sets (*Table 6.3*) and (*Table 6.4*). This includes genes such as *EGR1*, *ITGAV* and *KLK7*, highlighting their importance in the response of the developing HSE model to HBO treatment.

Table 6.5 Ontology of differentially expressed genes in HSEs involved 'dermatological diseases and conditions'

Time	P-value range	Focus Genes
Day 3	2.13E-06 – 4.08E-02	17
Day 5	1.57E-07 – 3.88E-02	28
Day 9	1.72E-07 – 2.06E-02	23

Table 6.6 Focus genes differentially expressed in HSEs in response to HBO treatment within the 'dermatological diseases and conditions' data set

Time	Focus Genes
Day 3	ALOX15B, DSC1, FKBP1A, IDO1, **KLK7**, KRT10, KRT13, LCE2B (includes others), MAD2L1, MUC6, PKM2, PLA2G16, PTGS1, RAN **S100A7A**, SMPD1, TYMP
Day 5	ATP1B1, CCL20, CD63, FKBP1A, GAL, GM2A, HLA-DRB5, HMOX1, IFI27, IFI6, IGFBP3, IL17RD, IL1R2, KRT4, KRT13, KRT15, MUC6, MUCL1, OASL, RAN, RARRES1, **S100A12, S100P**, SERPINA1, SLC9A1, TGM3, TGM5, TIMP2
Day 9	ACADVL, ALDH1A3, CCL20, CYP1B1, DEFB4A/DEFB4B, **EGR1,** GAL, GSTM1, HLA-DRB1, IFI27, IL1R2, **ITGAV,** KRT2, KRT13, KRT79, LAMC2, MUC6, NAMPT, OAS1, RARRES1, **S100A7A,** TCN1, ZBTB16

Genes in **bold** type were deemed as genes of interest and gene expression levels were validated in sections 6.3.6 - 6.3.11. Up-regulated genes are highlighted in red, whereas down-regulated genes are highlighted in blue.

6.3.4 Functional network analysis

Functional network diagrams were created in IPA from the microarray data input from each time point. The program determined functional network pathways based on the genes up- or down-regulated in response to HBO treatment. Furthermore, the data generated is different from previous functional analyses reported in this Chapter as it creates networks based on individual genes, rather than on functional ontology. Analysis of the networks generated at days 3, 5 and 9 revealed that there was a high level of variation in the functions of these networks, and none directly related to epidermal generation. The top 3 functional networks for each time point and the focus genes within these networks are listed in Appendix Table A39 – Table A44. Furthermore, the interactions of the genes within these networks are presented in Appendix Figures A10 – A18.

While functional network analysis can be useful in microarray studies such as this one, there was nevertheless a large amount of variation between the functional groups identified. Furthermore, the relevance of these networks to epidermogenesis was not clear. While many of the genes deemed as important and further investigated in sections 6.3.6 - 6.3.11, were present in these networks, the current analysis was not used as the sole basis for selecting genes for further studies

6.3.5 General conclusions regarding the microarray data analysis

Microarray analysis generates large amounts of data and through the use of functional analysis programs these data can be analysed and key information extracted. Throughout the gene microarray analysis data (section 6.3.3), a few gene families were consistently present. These genes were of the S100 family, the kallikreins (KLKs), in particular *KLK7*, transcription factor *EGR1* and epithelial cell-to-cell and cell-to-matrix adhesion markers; *CDCP1* and *ITGAV*. These genes were further investigated using real time PCR, discussed further in sections 6.3.6 - 6.3.11.

6.3.6 qRT-PCR expression validation of differentially regulated genes

As described above, the analysis of the microarray data uncovered several interesting and biologically relevant genes which were differentially regulated in response to HBO treatment in the HSE model. Validation of the expression of these genes of interest was therefore performed using qRT-PCR of RNA extracted from the group B skin samples.

6.3.7 Expression of metallothionein genes in response to HBO treatment in HSE models undergoing epidermogenesis.

Metallothionein (*MT*) mRNA has been reported to be up-regulated in both wound margins and newly-formed epidermis following wound closure (Iwata *et al.*, 1999). Therefore, analysis of *MT1G* and *MT2A* gene expression in the HSE model using qRT-PCR was performed to determine if the expression of these genes is affected by HBO treatment. Although the microarray data also revealed that *MT1H* and *MT4* were differentially regulated in response to HBO, amplification of these genes by qRT-PCR was not successful, presumably due to low copy numbers present in the total mRNA samples. Similarly, *MT1G* gene expression was undetectable in the RNA from sample 4.

qRT-PCR analysis of MT1G gene expression in HSE models undergoing epidermogenesis in response to HBO treatment

When comparing HBO treatment to control treatment, qRT-PCR analysis of the group B skin samples revealed that none of the HSEs followed a similar gene expression trend in response to HBO treatment (Appendix Table A45). Analysis of the qRT-PCR data demonstrated that generally, *MT1G* gene expression was up-regulated when compared to the day 0 control HSE (**Figure 6.5**).

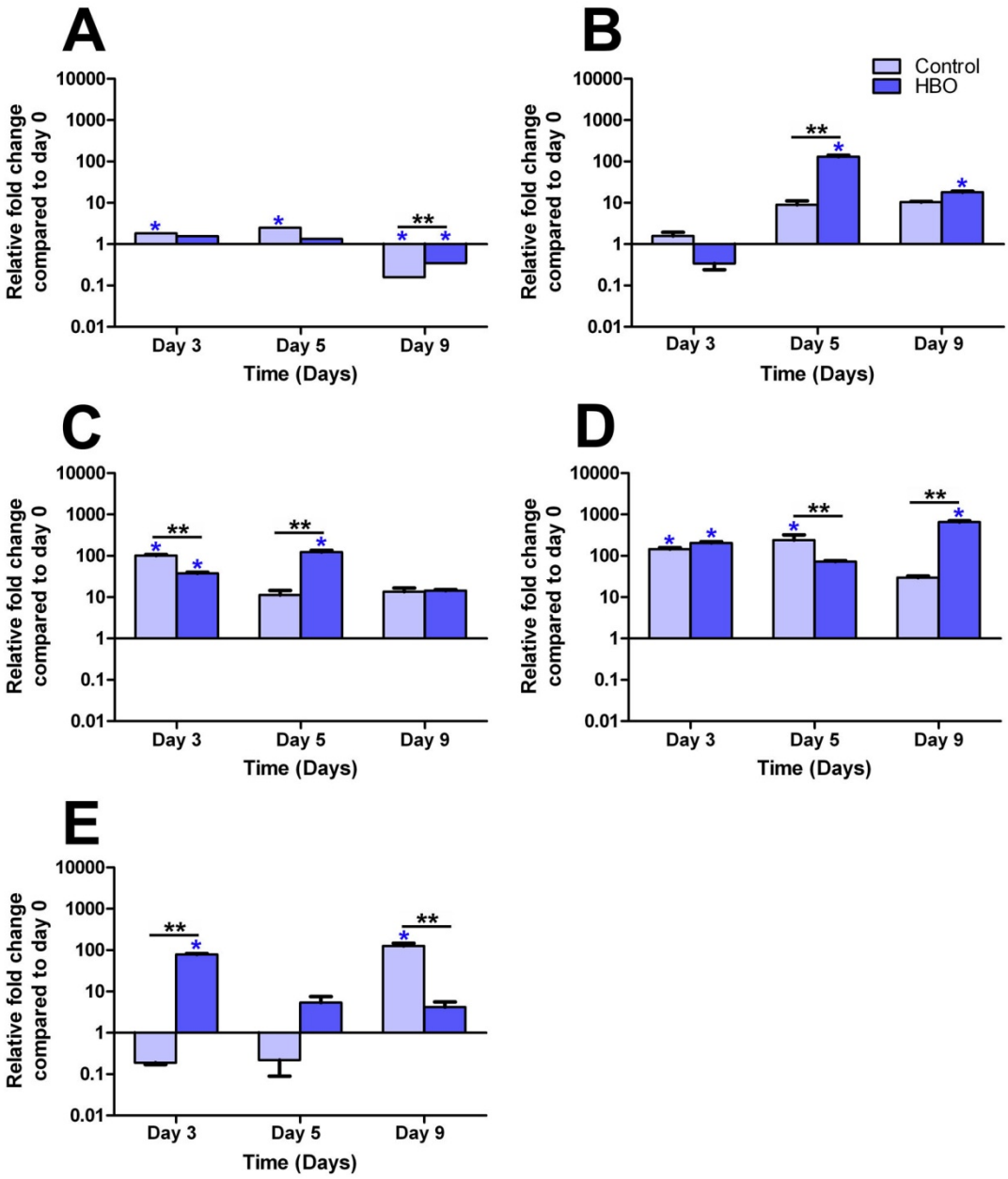

Figure 6.5 The effect of HBO treatment on *MT1G* gene expression in the developing HSE model
Gene expression analysis of *MT1G* was performed on total mRNA isolated from the epidermis of the developing HSE. The data was obtained from (**A**) microarray analysis of RNA pooled from group A skin samples, (**B**) *MT1G* qRT-PCR data from HSE models created using sample 5, (**C**) sample 6, (**D**) sample 7 and (**E**) sample 8. Data was normalised to the day 0 HSE and represents the mean *MT1G* fold change in gene expression ± standard deviation of technical replicates (n = 3). Statistical significance $p < 0.05$ between treatment groups on a given day was represented by **, whereas statistical difference $p < 0.05$ to the day 0 time point was represented by *.

qRT-PCR analysis of MT2A gene expression in HSE models undergoing epidermogenesis in response to HBO treatment

MT2A gene expression analysis was performed on the group B skin samples using qRT-PCR. This yielded results that did not correlate to the gene expression analysis performed on the group A skin samples using microarray technology (Appendix Table A46). Specifically, the temporal expression of *MT2A* in HSEs from group A remained relatively unchanged throughout the course of the experiment. Furthermore, there were no significant differences in *MT2A* expression between the control and HBO treatment at each time point (**Figure 6.6 A**). Samples 6, 7 and 8 from the group B skin samples had significantly lower levels of *MT2A* gene expression when compared to the day 0 control HSE ($p < 0.05$; **Figure 6.6 D - F**). Interestingly, a progressive temporal decrease in *MT2A* expression was observed in samples 6, 7 and 8. In general, it appears that the expression of *MT2A* was only similar in 3 of the 5 samples from group B

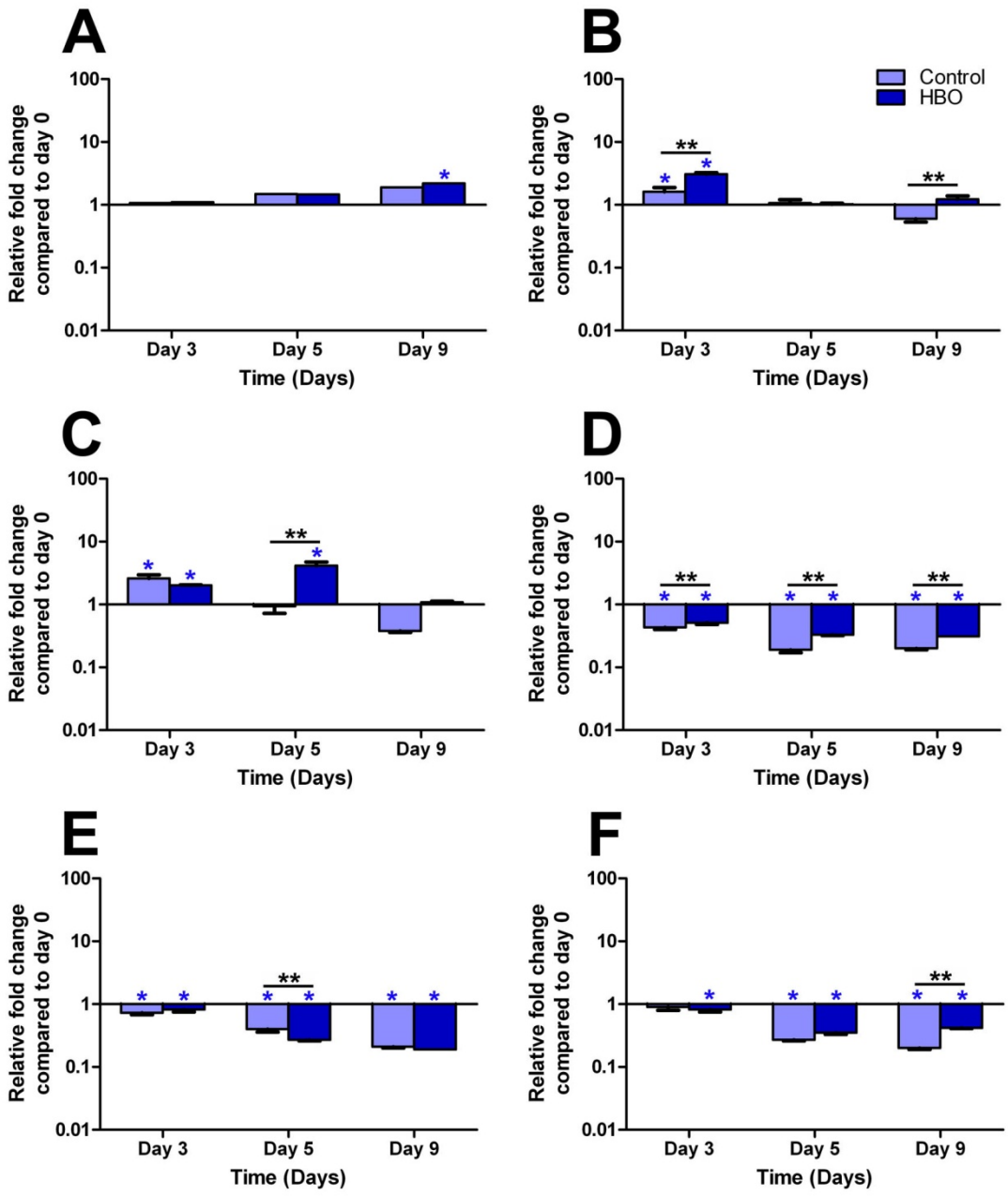

Figure 6.6 The effect of HBO treatment on *MT2A* gene expression in the developing HSE model
Gene expression analysis of *MT2A* was performed on total mRNA isolated from the epidermis of the developing HSE. The data was obtained from (**A**) microarray analysis of RNA pooled from group A skin samples. (**B**) *MT2A* qRT-PCR data from HSE models created using sample 4, (**C**) sample 5, (**D**) sample 6, (**E**) sample 7 and (**F**) sample 8. Data was normalised to the day 0 HSE and represents the mean *MT2A* fold change in gene expression ± standard deviation of technical replicates (n = 3). Statistical significance $p < 0.05$ between treatment groups on a given day was represented by **, whereas statistical difference $p < 0.05$ to the day 0 time point was represented by *.

6.3.8 Expression of kallikrein genes in response to HBO treatment in HSE models undergoing epidermogenesis.

Kallikrein 7 (*KLK7*) is a serine protease involved in skin desquamation and homeostasis and is almost exclusively expressed in skin (Hansson *et al.*, 1994). In addition, it was reported by Komatsu *et al*. (2003) that *KLK1* mRNA is present at a level five times greater than that of *KLK7* in native human skin. Interestingly, the microarray analysis revealed that expression of *KLK1* and *KLK7* was down-regulated in all treatments when compared to the day 0 control HSE. To validate these findings, qRT-PCR was performed to determine *KLK1* and *KLK7* expression levels in the HSE models.

qRT-PCR analysis of KLK1 gene expression in HSE models undergoing epidermogenesis in response to HBO treatment

When the microarray gene expression data was compared to the qRT-PCR validation data differences between the two gene analysis methods were apparent (Appendix Table A47). Specifically, microarray analysis revealed *KLK1* was persistently down-regulated in the HSE model over time (**Figure 6.7 A**). This however was not the case for the group B skin samples (**Figure 6.7 B-F**). When compared to the day 0 control HSE by qRT-PCR, most skin samples generally expressed significantly greater levels of *KLK1* ($p < 0.05$; **Figure 6.7**). In addition, the differential expression of KLK1 in response to HBO treatment was analysed in each sample, but no consistent trends in regulation of *KLK1* gene expression in the HSE models were observed.

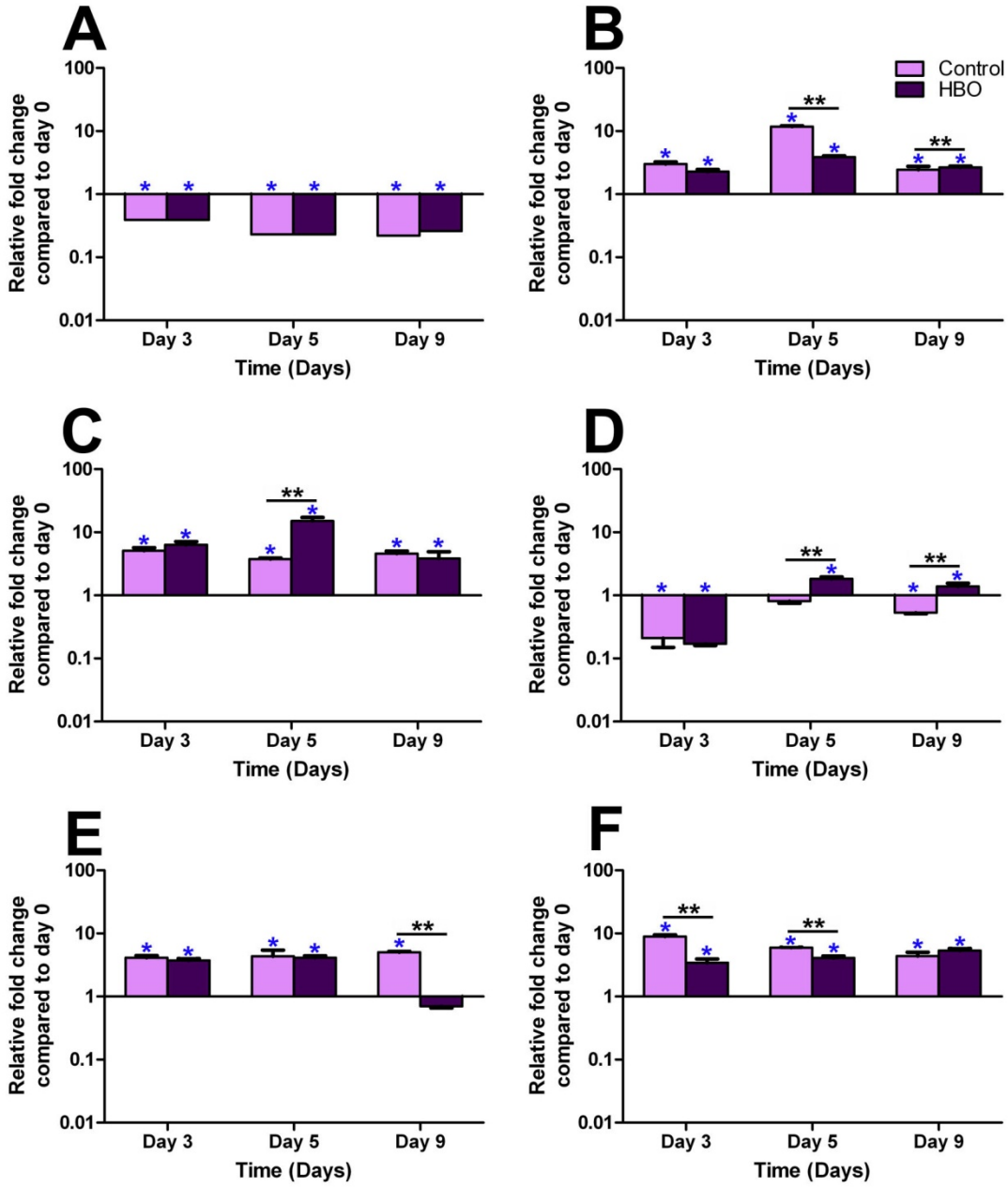

Figure 6.7 The effect of HBO treatment on *KLK1* gene expression in the developing HSE model
Gene expression analysis of *KLK1* was performed on total mRNA isolated from the epidermis of the developing HSE. The data was obtained from (**A**) microarray analysis of RNA pooled from group A skin samples. (**B**) *KLK1* qRT-PCR data from HSE models created using sample 4, (**C**) sample 5, (**D**) sample 6, (**E**) sample 7 and (**F**) sample 8. Data was normalised to the day 0 HSE and represents the mean *KLK1* fold change in gene expression ± standard deviation of technical replicates (n = 3). Statistical significance $p < 0.05$ between treatment groups on a given day was represented by **, whereas statistical difference $p < 0.05$ to the day 0 time point was represented by *.

qRT-PCR analysis of KLK7 gene expression in HSE models undergoing epidermogenesis in response to HBO treatment

KLK7 gene expression analysis was performed on the group B skin samples using qRT-PCR. This yielded results that did not correlate to the gene expression analysis performed on the group A skin samples using microarray technology (Appendix Table A48). In particular, *KLK7* was down-regulated at each time point in the microarray data (**Figure 6.8 A**), whereas, *KLK7* was up-regulated at most time points in all samples when analysed by qRT-PCR (**Figure 6.8 B - F**).

When compared to the day 0 control HSE model, *KLK7* expression was significantly up-regulated at most time points from skin samples 4, 5, 6 and 8 (**Figure 6.8 B, D** and **F**). Furthermore, *KLK7* was generally only up-regulated when compared to the day 0 control HSE, in skin sample 7 at day 5 (**Figure 6.8 E**). When comparing the presence of absence of HBO treatment of the HSE models by qRT-PCR, there were no distinct correlations between HBO treatment and *KLK7* expression.

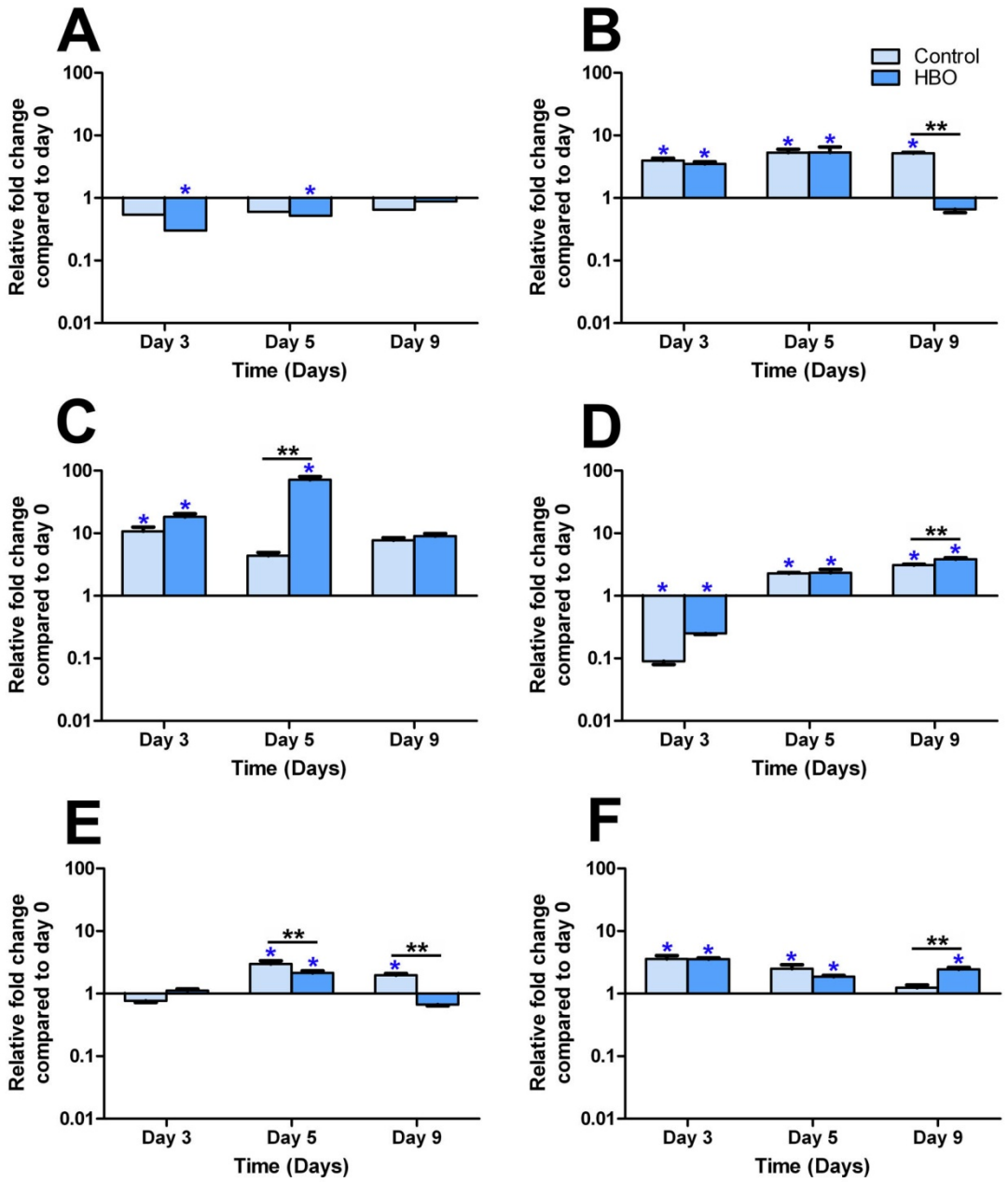

Figure 6.8 The effect of HBO treatment on *KLK7* gene expression in the HSE model
Gene expression analysis of *KLK7* was performed on total mRNA isolated from the epidermis of the developing HSE. The data was obtained from (**A**) microarray analysis of RNA pooled from group A skin samples. (**B**) *KLK7* qRT-PCR data from HSE models created using sample 4, (**C**) sample 5, (**D**) sample 6, (**E**) sample 7 and (**F**) sample 8. Data was normalised to the day 0 HSE and represents the mean *KLK7* fold change in gene expression ± standard deviation of technical replicates (n = 3). Statistical significance $p < 0.05$ between treatment groups on a given day was represented by **, whereas statistical difference $p < 0.05$ to the day 0 time point was represented by *.

6.3.9 Expression of genes for early growth response proteins in response to HBO treatment in HSE models undergoing epidermogenesis.

The genes of early growth response (EGR) proteins are rapidly up-regulated post-wounding (Amendt *et al*., 2002). This suggests that *EGRs* are possibly involved in the generation of a new epidermis. Furthermore, *EGRs* are induced in response to growth factors in order to stimulate mitogenic effects (Lemaire *et al*., 1988). Interestingly, *EGR* expression is also stimulated by hypoxia (Yan *et al.*, 1999).

qRT-PCR analysis of EGR1 gene expression in HSE models undergoing epidermogenesis in response to HBO treatment

EGR1 gene expression analysis was performed on the group B skin samples using qRT-PCR. This yielded results that did not correlate to the gene expression analysis performed on the group A skin samples using microarray technology (Appendix Table A49). When compared to the day 0 control HSE, *EGR1* gene expression was higher at most time points from skin samples 4, 5, 7 and 8 (**Figure 6.9 B, C, E** and **F**). Sample 6 differed from the others in that EGR1 was down-regulated at most time points when compared to the day 0 control HSE model (**Figure 6.9 D**). When comparing HBO treatment to the correlating control, it appeared that *EGR1* gene expression was highly variable between skin samples. This suggests that there were no distinct correlations between HBO treatment and *EGR1* expression.

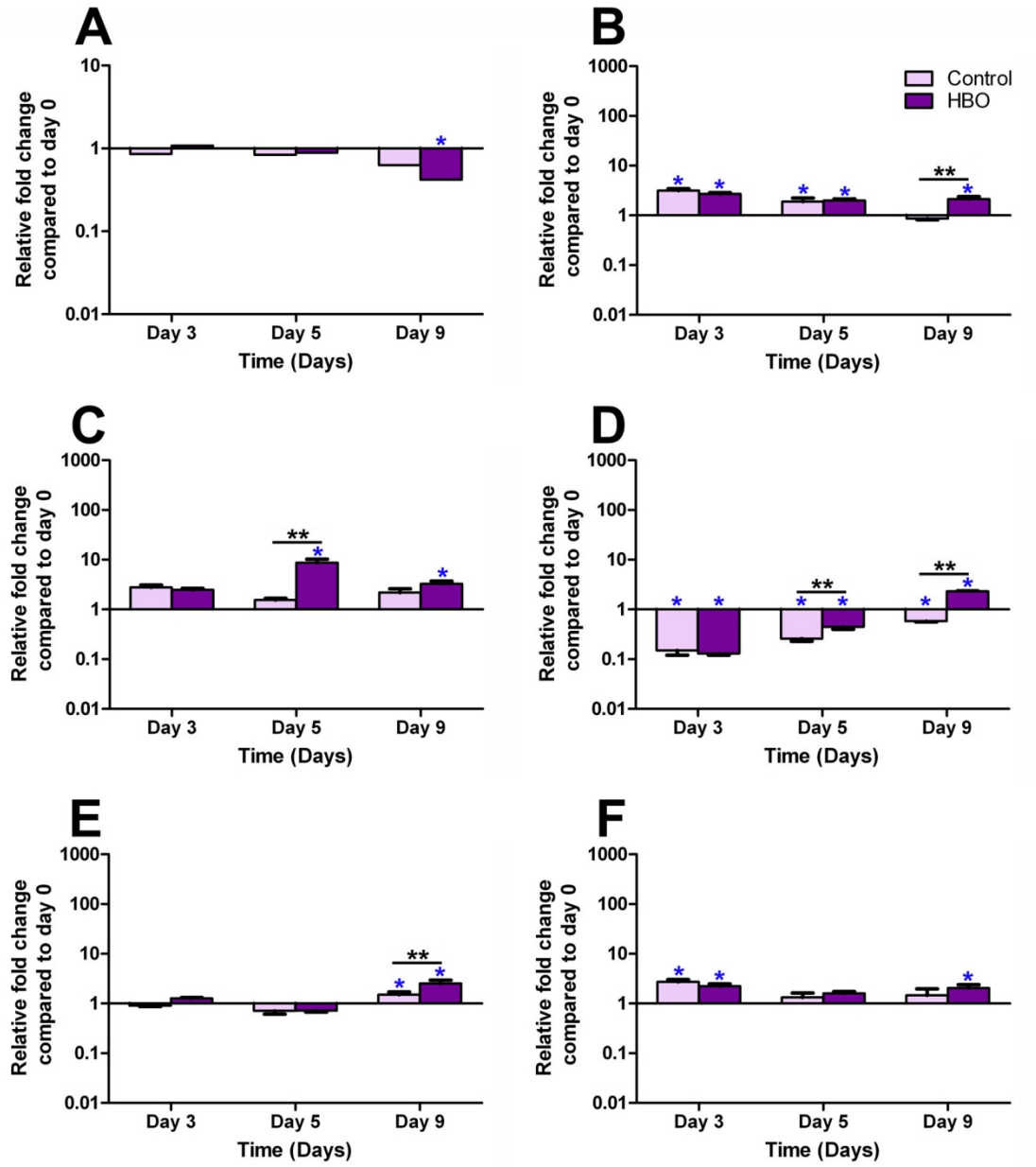

Figure 6.9 The effect of HBO treatment on *EGR1* gene expression in the HSE model
Gene expression analysis of *EGR1* was performed on total mRNA isolated from the epidermis of the developing HSE. The data was obtained from (**A**) microarray analysis of RNA pooled from group A skin samples. (**B**) *EGR1* qRT-PCR data from HSE models created using sample 4, (**C**) sample 5, (**D**) sample 6, (**E**) sample 7 and (**F**) sample 8. Data was normalised to the day 0 HSE and represents the mean *EGR1* fold change in gene expression ± standard deviation of technical replicates (n = 3). Statistical significance $p < 0.05$ between treatment groups on a given day was represented by **, whereas statistical difference $p < 0.05$ to the day 0 time point was represented by *.

6.3.10 Expression of the CDCP1 gene in response to HBO treatment in HSE models undergoing epidermogenesis.

Over-expression of *CDCP1* mRNA has been implicated in metastatic epithelial cancers, such as colorectal cancer (Scherl-Mostageer *et al.*, 2001). Furthermore, *CDCP1* has been hypothesised to be involved in regulating cell-to-cell junctions in epithelial tissues and may also play a role in wound healing (Spassov *et al.*, 2009). Microarray analysis was performed on pooled RNA from the group A skin samples, whereas qRT-PCR was performed on RNA from each of the group B skin samples. It was observed that *CDCP1* expression was up-regulated above the day 0 control HSE at each time point in the microarray data (Appendix Table A50).

Similar to the microarray data, *CDCP1* was up-regulated in samples 4 and 5, when compared to the day 0 control HSE (**Figure 6.10 B** and **C**). Conversely, *CDCP1* was generally down-regulated in samples 6, 7 and 8 when compared to the day 0 control HSE (**Figure 6.10 D – F**). When HBO treatment was compared to the correlating controls via qRT-PCR, HSE models from samples 4, 5, 6 and 7 all differentially expressed *CDCP1* in response to HBO treatment ($p < 0.05$; **Figure 6.10 B-E**). However, the expression of *CDCP1* was highly variable between skin samples, suggesting that there were no distinct correlations between HBO treatment and *CDCP1* expression.

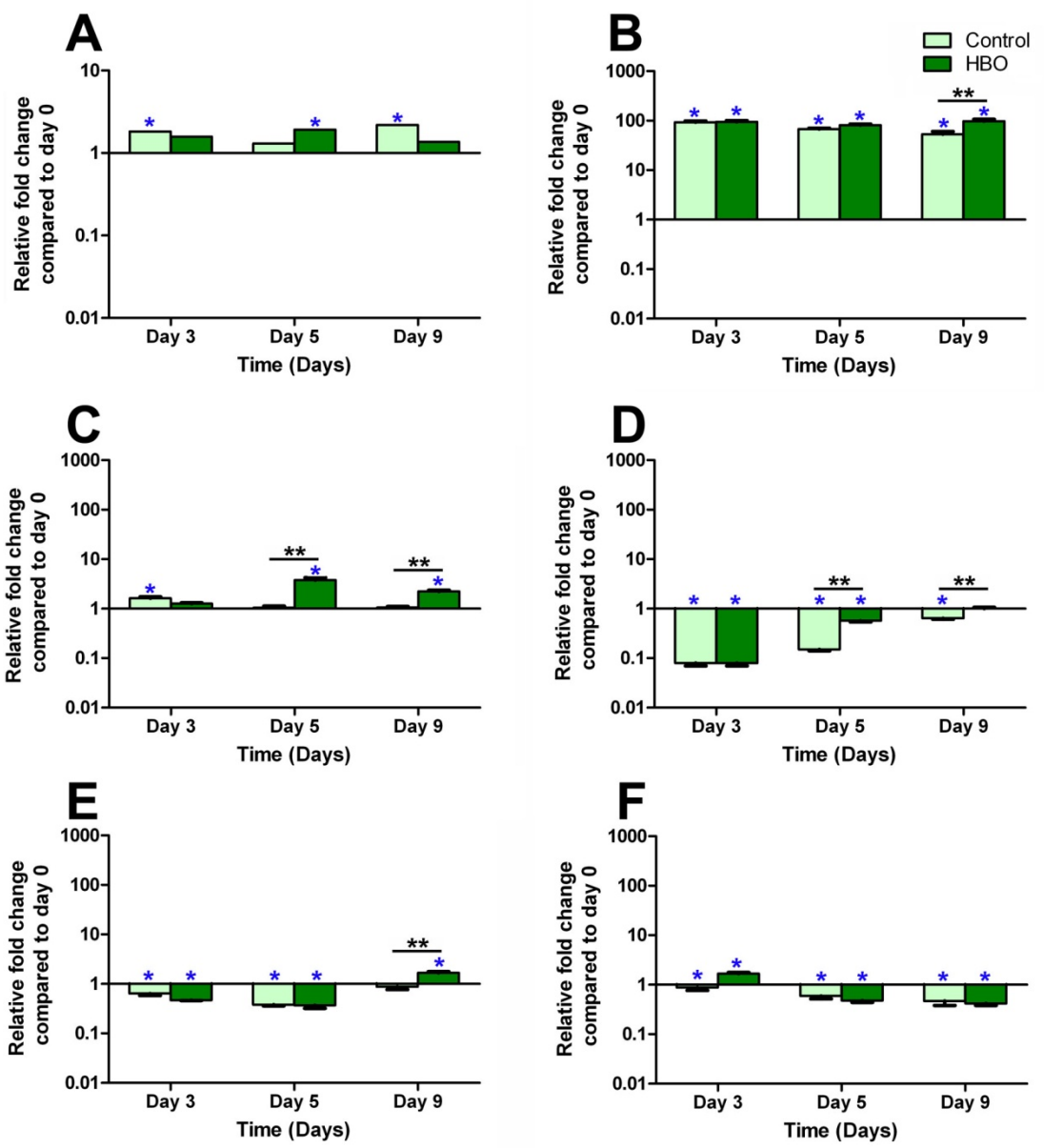

Figure 6.10 The effect of HBO treatment on CDCP1 gene expression in HSE models undergoing epidermogenesis

Gene expression analysis of *CDCP1* was performed on total mRNA isolated from the epidermis of the developing HSE. The data was obtained from (**A**) microarray analysis of RNA pooled from group A skin samples. (**B**) *CDCP1* qRT-PCR data from HSE models created using sample 4, (**C**) sample 5, (**D**) sample 6, (**E**) sample 7 and (**F**) sample 8. Data was normalised to the day 0 HSE and represents the mean *CDCP1* fold change in gene expression ± standard deviation of technical replicates (n = 3). Statistical significance $p < 0.05$ between treatment groups on a given day was represented by **, whereas statistical difference $p < 0.05$ to the day 0 time point was represented by *.

6.3.11 Other genes investigated by qRT-PCR

Early growth response 3 (*EGR3*) was investigated by qRT-PCR as members of the EGR family are up-regulated post wounding, involved in mitogenesis and in response to changes in oxygen tension (Amendt *et al.*, 2002; Lemaire *et al.*, 1988; Yan *et al.*, 1999). In addition, grainyhead-like 3 (*GRHL3*), which encodes the GRHL3 transcription factor protein was investigated due to its proposed role in keratinocyte migration, wound healing, epithelial development and barrier formation (Caddy *et al.*, 2010; Dai and Segre, 2004, Hislop *et al.*, 2008; Koster and Roop, 2007, Ting *et al.*, 2005; Yu *et al.*, 2008). Moreover, integrin α_v (*ITGAV*), heterodimerised to the integrin β_6 subunit, has been reported to be expressed exclusively in epithelial cells and its expression is up-regulated following injury (Huang *et al.*, 1996). Furthermore, Upton *et al.*, (2008) reported that α_v integrin is important in vitronectin:growth factor mediation of keratinocyte migration. Thus, the expression of the *ITGAV* gene in the HBO-treated HSE model was further investigated. Lastly, S100A8 gene expression was analysed by qRT-PCR as it has been reported to be induced upon stressful events within the skin, such as UV irradiation and in hyperproliferative skin disorders such as psoriasis (Lee *et al.*, 2009; Sugiura *et al.*, 2005). As with many of the other genes investigated via q-RT-PCR in sections 6.3.7 - 6.3.10, the expression of these genes did not correlate to the microarray data and there were also inconsistencies in expression trends between individual HSE models (Appendix Table A51 – Table A54 and Figure A19 – Figure A22).

6.3.12 Gene expression in replicate HSE models from the same skin sample is consistent

Gene expression data from sections 6.3.6 - 6.3.11, as determined by qRT-PCR, was highly variable between skin samples. To investigate the origin of the variation, replicate HSE models were generated from an additional skin sample (skin sample 9). The six replicate HSEs were cultured for 9 days at the air-liquid interface prior to extraction of total RNA from the epidermis of the HSEs, as described in section 6.2.3. Expression of genes; *CDCP1* (no consistent gene expression regulation in the group B skin samples when compared to the day 0 control HSE; **Figure 6.10**), *KLK1* (generally up-regulated in the group B skin samples when compared to the day 0 control HSE; **Figure 6.7**) and *MT2A* (generally down-regulated in the group B skin samples when compared to the day 0 control HSE; **Figure 6.6**) were investigated (**Figure 6.11**). The qRT-PCR data revealed that 5 of the 6 HSE models exhibited similar levels of expression, particularly evident in *CDCP1* (**Figure 6.11 A**) and *KLK1* (**Figure 6.11 B**). There appeared to be one outlier sample (HSE 1), which had significantly greater levels of *CDCP1* and *KLK1* gene expression when compared to the remaining five HSEs (**Figure 6.11 A** and **B**). Therefore, with the exception of the one outlier, gene expression as determined by qRT-PCR is relatively similar between replicate HSE models generated from the same skin sample. Thus, it seems that the variation between skin samples observed previously (sections 6.3.6 - 6.3.11) is due to sample-to-sample variation, as opposed to within sample variation.

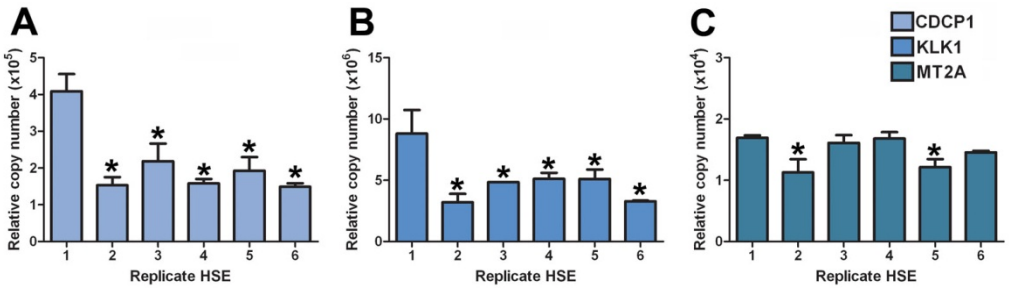

Figure 6.11 Expression of *CDCP1, KLK1* and *MT2A* genes in replicate HSE models from the same skin sample
Gene expression analysis of (**A**) *CDCP1,* (**B**) *KLK1* and (**C**) *MT2A* was performed on total mRNA isolated from the epidermis of 6 replicate HSE models generated from skin sample 9. Data was expressed as relative gene copy number ± standard deviation. Significant difference ($p < 0.05$) to replicate HSE 1 was denoted by the *.

6.3.13 Immunohistochemical validation of the HSE model in response to HBO treatment over time

The gene microarray data presented in sections 6.3.1 - 6.3.5 aimed to identify key epithelialisation-associated genes differentially regulated in response to HBO treatment in the HSE model. The expression of ten genes were subsequently further investigated using qRT-PCR, however, a high level of variation in gene expression was observed between skin samples (sections 6.3.6 - 6.3.11). In view of this, protein expression studies were also pursued in order to establish if the products of these genes exhibited less variability. Specifically, immunohistochemical analysis was performed on sections from the HSE models to determine differences in protein immunoreactivity and localisation of a select variety of epidermal markers. The five proteins examined; KLK1, KLK7, EGR1, CDCP1 and total MT1/2, were chosen based on their relevance to skin and epidermogenesis, in addition to the gene expression fold changes observed in the HSE models in response to HBO treatment.

6.3.14 Total Metallothionein expression in the HSE model in response to HBO treatment

Metallothioneins (MTs) are a family of proteins reported to play a role in epidermal proliferation and wound healing (Lansdown *et al.*, 2011). Furthermore, MTs have an established involvement in cellular protection from oxidative stress (Kumari *et al.*, 1998). Immunohistochemical analysis of MT expression using an antibody against total MT-1 and MT-2, which encompasses MT1G and MT2A, was performed. This was conducted to determine both the temporal expression and localisation of MT during epidermogenesis in response to HBO treatment.

MT was localised to the basal layers in sections from both native skin and the HSE model. The expression of MT protein was generally confined to no more than approximately 3 cell layers thick, extending from the basal region of the epidermis (**Figure 6.12 A**). Interestingly, in HSE sections from day 0, MT was localised to isolated regions of the epidermis, where the forming epidermis had begun to protrude into the rete ridges and was more than one cell layer thick (**Figure 6.12 B**).

The expression and localisation of MT was similar between treatment groups in HSE sections from days 3, 5 and 9 (**Figure 6.12 C - H**). The DAB staining, however, appeared to be more intense in the control-treated samples than in the HBO samples (**Figure 6.12 C - H**). In sections of HSEs from days 5 and 9, MT expression was also observed in isolated keratinocytes of the stratum spinosum, irrespective of treatment (**Figure 6.12 E - H**). Overall, MT appeared to follow the same pattern of temporal expression and localisation in both treatment groups. To establish if there were any quantitative differences in MT expression, the thickness of MT-positive epidermis was quantified using ImageJ analyses as described in section 2.11.2.

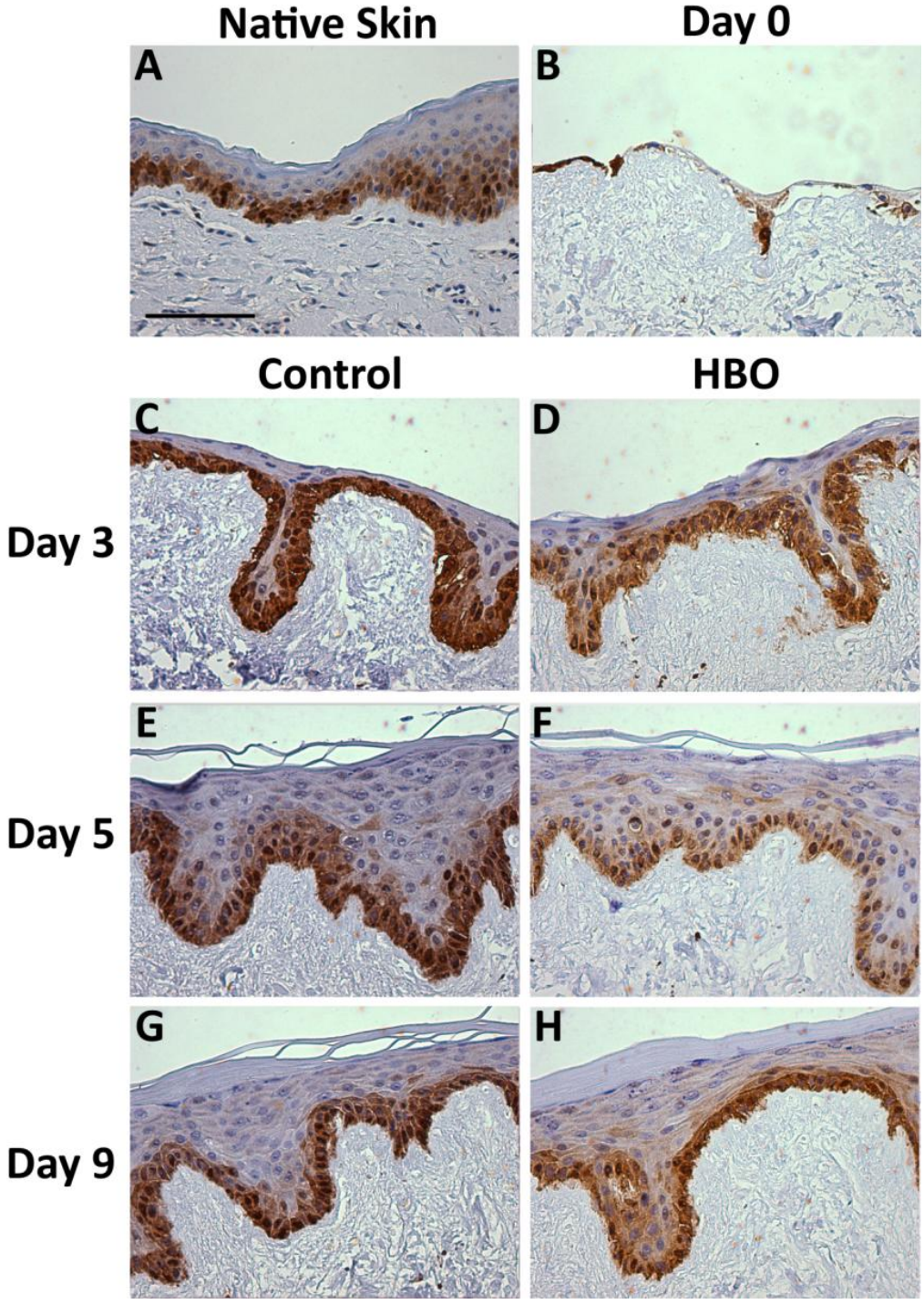

Figure 6.12 Localisation of MT in the HSE model undergoing epidermogenesis
Histological sections of native skin and HSE models were grown for 0, 3, 5 and 9 days at the air-liquid interface, treated with or without HBO and were probed for MT. The expression of MT in keratinocytes was detected in (**A**) native skin and in HSE models at (**B**) day 0, (**C, D**) day 3, (**E, F**) day 5 and (**G, H**) day 9. HBO-treated samples are represented by images **D, F** and **H**, whereas control samples were in images **C, E** and **G**. The presence of the MT antigen is represented by brown immunoreactivity, and all nuclei have been counterstained blue with haematoxylin. The scale bar represents 100 μm. These are representative figures using images captured from skin sample 2.

6.3.15 MT immunoreactivity is altered in the HSE model after 9 days of treatment with HBO

The immunoreactivity images described in section 6.3.14 were analysed using ImageJ to determine the thickness of the epidermis expressing MT (Appendix Table A55 and Table A56). MT protein expression was relatively similar between skin samples and was consistently higher in the HSEs than was present in native skin. In HSEs from group A samples and samples 4 – 6, the level of MT immunoreactivity increased between day 0 and day 3 and remained at this level until day 9, except in some instances where HBO treatment appeared to have an effect (**Figure 6.13 A - D**). Skin samples 7 and 8 were slightly different in that the level of MT immunoreactivity peaked in sections from day 3 HSEs and the levels progressively decreased after this time point (**Figure 6.13 E** and **F**).

Interestingly, all significant differences in MT immunoreactivity were observed at day 9, when the HSE model had formed a mature epidermis. MT immunoreactivity was up-regulated at day 9 in response to HBO treatment in the group A samples and sample 5, when compared to the equivalent control (51.27 µm ± 14.07 µm in HBO compared to 37.59 µm ± 10.44 µm in the control in the group A samples; $p < 0.05$ and 50.66 µm ± 11.82 µm in HBO compared to 31.81 µm ± 9.22 µm in the control in sample 5; $p < 0.01$; **Figure 6.13 A** and **C**). Conversely, MT immunoreactivity was down-regulated in response to HBO treatment in samples 4 and 6, when compared to the correlating controls (27.75 µm ± 9.35 µm in HBO compared to 53.94 µm ± 15.40 µm in the control in sample 4; $p < 0.001$ and 36.66 µm ± 12.99 µm in HBO compared to 51.90 µm ± 7.53 µm in the control in sample 6; $p < 0.05$; **Figure 6.13 B** and **D**). Together, these results suggest that HBO only impacts on MT protein expression after 9 days of treatment. The influence of HBO, however, is not consistent between samples.

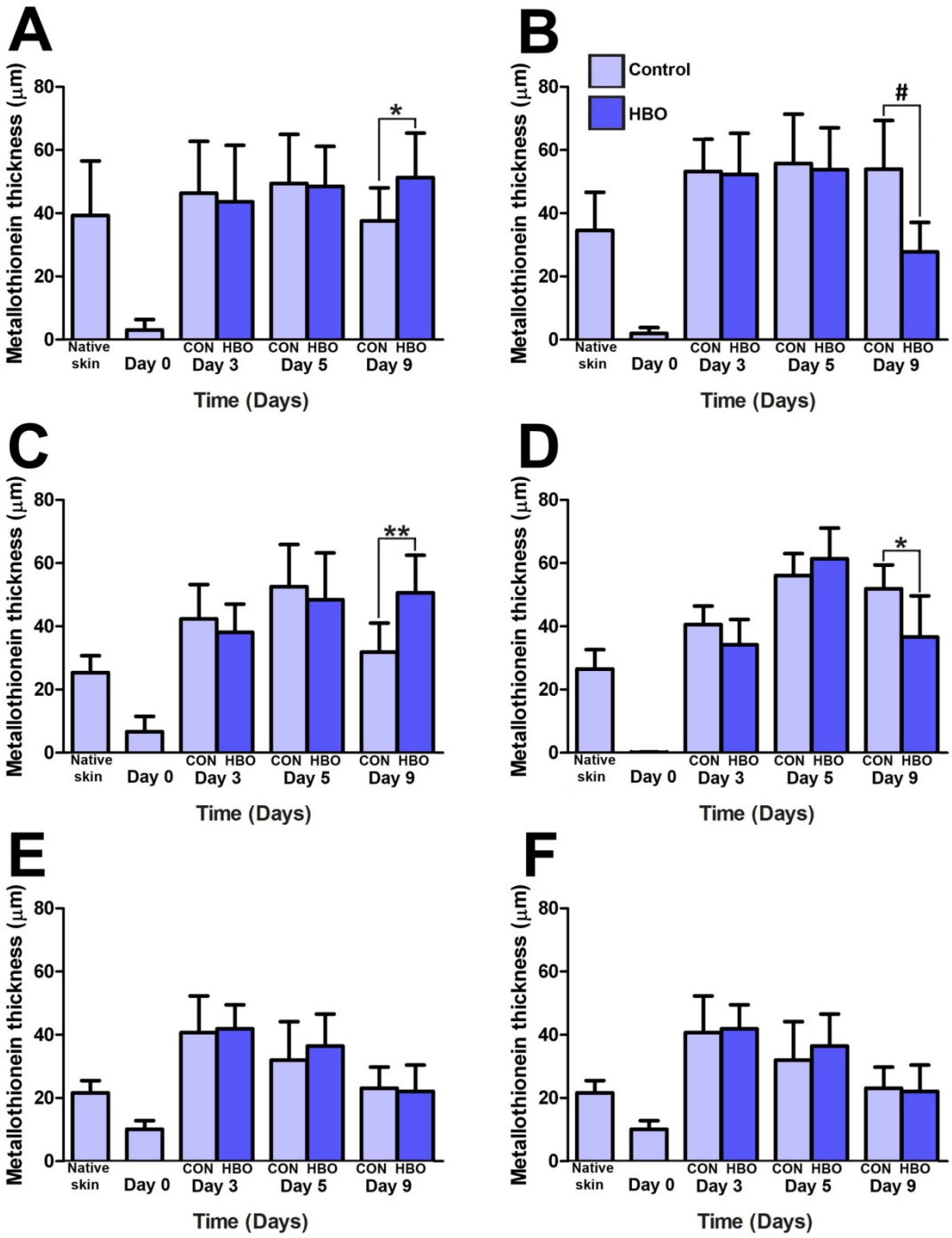

Figure 6.13 MT immunoreactivity in the HSE model over 9 days of treatment
The thickness of MT immunoreactivity in the epidermis was quantified from (**A**) the group A samples, (**B**) sample 4, (**C**) sample 5, (**D**) sample 6, (**E**) sample 7 and (**F**) sample 8. Data was obtained from n = 2 HSEs per time point, except sample 6, where n = 1 per time point. There were a total of 8 histological sections analysed per HSE model, therefore, 16 images for all samples, except sample 6. Data represent the mean thickness of MT immunoreactivity in the epidermis ± standard deviation. Significant difference $p < 0.05$ is indicated by *, $p < 0.01$ is indicated by **, and $p < 0.001$ is indicated by #.

6.3.16 Kallikrein 1 immunoreactivity in the HSE model in response to HBO treatment

Kallikrein 1 (KLK1), also known as tissue kallikrein, is a serine protease with a largely unknown role in the skin. KLK1 involvement, however, has previously been implicated in keratinocyte migration, wound healing and epidermal desquamation (Gao *et al*., 2010; Komatsu *et al*., 2003). Currently, the expression and localisation of KLK1 protein in human skin has not been previously described. Komatsu *et al*. (2003 and 2005) has, however, examined *KLK1* mRNA localisation in the epidermis and reported its localisation in all epidermal layers.

Similar to the gene expression data reported by Komatsu *et al*. (2003 and 2005), KLK1 antigen immunoreactivity was observed throughout the entire epidermis in all HSE sections, as well as in native skin. Furthermore, KLK1 immunoreactivity was also detected in dermal fibroblasts in native skin sections. More specifically, KLK1 antigen was detected in the apical layers of the stratum corneum, but was absent from the layers of the stratum corneum closest to the stratum granulosum (**Figure 6.14 A**). In addition, KLK1 immunoreactivity was observed in all epidermal keratinocytes of each HSE model from day 0 up until day 9. However, KLK1 immunoreactivity appeared absent from, or reduced in, the stratum corneum of some HSE models (**Figure 6.14 B - H**). No differences in KLK1 expression in response to HBO treatment of the HSE samples were apparent. To establish if there were any quantitative differences in KLK1 expression, the thickness of KLK1-positive epidermis was quantified using ImageJ analyses as described in section 2.11.2.

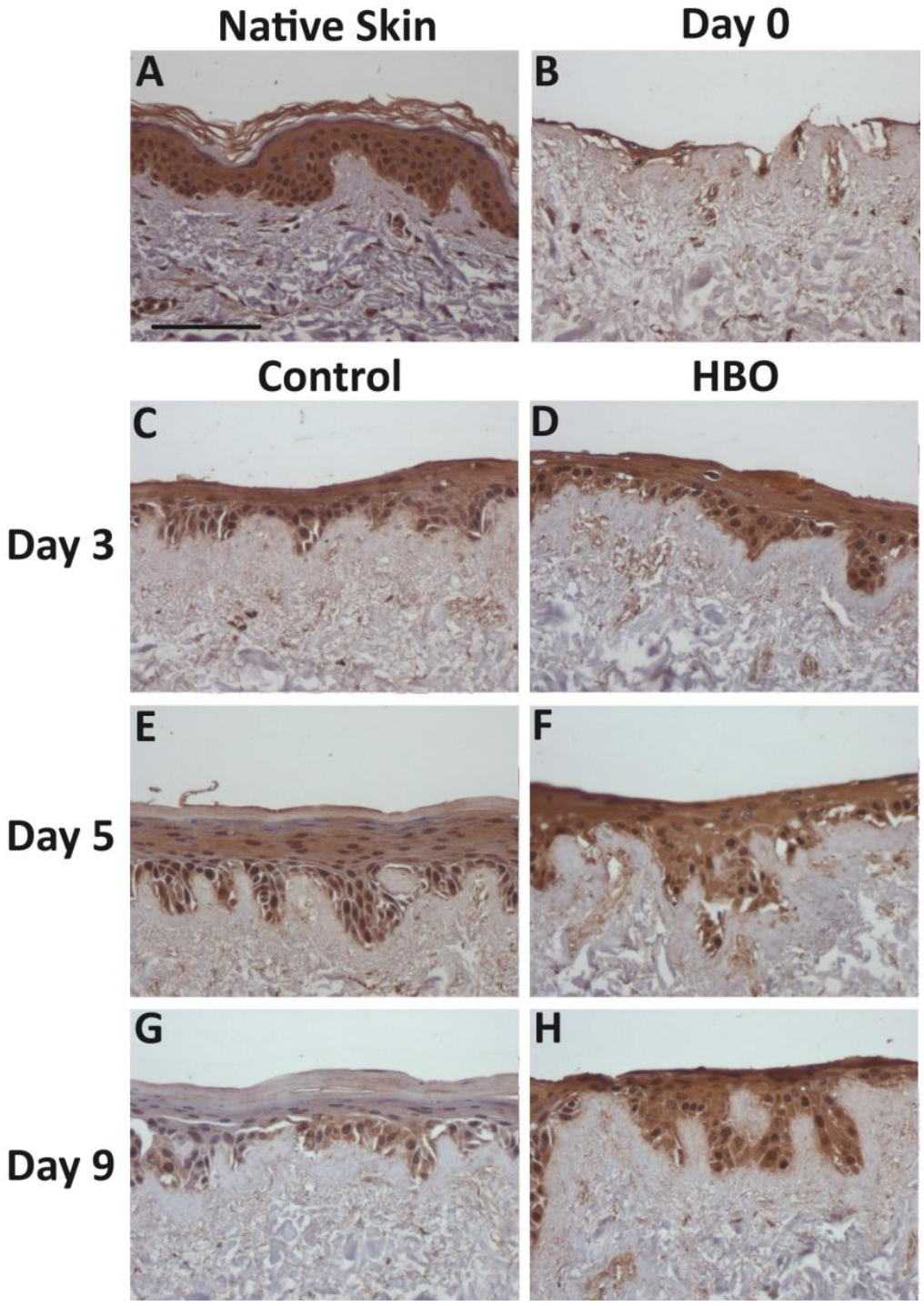

Figure 6.14 Localisation of KLK1 in the HSE model undergoing epidermogenesis
Histological sections of native skin and HSE models grown for 0, 3, 5 and 9 days at the air-liquid interface, treated with or without HBO and were probed for KLK1. The expression of KLK1 in keratinocytes was detected in (**A**) native skin and in HSE models at (**B**) day 0, (**C, D**) day 3, (**E, F**) day 5 and (**G, H**) day 9. HBO-treated samples are represented by images **D, F** and **H**, whereas control samples were in images **C, E** and **G**. The presence of the KLK1 antigen was represented by brown immunoreactivity, and all nuclei have been counterstained blue with haematoxylin. The scale bar represents 100 μm. These are representative images using images captured from skin sample 6.

6.3.17 KLK1 immunoreactivity in the HSE model is not consistently altered by HBO treatment

Images captured of the immunoreactivity described in section 6.3.16 were analysed using ImageJ to determine the thickness of the epidermis expressing KLK1 (Appendix Table A57 and Table A58). The temporal trend of KLK1 immunoreactivity was similar between skin samples. In sections from the HSE model at day 0, the expression of KLK1 was low. Between days 0 and 3, KLK1-positive epidermal thickness increased, then peaked at day 5, and by day 9 had decreased to levels similar to sections from the day 3 HSE (**Figure 6.15 A - D** and **F**). In skin sample 7, however, KLK1 immunoreactivity peaked in sections from the day 3 HSE model, before it progressively decreased over time (**Figure 6.15 E**).

The HSEs were also investigated to determine if HBO treatment influenced KLK1 immunoreactivity. At each time point, there was little difference in the detection of the KLK1 antigen between the two treatment groups. Indeed, only sample 8 demonstrated any significant differences from the control HSEs in response to HBO treatment. This occurred at day 3, where KLK1 immunoreactivity was significantly lower in the HBO-treated HSE model (50.62 µm ± 10.53 µm in HBO compared to 72.66 µm ± 17.39 µm in the control; $p < 0.01$; **Figure 6.15 F**). Taken together these results suggest that HBO treatment does not influence KLK1 immunoreactivity in the HSE model.

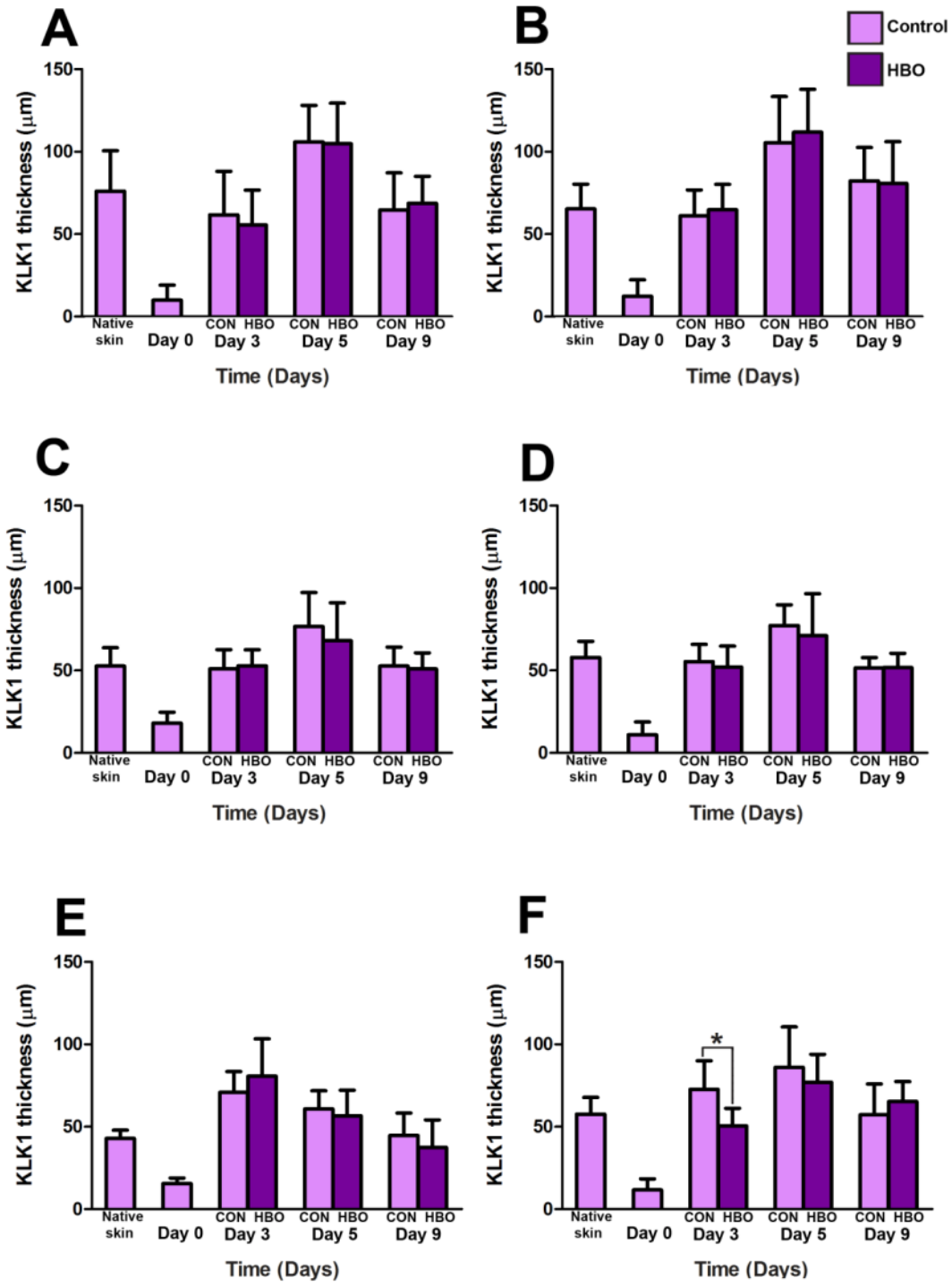

Figure 6.15 KLK1 immunoreactivity in the HSE model over 9 days of treatment
The thickness of KLK1 immunoreactivity in the epidermis was quantified from (**A**) the group A samples, (**B**) sample 4, (**C**) sample 5, (**D**) sample 6, (**E**) sample 7 and (**F**) sample 8. Data was obtained from n = 2 HSEs per time point, except sample 6, where n = 1 per time point. There were a total of 8 histological sections analysed per HSE model, therefore, 16 images for all samples, except sample 6. Data represent the mean thickness of KLK1-immunoreactivity in the epidermis ± standard deviation. Statistical significance $p < 0.01$ is indicated by *.

6.3.18 Kallikrein 7 immunoreactivity in the HSE model in response to HBO treatment

KLK7, also known as stratum corneum chymotryptic enzyme (SCCE), is a serine protease involved in maintaining the stratum corneum through participation in the desquamation process (Hansson *et al.*, 2002). Moreover, KLK7 expression has previously been demonstrated to localise to the supra-basal layers of the epidermis where corneocytes are sloughed off at the skin surface (Ekholm *et al.*, 2000).

Initial analysis of native skin images revealed that KLK7 expression was present and localised to the stratum corneum and in some instances, the most superficial layer of the stratum granulosum (**Figure 6.17 A**). In sections from the day 0 HSE, KLK7 was either absent, or expressed at almost undetectable levels, most likely due to the absence of a stratum corneum at this time point (**Figure 6.17 B**). By day 3 in the HSE model, KLK7 immunoreactivity was clearly present in the supra-basal epidermal layers, just beneath the stratum corneum (**Figure 6.17 C** and **D**). Continuing into day 5 (**Figure 6.17 E** and **F**) and day 9 (**Figure 6.17 G** and **H**), KLK7 expression remained localised to the superficial epidermal layers. Moreover, at days 5 and 9, KLK7 was localised to the edges of the epidermal cell surface and appeared to be reduced or absent from the cytoplasm (**Figure 6.17 E - H**). In general, the pattern of KLK7 immunoreactivity was similar between skin samples. In epidermal keratinocytes, KLK7 was localised mainly to the outer edges of the keratinocytes in the suprabasal layers of the epidermis (**Figure 6.16**).

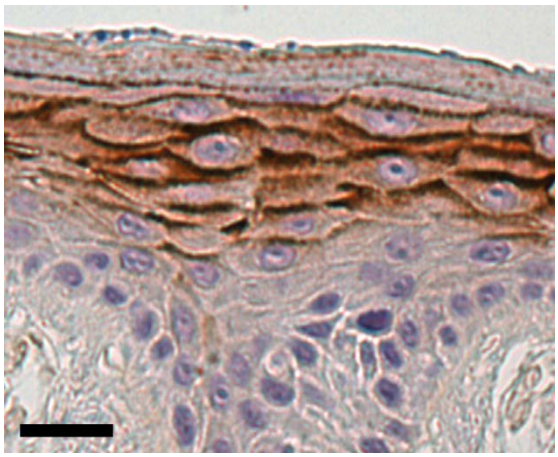

Figure 6.16 Localisation of KLK7 in epidermal keratinocytes
KLK7 was localised to edges of the suprabasal keratinocytes, but was absent from the cytoplasm. The scale bar represents 25 μm.

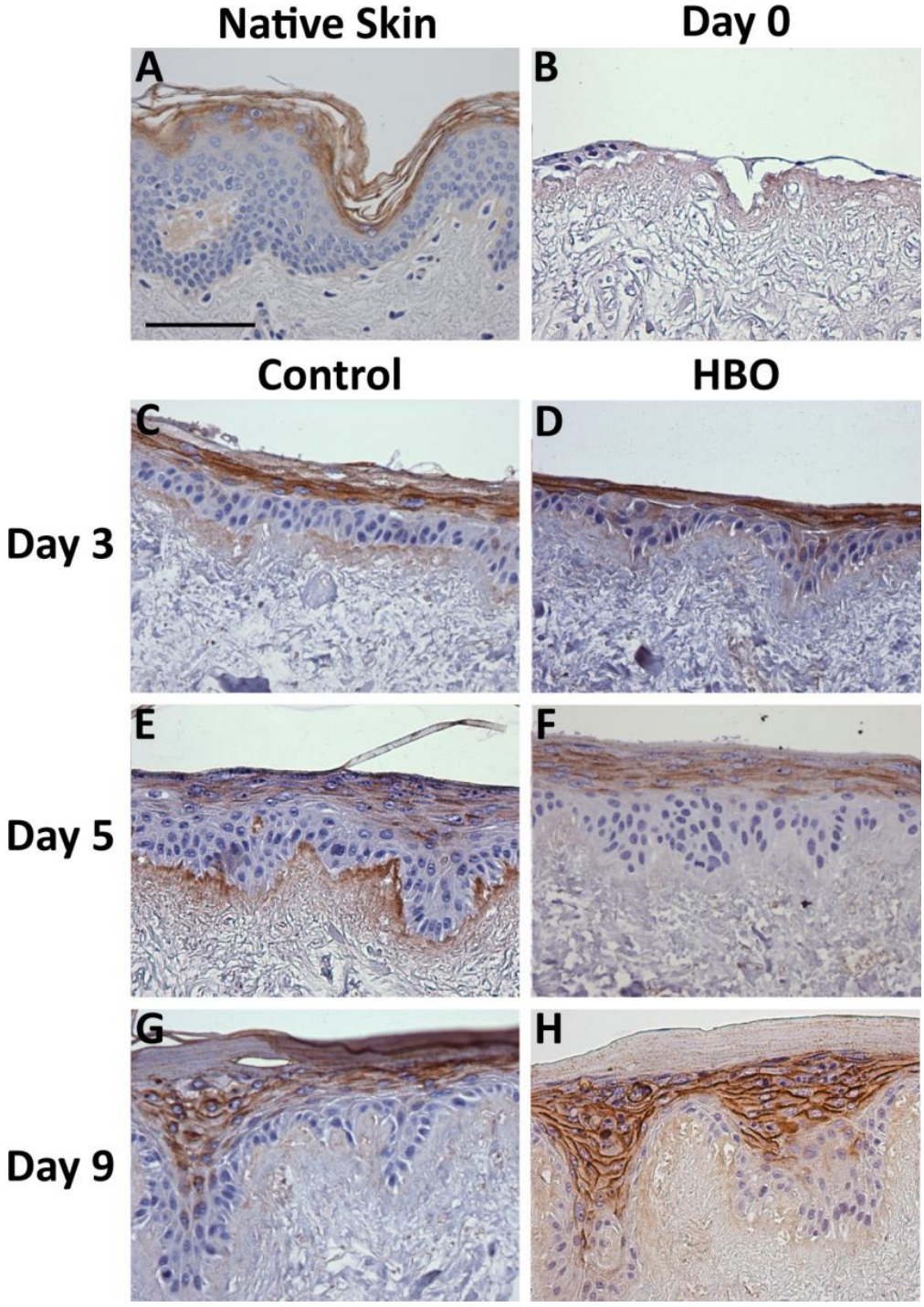

Figure 6.17 Localisation of KLK7 in the HSE model undergoing epidermogenesis in response to HBO treatment

Histological sections of native skin and HSE models were grown for 0, 3, 5 and 9 days at the air-liquid interface, treated with or without HBO and were probed for KLK7. The expression of KLK7 in keratinocytes was detected in (**A**) native skin and in HSE models at (**B**) day 0, (**C, D**) day 3, (**E, F**) day 5 and (**G, H**) day 9. HBO-treated samples were represented by figures (**D, F, H)**, whereas control samples were represented by figures (**C, E, G**). The presence of the KLK7 antigen was represented by brown immunoreactivity, and all nuclei were counterstained blue with haematoxylin. The scale bar represents 100 μm. These are representative figures using images captured from group A samples.

6.3.19 KLK7 immunoreactivity is not consistently altered by HBO treatment in the HSE model

Images captured of the immunoreactivity described in section 6.3.18 were analysed using ImageJ to determine the thickness of the epidermis which expressed KLK7 (Appendix Table A59 and Table A60). In sections from HSEs at day 0, KLK7 immunoreactivity was scarce. This was followed by an increase in the thickness of KLK7-positive epidermis at day 3, peaking at day 5, then decreasing by day 9 (**Figure 6.18**). In most skin samples the thickness of KLK7-positive epidermis was equivalent between treatment groups. At day 9, however, KLK7 immunoreactivity was significantly decreased in response to HBO treatment, when compared to the correlating control, in skin sample 4 (20.32 µm ± 15.82 µm in HBO compared to 35.80 µm ± 10.28 µm in the control; $p < 0.01$, **Figure 6.18 B**). Moreover, KLK7 immunoreactivity was significantly decreased in response to HBO treatment at all time points in skin sample 6 (8.88 µm ± 3.81 µm in HBO compared to 18.03 µm ± 3.49 µm in the control at day 3, 25.98 µm ± 3.20 µm in HBO compared to 36.60 µm ± 4.54 µm in the control at day 5 and 5.24 µm ± 1.14 µm in HBO compared to 25.61 µm ± 4.86 µm in the control at day 9; $p < 0.001$ for all, **Figure 6.18 D**). From these results it appears that HBO may cause a decrease in KLK7 immunoreactivity in some HSE models. Nevertheless it appears that HBO treatment does not consistently influence KLK7 immunoreactivity in the HSE model.

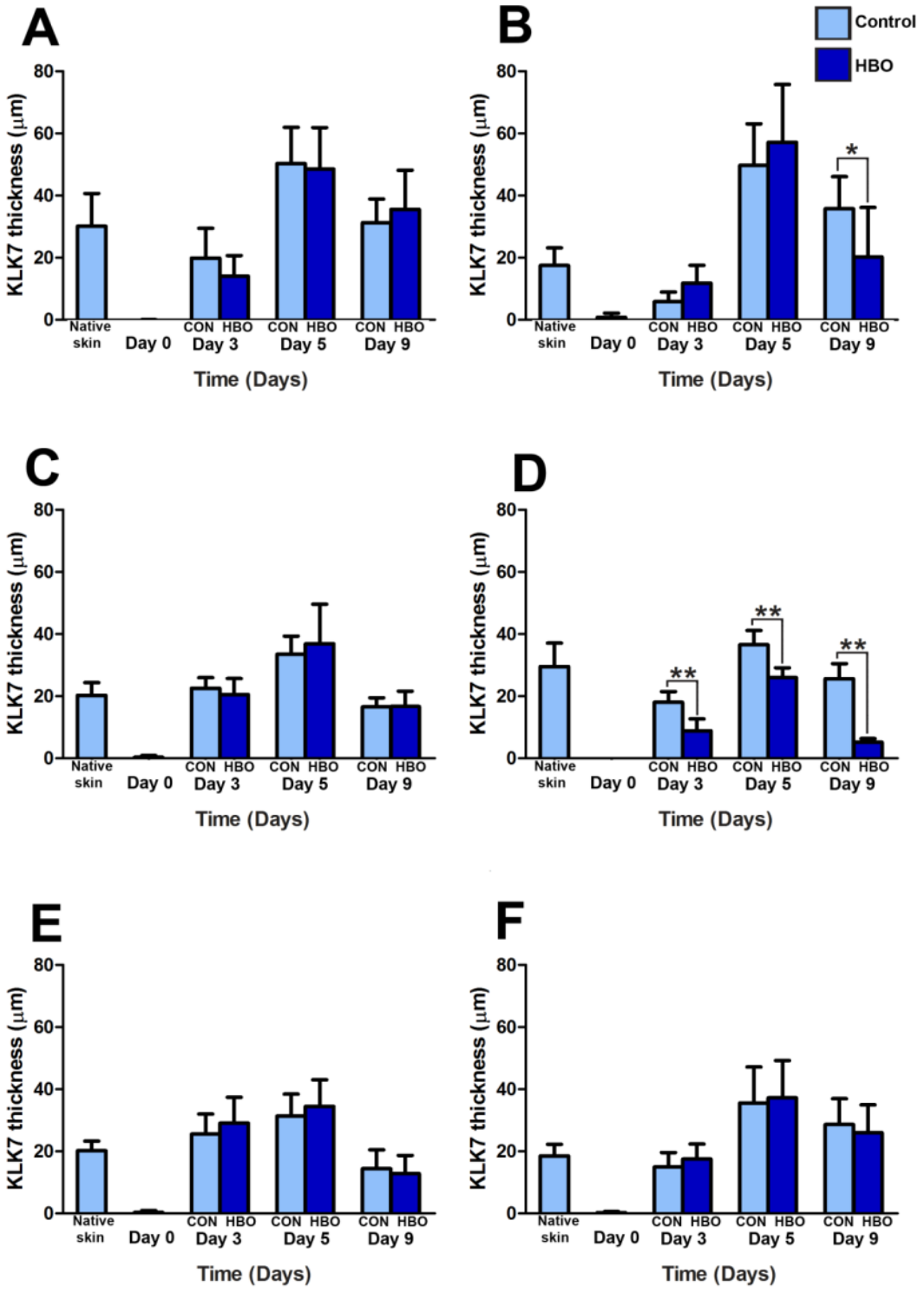

Figure 6.18 KLK7 immunoreactivity in the HSE model over 9 days of treatment
The thickness of KLK7 immunoreactivity in the HSE models was quantified from (**A**) the group A samples, (**B**) sample 4, (**C**) sample 5, (**D**) sample 6, (**E**) sample 7 and (**F**) sample 8. Data was obtained from n = 2 HSEs per time point, except sample 6, where n = 1 per time point. There were a total of 8 histological sections analysed per HSE model, therefore, 16 images for all samples, except sample 6. Data represent the mean thickness of KLK7-immunoreactivity in the epidermis ± standard deviation. Statistical significance $p < 0.01$ is indicated by *, and $p < 0.001$ is indicated by **.

6.3.20 EGR1 immunoreactivity in the HSE model in response to HBO treatment

EGR1 is a mammalian transcription factor that is involved in cellular growth, proliferation and differentiation (Sukhatme *et al.*, 1988). The expression of EGR1 was analysed by immunohistochemistry to detect the presence of this transcription factor in the HSE model and also to determine if HBO treatment influenced the relative abundance of this protein in the nuclei of the developing epidermis.

Analysis of sections from native skin samples revealed that there was a very high level of EGR1 expression. Almost all nuclei throughout native skin were EGR1 positive, including keratinocytes from the basal layer, through to the supra-basal layers (**Figure 6.19 A**). In the HSE models EGR1 was detected in the nuclei of all keratinocytes in the day 0 epidermis (**Figure 6.19 B**). In addition, sections of the HSE model from day 3 expressed EGR1 in most nuclei of the epidermis, with the exception of the supra-basal layers (**Figure 6.19 C** and **D**). This continued into day 5, where EGR1 positive nuclei were present in all but the supra-basal layers of the epidermis in both treatment groups (**Figure 6.19 E** and **F**). This expression trend was also observed at day 9 (**Figure 6.19 G** and **H**). To establish if there were any quantitative differences in EGR1 expression, the number of EGR1-positive nuclei were quantified using ImageJ analyses as described in section 2.11.2.

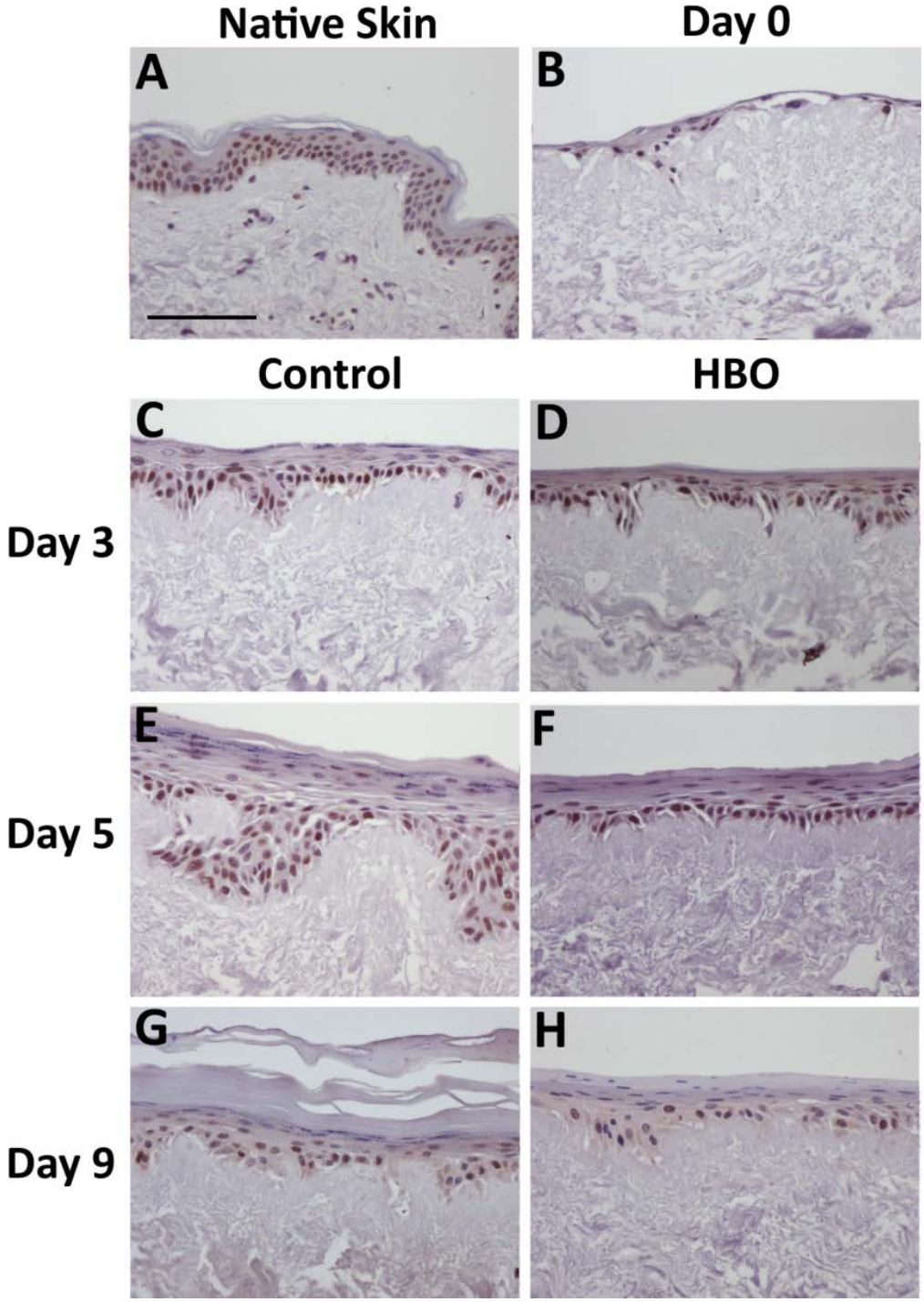

Figure 6.19 Localisation of EGR1 in the HSE model undergoing epidermogenesis
Histological sections of native skin and HSE models were grown fort 0, 3, 5 and 9 days at the air-liquid interface, treated with or without HBO and were probed for EGR1. The expression of EGR1 in the nuclei of keratinocytes was detected in (**A**) native skin and in HSE models at (**B**) day 0, (**C, D**) day 3, (**E, F**) day 5 and (**G, H**) day 9. HBO-treated samples are represented by figures **D, F** and **H**, whereas control samples were in figures **C, E** and **G**. The presence of the EGR1 antigen was represented by brown immunoreactivity, and all other nuclei were counterstained blue with haematoxylin. The scale bar represents 100 μm. These are representative figures using images captured from skin sample 5.

6.3.21 EGR1 immunoreactivity is not consistently affected by HBO treatment in the HSE model

Images captured of the immunoreactivity described in section 6.3.20 were analysed using ImageJ to determine the number of nuclei which expressed EGR1 (Appendix Table A61 and Table A62). The pattern of EGR1 expression in the HSE models was similar between skin samples analysed. Initially, there was an increase in the number of EGR1 positive nuclei between days 0 and 3, which then peaked in HSE sections from day 5, and decreased by day 9 (**Figure 6.20**). Sample 4, however, varied in that there was a progressive increase in the number of EGR1 positive nuclei over the course of the experiment (**Figure 6.20 B**). In contrast, the number of EGR1 positive nuclei progressively decreased in sections from day 3 to 9 in skin sample 8 (**Figure 6.20 F**).

Sections from the HSE models were also investigated to determine if HBO treatment influenced EGR1 immunoreactivity. Significant differences in EGR1 immunoreactivity between treatment groups were detected in some patients. Higher levels of EGR1 in response to HBO treatment were present in sections from day 3 in sample 4 (90.13 ± 18.37 in HBO compared to 61.38 ± 19.31 in the control; $p < 0.01$) and sample 7 (71.94 ± 14.91 in HBO compared to 49.13 ± 10.39 in the control; $p < 0.001$; **Figure 6.20 B** and **E**). Furthermore, sample 7 expressed significantly lower levels of EGR1 in the day 5 HBO sample (65.44 ± 21.65 in HBO compared to 72.13 ± 15.30 in the control; $p < 0.05$), as did sample 5 (54.69 ± 9.39 in HBO compared to 73.94 ± 24.08 in the control; $p < 0.01$; **Figure 6.20 C** and **E**). Lastly, sample 6 had lower levels of EGR1 positive nuclei in day 9 HBO-treated HSEs as compared to day 9 control (17.00 ± 10.92 in HBO compared to 39.38 ± 9.83 in the control; $p < 0.01$; **Figure 6.20 D**). Taken together, these results suggest that HBO treatment does not consistently influence EGR1 immunoreactivity in the HSE model.

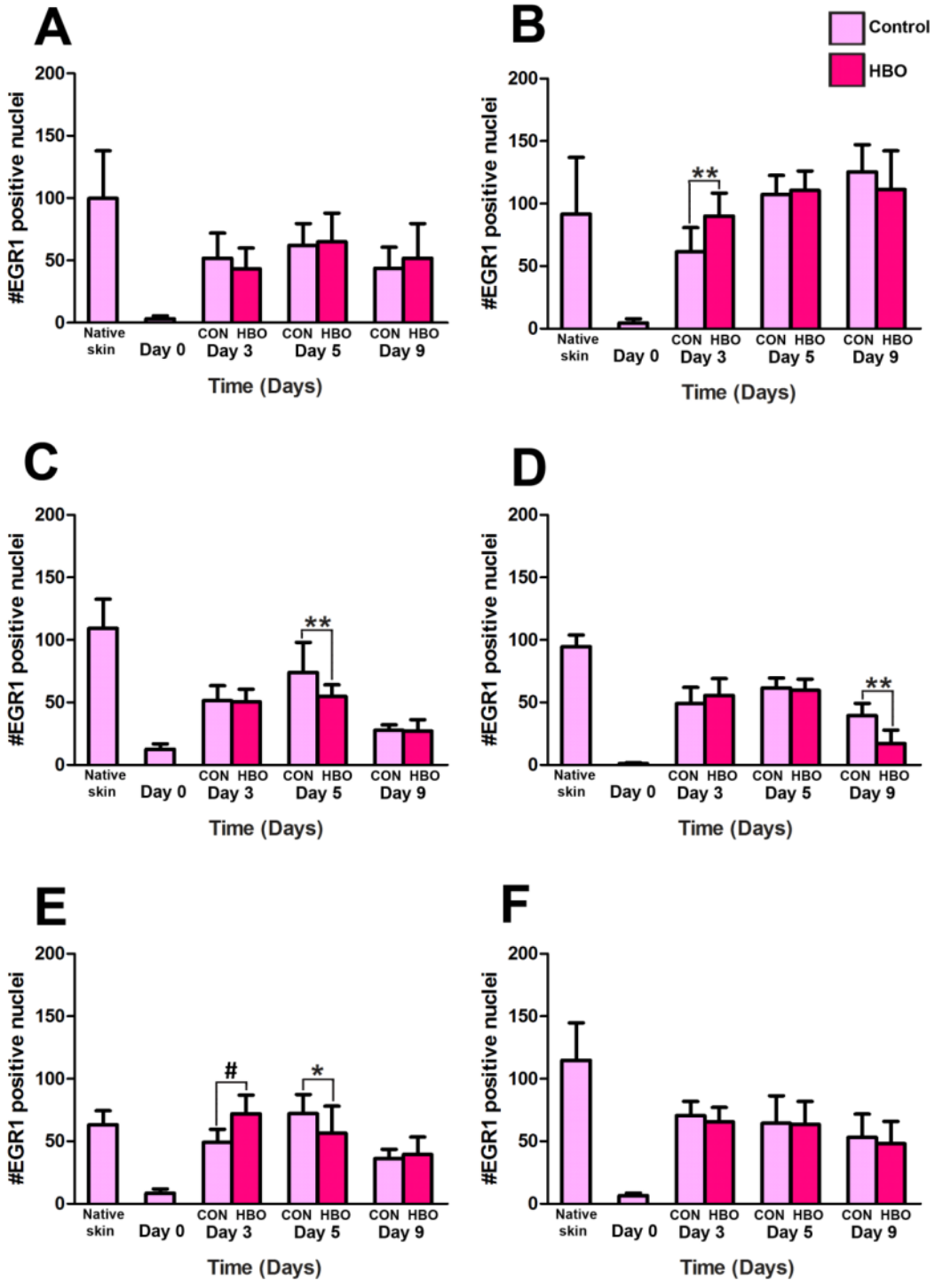

Figure 6.20 EGR1 immunoreactivity in the HSE model over 9 days of treatment
The number nuclei immunoreacting positive for EGR1 were counted using ImageJ in sequential histology sections. The data was obtained from (**A**) pooled EGR1 data from group A samples and (**B**) EGR1 data from sample 4, (**C**) sample 5, (**D**) sample 6, (**E**) sample 7 and (**F**) sample 8. Data was obtained from n = 2 HSEs per time point, except sample 6, where n = 1 per time point. There were a total of 8 histological sections analysed per HSE model, therefore, 16 images for all samples, except sample 6. Data represents the mean number of EGR1 positive nuclei ± standard deviation. Statistical significance $p < 0.05$ is indicated by*, $p < 0.01$ is indicated by **, and $p < 0.001$ is indicated by #.

6.3.22 CDCP1 immunoreactivity in the HSE model in response to HBO treatment

The transmembrane protein CDCP1 is a putative marker for cell-to-cell adhesion within epithelial tissue (Alvares *et al.,* 2008). In spite of this, the role of CDCP1 in stratified epithelial tissues is largely unknown. For these reasons the expression levels of this protein were evaluated in control and HBO-treated HSEs.

Analysis of immunohistological sections probed for CDCP1 revealed that CDCP1 was localised to the cell surfaces in contact with other epithelial cells and was absent from the cell surface of the keratinocytes that were in contact with the basement membrane (**Figure 6.21**). Interestingly, CDCP1 was present in both the stratum corneum and the stratum spinosum of the epidermis in native skin sections (**Figure 6.22 A**). In sections from day 0 HSE models, the cellular surfaces and cytoplasm of all keratinocytes were positive for CDCP1 expression (**Figure 6.22 B**). As the epidermis of the HSE model stratified, the localisation of CDCP1 became restricted to only cell-to-cell contacts (**Figure 6.22 C - H**). The expression of CDCP1 extended approximately 1 - 2 cell layers above the stratum basale. Furthermore, in native skin, CDCP1 expression was localised to the cell membrane and the cytoplasm, whereas CDCP1 was localised only to the cell membrane in the HSE model. To establish if there were any quantitative differences in CDCP1 expression, the thickness of CDCP1-positive epidermis was quantified using ImageJ analyses as described in section 2.11.2.

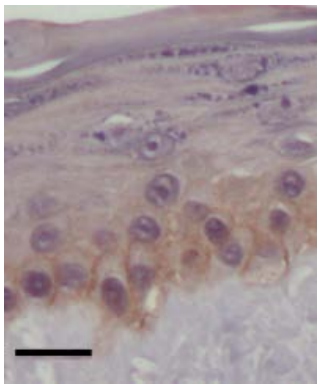

Figure 6.21 Localisation of CDCP1 in epidermal keratinocytes
CDCP1 was localised to surfaces of the keratinocytes in contact with other cells, but was absent from the cell surface in contact with the basement membrane. The scale bar represents 25 µm.

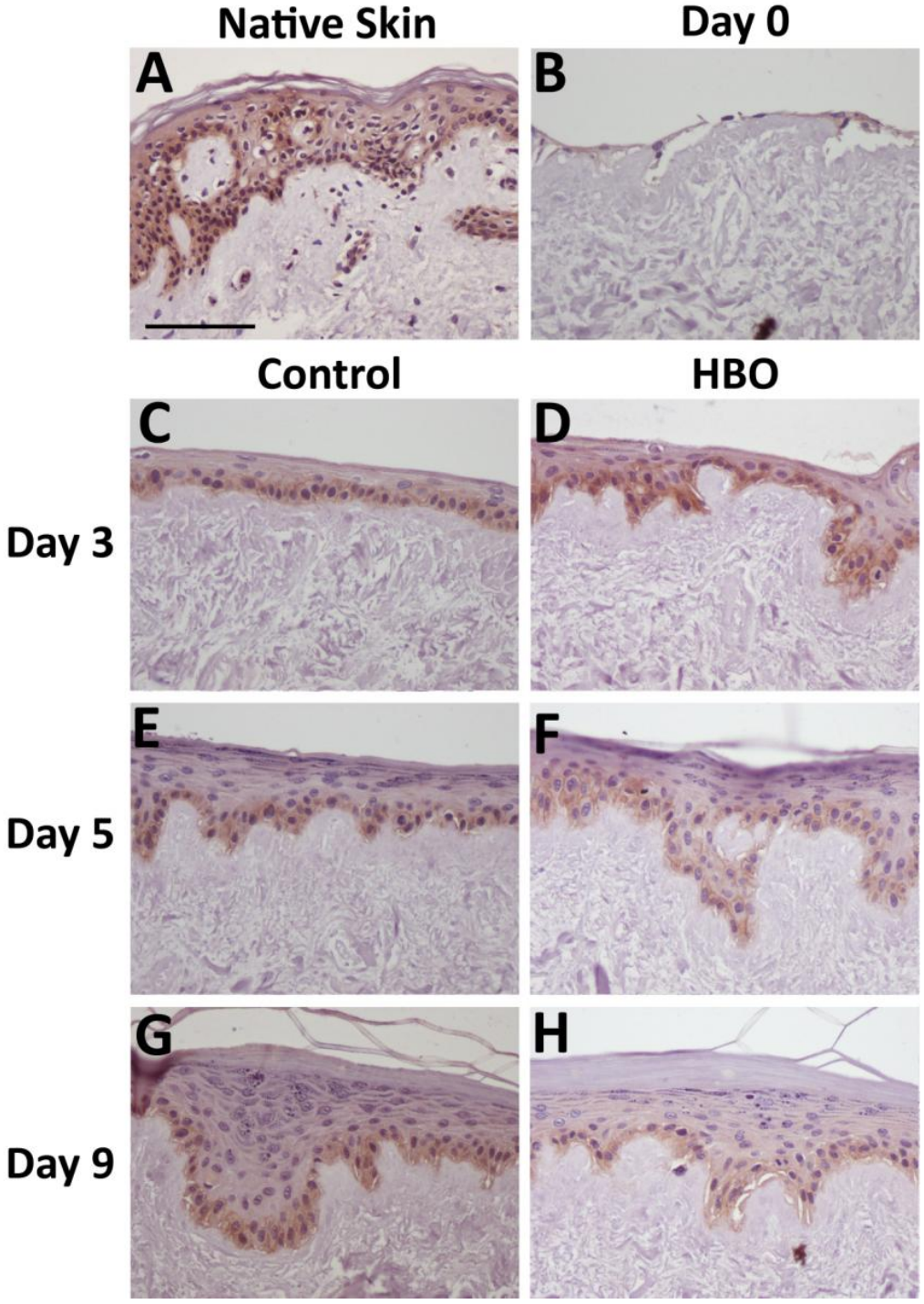

Figure 6.22 Localisation of CDCP1 in the HSE model undergoing epidermogenesis
Histological sections generated from native skin and HSE models grown for 0, 3, 5 and 9 days at the air-liquid interface, treated with or without HBO and were probed for CDCP1. The expression of CDCP1 in keratinocytes was detected in (**A**) native skin and in HSE models at (**B**) day 0, (**C, D**) day 3, (**E, F**) day 5 and (**G, H**) day 9. HBO-treated samples are represented by images **D, F** and **H**, whereas control samples were in images **C, E** and **G**. The presence of the CDCP1 antigen was represented by brown immunoreactivity, and all nuclei were counterstained blue with haematoxylin. The scale bar represents 100 μm. These are representative images using images captured from the group A skin samples.

6.3.23 CDCP1 immunoreactivity is not consistently affected by HBO treatment in the HSE model

Images captured of the immunoreactivity described in section 6.3.22 were analysed using ImageJ to determine the thickness of the epidermis which expressed CDCP1 (Appendix Table A63 and Table A64). CDCP1 immunoreactivity was analysed in sections of the HSE model and it was observed that CDCP1 antigen levels were relatively stable throughout the experiment (**Figure 6.23**). In general, CDCP1 immunoreactivity increased between days 0 and 3, then the thickness of the epidermis positive for CDCP1 remained consistent at day 5 and 9 (**Figure 6.23**).

The HSE sections were also investigated to determine if HBO treatment influenced CDCP1 immunoreactivity. Interestingly, all significant differences in CDCP1 immunoreactivity were observed at day 9. CDCP1 immunoreactivity was up-regulated in response to HBO treatment in skin sample 5, when compared to the day 9 control sample (35.35 µm ± 10.79 µm in HBO compared to 22.51 µm ± 4.91 µm in the control; $p < 0.001$; **Figure 6.23 C**). Conversely, CDCP1 immunoreactivity was significantly down-regulated in response to HBO treatment in sample 8 when compared to the correlating control (23.18 µm ± 4.66 µm in HBO compared to 32.39 µm ± 10.09 µm in the control; $p < 0.05$; **Figure 6.23 F**). Together, these results suggest that HBO only impacts CDCP1 immunoreactivity after 9 days of treatment. The influence of HBO, however, is not consistent between samples.

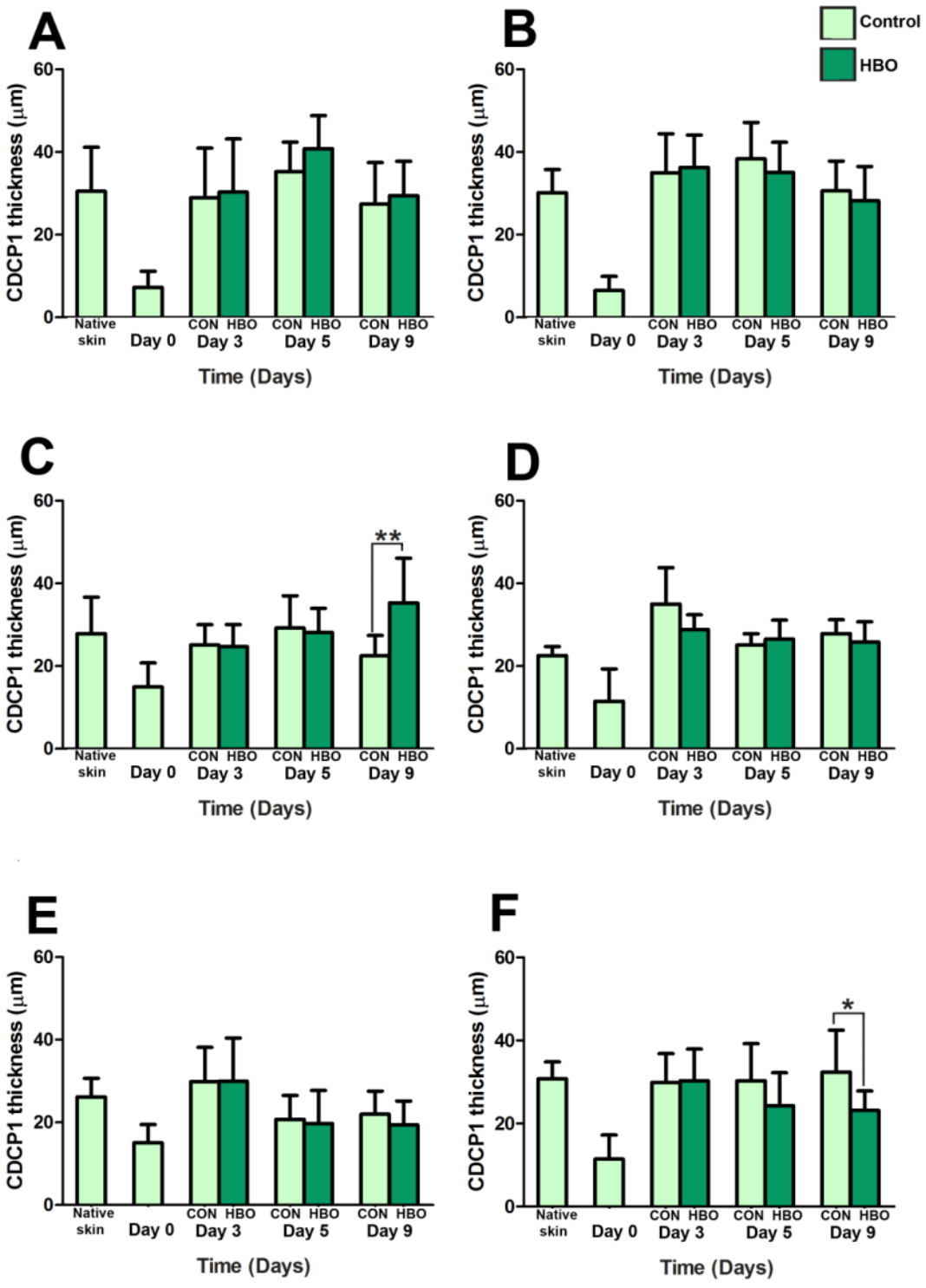

Figure 6.23 CDCP1 immunoreactivity in the HSE model over 9 days of treatment
The thickness of CDCP1-positive epidermis in the HSE models was quantified from (**A**) the group A samples, (**B**) sample 4, (**C**) sample 5, (**D**) sample 6, (**E**) sample 7 and (**F**) sample 8. Data was obtained from n = 2 HSEs per time point, except sample 6, where n = 1 per time point. There were a total of 8 histological sections analysed per HSE model, therefore, 16 images for all samples, except sample 6. Data represent the mean thickness of CDCP1-immunoreactivity in the epidermis ± standard deviation. Statistical significance $p < 0.05$ is indicated by *, and $p < 0.001$ is indicated by **.

6.4 DISCUSSION

This is the first study to investigate gene expression in HSE models treated with HBO using microarray approaches. It was later discovered, however, that pooling separate skin samples prior to microarray analysis was not the optimal approach (**Figure 6.11**). The expense associated with microarray analysis, combined with the limited quantity of RNA available from each HSE, persuaded us to pool samples from the HSEs from skin from 3 donors at each of the time points. This may have led to masking specific changes in gene expression detection via gene microarray analysis if the gene expression for each particular gene varied greatly between the three pooled skin samples. In light of this, in future studies triplicate HSE models from the same skin sample should be used to ensure a sufficient yield of RNA, thus overcoming the need to pool RNA from different skin samples. Nonetheless, the data generated from this Chapter, in addition its novelty, was a useful screening tool to identify a cohort of focus genes which were further investigated using qRT-PCR and immunohistochemistry.

The first approach employed to address the aim of this Chapter was to use gene microarray and functional analysis technologies to perform a genome-wide screen of genes differentially regulated in response to HBO treatment in the HSE model. Unsurprisingly, the top 5 ranking data sets at all three time points were associated with 'molecular and cellular function', such as cell cycle, small molecule biochemistry and cellular growth and proliferation (Appendix Tables A36 – A38). These were further analysed using Cytoscape® to visualise the change in gene number and relevance to the functional group over time (**Figure 6.3**). Furthermore, genes involved in 'hair and skin development and function' (*Table 6.3*), 'tissue development' (*Table 6.4*) and 'dermatological diseases and conditions' (*Table 6.6*) were analysed and a list of genes of interest was generated. These genes include those from the S100 family, as well as *ITGAV*, *GRHL3*, *CDCP1* and *KLK7*.

In addition to electing to further study the genes identified via the focus gene data from this microarray analysis, genes identified as likely to be relevant from the published literature were also examined. For example, Godman *et al.* (2010) examined the effect of HBO treatment on human microvascular endothelial cells. Similar to the data presented in this Chapter, Godman *et al*. (2010) reported that *EGR1* was a top responding gene following HBO treatment. Interestingly, however,

in this study most members of the Metallothionein family of genes were differentially regulated post-HBO treatment (Godman *et al.*, 2010). This highlights that the Metallothionein gene family may be important to HBO-mediated reponses in humans. Furthermore, Metallothioneins are known to have protective effects against oxidative stress, which is a reported side-effect of HBO treatment (Kumari *et al.*, 1998; Thom, 2009; Thornalley and Vasák, 1985). Investigation of functional network data reported in this Chapter revealed that *MT1H* was differentially regulated in response to HBO treatment (Appendix Table A12 and A16). Interestingly, microarray analysis of hypoxia-treated prostate cancer cells by Yamasaki *et al*. (2007) demonstrated that genes in the metallothionein family, in addition to *EGR1*, are up-regulated in response to hypoxia. It was reported in this Chapter that both *EGR1* and members of the metallothionein family were differentially regulated in response to HBO treatment (**Figure 6.13** and **Figure 6.20**). Taken together this suggested that both *EGR1* and the metallothionein family may be induced by exposure to either higher or low oxygen tensions and were therefore investigated by qRT-PCR in sections 6.3.7 and 6.3.9

When these genes of interest were investigated by qRT-PCR, a high level of variation between skin samples was revealed (**Figure 6.5** - **Figure 6.10**); there was a lack of correlation between gene expression (as determined by qRT-PCR) within skin samples from group B, and there was also a lack of correlation between the microarray data and the qRT-PCR data. It is possible that since microarray analysis was performed on pooled RNA from group A skin samples, the sample-to-sample variation may have 'dampened' any significant changes in gene expression. Indeed, in sections 6.3.6 - 6.3.11, significant sample-to-sample variation was observed, making it difficult to obtain any meaningful results. This also suggests that the pooling of separate skin samples to generate the gene microarray data was not optimal. Furthermore, Morey *et al* (2006) highlighted that there are fundamental differences between the normalisation processes in gene microarray and qRT-PCR. Specifically, microarray analysis involves normalisation based on global gene changes and signal intensity values, whereas qRT-PCR is based on normalisation of gene expression to a reference gene (Morey *et al.*, 2006). This can affect gene expression correlations between microarray and qRT-PCR. Additionally, Chuaqui *et al*. (2002) reported that qRT-PCR only correlates to microarray data when gene

expression fold change levels are quite high (> 4-fold). Given the large variation in gene expression between skin samples, immunohistochemical analysis was employed to investigate the presence of proteins within the HSE in response to HBO treatment.

The role of MT in epidermal proliferation has been suggested previously. Specifically, Hanada *et al*. (1998) used cholera toxin and UVB irradiation to stimulate epidermal hyperplasia in both wild-type and MT1/2 null mice. The authors found that null mice sequestered less zinc in the epidermis and had less hyperplasia, suggesting a role for MT in enhanced proliferation, possibly through the regulatory action on zinc metabolism required for cell growth (Hanada *et al.,* 1998). Moreover, Lansdown *et al.* (1999) and Iwata *et al.* (1999) both reported increased MT expression in newly formed epithelium, as compared to native skin. This is similar to the consistently higher MT immunoreactivity observed in the HSE model than in native skin in these studies (**Figure 6.13**). Moreover, MT immunoreactivity was constantly localised to the basal layers of the epidermis and never extended more than ~3 cell layers from the basement membrane (**Figure 6.12**), consistent with the basal-specific pattern of expression previously observed by Karasawa *et al*. (1991).

MT protein expression has also been investigated in hair follicles, an area of high keratinocyte proliferation and differentiation (Karasawa *et al.,* 1991). A study by Nishimura *et al.* (1996) reported the presence of MT immunoreactivity in the proliferative basal keratinocytes, but this tapered off once differentiation began. These findings not only concur with other published reports (Karasawa *et al*., 1991; Ma *et al*., 2011), but also correlate with the localisation of MT immunoreactivity to the basal layers of the epidermis in both native skin and HSE models reported herein (**Figure 6.12**). These data suggest that MT may be important in epidermal proliferation, but is only differentially regulated once a mature epidermis has formed.

The data reported in this Chapter indicate that KLK7 was localised to the supra-basal layers of the epidermis in the HSE model. In addition, KLK7 was determined to be absent from the stratum corneum in the HSE model, but present in the stratum corneum in native skin (**Figure 6.17**). Ekholm *et al.* (2000) and Hansson *et al*. (1994) similarly reported KLK7 localisation to the stratum corneum in native human skin. Our analysis also revealed that increased KLK7 immunoreactivity only occurred in the control-treated HSE samples (**Figure 6.18**). Interestingly, haematoxylin and eosin analysis of the HSE models revealed that the epidermis of

the HBO-treated HSEs possessed a thicker stratum corneum (**Figure 5.6**). This may suggest involvement of KLK7 in stratum corneum desquamation in the HSE model. Thus, higher levels of KLK7 in the epidermis of the control-treated HSEs may have a role in increased surface sloughing and hence decreased thickness of the stratum corneum (**Figure 5.6**).

KLK7 has been reported by others to be the major enzyme involved in maintenance of epidermal thickness and desquamation (Hansson *et al.*, 1994; Igarashi *et al.*, 2004). Interestingly, however, Ponec *et al*. (2002) investigated desquamation in their HSE model and found that treatment of HSEs with topical activators of proteases, such as KLK7, were ineffective at initiating desquamation (Ponec *et al.*, 2002). Furthermore, Ponec *et al.* (2002) reported that mechanical exfoliation of the HSE was the only effective method of countering excessive terminal differentiation that occurs within the HSE model. Therefore, while it would appear a correlation exists between stratum corneum thickness and KLK7 immunoreactivity levels (**Figure 5.6** and **Figure 6.18**), correlation does not necessarily equate to causation.

While KLK7 has been widely reported to have a role in skin homeostasis, currently no studies report the presence of KLK1 protein in native human skin or skin equivalent models. Studies investigating KLK1 mRNA expression in skin have, however, been reported (Komatsu *et al.*, 2003 and 2005). A functional role of KLK1 in the skin has not yet been fully elucidated; therefore, the possibility remains that KLK1 may be involved in similar functions as found for KLK7 within the skin. KLK1 has been reported, however, to act as an antioxidant and an anti-inflammatory in heart, kidney and blood vessels through processing of a vasoactive protein called kinin (Chao and Chao, 2005). More recently, Gao *et al.* (2010) reported a potential role of KLK1 in keratinocyte migration and also in a rat wound healing model. Specifically, Gao *et al*. (2010) demonstrated that KLK1 stimulated cell migration and proliferation through interactions with the epidermal growth factor receptor. The results presented in this Chapter demonstrate that KLK1 immunoreactivity is located both in the human epidermis and in the HSE model; hence the HSE may be useful as a model system to further investigate the role of KLK1 in skin.

The transcription factor EGR1 was investigated at both the gene and protein level. The functional ontology data indicated that this gene may have been regulated

by HBO treatment; however, comparison of the gene expression data with the protein data did not reflect any consistencies between the two (**Figure 6.9** and **Figure 6.20**). Interestingly, analysis of the EGR1 immunoreactivity revealed that differential expression of EGR1 generally occurred at the earlier time points; days 3 and 5 (**Figure 6.20**). Amendt *et al*. (2002) reported that EGR1 protein is up-regulated not only upon injury, it also remains up-regulated after re-epithelialisation. Furthermore, the authors propose that post-epithelialisation EGR1 expression is induced by TGF-ß (Amendt *et al*., 2002). These results seem contradictory as TGF-ß is a differentiation-inducing, growth restricting growth factor, whereas EGR1 has been demonstrated to induce the expression of mitogenic growth factors (Sukhatme, 1990; Riggs *et al.*, 2000). In contrast to published reports, the levels of EGR1 generally did not increase above native skin levels in the HSE models at any stage throughout the epidermogenesis process or in response to HBO treatment. Therefore, it is possible that EGR1 may not have a role in HBO-mediated effect on cell growth in the HSE model.

Comparison of the CDCP1 gene expression data and protein data for the most part, was inconsistent. Similar to MT immunoreactivity, significant differences in CDCP1 immunoreactivity were only present at day 9 and once the epidermis had formed, very little variation in the expression of CDCP1 was observed both over time and in response to HBO or control treatment (**Figure 6.23 C** and **F**). As mentioned earlier, CDCP1 is known to be expressed in the epidermis and is specifically localised to the basal keratinocytes (Alvares *et al.*, 2008). However, a specific role of CDCP1 in skin has yet to be elucidated. A general role of CDCP1 in epithelial cells has been reported by Spassov *et al*. (2009). The authors suggest that CDCP1 is involved in epithelial cell detachment during processes such as mitosis and migration. Furthermore, recently published data from Spassov *et al*. (2011) indicates that CDCP1 may be involved in controlling cell attachment and detachment in epithelial cells through interactions with integrins. As noted herein, CDCP1 is localised to the basal layer of keratinocytes in both the HSE model and native human skin. More recently a possible role for CDCP1 in keratinocyte migration has been identified (McGovern *et al*., 2012), with keratinocyte migration decreased by up to 68% in the presence of a CDCP1-function blocking antibody. CDCP1 therefore appears to have a role in migration, a key process during both epidermogenesis and

wound healing; however, the specific mechanisms behind its action remain to be elucidated. The HSE model appears to be an ideal model system to further elucidate the functions and molecular interactions of CDCP1 in human skin.

Overall, it appears there is differential regulation of KLK1, KLK7, EGR1, MT1/2 and CDCP1 in HSE models treated with and without HBO exposure. However, due to the small sample size and high sample-to-sample variability present in this study, it is difficult to determine any correlations between HBO treatment and differential gene and protein expression. Nevertheless, the above mentioned proteins clearly are involved in epithelial formation and possibly even wound healing, however, their specific role in HSE models requires further clarification.

Chapter 7: General Discussion

In Australia between 1% and 3% of the population is affected by chronic loss of skin integrity (Baker and Stacey, 1994; Gruen *et al.*, 1996). The high incidence of chronic wounds also results in a large economic burden, with the Australian Institute of Health and Welfare (AIHW) estimating in 2005-2006 that up to AU$ 2.6 billion or approximately 3% of the national health care budget was spent on the care and management of chronic wounds (Posnett and Franks, 2008). Importantly, chronic wounds impact on the quality of life of those affected, their families and friends. Thus the development of wound healing therapeutics is important to remediate both the financial costs of chronic wounds and to improvement of patient care. As reported in this thesis, epidermogenesis, an important process during wound healing, can be studied in a model system and provides a key tool to facilitate research to investigate and understand the mechanisms underlying wound healing.

The use of human skin equivalent (HSE) models has advanced our ability to study skin cells in a more biologically relevant system than traditional 2D cell culture approaches. The structural and morphological similarities of the HSE model to native skin make it a useful tool in studying human skin *in vitro* (Chakrabarty *et al.*, 1999). Furthermore, the development of HSE models has allowed the study of re-epithelialisation and epidermal generation in a controlled manner. Chapter 3 of this thesis focussed on investigating the phenotype and morphology of the HSE model undergoing epidermogenesis and is the first study to histologically characterise a HSE grown on de-epidermised dermis (DED; DED-HSE) over a 9 day period. Previously, a DED-HSE had been characterised in a similar manner as Chapter 3 (Parnigotto *et al.*, 1998). The authors, however, cultured the HSE at the air-liquid interface for 14 days prior to histological characterisation at this single time point. As reported herein, the authors noted a thicker stratum corneum in the HSE as compared to native skin and similarities in the localisation of standard skin markers. In addition, Ponec *et al.* (2002) compared the DED-HSE to native skin and commercially available HSE models (EpiDerm™ and SkinEthic™; stratified keratinocytes grown on non-DED substrates). Again, comparisons were made at a single time point when the HSEs had been cultured at the air-liquid interface for

between 13-20 days. The authors reported that the stratum corneum was thicker than native skin but all histological markers were similarly localised (Ponec *et al.*, 2002). Therefore, while DED-HSE models have previously been investigated and compared to native skin, the process of epidermogenesis encompassing multiple time points in the developing HSE model had not been reported until Chapter 3 of this thesis.

In addition to investigating epidermogenesis at the phenotypic level, changes in gene expression were also examined in the developing HSE in Chapter 4 using gene microarray analysis. Importantly, while a few gene microarray studies on stratification and differentiation of a HSE model have previously been reported (Koira and Andreadis, 2006; Mazar *et al*., 2010), these studies compared submerged HSEs to HSEs cultured at the air-liquid interface. Analysis of differential gene expression changes that take place during the epidermogenesis process in the HSE has not previously been performed. A comparison of the results reported by Koira and Andreadis (2006) and Mazar *et al.* (2010) to those reported in Chapter 4 highlighted the importance of a DED on keratinocyte gene expression. Specifically, Koira and Andreadis (2006) and Mazar *et al*. (2010) had technically more similar experimental design (comparing submerged versus standard HSE culture techniques) than the experimental design reported herein. However, the differentially regulated genes were more similar to my studies than to those highlighted by Mazar *et al*. (2010).

Ralston *et al.* (1999) highlighted the importance of the basement membrane in the HSE model, comparing DED-HSEs both with and without the native basement membrane. The authors reported that greater epidermal-dermal attachment and correct epidermal morphology was present in the HSEs with the intact basement membrane than those without (Ralston *et al.*, 1999). Subsequently, El Ghalbzouri *et al.* (2009) stimulated native human fibroblasts to generate a basement membrane and extracellular matrix, thus eliminating the need for skin donor-derived DED and the use of collagen scaffolds as a dermal substitute. The authors reported that their fibroblast-derived scaffold supported longer HSE culture (> 20 weeks) and proliferation, differentiation and morphology similar to native human skin (El Ghalbzouri *et al.*, 2009). Therefore, it is clear that the use of a DED-HSE is important in generating HSE models more similar to native skin than those generated using a collagen scaffold.

Once the DED-HSE model was characterised and validated as a suitable model of native human skin, investigation of the effect of hyperbaric oxygen (HBO) on the HSE was performed. HBO treatment was investigated as it has been reported to have beneficial effects on chronic wound healing (Abidia *et al*., 2003; Duzgun *et al*., 2008; Hammarlund and Sundberg, 1994; Kalani *et al*, 2002; May and Hodgson, 2002). The therapeutic principles underlying HBO as an effective wound healing adjunct lie in the ability of HBO to increase systemic oxygen content, thereby increasing tissue oxygenation and remediating the hypoxic nature of chronic wounds (Thom, 2009). However, the mechanistic and skin-specific processes of HBO action are yet to be elucidated. Kairuz *et al.* (2007) commenced studies in this area and employed HSE models treated with HBO for up to 5 consecutive days. The authors found that HBO significantly increased the thickness of the cellular layer and stratum corneum following 3 and 5 days of culture when compared to untreated controls (Kairuz *et al.*, 2007). Furthermore, immunohistochemical analysis demonstrated that HBO enhanced p63 immunoreactivity and K1/10/11, markers of epidermal proliferative capacity and differentiation, respectively (Kairuz *et al.*, 2007). Based on these measureable changes observed within the HSE model in response to HBO treatment, one of the hypotheses of this thesis was that those changes could be further investigated by evaluating gene and protein expression differences induced in response to HBO treatment in the HSEs. Moreover, it was reasoned that extending the analysis from 5 to 9 days would be beneficial to examine the longer term effects of HBO treatment of the HSE model. In addition, the HSE model was not cultured for more than 9 days as the HSE model was reaching the end of its lifespan. This was evidence by the excessive differentiation and decreased proliferation which was observed at this time point (**Figure 5.6** and **Figure 5.10**).

In Chapter 5, it was reported that some HSE models had enhanced epidermal thickness in response to HBO treatment, whereas no differences between HBO and control treatment were observed in others. In terms of epidermal proliferation and differentiation markers, consistent responses to HBO treatment on the HSE models were not observed; this contrasts with the report from Kairuz *et al.* (2007). Previously Dimitrijevich *et al.* (1999), the only other study to investigate HBO treatment on a HSE, reported that HBO treatment consistently enhanced epidermal thickness in HSE models after 10 days of treatment. These authors however, cultured

the HSEs using a collagen scaffold dermal-substitute rather than DED and used keratinocytes isolated from a single donor, thereby significantly reducing inherent donor-to-donor variation which could affect result reproducibility. In contrast with these previously published studies (Dimitrijevich *et al.*, 1999; Kairuz *et al.*, 2007), the data presented herein suggest that HBO may stimulate equivalent keratinocyte proliferation during epidermogenesis in all skin donors. In light of this, global changes in gene expression in response to HBO treatment in the HSEs were investigated using gene microarrays to identify potential differences between HBO and control treatment in the HSE model.

Many studies have been conducted using gene microarray analysis to study HSE models at the molecular level (Holland *et al*., 2009; Hu *et al*, 2010; Koira and Andreadis, 2006; Kurata *et al.*, 2010; Mazar *et al*., 2010). Interpretation of these studies needs to be considered with caution, however, as they all used replicate HSEs which were derived from the same biological source and were grown on collagen-coated tissue culture insets. Thus, inherent donor-to-donor variation which may affect results has not been addressed (Holland *et al*., 2009; Koira and Andreadis, 2006; Kurata *et al.*, 2010; Mazar *et al*., 2010). The exception, however, was the study reported by Hu *et al.* (2010) who investigated gene expression differences between EpiDerm™ obtained from 4 biologically different sources and native human skin obtained from 4 individual donors. Interestingly, the authors reported ~ 87% similarity in gene expression between the EpiDerm™ HSEs and the donor skin (Hu *et al.*, 2010). Nonetheless, the previously mentioned HSE gene microarray studies generated large amounts of data with many lists of potential gene candidates for their area of interest, which can be confusing without a focused analysis (Holland *et al*., 2009; Hu *et al*, 2010; Koira and Andreadis, 2006; Kurata *et al.*, 2010; Mazar *et al*., 2010). The underlying premise for the gene microarray studies reported in Chapter 6 was to determine gene expression alterations in response to HBO treatment in the HSE which may contribute to enhanced epidermogenesis. To assist with analysis of the gene microarray data, functional network analysis was performed to investigate relationships within and between the differentially expressed genes.

The gene network data generated using IPA software revealed that ERK/MAPK were not differentially regulated genes in the microarray data, but were central to many of the gene network pathways identified. In general, signal-

mediating molecules such as ERK/MAPK generally do not alter in gene expression in response to stimuli, rather the phosphorylation status of these proteins is modified and thereby, gene expression regulated by these signalling mediators is post-translational. Since ERK/MAPK were not identified as differentially regulated genes through the original microarray analysis, these genes and subsequent proteins were not further investigated by qRT-PCR or immunohistochemical analysis. A review of the published literature, however, reveals that the ERK/MAPK pathway may be highly relevant to keratinocytes and skin. Dumesic *et al.* (2009) studied keratinocytes within a HSE graft model and found that ERK/MAPK is involved in promoting cell cycle progression, specifically in epithelial cells. The authors also reported that ERK/MAPK is important for cellular growth in the epidermis (Dumesic *et al.*, 2009). Furthermore, Satoh *et al.* (2009) demonstrated in mice that ERK2 is involved in the re-epithelialisation process in burn wounds. The role of ERK/MAPK in inflammatory skin conditions such as psoriasis has been investigated and it appears to be involved in psoriasis pathophysiology. Specifically, Wang *et al*. (2009) studied phosphorylation of ERK/MAPK in sections of human native and psoriatic skin. The authors reported a significantly greater level of phosphorylated ERK1/2 was evidentin psoriatic skin as compared to native skin. This is supported by Yu *et al*. (2007) who also found increased ERK1/2 phosphorylation in skin sections from patients with psoriasis.

Interestingly, and in relation to the results reported in Chapters 5 and 6, Jeong *et al*. (2010) established that a cigarette smoke-induced inflammatory response in keratinocytes coincided with an up-regulation of EGR1 gene expression. Furthermore, the authors reported that the induced EGR1 gene expression could be inhibited by treating keratinocytes with an ERK1/2 phosphorylation inhibitor (Jeong *et al*., 2010). Of pertinence to this PhD project overall, Hsieh *et al.* (2010) reported increased proliferation and cell cycle progression of HBO-treated osetoblasts, in addition to an increase in the phosphorylation status of ERK1/2. A paper by Gazel *et al.* (2008) utilised microarray analysis to investigate genes up- and down-regulated in epidermal keratinocytes, treated with and without MAPK inhibitors. The authors demonstrated, for the first time, transcriptional targets of the ERK1/2 pathway in keratinocytes. These targets would be an excellent starting point for future studies of HBO on the skin (Gazel *et al.*, 2008). In general, it is apparent that the ERK/MAPK

pathway is of central importance to the epidermal layer of the skin, and furthermore, may be involved in the HBO-stimulated effects previously observed within the HSE model. Therefore, in future HBO studies, it may be worthwhile to focus on the ERK/MAPK pathway.

Functional gene network analysis using IPA software produced a series of gene networks that did not appear to be related to epidermogenesis in the HSE model and this is discussed in Chapter 6. Functional network analysis was performed using Cytoscape®, a network modelling platform used in this case for visualising functional ontology data, based on the functional ontologies assigned to the differentially regulated genes from the microarray data. When the gene microarray data were analysed in a functional sense the global changes occurring within the HSE were easier to visualise, as opposed to analysing changes in groups of genes over time. Previously Mohamed-Hussein and Harun (2009) applied Cytoscape® to analyse gene microarray data from polycystic ovary syndrome (PCOS) ovary samples compared to healthy, unaffected control ovary samples. The authors highlighted that PCOS is a complex and multi-faceted disease and analysis of gene expression data is overwhelming and undirected when not placed in a functional context (Mohamed-Hussein and Harun, 2009). From their analysis, molecular functions and biological processes likely to be altered in PCOS were discovered and concluded that the genes involved in these processes are likely to be mechanistically involved in PCOS (Mohamed-Hussein and Harun, 2009). Studies such as Mohamed-Hussein and Harun, (2009) and the results reported in Chapter 6 highlight the importance of functional and systems-focused analyses as a means of deriving meaningful and biologically relevant results from large data generating methods such as gene microarrays.

As mentioned earlier, skin is a complex structure that is formed through epidermal cell proliferation, stratification and differentiation. In addition, native human skin contains multiple cell types, such as Langerhan's cells, fibroblasts, melanocytes and keratinocytes (Kirfel and Herzog, 2004; Tsatmali *et al*., 2002; Woods *et al*., 2005). Studying gene expression, therefore, in a multi-layered and multi-cellular structure poses significant challenges. The implementation of a single-cell type HSE model, such as the keratinocyte-only model utilised for studies throughout this thesis, reduces gene expression variation induced by multiple cell

types. However, the gene expression variation in the stratified epidermis itself must be considered. Highly proliferative keratinocytes of the stratum basale express genes related to proliferation and cell cycle progression, whereas, keratinocytes in the supra-basal layers express genes related to terminal differentiation (Elias *et al*., 2002; Parsa *et al*., 1999). In view of this, sections of native skin have been analysed using *in situ* hybridisation to localise gene expression within the tissue. Byrne *et al*. (1994) demonstrated K15 gene expression was localised to basal keratinocytes, while K10 and loricrin were localised to the supra-basal and developing stratum corneum layers, respectively. This is also clearly apparent from the data presented herein, where protein expression markers generally are strata specific in both native skin and the HSE. This is evidence that each strata of the epidermis has a unique gene expression profile, therefore current whole-epidermis RNA extraction methods may be suboptimal and this should be considered carefully in future experiments.

The issues arising from the multi-layered nature of the skin in genomic profiling have been overcome by other researchers by utilising laser-capture microdissection (LCM) techniques, rather than total epidermal RNA extraction techniques. LCM allows the isolation of RNA and protein from a select population of cells within a heterogeneous tissue environment (Espina *et al*., 2006). Indeed, others have utilised LCM to investigate subpopulations of keratinocytes from skin. Specifically, Pedersen *et al*. (2003) utilised LCM to isolate RNA from wound-area keratinocytes and also adjacent unwounded keratinocytes. Kennedy-Crispin *et al.* (2012) used LCM to isolate epidermal cells only and prevent dermal fibroblast contamination. LCM was also utilised by Rittié *et al.* (2011) to specifically isolate RNA from total epidermis, specifically without hair follicle keratinocytes and dermal fibroblasts from the same section of skin. Therefore, LCM would be a highly effective tool when investigating RNA from specific populations of cells within complex tissues, such as skin.

In Chapter 6, the expression and localisation of 5 proteins were analysed by immunohistochemical methods in the HSE model. These 5 proteins were chosen as their respective genes were deemed to be significantly differentially regulated in the studies reported in Chapter 5. In general, HBO treatment did not appear to have a significant impact on the expression of any of these proteins and in light of this, this thesis does not provide definitive evidence that HBO treatment is an effective wound

healing therapeutic in the model system used. The results however, demonstrate that the HSE model described herein is a useful tool to study the expression and localisation of these proteins in future studies. In particular, Chapter 6 describes the first study to detect KLK1 protein expression in both native human skin and a HSE model. Moreover, the result presented in Chapter 6 highlighted that the HSE could be used to study CDCP1 expression during epidermogenesis and compares and contrasts its localisation to native human skin (McGovern *et al.,* 2012). Previously, the HSE model has also proved its effectiveness as a tool to investigate functional mechanisms within the skin. Xie *et al.* (2010) created a wounded HSE model and topically applied function blocking antibodies to assess impairment to keratinocyte migration into the wound bed.

As stated earlier, the HSE model is a biologically relevant tool to study epidermogenesis. It is clearly evident that inherent skin donor-to-donor variation exists and this impacted on the reproducibility of results throughout this thesis. Importantly however, it was determined in Chapter 6 that little variation is present between HSEs created from the same skin donor. Together this suggests that for future studies, larger cohorts of skin donors need to be utilised to provide greater resolution of results and to overcome this variation. Furthermore, Tara Fernandez from our laboratory (unpublished data) has highlighted the importance of incorporating both keratinocytes and fibroblasts into the HSE; data support prior reports that fibroblasts play an important role in regulating keratinocyte proliferation and differentiation (El Ghalbzouri *et al.,* 2002; Smola *et al.,* 2003). This may also play an important role in preventing the excessive stratum corneum thickening observed as the HSE models mature. In addition, and supported by Ponec *et al.* (2002), the natural, mechanical process of sloughing to regulate skin thickness should be incorporated into HSE model culture to maintain epidermal homeostasis.

Interestingly, the HSE model from one particular skin donor (skin sample 5) exhibited the most significant increase in HBO-induced stratum corneum thickness when compared to the control. This skin donor was subsequently found to have Cushing's syndrome, a disease characterised by excess glucocorticoids (GC) and an altered wound healing response (Afandi *et al.,* 2003; Bitar *et al.,* 1999). It is remarkable that a skin donor with a condition that impairs wound healing responded most strongly in terms of epidermal thickness to HBO treatment and suggests that

utilising donor skin from individuals predisposed to normal healing may not respond to HBO treatment, or other wound healing therapeutics. In future, it would be of interest to compare and contrast epidermogenesis in HSEs created from "normal" skin donors and those with compromised wound healing (e.g. diabetic individuals).

A commonly arising issue throughout this thesis was the presence of high inter-individual variation. Interestingly, this high level of variation between individuals was more pronounced when examining the responses to HBO treatment rather than the general epidermogenesis response overall. Slight variation of inter-individual variation was observed in the immunohistochemistry analysis of key epidermal markers in Chapters 5 and 6 and was highly prominent in the qRT-PCR data in Chapter 6. This may be attributed to the relative half-lives of mRNA and protein, which is reported to be 9 hours and 46 hours, respectively (Schwanhäusser *et al.*, 2011). Gene expression studies were conducted using mRNA isolated 24-hours post-HBO treatment, which is outside the 9 hour median half-life of mRNA and may have impacted on the results. Therefore, it is possible that inter-individual variability, particularly in the gene expression analysis, was exacerbated by poorly timed sample collection. In future studies, sample collection time should be optimised in order to capture samples when the lowest level of variation will be present.

In summary, the results presented in this thesis advance our understanding of skin repair and regeneration, reporting the first study to investigate epidermogenesis in a biologically relevant DED-HSE over a 9 day period. This body of work suggested that a HSE model, while having some *in vitro* limitations, is histologically similar to native human skin and is certainly no less clinically translatable, but is more ethically appealing than conducting similar studies in animal models. Additionally, this work differs from previous studies investigating HBO using a HSE model as it provides a greater depth of analysis through gene microarrays, functional ontology network analysis, qRT-PCR gene expression studies and immunohistochemistry analysis. The data presented herein did, however, suggest that HBO treatment may not be as clinically beneficial as initially proposed, at least as assessed in this experimental model system. Furthermore, the data suggest that the disease/clinical status of individual skin donors (e.g. Cushing's syndrome) may be evident in HSEs created from their tissue; thus the HSE may prove to be useful for research into certain disease states that affect skin development and repair.

References

Abidia, A., G. Laden, G. Kuhan, B. F. Johnson, A. R. Wilkinson, P. M. Renwick, E. A. Masson and P. T. McCollum (2003). "The role of hyperbaric oxygen therapy in ischaemic diabetic lower extremity ulcers: a double-blind randomised-controlled trial." Eur J Vasc Endovasc Surg **25**(6): 513-518.

Afandi, B., M. S. Toumeh and H. F. Saadi (2003). "Cushing's syndrome caused by unsupervised use of ocular glucocorticoids." Endocr Pract **9**(6): 526-529.

Alam, H., L. Sehgal, S. T. Kundu, S. N. Dalal and M. M. Vaidya (2011). "Novel function of keratins 5 and 14 in proliferation and differentiation of stratified epithelial cells." Mol Biol Cell **22**(21): 4068-4078.

Alleva, R., M. Tomasetti, D. Sartini, M. Emanuelli, E. Nasole, F. Di Donato, B. Borghi, L. Santarelli and J. Neuzil (2008). "alpha-Lipoic acid modulates extracellular matrix and angiogenesis gene expression in non-healing wounds treated with hyperbaric oxygen therapy." Mol Med **14**(3-4): 175-183.

Alvares, S. M., C. A. Dunn, T. A. Brown, E. E. Wayner and W. G. Carter (2008). "The role of membrane microdomains in transmembrane signaling through the epithelial glycoprotein Gp140/CDCP1." Biochimica et Biophysica Acta **1780**(3): 486-496.

Amendt, C., A. Mann, P. Schirmacher and M. Blessing (2002). "Resistance of keratinocytes to TGFbeta-mediated growth restriction and apoptosis induction accelerates re-epithelialization in skin wounds." Journal of Cell Science **115**(Pt 10): 2189-2198.

Archambault, M., M. Yaar and B. A. Gilchrest (1995). "Keratinocytes and fibroblasts in a human skin equivalent model enhance melanocyte survival and melanin synthesis after ultraviolet irradiation." J Invest Dermatol **104**(5): 859-867.

Asano, T., E. Kaneko, S. Shinozaki, Y. Imai, M. Shibayama, T. Chiba, M. Ai, A. Kawakami, H. Asaoka, T. Nakayama, Y. Mano and K. Shimokado (2007). "Hyperbaric oxygen induces basic fibroblast growth factor and hepatocyte growth factor expression, and enhances blood perfusion and muscle regeneration in mouse ischemic hind limbs." Circ J **71**(3): 405-411.

Ayello, E. A., C. Dowsett, G. S. Schultz, R. G. Sibbald, V. Falanga, K. Harding, M. Romanelli, M. Stacey, T. E. L and W. Vanscheidt (2004). "TIME heals all wounds." Nursing **34**(4): 36-41; quiz, 41-32.

Baker, S. R. and M. C. Stacey (1994). "Epidemiology of chronic leg ulcers in Australia." Australia and New Zealand Journal of Surgery **64**(4): 258-261.

Bannasch, H., G. B. Stark, F. Knam, R. E. Horch and M. Föhn (2007). "Decellularized dermis in combination with cultivated keratinocytes in a short- and long-term animal experimental investigation." Journal of the European Academy of Dermatology and Venereology **22**(1): 41-49.

Barthel, D., B. Matthé, C. S. Potten, G. Owen and M. Loeffler (2000). "Proliferation in murine epidermis after minor mechanical stimulation. Part 2. Alterations in keratinocyte cell cycle fluxes." Cell Proliferation **33**(4): 247-259.

Bechetoille, N., C. Dezutter-Dambuyant, O. Damour, V. Andre, I. Orly and E. Perrier (2007). "Effects of solar ultraviolet radiation on engineered human skin equivalent containing both Langerhans cells and dermal dendritic cells." Tissue Engineering **13**(11): 2667-2679.

Benoit, S., A. Toksoy, M. Ahlmann, M. Schmidt, C. Sunderkotter, D. Foell, M. Pasparakis, J. Roth and M. Goebeler (2006). "Elevated serum levels of calcium-binding S100 proteins A8 and A9 reflect disease activity and abnormal differentiation of keratinocytes in psoriasis." Br J Dermatol **155**(1): 62-66.

Bernot, K. M., P. A. Coulombe and K. M. McGowan (2002). "Keratin 16 expression defines a subset of epithelial cells during skin morphogenesis and the hair cycle." J Invest Dermatol **119**(5): 1137-1149.

Berthod, F., L. Germain, N. Tremblay and F. A. Auger (2006). "Extracellular matrix deposition by fibroblasts is necessary to promote capillary-like tube formation in vitro." J Cell Physiol **207**(2): 491-498.

Betz, P., A. Nerlich, J. Wilske, J. Tubel, R. Penning and W. Eisenmenger (1993). "The time-dependent localization of Ki67 antigen-positive cells in human skin wounds." Int J Legal Med **106**(1): 35-40.

Bickenbach, J. R., J. M. Greer, D. S. Bundman, J. A. Rothnagel and D. R. Roop (1994). "Loricrin expression is coordinated with other epidermal proteins and the appearance of lipid lamellar granules in development." Journal of Investigative Dermatology **104**(3): 405-410.

Biedermann, T., L. Pontiggia, S. Bottcher-Haberzeth, S. Tharakan, E. Braziulis, C. Schiestl, M. Meuli and E. Reichmann (2010). "Human eccrine sweat gland cells can reconstitute a stratified epidermis." J Invest Dermatol **130**(8): 1996-2009.

Bishop, A. (2008). "Role of oxygen in wound healing." Journal of Wound Care **17**(9): 399-402.

Bitar, M. S., T. Farook, B. John and I. M. Francis (1999). "Heat-shock protein 72/73 and impaired wound healing in diabetic and hypercortisolemic states." Surgery **125**(6): 594-601.

Boraldi, F., G. Annovi, F. Carraro, A. Naldini, R. Tiozzo, P. Sommer and D. Quaglino (2007). "Hypoxia influences the cellular cross-talk of human dermal fibroblasts. A proteomic approach." Biochimica et Biophysica Acta **1774**(11): 1402-1413.

Borg, D. J., R. A. Dawson, D. I. Leavesley, D. W. Hutmacher, Z. Upton and J. Malda (2009). "Functional and phenotypic characterization of human keratinocytes expanded in microcarrier culture." J Biomed Mater Res A **88**(1): 184-194.

Bowler, P. G. (2002). "Wound pathophysiology, infection and therapeutic options." Annals of Medicine **34**(6): 419-427.

Brattsand, M. and T. Egelrud (1999). "Purification, molecular cloning, and expression of a human stratum corneum trypsin-like serine protease with possible function in desquamation." J Biol Chem **274**(42): 30033-30040.

Broome, A. M., D. Ryan and R. L. Eckert (2003). "S100 protein subcellular localization during epidermal differentiation and psoriasis." J Histochem Cytochem **51**(5): 675-685.

Burgeson, R. E. and A. M. Christiano (1997). "The dermal-epidermal junction." Curr Opin Cell Biol **9**(5): 651-658.

Byrne, C., M. Tainsky and E. Fuchs (1994). "Programming gene expression in developing epidermis." Development **120**(9): 2369-2383.

Caddy, J., T. Wilanowski, C. Darido, S. Dworkin, S. B. Ting, Q. Zhao, G. Rank, A. Auden, S. Srivastava, T. A. Papenfuss, J. N. Murdoch, P. O. Humbert, V. Parekh, N. Boulos, T. Weber, J. Zuo, J. M. Cunningham and S. M. Jane

(2010). "Epidermal wound repair is regulated by the planar cell polarity signaling pathway." Dev Cell **19**(1): 138-147.
Candi, E., R. Schmidt and G. Melino (2005). "The cornified envelope: A model of cell death in the skin." Nature Reviews. Molecular Cell Biology **6**(4): 328-340.
Castelijns, F. A., M. J. Gerritsen, P. E. van Erp and P. C. van de Kerkhof (1999). "Immunohistochemical assessment of keratin 16 on paraffin-embedded sections of normal and hyperproliferative skin: monoclonal antibodies Ks8.12 and LL025 in a comparative study." Arch Dermatol Res **291**(1): 59-63.
Cavani, A., G. Zambruno, A. Marconi, V. Manca, M. Marchetti and A. Giannetti (1993). "Distinctive integrin expression in the newly forming epidermis during wound healing in humans." J Invest Dermatol **101**(4): 600-604.
Ceccarini, C. and H. Eagle (1971). "pH as a determinant of cellular growth and contact inhibition." Proc Natl Acad Sci U S A **68**(1): 229-233.
Chakrabarty, K. H., R. A. Dawson, P. Harris, C. Layton, M. Babu, L. Gould, J. Phillips, I. Leigh, C. Green, E. Freelander and S. M. Neil (1999). "Development of autologous human dermal-epidermal composites based on sterilized human allodermis for clinical use." British Journal of Dermatology **141**(5): 811-823.
Chao, J. and L. Chao (2005). "Kallikrein-kinin in stroke, cardiovascular and renal disease." Exp Physiol **90**(3): 291-298.
Chen, H., J. C. Ho, A. Sandilands, Y. C. Chan, Y. C. Giam, A. T. Evans, E. B. Lane and W. H. McLean (2008). "Unique and recurrent mutations in the filaggrin gene in Singaporean Chinese patients with ichthyosis vulgaris." J Invest Dermatol **128**(7): 1669-1675.
Chen, L., Z. H. Arbieva, S. Guo, P. T. Marucha, T. A. Mustoe and L. A. DiPietro (2010). "Positional differences in the wound transcriptome of skin and oral mucosa." BMC Genomics **11**: 471.
Chuaqui, R. F., R. F. Bonner, C. J. Best, J. W. Gillespie, M. J. Flaig, S. M. Hewitt, J. L. Phillips, D. B. Krizman, M. A. Tangrea, M. Ahram, W. M. Linehan, V. Knezevic and M. R. Emmert-Buck (2002). "Post-analysis follow-up and validation of microarray experiments." Nat Genet **32 Suppl**: 509-514.
Collins, B., T. O. Poehler and W. A. Bryden (1995). "EPR persistence measurements of UV-induced melanin free radicals in whole skin." Photochem Photobiol **62**(3): 557-560.
Compton, C. C., H. B. Nadire, S. Regauer, M. Simon, G. Warland, N. E. O'Connor, G. G. Gallico and D. B. Landry (1998). "Cultured human sole-derived keratinocyte grafts re-express site-specific differentiation after transplantation." Differentiation **64**(1): 45-53.
Dai, X. and J. A. Segre (2004). "Transcriptional control of epidermal specification and differentiation." Curr Opin Genet Dev **14**(5): 485-491.
Dale, B. A., K. A. Holbrook, J. R. Kimball, M. Hoff and T. T. Sun (1985). "Expression of epidermal keratins and filaggrin during Human fetal skin development." The Journal of Cell Biology **101**(4): 1257-1269.
Davidovici, B. B., E. Orion and R. Wolf (2008). "Cutaneous manifestations of pituitary gland diseases." Clinics in Dermatology **26**(3): 288-295.
Davis, S. C., A. L. Cazzaniga, C. Ricotti, P. Zalesky, L. C. Hsu, J. Creech, W. H. Eaglstein and P. M. Mertz (2007). "Topical oxygen emulsion: A novel wound therapy." Archives of Dermatology **143**(10): 1252-1256.

de Sousa Abreu, R., L. O. Penalva, E. M. Marcotte and C. Vogel (2009). "Global signatures of protein and mRNA expression levels." Mol Biosyst **5**(12): 1512-1526.
Devenport, D. and E. Fuchs (2008). "Planar polarization in embryonic epidermis orchestrates global assymetric morphogenesis of hair follicles." Nature Cell Biology **10**(11): 1257-1268.
DiColandrea, T., T. Karashima, A. Maatta and F. M. Watt (2000). "Subcellular distribution of envoplakin and periplakin: insights into their role as precursors of the epidermal cornified envelope." The Journal of Cell Biology **151**(3): 573-586.
Dimitrijevich, S. D., S. Paranjape, J. R. Wilson, R. W. Gracy and J. G. Mills (1999). "Effect of hyperbaric oxygen on human skin cells in culture and in human dermal and skin equivalents." Wound Repair Regen **7**(1): 53-64.
Dumesic, P. A., F. A. Scholl, D. I. Barragan and P. A. Khavari (2009). "Erk1/2 MAP kinases are required for epidermal G2/M progression." The Journal of Cell Biology **185**(3): 409-422.
Duzgun, A. P., H. Z. Satir, O. Ozozan, B. Saylam, B. Kulah and F. Coskun (2008). "Effect of hyperbaric oxygen therapy on healing diabetic foot ulcers." The Journal of Foot and Ankle Surgery **47**(6): 515-519.
Ebert, L. M., S. Meuter and B. Moser (2006). "Homing and function of human skin gammadelta T cells and NK cells: relevance for tumor surveillance." J Immunol **176**(7): 4331-4336.
Ekholm, E. and T. Egelrud (2000). "Expression of stratum corneum chymotryptic enzyme in relation to other markers of epidermal differentiation in a skin explant model." Experimental Dermatology **9**(1): 65-70.
Ekholm, I. E., M. Brattsand and T. Egelrud (2000). "Stratum corneum tryptic enzyme in normal epidermis: a missing link in the desquamation process?" J Invest Dermatol **114**(1): 56-63.
El Ghalbzouri, A., S. Commandeur, M. H. Rietveld, A. A. Mulder and R. Willemze (2009). "Replacement of animal-derived collagen matrix by human fibroblast-derived dermal matrix for human skin equivalent products." Biomaterials **30**(1): 71-78.
El Ghalbzouri, A., S. Gibbs, E. Lamme, C. A. Van Blitterswijk and M. Ponec (2002). "Effect of fibroblasts on epidermal regeneration." Br J Dermatol **147**(2): 230-243.
El Ghalbzouri, A., E. Lamme and M. Ponec (2002). "Crucial role of fibroblasts in regulating epidermal morphogenesis." Cell Tissue Res **310**(2): 189-199.
Elias, P. M., S. K. Ahn, M. Denda, B. E. Brown, D. Crumrine, L. K. Kimutai, L. Komuves, S. H. Lee and K. R. Feingold (2002). "Modulations in epidermal calcium regulate the expression of differentiation-specific markers." J Invest Dermatol **119**(5): 1128-1136.
Espina, V., J. Milia, G. Wu, S. Cowherd and L. A. Liotta (2006). "Laser capture microdissection." Methods Mol Biol **319**: 213-229.
Espina, V., J. D. Wulfkuhle, V. S. Calvert, A. VanMeter, W. Zhou, G. Coukos, D. H. Geho, E. F. Petricoin, 3rd and L. A. Liotta (2006). "Laser-capture microdissection." Nat Protoc **1**(2): 586-603.
Feldmeier, J. J., H. W. Hopf, R. A. W. III, C. E. Fife, L. B. Gesell and M. Bennett (2005). "UHMS position statment: Topical oxygen for chronic wounds." Undersea and Hyperbaric Medicine **32**(3): 157-168.

Fernandez-Rodriguez, E., P. M. Stewart and M. S. Cooper (2009). "The pituitary-adrenal axis and body composition." Pituitary **12**(2): 105-115.
Flasher, D., K. Konopka, S. M. Chamow, P. Dazin, A. Ashkenazi, E. Pretzer and N. Duzgunes (1994). "Liposome targeting to human immunodeficiency virus type 1-infected cells via recombinant soluble CD4 and CD4 immunoadhesin (CD4-IgG)." Biochimica et Biophysica Acta **1194**(1): 185-196.
Fleischmajer, R., S. Gay, J. S. Perlish and J. P. Cesarini (1980). "Immunoelectron microscopy of type III collagen in normal and scleroderma skin." J Invest Dermatol **75**(2): 189-191.
Franzke, C. W., A. Baici, J. Bartels, E. Christophers and O. Wiedow (1996). "Antileukoprotease inhibits stratum corneum chymotryptic enzyme. Evidence for a regulative function in desquamation." J Biol Chem **271**(36): 21886-21890.
Fries, R. B., W. A. Wallace, S. Roy, P. Kuppusamy, V. Bergdall, G. M. Gordillo, W. S. Melvin and C. K. Sen (2005). "Dermal excisional wound healing in pigs following treatment with topically applied pure oxygen." Mutation Research **579**(1-2): 172-181.
Fuchs, E. (2007). "Scratching the surface of skin development." Nature **445**(7130): 834-842.
Gailit, J., M. P. Welch and R. A. Clark (1994). "TGF-beta 1 stimulates expression of keratinocyte integrins during re-epithelialization of cutaneous wounds." J Invest Dermatol **103**(2): 221-227.
Gao, L., L. Chao and J. Chao (2010). "A novel signaling pathway of tissue kallikrein in promoting keratinocyte migration: activation of proteinase-activated receptor 1 and epidermal growth factor receptor." Exp Cell Res **316**(3): 376-389.
Garrone, R., C. Lethias and D. Le Guellec (1997). "Distribution of minor collagens during skin development." Microscopy Research and Technique **38**(4): 407-412.
Gazel, A., R. I. Nijhawan, R. Walsh and M. Blumenberg (2008). "Transcriptional profiling defines the roles of ERK and p38 kinases in epidermal keratinocytes." J Cell Physiol **215**(2): 292-308.
Gibbs, N. F. (1998). "Anogenital papillomavirus infections in children." Curr Opin Pediatr **10**(4): 393-397.
Gibbs, S. and M. Ponec (2000). "Intrinsic regulation of differentiation markers in human epidermis, hard palate and buccal mucosa." Arch Oral Biol **45**(2): 149-158.
Gill, A. L. and C. N. Bell (2004). "Hyperbaric oxygen: its uses, mechanisms of action and outcomes." Qjm **97**(7): 385-395.
Gill, E. M., J. A. Straseski, C. A. Rasmussen, S. J. Liliensiek, K. W. Eliceiri, N. Ramanujam, J. G. White and B. L. Allen-Hoffmann (2010). "Visualization of morphological and molecular features associated with chronic ischemia in bioengineered human skin." Microsc Microanal **16**(2): 117-131.
Glickman, M. H. and A. Ciechanover (2002). "The ubiquitin-proteasome proteolytic pathway: destruction for the sake of construction." Physiol Rev **82**(2): 373-428.
Godman, C. A., R. Joshi, C. Giardina, G. Perdrizet and L. E. Hightower (2010). "Hyperbaric oxygen treatment induces antioxidant gene expression." Ann N Y Acad Sci **1197**: 178-183.

Gordillo, G. M., S. Roy, S. Khanna, R. Schlanger, S. Khandelwal, G. Phillips and C. K. Sen (2008). "Topical oxygen therapy induces vascular endothelial growth factor expression and improves closure of clinically presented chronic wounds." Clinical and Experimental Pharmacology and Physiology **35**(8): 957-964.

Gordillo, G. M. and C. K. Sen (2003). "Revisiting the essential role of oxygen in wound healing." The American Journal of Surgery **186**(3): 259-263.

Green, J. and R. Jester (2010). "Health-related quality of life and chronic venous leg ulceration: Part 2." Br J Community Nurs **15**(3): S4-6, S8, S10, passim.

Greenbaum, D., C. Colangelo, K. Williams and M. Gerstein (2003). "Comparing protein abundance and mRNA expression levels on a genomic scale." Genome Biol **4**(9): 117.

Gröger, M., S. Öter, V. Simkova, M. Bolten, A. Koch, V. Warninghoff, M. Georgieff, C.-M. Muth, G. Speit and P. Radermacher (2009). "DNA damage after long-term repetitive hyperbaric oxygen exposure." Journal of Applied Physiology **106**(1): 311-315.

Grubauer, G., K. R. Feingold, R. M. Harris and P. M. Elias (1989). "Lipid content and lipid type as determinants of the epidermal permeability barrier." Journal of Lipid Research **30**(1): 89-96.

Gruber, R., P. M. Elias, D. Crumrine, T. K. Lin, J. M. Brandner, J. P. Hachem, R. B. Presland, P. Fleckman, A. R. Janecke, A. Sandilands, W. H. McLean, P. O. Fritsch, M. Mildner, E. Tschachler and M. Schmuth (2011). "Filaggrin genotype in ichthyosis vulgaris predicts abnormalities in epidermal structure and function." The American Journal of Pathology **178**(5): 2252-2263.

Gruen, R. L., S. Chang and D. G. MacLellan (1996). "Optimizing the hospital management of leg ulcers." ANZ Journal of Surgery **66**(3): 171-174.

Gry, M., R. Rimini, S. Stromberg, A. Asplund, F. Ponten, M. Uhlen and P. Nilsson (2009). "Correlations between RNA and protein expression profiles in 23 human cell lines." BMC Genomics **10**: 365.

Haake, A. R. and G. A. Scott (1991). "Physiologic distribution and differentiation of melanocytes in Human fetal and neonatal skin equivalents." Journal of Investigative Dermatology **96**(1): 71-77.

Hammarlund, C. and T. Sundberg (1994). "Hyperbaric oxygen reduced size of chronic leg ulcers: A randomized double-blind study." Plastic and Reconstructive Surgery **93**(4): 829-834.

Hanada, K., D. Sawamura, I. Hashimoto, K. Kida and A. Naganuma (1998). "Epidermal proliferation of the skin in metallothionein-null mice." J Invest Dermatol **110**(3): 259-262.

Hansson, L., M. Stromqvist, A. Backman, P. Wallbrandt, A. Carlstein and T. Egelrud (1994). "Cloning, expression, and characterization of stratum corneum chymotryptic enzyme. A skin-specific human serine proteinase." J Biol Chem **269**(30): 19420-19426.

Harper, R. A. and G. Grove (1979). "Human skin fibroblasts derived from papillary and reticular dermis: differences in growth potential in vitro." Science **204**(4392): 526-527.

Hata, R. and H. Senoo (1989). "L-ascorbic acid 2-phosphate stimulates collagen accumulation, cell proliferation, and formation of a three-dimensional tissuelike substance by skin fibroblasts." J Cell Physiol **138**(1): 8-16.

Heng, M. C. and S. G. Kloss (1986). "Endothelial cell toxicity in leg ulcers treated with topical hyperbaric oxygen." The American Journal of Dermatopathology **8**(5): 403-410.

Heng, M. C. Y. (1993). "Topical hyperbaric therapy for problem skin wounds." The Journal of Dermatologic Surgery and Oncology **19**(8): 784-793.

Hinchliffe, R. J., G. D. Valk, J. Apelqvist, D. G. Armstrong, K. Bakker, F. L. Game, A. Hartemann-Heurtier, M. Löndahl, P. E. Price, W. H. v. Houtum and W. J. Jeffcoate (2008). "A systematic review of the effectiveness of interventions to enhance the healing of chronic ulcers of the foot in diabetes." Diabetes/Metabolism Research and Reviews **24**(Suppl 1): S119-S144.

Hink, J. and E. Jansen (2001). "Are superoxide and/or hydrogen peroxide responsible for some of the beneficial effects of hyperbaric oxygen therapy?" Med Hypotheses **57**(6): 764-769.

Hirata, T., Y. J. Cui, T. Funakoshi, Y. Mizukami, Y. Ishikawa, F. Shibasaki, M. Matsumoto and T. Sakabe (2007). "The temporal profile of genomic responses and protein synthesis in ischemic tolerance of the rat brain induced by repeated hyperbaric oxygen." Brain Res **1130**(1): 214-222.

Hislop, N. R., J. Caddy, S. B. Ting, A. Auden, S. Vasudevan, S. L. King, G. J. Lindeman, J. E. Visvader, J. M. Cunningham and S. M. Jane (2008). "Grhl3 and Lmo4 play coordinate roles in epidermal migration." Dev Biol **321**(1): 263-272.

HogenEsch, H., D. Boggess and J. P. Sundberg (1999). "Changes in keratin and filaggrin expression in the skin of chronic proliferative dermatitis (*cpdm*) mutant mice." Pathobiology **67**(1): 45-50.

Holick, M. F., J. A. MacLaughlin, M. B. Clark, S. A. Holick, J. T. Potts, R. R. Anderson, I. H. Blank, J. A. Parrish and P. Elias (1980). "Photosynthesis of previtamin D_3 in human skin and the physiologic consequences." Science **210**(4466): 203-205.

Holland, D. B., R. A. Bojar, M. D. Farrar and K. T. Holland (2009). "Differential innate immune responses of a living skin equivalent model colonized by Staphylococcus epidermidis or Staphylococcus aureus." FEMS Microbiol Lett **290**(2): 149-155.

Hollander, D. A., M. Y. Hakimi, A. Hartmann, K. Wilhelm and J. Windolf (2000). "The Influence of Hyperbaric Oxygenation (HBO) on Proliferation and Differentiation of Human Keratinocyte Cultures In Vitro." Cell and Tissue Banking **1**(4): 261-269.

Hsieh, C. P., Y. L. Chiou and C. Y. Lin (2010). "Hyperbaric oxygen-stimulated proliferation and growth of osteoblasts may be mediated through the FGF-2/MEK/ERK 1/2/NF-kappaB and PKC/JNK pathways." Connect Tissue Res **51**(6): 497-509.

Hu, T., Z. S. Khambatta, P. J. Hayden, J. Bolmarcich, R. L. Binder, M. K. Robinson, G. J. Carr, J. P. Tiesman, B. B. Jarrold, R. Osborne, T. D. Reichling, S. T. Nemeth and M. J. Aardema (2010). "Xenobiotic metabolism gene expression in the EpiDermin vitro 3D human epidermis model compared to human skin." Toxicol In Vitro **24**(5): 1450-1463.

Huang, X. Z., J. F. Wu, D. Cass, D. J. Erle, D. Corry, S. G. Young, R. V. Farese, Jr. and D. Sheppard (1996). "Inactivation of the integrin beta 6 subunit gene reveals a role of epithelial integrins in regulating inflammation in the lung and skin." The Journal of Cell Biology **133**(4): 921-928.

Hudon, V., F. Berthod, A. F. Black, O. Damour, L. Germain and F. A. Auger (2003). "A tissue-engineered endothelialized dermis to study the modulation of angiogenic and angiostatic molecules on capillary-like tube formation in vitro." Br J Dermatol **148**(6): 1094-1104.

Hueber, F., M. Besnard, H. Schaefer and J. Wepierre (1994). "Percutaneous absorption of estradiol and progesterone in normal and appendage-free skin of the hairless rat: lack of importance of nutritional blood flow." Skin Pharmacol **7**(5): 245-256.

Hueber, F., H. Schaefer and J. Wepierre (1994). "Role of transepidermal and transfollicular routes in percutaneous absorption of steroids: in vitro studies on human skin." Skin Pharmacol **7**(5): 237-244.

Igarashi, S., T. Takizawa, Y. Yasuda, H. Uchiwa, S. Hayashi, H. Brysk, J. M. Robinson, K. Yamamoto, M. M. Brysk and T. Horikoshi (2004). "Cathepsin D, but not cathepsin E, degrades desmosomes during epidermal desquamation." Br J Dermatol **151**(2): 355-361.

Iozzo, R. V. and A. D. Murdoch (1996). "Proteoglycans of the extracellular environment: clues from the gene and protein side offer novel perspectives in molecular diversity and function." Faseb J **10**(5): 598-614.

Iwata, M., T. Takebayashi, H. Ohta, R. E. Alcalde, Y. Itano and T. Matsumura (1999). "Zinc accumulation and metallothionein gene expression in the proliferating epidermis during wound healing in mouse skin." Histochem Cell Biol **112**(4): 283-290.

Jeong, S. H., J. H. Park, J. N. Kim, Y. H. Park, S. Y. Shin, Y. H. Lee, Y. C. Kye and S. W. Son (2010). "Up-regulation of TNF-alpha secretion by cigarette smoke is mediated by Egr-1 in HaCaT human keratinocytes." Experimental Dermatology **19**(8): e206-212.

Jonca, N., M. Guerrin, K. Hadjiolova, C. Caubet, H. Gallinaro, M. Simon and G. Serre (2002). "Corneodesmosin, a component of epidermal corneocyte desmosomes, displays homophilic adhesive properties." J Biol Chem **277**(7): 5024-5029.

Kairuz, E., Z. Upton, R. A. Dawson and J. Malda (2007). "Hyperbaric oxygen stimulates epidermal reconstruction in human skin equivalents." Wound Repair Regen **15**(2): 266-274.

Kalani, M., G. Jörneskog, N. Naderi, F. Lind and K. Brismar (2002). "Hyperbaric oxygen (HBO) therapy in treatment of diabetic foot ulcers: Long-term follow-up." Journal of Diabetes and Its Complications **16**(2): 153-158.

Kao, J. S., J. W. Fluhr, M. Q. Man, A. J. Fowler, J. P. Hachem, D. Crumrine, S. K. Ahn, B. E. Brown, P. M. Elias and K. R. Feingold (2003). "Short-term glucocorticoid treatment compromises both permeability barrier homeostasis and stratum corneum integrity: inhibition of epidermal lipid synthesis accounts for functional abnormalities." J Invest Dermatol **120**(3): 456-464.

Karasawa, M., N. Nishimura, H. Nishimura, C. Tohyama, H. Hashiba and T. Kuroki (1991). "Localization of metallothionein in hair follicles of normal skin and the basal cell layer of hyperplastic epidermis: possible association with cell proliferation." J Invest Dermatol **97**(1): 97-100.

Kennedy-Crispin, M., E. Billick, H. Mitsui, N. Gulati, H. Fujita, P. Gilleaudeau, M. Sullivan-Whalen, L. M. Johnson-Huang, M. Suarez-Farinas and J. G. Krueger (2012). "Human keratinocytes' response to injury upregulates CCL20 and other genes linking innate and adaptive immunity." J Invest Dermatol **132**(1): 105-113.

Kirfel, G. and V. Herzog (2004). "Migration of epidermal keratinocytes: mechanisms, regulation, and biological significance." Protoplasma **223**(2-4): 67-78.

Kojima, S., H. Yamaguchi, K. Morita and Y. Ueno (1995). "Inhibitory effect of sodium 5,6-benzylidene ascorbate (SBA) on the elevation of melanin biosynthesis induced by ultraviolet-A (UV-A) light in cultured B-16 melanoma cells." Biol Pharm Bull **18**(8): 1076-1080.

Komatsu, N., K. Saijoh, C. Kuk, A. C. Liu, S. Khan, F. Shirasaki, K. Takehara and E. P. Diamandis (2007). "Human tissue kallikrein expression in the stratum corneum and serum of atopic dermatitis patients." Experimental Dermatology **16**(6): 513-519.

Komatsu, N., K. Saijoh, C. Kuk, F. Shirasaki, K. Takehara and E. P. Diamandis (2007). "Aberrant human tissue kallikrein levels in the stratum corneum and serum of patients with psoriasis: dependence on phenotype, severity and therapy." Br J Dermatol **156**(5): 875-883.

Komatsu, N., K. Saijoh, T. Toyama, R. Ohka, N. Otsuki, G. Hussack, K. Takehara and E. P. Diamandis (2005). "Multiple tissue kallikrein mRNA and protein expression in normal skin and skin diseases." Br J Dermatol **153**(2): 274-281.

Komatsu, N., M. Takata, N. Otsuki, T. Toyama, R. Ohka, K. Takehara and K. Saijoh (2003). "Expression and localization of tissue kallikrein mRNAs in human epidermis and appendages." J Invest Dermatol **121**(3): 542-549.

Koria, P. and S. T. Andreadis (2006). "Epidermal morphogenesis: the transcriptional program of human keratinocytes during stratification." J Invest Dermatol **126**(8): 1834-1841.

Koster, M. I. and D. R. Roop (2007). "Mechanisms regulating epithelial stratification." Annu Rev Cell Dev Biol **23**: 93-113.

Kremer, M., E. Lang and A. C. Berger (2000). "Evaluation of dermal-epidermal skin equivalents ('composite-skin') of human keratinocytes in a collagen-glycosaminoglycan matrix(Integra artificial skin)." Br J Plast Surg **53**(6): 459-465.

Kulikovsky, M., T. Gil, I. Mettanes, R. Karmeli and Y. Har-Shai (2009). "Hyperbaric oxygen therapy for non-healing wounds." Isr Med Assoc J **11**(8): 480-485.

Kulonen, E. and J. Niinikoski (1968). "Effect of hyperbaric oxygenation on wound healing and experimental granuloma." Acta Physiologica Scandinavica **73**(3): 383-384.

Kurata, R., F. Fujita, K. Oonishi, K. I. Kuriyama and S. Kawamata (2010). "Inhibition of the CXCR3-mediated pathway suppresses ultraviolet B-induced pigmentation and erythema in skin." Br J Dermatol **163**(3): 593-602.

Ladwig, G. P., M. C. Robson, R. Liu, M. A. Kuhn, D. F. Muir and G. S. Schultz (2002). "Ratios of activated matrix metalloproteinase-9 to tissue inhibitor of matrix metalloproteinase-1 in wound fluids are inversely correlated with healing of pressure ulcers." Wound Repair and Regeneration **10**(1): 26-37.

Lansdown, A. B., B. Sampson and A. Rowe (1999). "Sequential changes in trace metal, metallothionein and calmodulin concentrations in healing skin wounds." Journal of Anatomy **195 (Pt 3)**: 375-386.

Laubach, V., N. Zoller, M. Rossberg, K. Gorg, S. Kippenberger, J. Bereiter-Hahn, R. Kaufmann and A. Bernd (2011). "Integration of Langerhans-like cells into a human skin equivalent." Arch Dermatol Res **303**(2): 135-139.

Leach, R. M., P. J. Rees and P. Wilmshurst (1998). "Hyperbaric oxygen therapy." Bmj **317**(7166): 1140-1143.

Lee, Y. M., Y. K. Kim, H. C. Eun and J. H. Chung (2009). "Changes in S100A8 expression in UV-irradiated and aged human skin in vivo." Arch Dermatol Res **301**(7): 523-529.
Leigh, I. M., P. E. Purkis, P. Whitehead and E. B. Lane (1993). "Monospecific monoclonal antibodies to keratin 1 carboxy terminal (synthetic peptide) and to keratin 10 as markers of epidermal differentiation." Br J Dermatol **129**(2): 110-119.
Lemaire, P., O. Revelant, R. Bravo and P. Charnay (1988). "Two mouse genes encoding potential transcription factors with identical DNA-binding domains are activated by growth factors in cultured cells." Proc Natl Acad Sci U S A **85**(13): 4691-4695.
Liu, F., X. S. Luo, H. Y. Shen, J. S. Dong and J. Yang (2011). "Using human hair follicle-derived keratinocytes and melanocytes for constructing pigmented tissue-engineered skin." Skin Res Technol.
Ma, C., L. F. Li and X. Chen (2011). "Expression of metallothionein-I and II in skin ageing and its association with skin proliferation." Br J Dermatol **164**(3): 479-482.
Määttä, A., T. DiColandrea, K. Groot and F. M. Watt (2001). "Gene targeting of envoplakin, a cytoskeletal linker protein and precursor of the epidermal cornified envelope." Mol Cell Biol **21**(20): 7047-7053.
Malda, J., T. J. Klein and Z. Upton (2007). "The roles of hypoxia in the *in vitro* engineering of tissues." Tissue Engineering **13**(9): 2153-2162.
Martin, P. (1997). "Wound healing--aiming for perfect skin regeneration." Science **276**(5309): 75-81.
Martin, P. and S. J. Leibovich (2005). "Inflammatory cells during wound repair: the good, the bad and the ugly." Trends in Cell Biology **15**(11): 599-607.
May, K. and M. Hodgson (2002). "Chronic wound healing with hyperbaric oxygen." Primary Intention **10**(4): 145-149.
Mazar, J., S. Sinha, M. E. Dinger, J. S. Mattick and R. J. Perera (2010). "Protein-coding and non-coding gene expression analysis in differentiating human keratinocytes using a three-dimensional epidermal equivalent." Mol Genet Genomics **284**(1): 1-9.
McGovern, J. A., J. R. Heinemann, L. J. Burke, R. Dawson, T. J. Parker, Z. Upton, J. D. Hooper and K. J. Manton (2012). "Stratum basale keratinocyte expression of the cell surface glycoprotein CDCP1 during epidermogenesis and its role in keratinocyte migration." Br J Dermatol.
McKeon, F. (2004). "p63 and the epithelial stem cell: more than status quo?" Genes Dev **18**(5): 465-469.
Meigel, W. N., S. Gay and L. Weber (1977). "Dermal architecture and collagen type distribution." Archives for Dermatological Research **259**(1): 1-10.
Menke, N. B., K. R. Ward, T. M. Witten, D. G. Bonchev and R. F. Diegelmann (2007). "Impaired wound healing." Clinics in Dermatology **25**(1): 19-25.
Menon, G. K., K. R. Feingold and P. M. Elias (1992). "Lamellar body secretory response to barrier disruption." J Invest Dermatol **98**(3): 279-289.
Michel, M., N. L'Heureux, R. Pouliot, W. Xu, F. A. Auger and L. Germain (1999). "Characterization of a new tissue-engineered human skin equivalent with hair." In Vitro Cell Dev Biol Anim **35**(6): 318-326.
Mills, A. A., B. Zheng, X. J. Wang, H. Vogel, D. R. Roop and A. Bradley (1999). "p63 is a p53 homologue required for limb and epidermal morphogenesis." Nature **398**(6729): 708-713.

Mirastschijski, U., R. Bugdahl, O. Rollman, B. R. Johansson and M. S. Agren (2006). "Epithelial regeneration from bioengineered skin explants in culture." Br J Dermatol **154**(1): 42-49.

Miyamura, Y., S. G. Coelho, K. Schlenz, J. Batzer, C. Smuda, W. Choi, M. Brenner, T. Passeron, G. Zhang, L. Kolbe, R. Wolber and V. J. Hearing (2011). "The deceptive nature of UVA tanning versus the modest protective effects of UVB tanning on human skin." Pigment Cell Melanoma Res **24**(1): 136-147.

Miyamura, Y., S. G. Coelho, R. Wolber, S. A. Miller, K. Wakamatsu, B. Z. Zmudzka, S. Ito, C. Smuda, T. Passeron, W. Choi, J. Batzer, Y. Yamaguchi, J. Z. Beer and V. J. Hearing (2007). "Regulation of human skin pigmentation and responses to ultraviolet radiation." Pigment Cell Res **20**(1): 2-13.

Mohamed-Hussein, Z. A. and S. Harun (2009). "Construction of a polycystic ovarian syndrome (PCOS) pathway based on the interactions of PCOS-related proteins retrieved from bibliomic data." Theor Biol Med Model **6**: 18.

Molhuizen, H. O., H. A. Alkemade, P. L. Zeeuwen, G. J. de Jongh, B. Wieringa and J. Schalkwijk (1993). "SKALP/elafin: an elastase inhibitor from cultured human keratinocytes. Purification, cDNA sequence, and evidence for transglutaminase cross-linking." J Biol Chem **268**(16): 12028-12032.

Moll, I., H. Heid, W. W. Franke and R. Moll (1987). "Distribution of a special subset of keratinocytes characterized by the expression of cytokeratin 9 in adult and fetal human epidermis of various body sites." Differentiation; research in biological diversity **33**(3): 254-265.

Mommaas, A. M., R. G. C. Teepe, I. M. Leigh, A. A. Mulder, E. J. Koebrugge and B. J. Vermeer (1992). "Ontogenesis of the basement membrane zone after grafting cultured Human epithelium: A morphologic and immunoelectron microscopic study." Journal of Investigative Dermatology **99**(1): 71-77.

Morey, J. S., J. C. Ryan and F. M. Van Dolah (2006). "Microarray validation: factors influencing correlation between oligonucleotide microarrays and real-time PCR." Biol Proced Online **8**: 175-193.

Mujaj, S., K. Manton, Z. Upton and S. Richards (2010). "Serum-free primary human fibroblast and keratinocyte coculture." Tissue Eng Part A **16**(4): 1407-1420.

Mustoe, T. A., S. T. Ahn, J. E. Tarpley and G. F. Pierce (1994). "Role of hypoxia in growth factor responses: Differential effects of basic fibroblast growth factor and platelet-derived growth factor in an ischemic wound model." Wound Repair and Regeneration **2**(4): 277-283.

Myers, S. R., I. M. Leigh and H. Navsaria (2007). "Epidermal repair results from activation of follicular and epidermal progenitor keratinocytes mediated by a growth factor cascade." Wound Repair Regen **15**(5): 693-701.

Nickoloff, B. J., R. S. Mitra, B. L. Riser, V. M. Dixit and J. Varani (1988). "Modulation of keratinocyte motility. Correlation with production of extracellular matrix molecules in response to growth promoting and antiproliferative factors." The American Journal of Pathology **132**(3): 543-551.

Nishimura, N., G. R. Cam, H. Nishimura, C. Tohyama, Y. Saitoh and D. L. Adelson (1996). "Evidence for developmentally regulated transcriptional, translational and post-translational control of metallothionein gene expression in hair follicles." Reprod Fertil Dev **8**(7): 1089-1096.

Noszczyk, B. H. and S. T. Majewski (2001). "p63 expression during normal cutaneous wound healing in humans." Plastic and Reconstructive Surgery **108**(5): 1242-1247; discussion 1248-1250.

Nukui, T., R. Ehama, M. Sakaguchi, H. Sonegawa, C. Katagiri, T. Hibino and N. H. Huh (2008). "S100A8/A9, a key mediator for positive feedback growth stimulation of normal human keratinocytes." J Cell Biochem **104**(2): 453-464.

O'Reilly, D., R. Linden, L. Fedorko, J. E. Tarride, W. G. Jones, J. M. Bowen and R. Goeree (2011). "A prospective, double-blind, randomized, controlled clinical trial comparing standard wound care with adjunctive hyperbaric oxygen therapy (HBOT) to standard wound care only for the treatment of chronic, non-healing ulcers of the lower limb in patients with diabetes mellitus: a study protocol." Trials **12**(1): 69.

O'Toole, E. A., M. P. Marinkovich, C. L. Peavey, M. R. Amieva, H. Furthmayr, T. A. Mustoe and D. T. Woodley (1997). "Hypoxia increases human keratinocyte motility on connective tissue." J Clin Invest **100**(11): 2881-2891.

Odland, G. and R. Ross (1968). "Human wound repair. I. Epidermal regeneration." The Journal of Cell Biology **39**(1): 135-151.

Olsen, L. O., H. Takiwaki and J. Serup (1995). "High-frequency ultrasound characterization of normal skin. Skin thickness and echographic density of 22 anatomical sites." Skin Research and Technology **1**(2): 74-80.

Ozoran, K., S. Ataman, O. Aydintug, N. Tulek and N. Duzgun (1994). "Remitting seronegative symmetrical synovitis with pitting edema: an adult case with excellent prognosis." Rheumatol Int **13**(5): 215-216.

Paladini, R. D., K. Takahashi, N. S. Bravo and P. A. Coulombe (1996). "Onset of re-epithelialization after skin injury correlates with a reorganization of keratin filaments in wound edge keratinocytes: defining a potential role for keratin 16." The Journal of Cell Biology **132**(3): 381-397.

Paladini, R. D., K. Takahashi, T. M. Gant and P. A. Coulombe (1995). "cDNA cloning and bacterial expression of the human type I keratin 16." Biochem Biophys Res Commun **215**(2): 517-523.

Parnigotto, P. P., S. Bernuzzo, P. Bruno, M. T. Conconi and F. Montesi (1998). "Characterization and applications of human epidermis reconstructed in vitro on de-epidermized derma." Farmaco **53**(2): 125-131.

Parsa, R., A. Yang, F. McKeon and H. Green (1999). "Association of p63 with proliferative potential in normal and neoplastic human keratinocytes." J Invest Dermatol **113**(6): 1099-1105.

Pascal, L. E., L. D. True, D. S. Campbell, E. W. Deutsch, M. Risk, I. M. Coleman, L. J. Eichner, P. S. Nelson and A. Y. Liu (2008). "Correlation of mRNA and protein levels: cell type-specific gene expression of cluster designation antigens in the prostate." BMC Genomics **9**: 246.

Patel, G. K., C. H. Wilson, K. G. Harding, A. Y. Finlay and P. E. Bowden (2006). "Numerous keratinocyte subtypes involved in wound re-epithelialization." J Invest Dermatol **126**(2): 497-502.

Pedersen, T. X., C. Leethanakul, V. Patel, D. Mitola, L. R. Lund, K. Dano, M. Johnsen, J. S. Gutkind and T. H. Bugge (2003). "Laser capture microdissection-based in vivo genomic profiling of wound keratinocytes identifies similarities and differences to squamous cell carcinoma." Oncogene **22**(25): 3964-3976.

Ponec, M. (1991). "Reconstruction of human epidermis on de-epidermized dermis: Expression of differentiation-specific protein markers and lipid composition." Toxicol In Vitro **5**(5-6): 597-606.

Ponec, M., J. Kempenaar and A. Weerheim (2002). "Lack of desquamation - the Achilles heel of the reconstructed epidermis." International Journal of Cosmetic Science **24**(5): 263-272.

Pontiggia, L., T. Biedermann, M. Meuli, D. Widmer, S. Bottcher-Haberzeth, C. Schiestl, J. Schneider, E. Braziulis, I. Montano, C. Meuli-Simmen and E. Reichmann (2009). "Markers to evaluate the quality and self-renewing potential of engineered human skin substitutes in vitro and after transplantation." J Invest Dermatol **129**(2): 480-490.

Porter, R. M., D. P. Lunny, P. H. Ogden, S. M. Morley, W. H. McLean, A. Evans, D. L. Harrison, E. L. Rugg and E. B. Lane (2000). "K15 expression implies lateral differentiation within stratified epithelial basal cells." Lab Invest **80**(11): 1701-1710.

Posnett, J. and P. J. Franks (2008). "The burden of chronic wounds in the UK." Nursing Times **104**(3): 44-45.

Potten, C. S., D. Barthel, Y. Q. Li, R. Ohlrich, B. Matthé and M. Loeffler (2000). "Proliferation in murine epidermis after minor mechanical stimulation. Part 1. Sustained increase in keratinocyte production and migration." Cell Proliferation **33**(4): 231-246.

Potts, R. O. and M. L. Francoeur (1991). "The influence of stratum corneum morphology on water permeability." Journal of Investigative Dermatology **96**(4): 495-499.

Proksch, E., J. M. Brandner and J. Jensen (2008). "The skin: an indispensable barrier." Experimental Dermatology **17**(12): 1063-1072.

Racila, D. and J. R. Bickenbach (2009). "Are epidermal stem cells unique with respect to aging?" Aging **1**(8): 746-750.

Ralston, D. R., C. Layton, A. J. Dalley, S. G. Boyce, E. Freedlander and S. M. Neil (1999). "The requirement for basement membrane antigens in the production of human epidermal/dermal composites *in vitro*." British Journal of Dermatology **140**(4): 605-615.

Rawlings, A. V. and C. R. Harding (2004). "Moisturization and skin barrier function." Dermatol Ther **17 Suppl 1**: 43-48.

Rayment, E. A., Z. Upton and G. K. Shooter (2008). "Increased matrix metalloproteinase-9 (MMP-9) activity observed in chronic wound fluid is related to the clinical severity of the ulcer." British Journal of Dermatology **158**(5): 951-961.

Remensnyder, J. P. and G. Majno (1968). "Oxygen gradients in healing wounds." The American Journal of Pathology **52**(2): 301-323.

Riggs, P. K., O. Rho and J. DiGiovanni (2000). "Alteration of Egr-1 mRNA during multistage carcinogenesis in mouse skin." Mol Carcinog **27**(4): 247-251.

Rink, C., S. Roy, M. Khan, P. Ananth, P. Kuppusamy, C. K. Sen and S. Khanna (2010). "Oxygen-sensitive outcomes and gene expression in acute ischemic stroke." J Cereb Blood Flow Metab **30**(7): 1275-1287.

Rittié, L., B. Perbal, J. J. Castellot, Jr., J. S. Orringer, J. J. Voorhees and G. J. Fisher (2011). "Spatial-temporal modulation of CCN proteins during wound healing in human skin in vivo." J Cell Commun Signal **5**(1): 69-80.

Rodriguez, P. G., F. N. Felix, D. T. Woodley and E. K. Shim (2008). "The role of oxygen in wound healing: a review of the literature." Dermatol Surg **34**(9): 1159-1169.

Rugg, E. L., J. E. Common, A. Wilgoss, H. P. Stevens, J. Buchan, I. M. Leigh and D. P. Kelsell (2002). "Diagnosis and confirmation of epidermolytic palmoplantar

keratoderma by the identification of mutations in keratin 9 using denaturing high-performance liquid chromatography." Br J Dermatol **146**(6): 952-957.
Ruhrberg, C., M. A. Hajibagheri, M. Simon, T. P. Dooley and F. M. Watt (1996). "Envoplakin, a novel precursor of the cornified envelope that has homology to desmoplakin." The Journal of Cell Biology **134**(3): 715-729.
Satoh, Y., D. Saitoh, A. Takeuchi, K. Ojima, K. Kouzu, S. Kawakami, M. Ito, M. Ishihara, S. Sato and K. Takishima (2009). "ERK2 dependent signaling contributes to wound healing after a partial-thickness burn." Biochem Biophys Res Commun **381**(1): 118-122.
Savagner, P., D. F. Kusewitt, E. A. Carver, F. Magnino, C. Choi, T. Gridley and L. G. Hudson (2005). "Developmental transcription factor slug is required for effective re-epithelialization by adult keratinocytes." J Cell Physiol **202**(3): 858-866.
Schäfer, M., H. Farwanah, A. H. Willrodt, A. J. Huebner, K. Sandhoff, D. Roop, D. Hohl, W. Bloch and S. Werner (2012). "Nrf2 links epidermal barrier function with antioxidant defense." EMBO Mol Med **4**(5): 364-379.
Scherl-Mostageer, M., W. Sommergruber, R. Abseher, R. Hauptmann, P. Ambros and N. Schweifer (2001). "Identification of a novel gene, CDCP1, overexpressed in human colorectal cancer." Oncogene **20**(32): 4402-4408.
Schiller, M., D. Metze, T. A. Luger, S. Grabbe and M. Gunzer (2006). "Immune response modifiers - mode of action." Experimental Dermatology **15**(5): 331-341.
Schwanhäusser, B., D. Busse, N. Li, G. Dittmar, J. Schuchhardt, J. Wolf, W. Chen and M. Selbach (2011). "Global quantification of mammalian gene expression control." Nature **473**(7347): 337-342.
Schweizer, J., P. E. Bowden, P. A. Coulombe, L. Langbein, E. B. Lane, T. M. Magin, L. Maltais, M. B. Omary, D. A. D. Parry, M. A. Rogers and M. W. Wright (2006). "New consensus nomenclature for mammalian keratins." The Journal of Cell Biology **174**(2): 169-174.
Sen, C. K. (2000). "Cellular thiols and redox-regulated signal transduction." Curr Top Cell Regul **36**: 1-30.
Sen, C. K. (2003). "The general case for redox control of wound repair." Wound Repair and Regeneration **11**(6): 431-438.
Sen, C. K. (2009). "Wound healing essentials: Let there be oxygen." Wound Repair and Regeneration **17**(1): 1-18.
Senoo, M., F. Pinto, C. P. Crum and F. McKeon (2007). "p63 Is essential for the proliferative potential of stem cells in stratified epithelia." Cell **129**(3): 523-536.
Simon, M., N. Jonca, M. Guerrin, M. Haftek, D. Bernard, C. Caubet, T. Egelrud, R. Schmidt and G. Serre (2001). "Refined characterization of corneodesmosin proteolysis during terminal differentiation of human epidermis and its relationship to desquamation." J Biol Chem **276**(23): 20292-20299.
Smola, H., G. Thiekötter and N. E. Fusenig (1993). "Mutual induction of growth factor gene expression by epidermal-dermal cell interaction." The Journal of Cell Biology **122**(2): 417-429.
Smoot, M. E., K. Ono, J. Ruscheinski, P. L. Wang and T. Ideker (2011). "Cytoscape 2.8: new features for data integration and network visualization." Bioinformatics **27**(3): 431-432.

Spassov, D. S., D. Ahuja, C. H. Wong and M. M. Moasser (2011). "The structural features of Trask that mediate its anti-adhesive functions." PLoS ONE **6**(4): e19154.

Spassov, D. S., F. L. Baehner, C. H. Wong, S. McDonough and M. M. Moasser (2009). "The transmembrane src substrate Trask is an epithelial protein that signals during anchorage deprivation." The American Journal of Pathology **174**(5): 1756-1765.

Spassov, D. S., C. H. Wong, G. Harris, S. McDonough, P. Phojanakong, D. Wang, B. Hann, A. V. Bazarov, P. Yaswen, E. Khanafshar and M. M. Moasser (2012). "A tumor-suppressing function in the epithelial adhesion protein Trask." Oncogene **31**(4): 419-431.

Spassov, D. S., C. H. Wong and M. M. Moasser (2011). "Trask phosphorylation defines the reverse mode of a phosphotyrosine signaling switch that underlies cell anchorage state." Cell Cycle **10**(8): 1225-1232.

Spassov, D. S., C. H. Wong, N. Sergina, D. Ahuja, M. Fried, D. Sheppard and M. M. Moasser (2011). "Phosphorylation of Trask by Src kinases inhibits integrin clustering and functions in exclusion with focal adhesion signaling." Mol Cell Biol **31**(4): 766-782.

Speit, G., C. Dennog, P. Radermacher and A. Rothfuss (2002). "Genotoxicity of hyperbaric oxygen." Mutation Research **512**(2-3): 111-119.

Steven, A. C. and P. M. Steinert (1994). "Protein composition of cornified cell envelopes of epidermal keratinocytes." Journal of Cell Science **107**(Part 2): 693-700.

Sugita, K., K. Kabashima, K. Atarashi, T. Shimauchi, M. Kobayashi and Y. Tokura (2007). "Innate immunity mediated by epidermal keratinocytes promotoes acquired immunity involving Langerhans cells and T cells in the skin." Clinical and Experimental Immunology **147**(1): 176-183.

Sugiura, H., H. Ebise, T. Tazawa, K. Tanaka, Y. Sugiura, M. Uehara, K. Kikuchi and T. Kimura (2005). "Large-scale DNA microarray analysis of atopic skin lesions shows overexpression of an epidermal differentiation gene cluster in the alternative pathway and lack of protective gene expression in the cornified envelope." Br J Dermatol **152**(1): 146-149.

Sukhatme, V. P. (1990). "Early transcriptional events in cell growth: the Egr family." J Am Soc Nephrol **1**(6): 859-866.

Sullivan, T. P., W. H. Eaglstein, S. C. Davis and P. Mertz (2001). "The pig as a model for human wound healing." Wound Repair and Regeneration **9**(2): 66-76.

Takahashi, P. Y., L. J. Kiemelle and J. P. Jones (2004). "Wound care for elderly patients: Advances and clinical applications for practicing physicians." Mayo Clinic Proceedings **79**(2): 260-267.

Tandara, A. A. and T. A. Mustoe (2004). "Oxygen in wound healing--more than a nutrient." World J Surg **28**(3): 294-300.

Thackham, J. A., D. L. S. McElwain and R. J. Long (2008). "The use of hyperbaric oxygen therapy to treat chronic wounds: A review." Wound Repair and Regeneration **16**(3): 321-330.

Thom, S. R. (2009). "Oxidative stress is fundamental to hyperbaric oxygen therapy." Journal of Applied Physiology **106**(3): 988-995.

Thornalley, P. J. and M. Vasák (1985). "Possible role for metallothionein in protection against radiation-induced oxidative stress. Kinetics and mechanism

of its reaction with superoxide and hydroxyl radicals." Biochimica et Biophysica Acta **827**(1): 36-44.
Ting, S. B., J. Caddy, N. Hislop, T. Wilanowski, A. Auden, L. L. Zhao, S. Ellis, P. Kaur, Y. Uchida, W. M. Holleran, P. M. Elias, J. M. Cunningham and S. M. Jane (2005). "A homolog of Drosophila grainy head is essential for epidermal integrity in mice." Science **308**(5720): 411-413.
Ting, S. B., J. Caddy, T. Wilanowski, A. Auden, J. M. Cunningham, P. M. Elias, W. M. Holleran and S. M. Jane (2005). "The epidermis of grhl3-null mice displays altered lipid processing and cellular hyperproliferation." Organogenesis **2**(2): 33-35.
Topol, B. M., H. B. Haimes, L. Dubertret and E. Bell (1986). "Transfer of melanosomes in a skin equivalent model in vitro." J Invest Dermatol **87**(5): 642-647.
Topping, G., J. Malda, R. Dawson and Z. Upton (2006). "Development and characterisation of human skin equivalents and their potential application as a burn wound model." Primary Intention **14**(1): 14-21.
Trengove, N. J., M. C. Stacey, S. MacAuley, N. Bennett, J. Gibson, F. Burslem, G. Murphy and G. Schultz (1999). "Analysis of the acute and chronic wound environments: the role of proteases and their inhibitors." Wound Repair Regen **7**(6): 442-452.
Truong, A. B. and P. A. Khavari (2007). "Control of keratinocyte proliferation and differentiation by p63." Cell Cycle **6**(3): 295-299.
Tsatmali, M., J. Ancans and A. J. Thody (2002). "Melanocyte function and its control by melanocortin peptides." J Histochem Cytochem **50**(2): 125-133.
Türkaslan, T., N. Yogun, M. Cimsit, S. Solakoglu, C. Ozdemir and Z. Ozsoy (2010). "Is HBOT treatment effective in recovering zone of stasis? An experimental immunohistochemical study." Burns **36**(4): 539-544.
Umehara, K. I., Y. Susaki, R. H. Van Teylingen, J. N. Neat, F. Ndikum-Moffor, K. Noguchi, T. Usui, A. Parkinson and H. Kamimura (2008). "Evaluation of the inhibitory and induction potential of YM758, a novel If channel inhibitor, for human P450-mediated metabolism." Eur J Drug Metab Pharmacokinet **33**(4): 211-223.
Upton, Z., L. Cuttle, A. Noble, M. Kempf, G. Topping, J. Malda, Y. Xie, J. Mill, D. G. Harkin, O. Kravchuk, D. I. Leavesley and R. M. Kimble (2008). "Vitronectin: growth factor complexes hold potential as a wound therapy approach." J Invest Dermatol **128**(6): 1535-1544.
Usui, C., K. Hatta, H. Arai and Y. Kikuchi (2009). "Brain-skin connection: is atopic dermatitis associated with demonstrable basal ganglia dysfunction?" Prog Neuropsychopharmacol Biol Psychiatry **33**(1): 164-165.
Usui, M. L., J. N. Mansbridge, W. G. Carter, M. Fujita and J. E. Olerud (2008). "Keratinocyte migration, proliferation, and differentiation in chronic ulcers from patients with diabetes and normal wounds." J Histochem Cytochem **56**(7): 687-696.
Usui, M. L., R. A. Underwood, J. N. Mansbridge, L. A. Muffley, W. G. Carter and J. E. Olerud (2005). "Morphological evidence for the role of suprabasal keratinocytes in wound reepithelialization." Wound Repair Regen **13**(5): 468-479.
Vardaxis, N. J., T. A. Brans, M. E. Boon, R. W. Kreis and L. M. Marres (1997). "Confocal laser scanning microscopy of porcine skin: implications for human wound healing studies." Journal of Anatomy **190**(4): 601-611.

Vermeij, W. P., A. Alia and C. Backendorf (2011). "ROS quenching potential of epidermal cornified cell envelope." Journal of Investigative Dermatology **131**(7): 1435-1441.
Vermeij, W. P. and C. Backendorf (2010). "Skin cornification proteins provide global link between ROS detoxification and cell migration during wound healing." PLoS ONE **5**(8): 1-7.
Villanueva, E. (2003). Hyperbaric oxygen therapy for the treatment of non-healing, refractory wounds in non-diabetic patients and refractory soft tissue radiation injuries: assessment report. Medical Services Advisory Committee, Department of Health and Ageing. Canberra.
Wang, S., H. Uchi, S. Hayashida, K. Urabe, Y. Moroi and M. Furue (2009). "Differential expression of phosphorylated extracellular signal-regulated kinase 1/2, phosphorylated p38 mitogen-activated protein kinase and nuclear factor-kappaB p105/p50 in chronic inflammatory skin diseases." J Dermatol **36**(10): 534-540.
Watt, F. M. and H. Green (1982). "Stratification and terminal differentiation of cultured epidermal cells." Nature **295**(5848): 434-436.
Watt, F. M., M. D. Kubler, N. A. Hotchin, L. J. Nicholson and J. C. Adams (1993). "Regulation of keratinocyte terminal differentiation by integrin-extracellular matrix interactions." Journal of Cell Science **106 (Pt 1)**: 175-182.
Werner, S., T. Krieg and H. Smola (2007). "Keratinocyte-fibroblast interactions in wound healing." Journal of Investigative Dermatology **127**(5): 998-1008.
Wilgus, T. A. (2008). "Immune cells in the healing skin wound: Influential players at each stage of repair." Pharmacological Research **58**(2): 112-116.
Wingens, M., B. H. van Bergen, P. S. Hiemstra, J. F. Meis, I. M. van Vlijmen-Willems, P. L. Zeeuwen, J. Mulder, H. A. Kramps, F. van Ruissen and J. Schalkwijk (1998). "Induction of SLPI (ALP/HUSI-I) in epidermal keratinocytes." J Invest Dermatol **111**(6): 996-1002.
Winkelmann, R. K. and A. S. Breathnach (1973). "The Merkel cell." J Invest Dermatol **60**(1): 2-15.
Wong, A. K., B. H. Schonmeyr, M. A. Soares, S. Li and B. J. Mehrara (2008). "Hyperbaric oxygen inhibits growth but not differentiation of normal and irradiated osteoblasts." J Craniofac Surg **19**(3): 757-765.
Wood, Z. (2002). "Hyperbaric oxygen in the management of chronic wounds." British Journal of Nursing **11 (Supplement)**(16): S16-S24.
Woods, G. M., R. C. Malley and H. K. Muller (2005). "The skin immune system and the challenge of tumour immunosurveillance." Eur J Dermatol **15**(2): 63-69.
Wruck, C. J., A. Fragoulis, A. Gurzynski, L. O. Brandenburg, Y. W. Kan, K. Chan, J. Hassenpflug, S. Freitag-Wolf, D. Varoga, S. Lippross and T. Pufe (2011). "Role of oxidative stress in rheumatoid arthritis: insights from the Nrf2-knockout mice." Ann Rheum Dis **70**(5): 844-850.
Wysocki, A. B. (1996). "Wound fluids and the pathogenesis of chronic wounds." J Wound Ostomy Continence Nurs **23**(6): 283-290.
Wysocki, A. B., A. O. Kusakabe, S. Chang and T. L. Tuan (1999). "Temporal expression of urokinase plasminogen activator, plasminogen activator inhibitor and gelatinase-B in chronic wound fluid switches from a chronic to acute wound profile with progression to healing." Wound Repair and Regeneration **7**(3): 154-165.
Xie, Y., S. C. Rizzi, R. Dawson, E. Lunam, S. Richards, D. I. Leavesley and Z. Upton (2010). "Development of a three-dimensional human skin equivalent

model for investigating novel wound healing therapies." Tissue Engineering: Part C **16**(5): 1111-1123.
Xie, Y., Z. Upton, S. Richards, S. C. Rizzi and D. I. Leavesley (2011). "Hyaluronic acid: Evaluation as a potnetial delivery vehicle for vitronectin:growth factor complexes in wound healing applications." Journal of Controlled Release **153**(3): 225-232.
Xu, J. and R. A. Clark (1996). "Extracellular matrix alters PDGF regulation of fibroblast integrins." The Journal of Cell Biology **132**(1-2): 239-249.
Yager, D. R. and B. C. Nwomeh (1999). "The proteolytic environment of chronic wounds." Wound Repair and Regeneration **7**(6): 433-441.
Yamada, Y., D. Yamauchi, H. Usui, H. Zhao, M. Yokoo, K. Ohinata, M. Iwai, M. Horiuchi and M. Yoshikawa (2008). "Hypotensive activity of novokinin, a potent analogue of ovokinin(2-7), is mediated by angiotensin AT(2) receptor and prostaglandin IP receptor." Peptides **29**(3): 412-418.
Yamaguchi, Y., S. Itami, M. Tarutani, K. Hosokawa, H. Miura and K. Yoshikawa (1999). "Regulation of keratin 9 in nonpalmoplantar keratinocytes by palmoplantar fibroblasts through epithelial-mesenchymal interactions." Journal of Investigative Dermatology **112**(4): 483-488.
Yamasaki, M., T. Nomura, F. Sato and H. Mimata (2007). "Metallothionein is up-regulated under hypoxia and promotes the survival of human prostate cancer cells." Oncol Rep **18**(5): 1145-1153.
Yan, S. F., J. Lu, Y. S. Zou, J. Soh-Won, D. M. Cohen, P. M. Buttrick, D. R. Cooper, S. F. Steinberg, N. Mackman, D. J. Pinsky and D. M. Stern (1999). "Hypoxia-associated induction of early growth response-1 gene expression." J Biol Chem **274**(21): 15030-15040.
Yang, A., R. Schweitzer, D. Sun, M. Kaghad, N. Walker, R. T. Bronson, C. Tabin, A. Sharpe, D. Caput, C. Crum and F. McKeon (1999). "p63 is essential for regenerative proliferation in limb, craniofacial and epithelial development." Nature **398**(6729): 714-718.
Yoneda, K. and P. M. Steinert (1993). "Overexpression of human loricrin in transgenic mice produces a normal phenotype." Proc Natl Acad Sci U S A **90**(22): 10754-10758.
Yu, X. J., C. Y. Li, H. Y. Dai, D. X. Cai, K. Y. Wang, Y. H. Xu, L. M. Chen and C. L. Zhou (2007). "Expression and localization of the activated mitogen-activated protein kinase in lesional psoriatic skin." Exp Mol Pathol **83**(3): 413-418.
Yu, Z., A. Bhandari, J. Mannik, T. Pham, X. Xu and B. Andersen (2008). "Grainyhead-like factor Get1/Grhl3 regulates formation of the epidermal leading edge during eyelid closure." Dev Biol **319**(1): 56-67.
Zhang, Q., Q. Chang, R. A. Cox, X. Gong and L. J. Gould (2008). "Hyperbaric oxygen attenuates apoptosis and decreases inflammation in an ischemic wound model." Journal of Investigative Dermatology **128**(8): 2102-2112.
Zhao, L. L., J. D. Davidson, S. C. Wee, S. I. Roth and T. A. Mustoe (1994). "Effect of hyperbaric oxygen and growth factors on rabbit ear ischemic ulcers." Arch Surg **129**(10): 1043-1049.
Zöller, N. N., S. Kippenberger, D. Thaçi, K. Mewes, M. Spiegel, A. Sättler, M. Schultz, J. Bereiter-Hahn, R. Kaufmann and A. Bernd (2008). "Evaluation of beneficial and adverse effects of glucocorticoids on a newly developed full-thickness skin model." Toxicol In Vitro **22**(3): 747-759.

Appendices

Table A1. Summary of epidermal outgrowth over the DED: Group A

Group A	Sample 1 (mm^2)	Sample 2 (mm^2)	Sample 3 (mm^2)	Average (mm^2)
Day 0	19.81 ± 0.16	16.15 ± 2.57	12.69 ± 0.49	16.22 ± 3.39
Day 3	36.17 ± 3.10	25.46 ± 0.07	24.87 ± 0.10	28.83 ± 5.86
Day 5	55.22 ± 0.90	34.62 ± 2.05	33.25 ± 2.40	41.03 ± 11.10
Day 9	96.75 ± 1.30	60.63 ± 1.52	71.26 ± 2.54	76.21 ± 16.66

Table A2. Summary of epidermal outgrowth over the DED: Group B

Group B	Sample 4 (mm^2)	Sample 5 (mm^2)	Sample 6 (mm^2)	Sample 7 (mm^2)	Sample 8 (mm^2)
Day 0	15.46 ± 0.41	18.72 ± 0.21	21.36 ± 0.00	21.00 ± 0.98	19.45 ± 0.03
Day 3	36.53 ± 2.71	32.49 ± 5.20	30.90 ± 0.00	43.69 ± 9.04	36.38 ± 2.65
Day 5	42.54 ± 0.48	44.66 ± 3.37	39.31 ± 0.00	68.09 ± 11.89	48.79 ± 6.69
Day 9	74.26 ± 12.21	77.54 ± 12.16	72.84 ± 0.00	72.33 ± 1.02	104.30 ± 1.06

Table A3. Summary of stratum corneum thickness in the HSE epidermis: Group A

SC	Sample 1 (µm)	Sample 2 (µm)	Sample 3 (µm)	Average (µm)
Native skin	n/a	n/a	n/a	24.52 ± 6.73
Day 0	1.90 ± 2.21	1.04 ± 1.08	1.86 ± 2.95	1.60 ± 2.21
Day 3	5.32 ± 3.66	5.92 ± 2.17	2.24 ± 1.17	4.49 ± 2.98
Day 5	10.00 ± 4.53	12.77 ± 2.10	14.74 ± 4.55	12.50 ± 4.29
Day 9	49.30 ± 15.34	48.50 ± 16.72	26.86 ± 3.66	41.55 ± 16.70

Table A4. Summary of cellular layer thickness in the HSE epidermis: Group A

Cell	Sample 1 (µm)	Sample 2 (µm)	Sample 3 (µm)	Average (µm)
Native skin	n/a	n/a	n/a	79.99 ± 28.21
Day 0	7.41 ± 3.11	4.95 ± 3.20	12.49 ± 8.07	8.28 ± 6.10
Day 3	94.18 ± 15.75	92.39 ± 14.57	53.00 ± 11.99	79.86 ± 23.70
Day 5	83.58 ± 10.29	117.34 ± 25.94	112.48 ± 32.05	104.46 ± 28.34
Day 9	71.26 ± 12.56	49.09 ± 15.33	71.44 ± 28.60	63.93 ± 22.33

Table A5. Summary of stratum corneum thickness in the HSE epidermis: Group B

SC	Sample 4 (µm)	Sample 5 (µm)	Sample 6 (µm)	Sample 7 (µm)	Sample 8 (µm)
Native skin	17.03 ± 4.18	24.36 ± 5.50	30.27 ± 5.43	20.69 ± 3.14	20.33 ± 5.38
Day 0	1.77 ± 2.43	2.58 ± 1.45	1.81 ± 1.38	2.75 ± 3.41	1.79 ± 2.31
Day 3	7.53 ± 2.44	4.67 ± 1.53	1.70 ± 1.39	3.42 ± 1.59	3.90 ± 1.54
Day 5	12.51 ± 3.43	18.21 ± 6.24	10.99 ± 2.14	11.60 ± 3.58	11.17 ± 3.16
Day 9	38.21 ± 11.93	45.84 ± 9.15	54.88 ± 9.93	65.70 ± 21.89	30.26 ± 12.32

Table A6. Summary of cellular layer thickness in the HSE epidermis: Group B

Cell	Sample 4 (µm)	Sample 5 (µm)	Sample 6 (µm)	Sample 7 (µm)	Sample 8 (µm)
Native skin	79.30 ± 10.14	46.48 ± 16.31	45.09 ± 7.86	43.89 ± 5.96	59.43 ± 4.92
Day 0	6.98 ± 3.33	12.52 ± 5.40	7.12 ± 4.62	11.13 ± 5.73	9.55 ± 4.38
Day 3	49.66 ± 14.83	71.00 ± 29.62	61.46 ± 13.44	62.38 ± 27.21	51.32 ± 15.33
Day 5	105.15 ± 31.81	90.48 ± 18.28	97.65 ± 13.78	51.66 ± 11.48	67.54 ± 15.74
Day 9	83.41 ± 31.92	46.74 ± 16.86	42.97 ± 6.00	28.08 ± 8.00	45.29 ± 18.04

Table A7. Summary of the number of p63-positive nuclei in the HSE epidermis: Group A

p63	Sample 1 (# nuclei)	Sample 2 (# nuclei)	Sample 3 (# nuclei)	Average (# nuclei)
Native skin	n/a	n/a	n/a	192.95 ± 52.25
Day 0	11.75 ± 5.47	6.38 ± 2.77	8.00 ± 2.62	8.71 ± 4.34
Day 3	127.00 ± 15.03	128.13 ± 30.90	34.75 ± 11.25	86.88 ± 44.45
Day 5	127.00 ± 26.77	116.5 ± 24.43	97.88 ± 25.31	113.88 ± 27.32
Day 9	81.00 ± 14.24	83.63 ± 33.91	94.63 ± 22.44	86.42 ± 24.52

Table A8. Summary of the number of p63 positive nuclei in the HSE epidermis: Group B

p63	Sample 4 (# nuclei)	Sample 5 (# nuclei)	Sample 6 (# nuclei)	Sample 7 (# nuclei)	Sample 8 (# nuclei)
Native skin	154.75 ± 22.91	169.25 ± 36.21	169.50 ± 40.30	104.50 ± 26.61	127.88 ± 27.65
Day 0	9.75 ± 7.37	14.94 ± 6.24	4.13 ± 1.36	12.63 ± 9.51	12.25 ± 3.32
Day 3	79.00 ± 20.04	47.31 ± 13.28	69.13 ± 15.26	64.31 ± 23.98	68.75 ± 17.38
Day 5	105.88 ± 26.43	46.25 ± 9.46	63.00 ± 8.42	54.31 ± 12.66	59.31 ± 17.45
Day 9	93.31 ± 18.42	30.88 ± 8.21	43.25 ± 9.59	28.94 ± 7.42	46.13 ± 18.20

Table A9. Summary of the number of ki-67 positive nuclei in the HSE epidermis: Group A

ki-67	Sample 1 (# nuclei)	Sample 2 (# nuclei)	Sample 3 (# nuclei)	Average (# nuclei)
Native skin	n/a	n/a	n/a	31.25 ± 17.33
Day 0	6.38 ± 2.83	7.63 ± 5.40	15.50 ± 6.41	9.83 ± 3.69
Day 3	51.00 ± 9.58	94.63 ± 12.41	50.88 ± 10.55	65.50 ± 13.56
Day 5	53.25 ± 12.59	46.25 ± 18.93	43.13 ± 14.25	47.54 ± 8.90
Day 9	36.57 ± 7.67	6.25 ± 1.83	25.00 ± 2.67	22.67 ± 7.87

Table A10. Summary of the number of ki-67 positive nuclei in the HSE epidermis: Group B

ki-67	Sample 4 (# nuclei)	Sample 5 (# nuclei)	Sample 6 (# nuclei)	Sample 7 (# nuclei)	Sample 8 (# nuclei)
Native skin	23.63 ± 6.61	22.00 ± 6.48	23.63 ± 6.61	17.00 ± 3.07	18.75 ± 6.23
Day 0	15.50 ± 10.12	17.44 ± 7.28	9.13 ± 2.42	25.31 ± 6.96	14.00 ± 4.98
Day 3	78.81 ± 11.44	46.56 ± 10.46	66.00 ± 13.43	61.25 ± 23.29	68.75 ± 23.17
Day 5	42.19 ± 8.60	23.25 ± 7.61	20.25 ± 15.69	24.06 ± 11.85	42.94 ± 13.73
Day 9	20.75 ± 6.03	13.50 ± 2.93	21.88 ± 4.02	8.69 ± 4.47	20.88 ± 8.10

Table A11. Summary of the thickness of K1-positive epidermis in the HSE epidermis: Group A

Keratin 1	Sample 1 (µm)	Sample 2 (µm)	Sample 3 (µm)	Average (µm)
Native skin	n/a	n/a	n/a	57.71 ± 16.91
Day 0	4.48 ± 1.72	0.24 ± 0.67	2.99 ± 3.32	2.57 ± 2.76
Day 3	9.00 ± 3.01	39.06 ± 19.02	8.83 ± 4.45	18.96 ± 18.15
Day 5	53.09 ± 8.65	82.18 ± 19.21	62.06 ± 16.55	65.78 ± 19.31
Day 9	45.87 ± 8.12	38.11 ± 13.93	43.19 ± 10.15	42.39 ± 11.01

Table A12. Summary of the thickness of K1-positive epidermis in the HSE epidermis: Group B

Keratin 1	Sample 4 (µm)	Sample 5 (µm)	Sample 6 (µm)	Sample 7 (µm)	Sample 8 (µm)
Native skin	53.10 ± 11.97	45.48 ± 19.77	5.46 ± 7.72	38.97 ± 4.08	45.08 ± 10.16
Day 0	5.76 ± 4.99	6.05 ± 4.20	2.73 ± 1.10	1.74 ± 2.04	3.21 ± 2.18
Day 3	17.90 ± 8.16	15.00 ± 4.30	17.42 ± 4.26	11.90 ± 7.20	17.16 ± 12.43
Day 5	76.04 ± 17.74	36.65 ± 10.66	37.97 ± 5.15	36.79 ± 12.31	40.11 ± 10.21
Day 9	61.17 ± 24.82	23.30 ± 4.56	20.40 ± 4.59	19.45 ± 7.13	32.08 ± 12.03

Table A13. Summary of the thickness of loricrin-positive epidermis in the HSE epidermis: Group A

Loricrin	Sample 1 (µm)	Sample 2 (µm)	Sample 3 (µm)	Average (µm)
Native skin	n/a	n/a	n/a	7.53 ± 2.71
Day 0	0.00 ± 0.00	0.00 ± 0.00	0.06 ± 0.16	0.02 ± 0.09
Day 3	3.36 ± 4.04	5.18 ± 3.20	8.87 ± 6.78	5.81 ± 5.25
Day 5	32.15 ± 5.62	31.34 ± 12.10	35.40 ± 11.39	32.96 ± 9.84
Day 9	22.62 ± 6.07	19.98 ± 6.16	23.68 ± 4.94	22.09 ± 5.72

Table A14. Summary of the thickness of loricrin-positive epidermis in the HSE epidermis: Group B

Loricrin	Sample 4 (µm)	Sample 5 (µm)	Sample 6 (µm)	Sample 7 (µm)	Sample 8 (µm)
Native skin	8.54 ± 2.82	5.58 ± 1.23	9.51 ± 2.01	5.53 ± 1.93	5.18 ± 1.23
Day 0	0.39 ± 1.39	1.34 ± 3.30	0.00 ± 0.00	0.15 ± 0.33	0.38 ± 1.08
Day 3	4.83 ± 4.57	10.73 ± 4.33	5.70 ± 3.19	12.15 ± 3.10	17.25 ± 5.30
Day 5	39.14 ± 10.29	30.10 ± 6.69	28.76 ± 6.06	21.88 ± 5.13	26.21 ± 7.82
Day 9	28.31 ± 8.13	22.56 ± 3.17	14.25 ± 1.96	19.73 ± 7.60	21.83 ± 5.79

Table A15. Summary of the thickness of K16-positive epidermis in the HSE epidermis: Group A

Keratin 16	Sample 1 (µm)	Sample 2 (µm)	Sample 3 (µm)	Average (µm)
Native skin	n/a	n/a	n/a	40.95 ± 15.02
Day 0	6.66 ± 3.50	4.20 ± 1.54	5.00 ± 1.00	6.23 ± 3.88
Day 3	46.32 ± 16.91	55.75 ± 19.12	7.84 ± 5.19	46.07 ± 16.96
Day 5	80.66 ± 21.85	94.59 ± 15.84	29.97 ± 6.17	84.25 ± 17.78
Day 9	69.37 ± 17.49	42.40 ± 13.08	77.50 ± 13.02	51.35 ± 18.78

Table A16. Summary of the thickness of K16-positive epidermis in the HSE epidermis: Group B

Keratin 16	Sample 4 (µm)	Sample 5 (µm)	Sample 6 (µm)	Sample 7 (µm)	Sample 8 (µm)
Native skin	24.20 ± 4.21	26.68 ± 8.56	31.88 ± 7.22	26.82 ± 4.80	32.85 ± 7.90
Day 0	5.37 ± 4.28	12.09 ± 10.18	7.49 ± 6.57	8.45 ± 3.24	6.05 ± 3.55
Day 3	44.95 ± 15.07	44.56 ± 14.76	35.91 ± 5.27	49.55 ± 10.93	55.65 ± 18.42
Day 5	97.69 ± 21.02	47.77 ± 11.20	64.39 ± 7.10	44.49 ± 10.78	59.88 ± 14.45
Day 9	81.41 ± 36.61	39.03 ± 8.02	43.07 ± 3.64	42.07 ± 16.18	46.11 ± 16.08

Table A17. Ontology of differentially expressed genes at day 3

Molecular and Cellular Functions	Significance P-value	Focus Genes
Cell Cycle	3.41E-04 – 4.48E-02	15
Cellular Assembly and Organization	3.41E-04 – 4.88E-02	12
DNA Replication, Recombination, and Repair	3.41E-04 – 4.08E-02	7
Lipid Metabolism	5.65E-04 – 4.48E-02	11
Small Molecule Biochemistry	5.65E-04 – 4.48E-02	18

Table A18. Ontology of differentially expressed genes at day 5

Molecular and Cellular Functions	Significance P-value	Focus Genes
Cellular Movement	1.02E-04 – 4.05E-02	21
Lipid Metabolism	4.66E-04 – 4.38E-02	17
Molecular Transport	4.66E-04 – 4.14E-02	20
Small Molecule Biochemistry	4.66E-04 – 4.38E-02	29
Cellular Growth and Proliferation	4.91E-04 – 3.88E-02	39

Table A19. Ontology of differentially expressed genes at day 9

Molecular and Cellular Functions	Significance P-value	Focus Genes
Lipid Metabolism	7.48E-08 – 2.31E-02	17
Small Molecule Biochemistry	7.48E-08 – 2.31E-02	26
Vitamin and Mineral Metabolism	7.48E-08 – 2.318E-02	8
Drug Metabolism	6.63E-06 – 2.318E-02	11
Cellular Growth and Proliferation	2.91E-05 – 2.31E-02	34

Data presented in these tables contains a range of p-values as each molecular and cellular functions category contains multiple sub-groups and each sub-group has a p-value assigned to it.

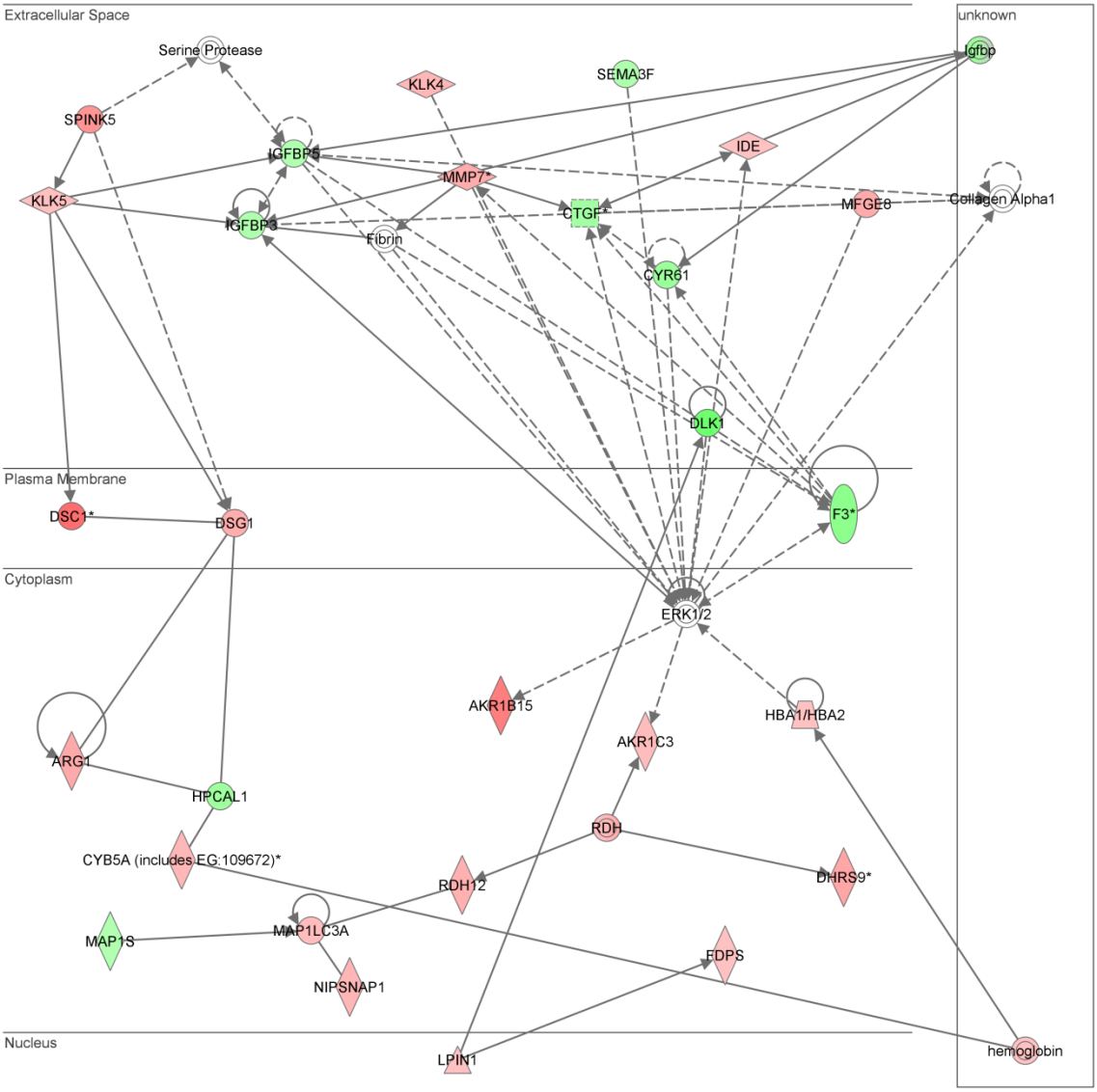

Figure A1. Functional network 1 of differentially regulated genes in the developing HSE model at day 3

A top ranking network of significantly associated genes identified to be differentially regulated in the developing HSE model at day 3. Each of the nodes represents a gene and they are colour-coded to reflect their expression; genes in red were up-regulated, whereas genes in green were down-regulated. The colourless nodes represent genes which were not present in the microarray data, but were added to the network by IPA. The bold line indicates that a gene acts directly on the other gene it was connected to, whereas the dotted line represents a gene indirectly acting on another gene. The gene network was divided into cellular location, including extracellular space, plasma membrane, cytoplasm and nucleus.

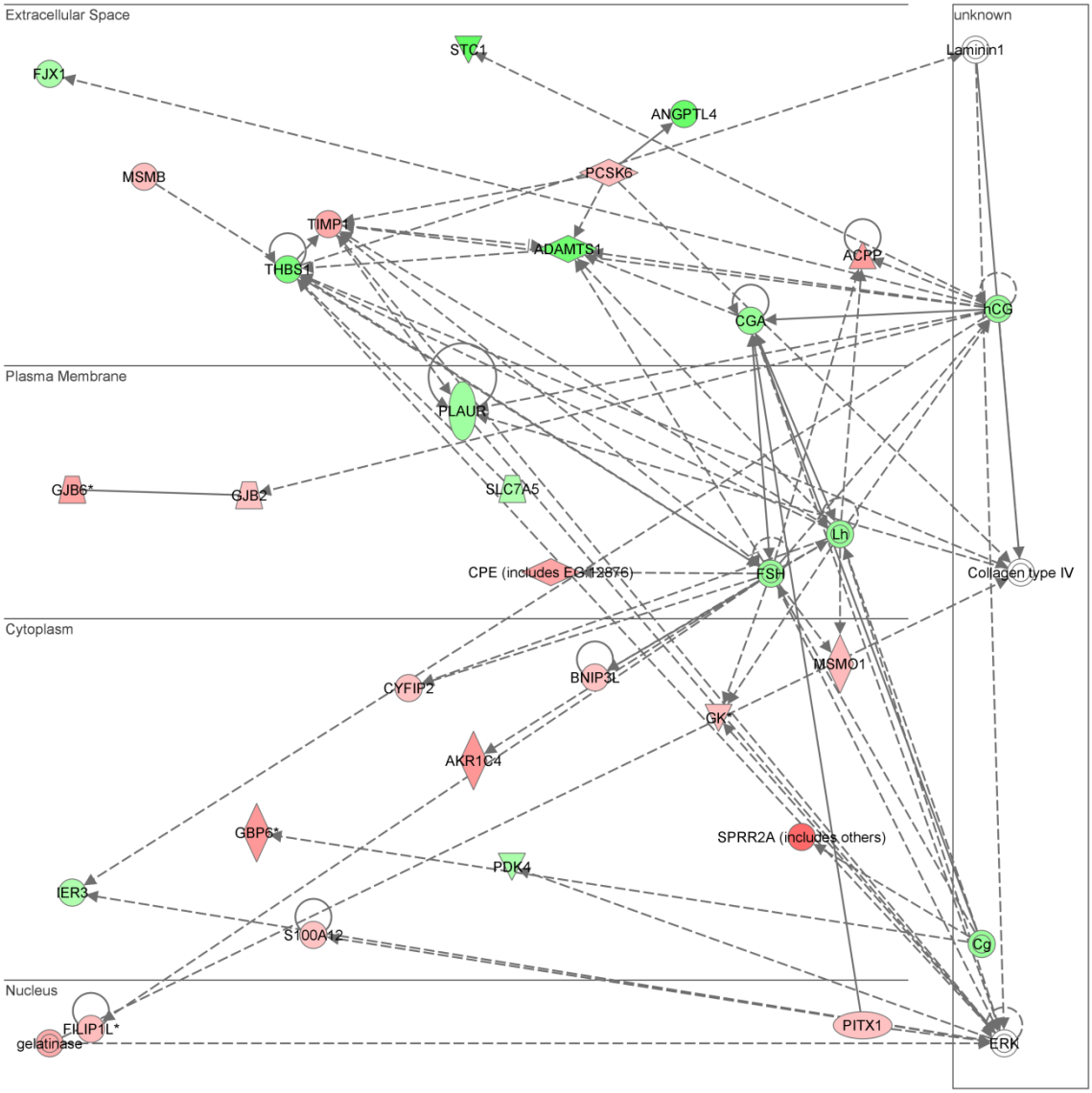

Figure A2. Functional network 2 of differentially regulated genes in the developing HSE model at day 3

A top ranking network of significantly associated genes identified to be differentially regulated in the developing HSE model at day 3. Each of the nodes represents a gene and they are colour-coded to reflect their expression; genes in red were up-regulated, whereas genes in green were down-regulated. The colourless nodes represent genes which were not present in the microarray data, but were added to the network by IPA. The bold line indicates that a gene acts directly on the other gene it was connected to, whereas the dotted line represents a gene indirectly acting on another gene. The gene network was divided into cellular location, including extracellular space, plasma membrane, cytoplasm and nucleus.

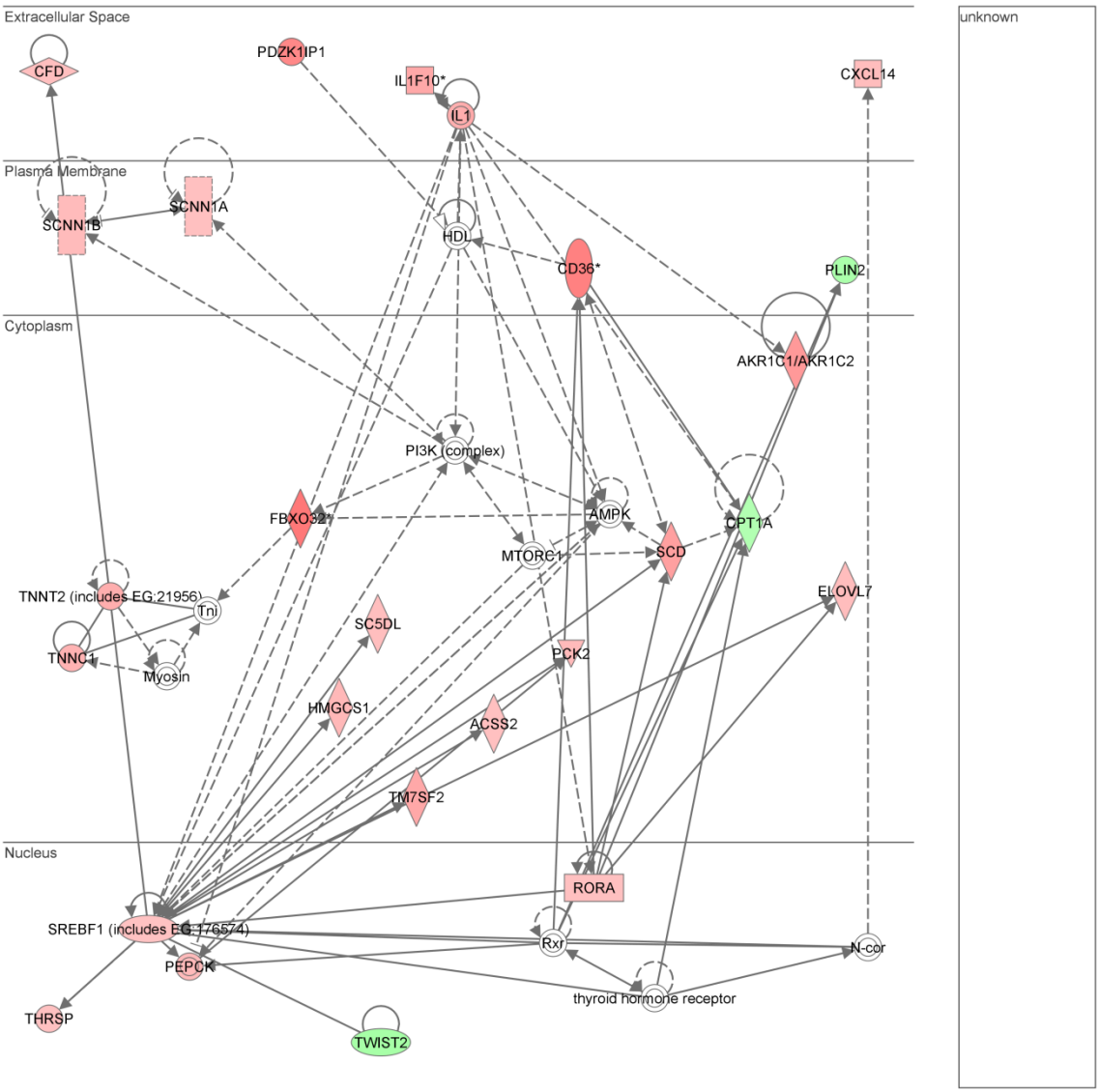

Figure A3. Functional network 3 of differentially regulated genes in the developing HSE model at day 3

A top ranking network of significantly associated genes identified to be differentially regulated in the developing HSE model at day 3. Each of the nodes represents a gene and they are colour-coded to reflect their expression; genes in red were up-regulated, whereas genes in green were down-regulated. The colourless nodes represent genes which were not present in the microarray data, but were added to the network by IPA. The bold line indicates that a gene acts directly on the other gene it was connected to, whereas the dotted line represents a gene indirectly acting on another gene. The gene network was divided into cellular location, including extracellular space, plasma membrane, cytoplasm and nucleus.

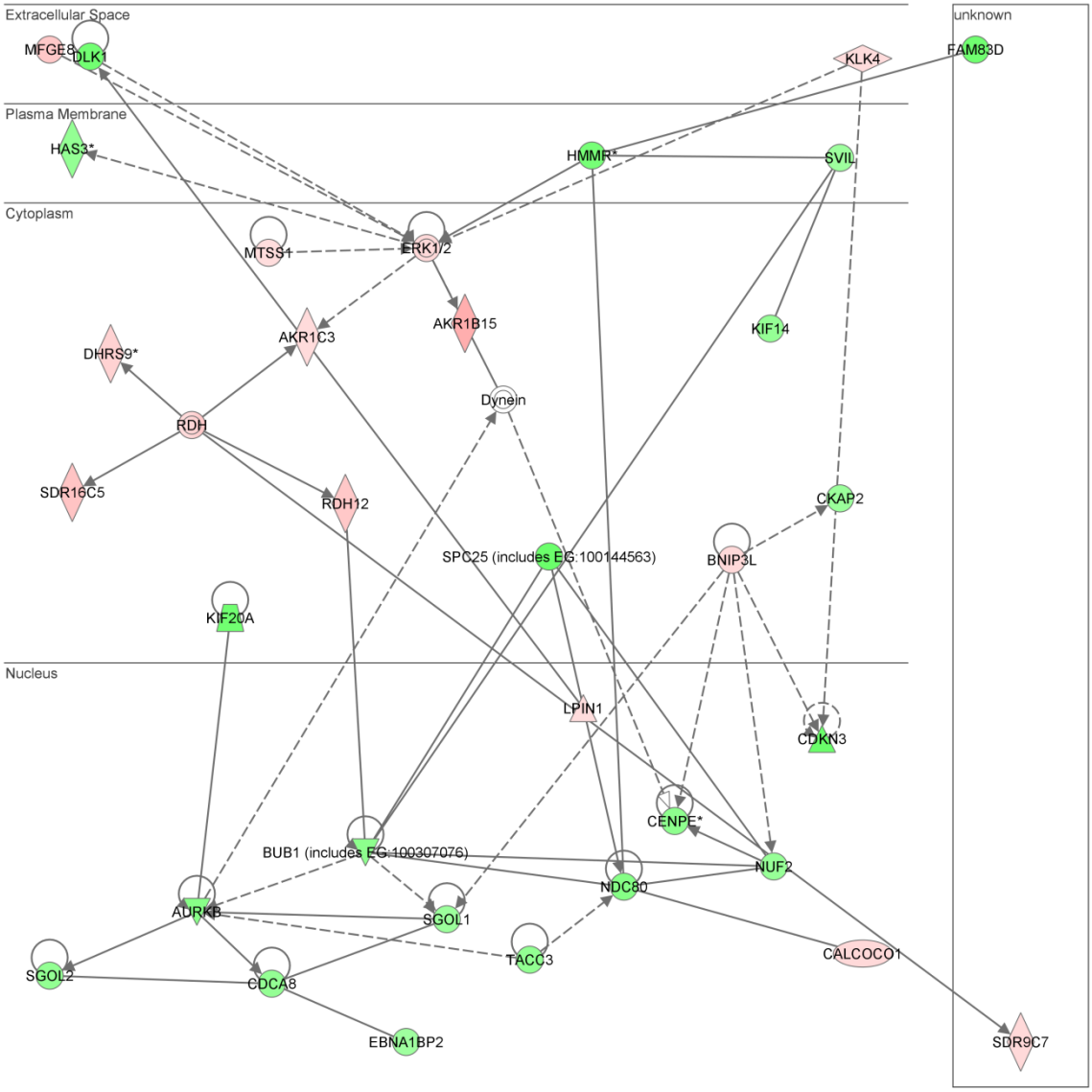

Figure A4. Functional network 1 of differentially regulated genes in the developing HSE model at day 5

A top ranking network of significantly associated genes identified to be differentially regulated in the developing HSE model at day 5. Each of the nodes represents a gene and they are colour-coded to reflect their expression; genes in red were up-regulated, whereas genes in green were down-regulated. The colourless nodes represent genes which were not present in the microarray data, but were added to the network by IPA. The bold line indicates that a gene acts directly on the other gene it was connected to, whereas the dotted line represents a gene indirectly acting on another gene. The gene network was divided into cellular location, including extracellular space, plasma membrane, cytoplasm and nucleus.

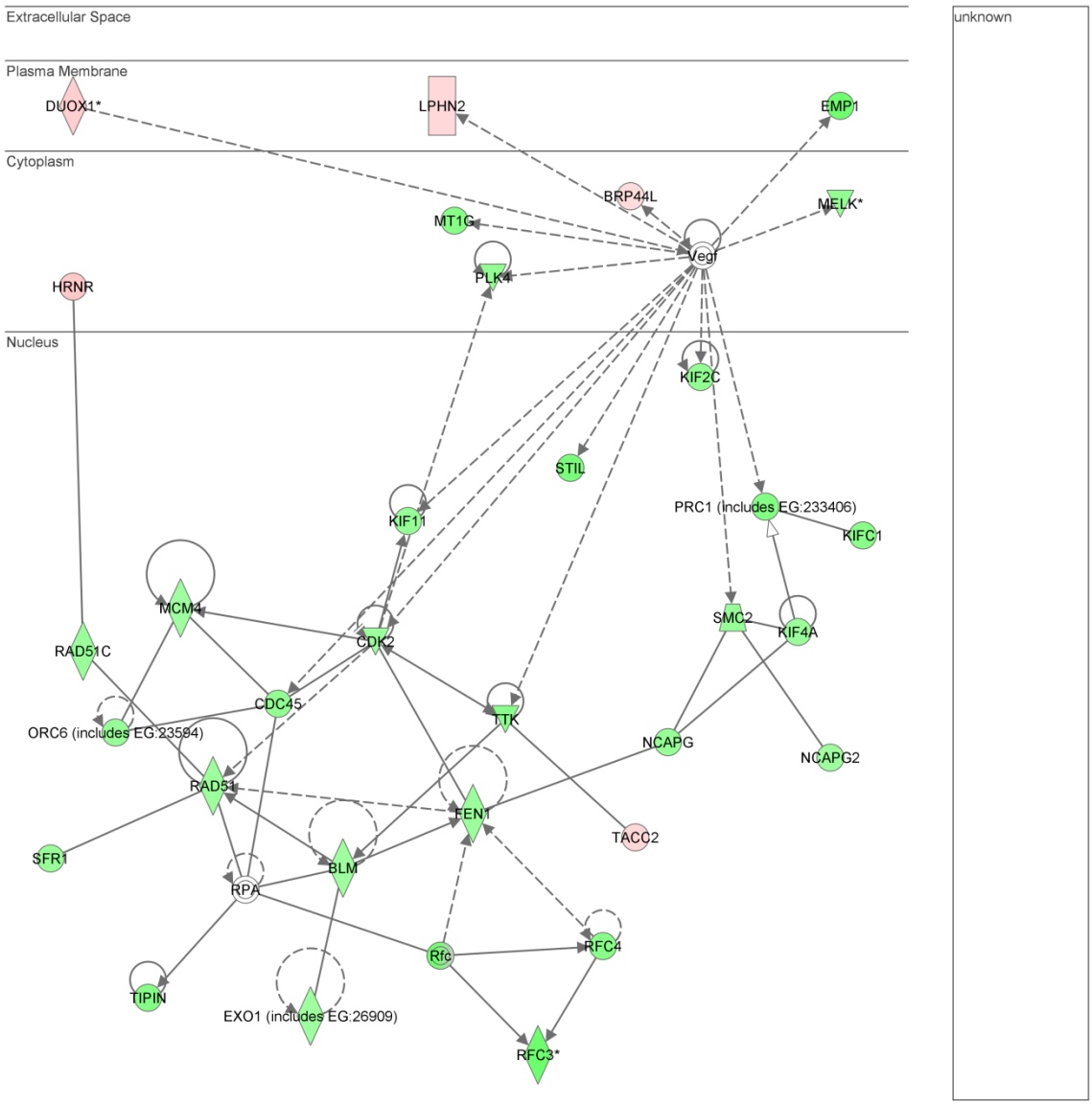

Figure A5. Functional network 2 of differentially regulated genes in the developing HSE model at day 5

A top ranking network of significantly associated genes identified to be differentially regulated in the developing HSE model at day 5. Each of the nodes represents a gene and they are colour-coded to reflect their expression; genes in red were up-regulated, whereas genes in green were down-regulated. The colourless nodes represent genes which were not present in the microarray data, but were added to the network by IPA. The bold line indicates that a gene acts directly on the other gene it was connected to, whereas the dotted line represents a gene indirectly acting on another gene. The gene network was divided into cellular location, including extracellular space, plasma membrane, cytoplasm and nucleus.

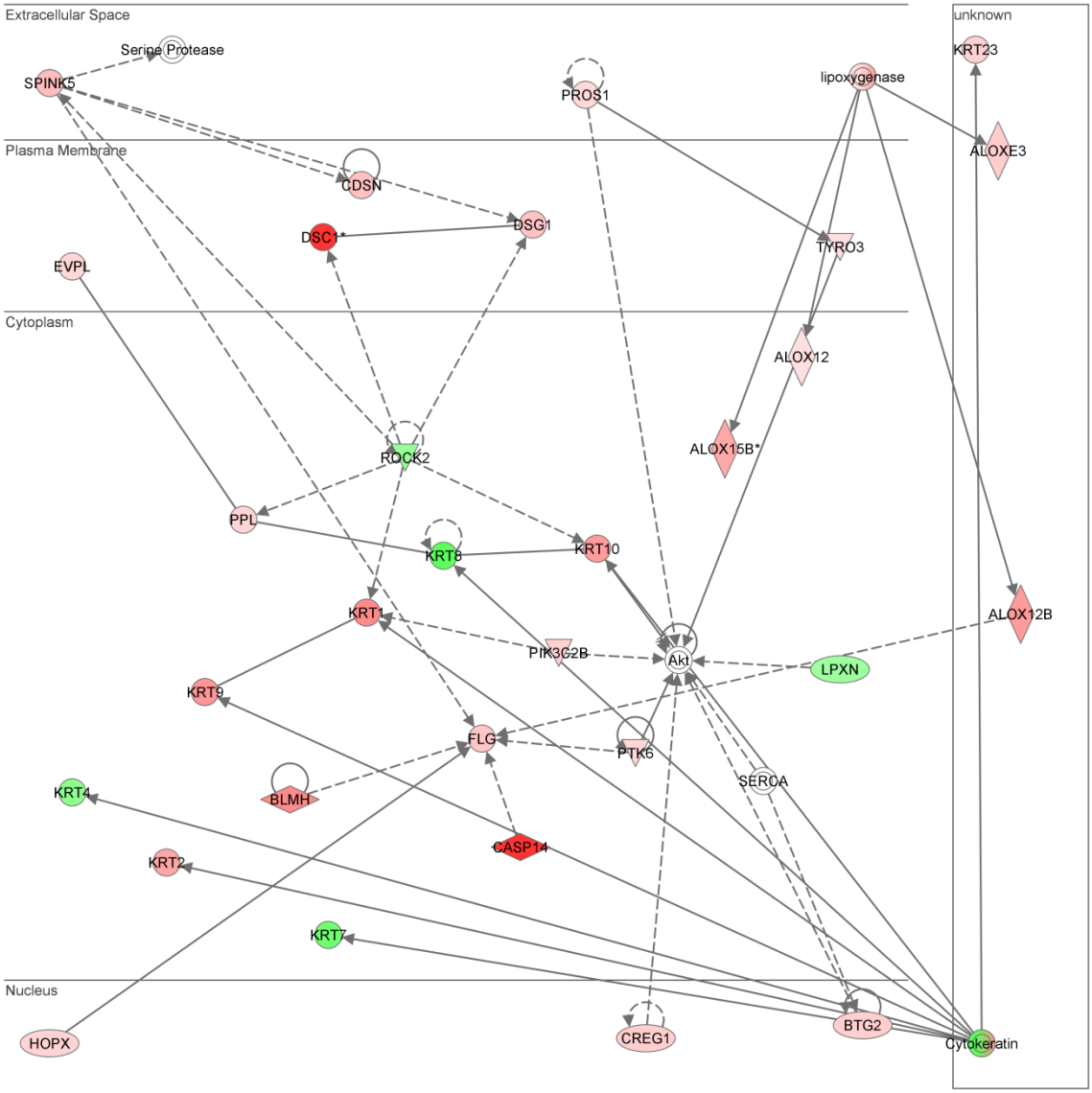

Figure A6. Functional network 3 of differentially regulated genes in the developing HSE model at day 5

A top ranking network of significantly associated genes identified to be differentially regulated in the developing HSE model at day 5. Each of the nodes represents a gene and they are colour-coded to reflect their expression; genes in red were up-regulated, whereas genes in green were down-regulated. The colourless nodes represent genes which were not present in the microarray data, but were added to the network by IPA. The bold line indicates that a gene acts directly on the other gene it was connected to, whereas the dotted line represents a gene indirectly acting on another gene. The gene network was divided into cellular location, including extracellular space, plasma membrane, cytoplasm and nucleus.

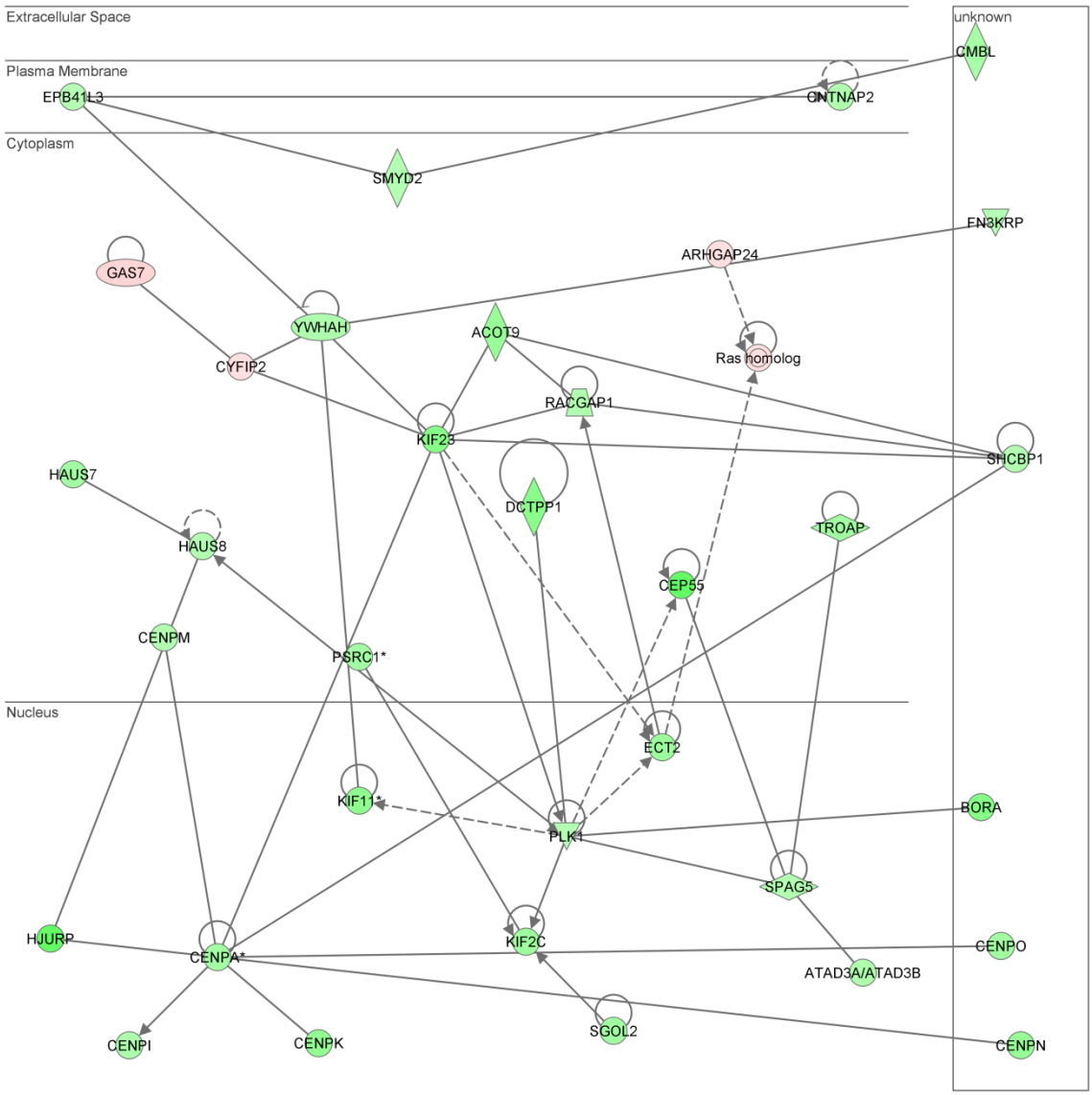

Figure A7. Functional network 1 of differentially regulated genes in the developing HSE model at day 9

A top ranking network of significantly associated genes identified to be differentially regulated in the developing HSE model at day 9. Each of the nodes represents a gene and they are colour-coded to reflect their expression; genes in red were up-regulated, whereas genes in green were down-regulated. The colourless nodes represent genes which were not present in the microarray data, but were added to the network by IPA. The bold line indicates that a gene acts directly on the other gene it was connected to, whereas the dotted line represents a gene indirectly acting on another gene. The gene network was divided into cellular location, including extracellular space, plasma membrane, cytoplasm and nucleus.

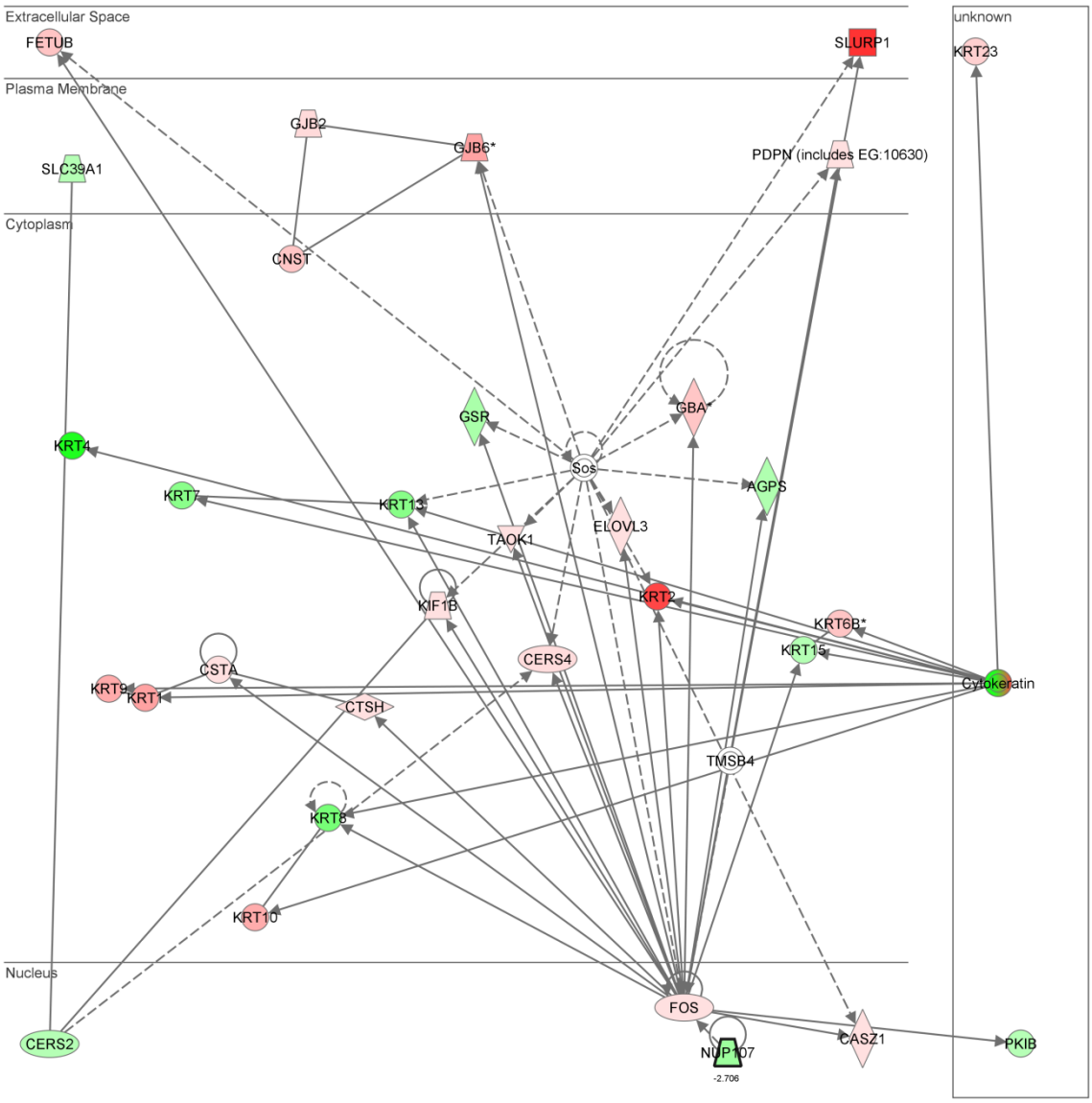

Figure A8. Functional network 2 of differentially regulated genes in the developing HSE model at day 9

A top ranking network of significantly associated genes identified to be differentially regulated in the developing HSE model at day 9. Each of the nodes represents a gene and they are colour-coded to reflect their expression; genes in red were up-regulated, whereas genes in green were down-regulated. The colourless nodes represent genes which were not present in the microarray data, but were added to the network by IPA. The bold line indicates that a gene acts directly on the other gene it was connected to, whereas the dotted line represents a gene indirectly acting on another gene. The gene network was divided into cellular location, including extracellular space, plasma membrane, cytoplasm and nucleus.

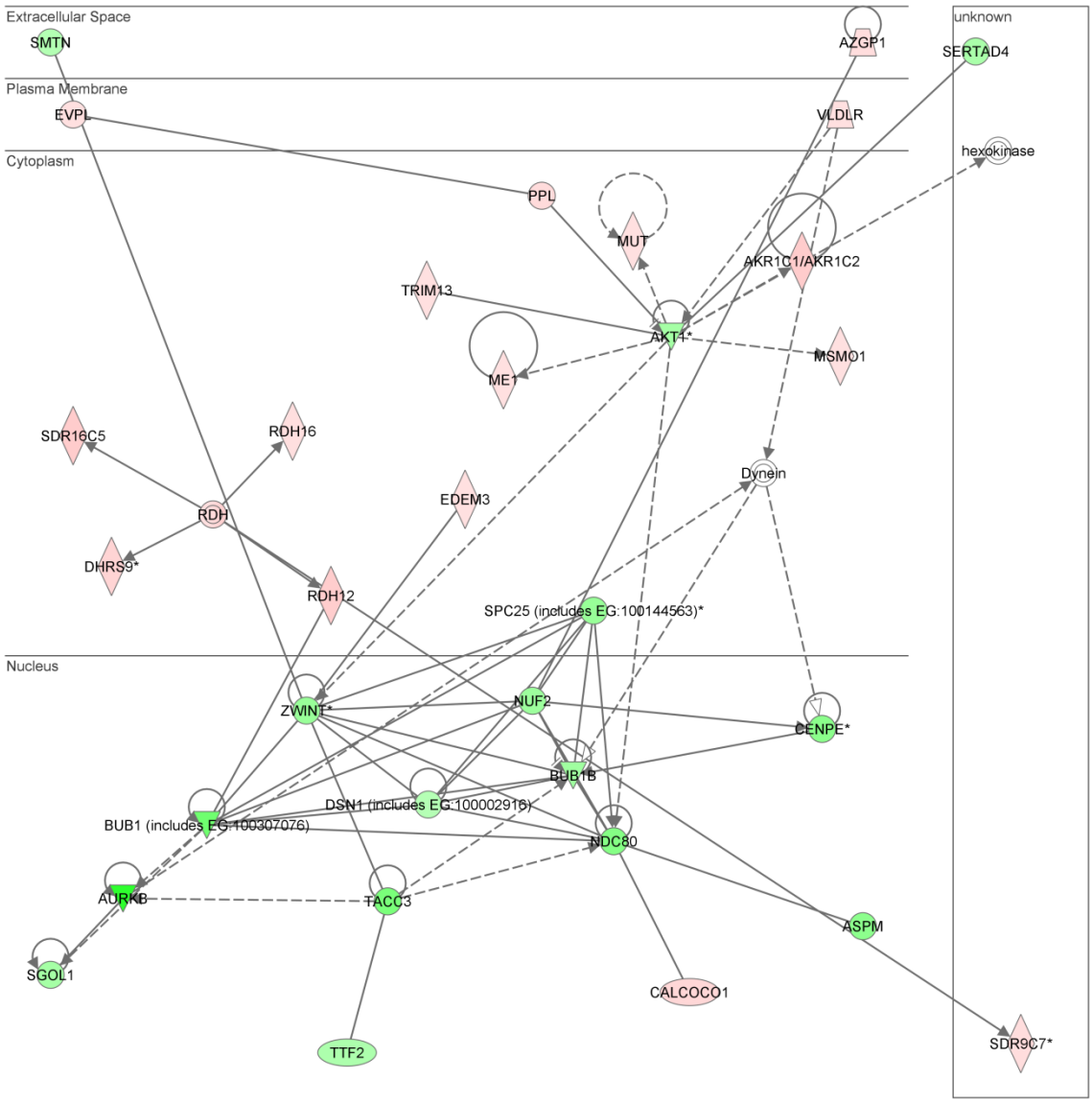

Figure A9. Functional network 3 of differentially regulated genes in the developing HSE model at day 9

A top ranking network of significantly associated genes identified to be differentially regulated in the developing HSE model at day 9. Each of the nodes represents a gene and they are colour-coded to reflect their expression; genes in red were up-regulated, whereas genes in green were down-regulated. The colourless nodes represent genes which were not present in the microarray data, but were added to the network by IPA. The bold line indicates that a gene acts directly on the other gene it was connected to, whereas the dotted line represents a gene indirectly acting on another gene. The gene network was divided into cellular location, including extracellular space, plasma membrane, cytoplasm and nucleus.

Table A20. Summary of lateral epidermal outgrowth over the DED: Group A

	Sample 1 (mm^2)	Sample 2 (mm^2)	Sample 3 (mm^2)	Average (mm^2)
Day 0	19.81 ± 0.16	16.15 ± 2.57	12.69 ± 0.49	16.22 ± 3.39
Day 3 CON	36.17 ± 3.10	25.46 ± 0.07	24.87 ± 0.10	28.83 ± 5.86
Day 3 HBO	31.11 ± 7.18	23.11 ± 0.88	26.76 ± 3.88	26.99 ± 5.13
Day 5 CON	55.22 ± 0.90	34.62 ± 2.05	33.25 ± 2.40	41.03 ± 11.10
Day 5 HBO	40.22 ± 0.15	33.33 ± 1.35	36.74 ± 1.35	36.76 ± 3.20
Day 9 CON	96.75 ± 1.30	60.63 ± 1.52	71.26 ± 2.54	76.21 ± 16.66
Day 9 HBO	79.32 ± 5.12	63.26 ± 6.52	56.50 ± 3.54	66.36 ± 11.23

Table A21. Summary of lateral epidermal outgrowth over the DED: Group B

	Sample 4 (mm^2)	Sample 5 (mm^2)	Sample 6 (mm^2)	Sample 7 (mm^2)	Sample 8 (mm^2)
Day 0	15.46 ± 0.41	18.72 ± 0.21	21.36 ± 0.00	21.00 ± 0.98	19.45 ± 0.03
Day 3 CON	36.53 ± 2.71	32.49 ± 5.20	30.90 ± 0.00	43.69 ± 9.04	36.38 ± 2.65
Day 3 HBO	31.19 ± 4.99	34.53 ± 0.57	25.72 ± 0.00	32.65 ± 1.84	34.72 ± 0.95
Day 5 CON	42.54 ± 0.48	44.66 ± 3.37	39.31 ± 0.00	68.09 ± 11.89	48.79 ± 6.69
Day 5 HBO	41.12 ± 4.13	41.61 ± 6.42	37.88 ± 0.00	65.24 ± 0.98	43.69 ± 4.04
Day 9 CON	74.26 ± 12.21	77.54 ± 12.16	72.84 ± 0.00	72.33 ± 1.02	104.30 ± 1.06
Day 9 HBO	76.70 ± 7.68	68.33 ± 10.89	69.21 ± 0.00	71.04 ± 4.36	89.31 ± 9.98

Table A22. Summary of stratum corneum thickness in the HSE epidermis: Group A

SC	Sample 1 (µm)	Sample 2 (µm)	Sample 3 (µm)	Average (µm)
Native skin	n/a	n/a	n/a	24.52 ± 6.73
Day 0	1.90 ± 2.21	1.04 ± 1.08	1.86 ± 2.95	1.60 ± 2.21
Day 3 CON	5.32 ± 3.66	5.92 ± 2.17	2.24 ± 1.17	4.49 ± 2.98
Day 3 HBO	4.46 ± 3.66	7.52 ± 1.33	2.62 ± 1.66	4.33 ± 3.13
Day 5 CON	10.00 ± 4.53	12.77 ± 2.10	14.74 ± 4.55	12.50 ± 4.29
Day 5 HBO	8.09 ± 2.05	11.42 ± 3.11	14.41 ± 10.95	11.31 ± 7.04
Day 9 CON	49.30 ± 15.34	48.50 ± 16.72	26.86 ± 3.66	41.55 ± 16.70
Day 9 HBO	62.36 ± 13.79	70.83 ± 21.89	33.29 ± 9.51	55.50 ± 22.51

Table A23. Summary of cellular layer thickness in the HSE epidermis: Group A

Cell	Sample 1 (µm)	Sample 2 (µm)	Sample 3 (µm)	Average (µm)
Native skin	n/a	n/a	n/a	79.99 ± 28.21
Day 0	7.41 ± 3.11	4.95 ± 3.20	12.49 ± 8.07	8.28 ± 6.10
Day 3 CON	94.18 ± 15.75	92.39 ± 14.57	53.00 ± 11.99	79.86 ± 23.70
Day 3 HBO	71.45 ± 20.04	78.34 ± 16.41	39.31 ± 8.82	59.97 ± 23.05
Day 5 CON	83.58 ± 10.29	117.34 ± 25.94	112.48 ± 32.05	104.46 ± 28.34
Day 5 HBO	129.49 ± 30.17	120.07 ± 25.47	88.58 ± 12.58	116.38 ± 26.60
Day 9 CON	71.26 ± 12.56	49.09 ± 15.33	71.44 ± 28.60	63.93 ± 22.33
Day 9 HBO	81.72 ± 13.78	66.71 ± 22.72	67.22 ± 13.39	71.88 ± 18.22

Table A24. Summary of stratum corneum thickness in the HSE epidermis: Group B

SC	Sample 4 (µm)	Sample 5 (µm)	Sample 6 (µm)	Sample 7 (µm)	Sample 8 (µm)
Native skin	17.03 ± 4.18	24.36 ± 5.50	30.27 ± 5.43	20.69 ± 3.14	20.33 ± 5.38
Day 0	1.77 ± 2.43	2.58 ± 1.45	1.81 ± 1.38	2.75 ± 3.41	1.79 ± 2.31
Day 3 CON	7.53 ± 2.44	4.67 ± 1.53	1.70 ± 1.39	3.42 ± 1.59	3.90 ± 1.54
Day 3 HBO	8.69 ± 2.31	5.94 ± 5.51	11.00 ± 12.92	5.02 ± 1.80	6.36 ± 5.35
Day 5 CON	12.51 ± 3.43	18.21 ± 6.24	10.99 ± 2.14	11.60 ± 3.58	11.17 ± 3.16
Day 5 HBO	11.72 ± 3.47	23.46 ± 7.13	15.82 ± 3.71	10.42 ± 4.38	10.44 ± 3.00
Day 9 CON	38.21 ± 11.93	45.84 ± 9.15	54.88 ± 9.93	65.70 ± 21.89	30.26 ± 12.32
Day 9 HBO	29.07 ± 9.96	84.44 ± 48.01	83.21 ± 18.03	55.08 ± 23.66	50.23 ± 13.36

Table A25. Summary of cellular layer thickness in the HSE epidermis: Group B

Cell	Sample 4 (µm)	Sample 5 (µm)	Sample 6 (µm)	Sample 7 (µm)	Sample 8 (µm)
Native skin	79.30 ± 10.14	46.48 ± 16.31	45.09 ± 7.86	43.89 ± 5.96	59.43 ± 4.92
Day 0	6.98 ± 3.33	12.52 ± 5.40	7.12 ± 4.62	11.13 ± 5.73	9.55 ± 4.38
Day 3 CON	49.66 ± 14.83	71.00 ± 29.62	61.46 ± 13.44	62.38 ± 27.21	51.32 ± 15.33
Day 3 HBO	60.22 ± 10.67	68.79 ± 21.48	77.73 ± 11.28	78.17 ± 30.50	68.55 ± 12.32
Day 5 CON	105.15 ± 31.81	90.48 ± 18.28	97.65 ± 13.78	51.66 ± 11.48	67.54 ± 15.74
Day 5 HBO	114.90 ± 18.22	87.68 ± 19.68	79.85 ± 6.46	56.06 ± 21.30	81.87 ± 13.18
Day 9 CON	83.41 ± 31.92	46.74 ± 16.86	42.97 ± 6.00	28.08 ± 8.00	45.29 ± 18.04
Day 9 HBO	67.74 ± 18.38	59.18 ± 19.08	49.00 ± 7.94	32.57 ± 10.42	64.35 ± 14.57

Table A26. Summary of the number of p63 positive nuclei in the HSE epidermis: Group A

p63	Sample 1 (# nuclei)	Sample 2 (# nuclei)	Sample 3 (# nuclei)	Average (# nuclei)
Native skin	n/a	n/a	n/a	192.95 ± 52.25
Day 0	11.75 ± 5.47	6.38 ± 2.77	8.00 ± 2.62	8.71 ± 4.34
Day 3 CON	127.00 ± 15.03	128.13 ± 30.90	34.75 ± 11.25	86.88 ± 44.45
Day 3 HBO	103.13 ± 31.95	81.13 ± 17.82	55.88 ± 10.19	80.04 ± 28.77
Day 5 CON	127.00 ± 26.77	116.5 ± 24.43	97.88 ± 25.31	113.88 ± 27.32
Day 5 HBO	122.50 ± 28.84	131.25 ± 32.40	108.38 ± 26.01	120.71 ± 29.52
Day 9 CON	81.00 ± 14.24	83.63 ± 33.91	94.63 ± 22.44	86.42 ± 24.52
Day 9 HBO	91.63 ± 13.49	77.13 ± 9.36	95.63 ± 14.11	88.13 ± 14.44

Table A27. Summary of the number of p63 positive nuclei in the HSE epidermis: Group B

p63	Sample 4 (# nuclei)	Sample 5 (# nuclei)	Sample 6 (# nuclei)	Sample 7 (# nuclei)	Sample 8 (# nuclei)
Native skin	154.75 ± 22.91	169.25 ± 36.21	169.50 ± 40.30	104.50 ± 26.61	127.88 ± 27.65
Day 0	9.75 ± 7.37	14.94 ± 6.24	4.13 ± 1.36	12.63 ± 9.51	12.25 ± 3.32
Day 3 CON	79.00 ± 20.04	47.31 ± 13.28	69.13 ± 15.26	64.31 ± 23.98	68.75 ± 17.38
Day 3 HBO	90.00 ± 23.42	47.94 ± 13.16	69.13 ± 14.63	74.56 ± 26.38	82.81 ± 22.49
Day 5 CON	105.88 ± 26.43	46.25 ± 9.46	63.00 ± 8.42	54.31 ± 12.66	59.31 ± 17.45
Day 5 HBO	138.88 ± 37.61	61.94 ± 19.96	62.38 ± 6.99	34.81 ± 10.11	88.94 ± 21.62
Day 9 CON	93.31 ± 18.42	30.88 ± 8.21	43.25 ± 9.59	28.94 ± 7.42	46.13 ± 18.20
Day 9 HBO	93.75 ± 36.21	32.38 ± 7.94	29.75 ± 9.79	28.63 ± 7.34	51.63 ± 15.10

Table A28. Summary of the number of ki-67 positive nuclei in the HSE epidermis: Group A

ki-67	Sample 1 (# nuclei)	Sample 2 (# nuclei)	Sample 3 (# nuclei)	Average (# nuclei)
Native skin	n/a	n/a	n/a	31.25 ± 17.33
Day 0	6.38 ± 2.83	7.63 ± 5.40	15.50 ± 6.41	9.83 ± 3.69
Day 3 CON	51.00 ± 9.58	94.63 ± 12.41	50.88 ± 10.55	65.50 ± 13.56
Day 3 HBO	49.75 ± 16.79	50.88 ± 18.04	51.88 ± 17.30	50.83 ± 9.60
Day 5 CON	53.25 ± 12.59	46.25 ± 18.93	43.13 ± 14.25	47.54 ± 8.90
Day 5 HBO	25.13 ± 12.19	31.50 ± 8.04	67.75 ± 12.16	41.46 ± 12.62
Day 9 CON	36.57 ± 7.67	6.25 ± 1.83	25.00 ± 2.67	22.67 ± 7.87
Day 9 HBO	25.63 ± 4.03	21.25 ± 8.03	34.25 ± 8.15	27.04 ± 5.01

Table A29. Summary of the number of ki-67 positive nuclei in the HSE epidermis: Group B

ki-67	Sample 4 (# nuclei)	Sample 5 (# nuclei)	Sample 6 (# nuclei)	Sample 7 (# nuclei)	Sample 8 (# nuclei)
Native skin	23.63 ± 6.61	22.00 ± 6.48	23.63 ± 6.61	17.00 ± 3.07	18.75 ± 6.23
Day 0	15.50 ± 10.12	17.44 ± 7.28	9.13 ± 2.42	25.31 ± 6.96	14.00 ± 4.98
Day 3 CON	78.81 ± 11.44	46.56 ± 10.46	66.00 ± 13.43	61.25 ± 23.29	68.75 ± 23.17
Day 3 HBO	90.69 ± 13.30	41.19 ± 7.14	54.00 ± 11.61	55.63 ± 14.08	70.50 ± 16.84
Day 5 CON	42.19 ± 8.60	23.25 ± 7.61	20.25 ± 15.69	24.06 ± 11.85	42.94 ± 13.73
Day 5 HBO	41.31 ± 14.55	29.50 ± 5.47	34.88 ± 11.74	21.19 ± 9.60	26.63 ± 6.49
Day 9 CON	20.75 ± 6.03	13.50 ± 2.93	21.88 ± 4.02	8.69 ± 4.47	20.88 ± 8.10
Day 9 HBO	23.75 ± 9.50	16.56 ± 3.39	20.75 ± 5.68	16.94 ± 7.02	22.63 ± 5.97

Table A30. Summary of the thickness of K1-positive epidermis in the HSE epidermis: Group A

Keratin 1	Sample 1 (µm)	Sample 2 (µm)	Sample 3 (µm)	Average (µm)
Native skin	n/a	n/a	n/a	57.71 ± 16.91
Day 0	4.48 ± 1.72	0.24 ± 0.67	2.99 ± 3.32	2.57 ± 2.76
Day 3 CON	9.00 ± 3.01	39.06 ± 19.02	8.83 ± 4.45	18.96 ± 18.15
Day 3 HBO	7.92 ± 2.98	7.99 ± 2.50	5.88 ± 1.19	7.26 ± 2.46
Day 5 CON	53.09 ± 8.65	82.18 ± 19.21	62.06 ± 16.55	65.78 ± 19.31
Day 5 HBO	25.09 ± 16.68	70.57 ± 17.75	41.57 ± 16.03	45.74 ± 25.06
Day 9 CON	45.87 ± 8.12	38.11 ± 13.93	43.19 ± 10.15	42.39 ± 11.01
Day 9 HBO	35.70 ± 2.08	36.65 ± 10.70	34.30 ± 5.19	35.62 ± 6.72

Table A31. Summary of the thickness of K1-positive epidermis in the HSE epidermis: Group B

Keratin 1	Sample 4 (µm)	Sample 5 (µm)	Sample 6 (µm)	Sample 7 (µm)	Sample 8 (µm)
Native skin	53.10 ± 11.97	45.48 ± 19.77	5.46 ± 7.72	38.97 ± 4.08	45.08 ± 10.16
Day 0	5.76 ± 4.99	6.05 ± 4.20	2.73 ± 1.10	1.74 ± 2.04	3.21 ± 2.18
Day 3 CON	17.90 ± 8.16	15.00 ± 4.30	17.42 ± 4.26	11.90 ± 7.20	17.16 ± 12.43
Day 3 HBO	20.75 ± 7.91	15.20 ± 6.41	17.24 ± 5.63	20.41 ± 11.10	8.44 ± 5.83
Day 5 CON	76.04 ± 17.74	36.65 ± 10.66	37.97 ± 5.15	36.79 ± 12.31	40.11 ± 10.21
Day 5 HBO	76.25 ± 20.11	47.23 ± 14.13	25.50 ± 3.29	30.15 ± 9.37	37.15 ± 11.99
Day 9 CON	61.17 ± 24.82	23.30 ± 4.56	20.40 ± 4.59	19.45 ± 7.13	32.08 ± 12.03

Table A32. Summary of the thickness of loricrin-positive epidermis in the HSE epidermis: Group A

Loricrin	Sample 1 (µm)	Sample 2 (µm)	Sample 3 (µm)	Average (µm)
Native skin	n/a	n/a	n/a	7.53 ± 2.71
Day 0	0.00 ± 0.00	0.00 ± 0.00	0.06 ± 0.16	0.02 ± 0.09
Day 3 CON	3.36 ± 4.04	5.18 ± 3.20	8.87 ± 6.78	5.81 ± 5.25
Day 3 HBO	0.78 ± 0.73	2.14 ± 3.49	4.84 ± 1.90	2.59 ± 2.82
Day 5 CON	32.15 ± 5.62	31.34 ± 12.10	35.40 ± 11.39	32.96 ± 9.84
Day 5 HBO	33.49 ± 18.50	38.90 ± 14.25	39.25 ± 5.00	37.21 ± 13.45
Day 9 CON	22.62 ± 6.07	19.98 ± 6.16	23.68 ± 4.94	22.09 ± 5.72
Day 9 HBO	26.54 ± 8.99	21.10 ± 3.82	28.16 ± 6.32	25.27 ± 7.12

Table A33. Summary of the thickness of loricrin-positive epidermis in the HSE epidermis: Group B

Loricrin	Sample 4 (µm)	Sample 5 (µm)	Sample 6 (µm)	Sample 7 (µm)	Sample 8 (µm)
Native skin	8.54 ± 2.82	5.58 ± 1.23	9.51 ± 2.01	5.53 ± 1.93	5.18 ± 1.23
Day 0	0.39 ± 1.39	1.34 ± 3.30	0.00 ± 0.00	0.15 ± 0.33	0.38 ± 1.08
Day 3 CON	4.83 ± 4.57	10.73 ± 4.33	5.70 ± 3.19	12.15 ± 3.10	17.25 ± 5.30
Day 3 HBO	6.80 ± 3.22	9.23 ± 6.14	5.03 ± 2.24	14.60 ± 4.37	14.48 ± 5.74
Day 5 CON	39.14 ± 10.29	30.10 ± 6.69	28.76 ± 6.06	21.88 ± 5.13	26.21 ± 7.82
Day 5 HBO	43.79 ± 8.94	36.27 ± 21.46	18.97 ± 2.69	29.33 ± 6.79	28.43 ± 6.50
Day 9 CON	28.31 ± 8.13	22.56 ± 3.17	14.25 ± 1.96	19.73 ± 7.60	21.83 ± 5.79
Day 9 HBO	23.35 ± 7.95	12.96 ± 7.31	4.03 ± 2.95	9.52 ± 4.46	18.41 ± 3.95

Table A34. Summary of the thickness of K16-positive epidermis in the HSE epidermis: Group A

K16	Sample 1 (µm)	Sample 2 (µm)	Sample 3 (µm)	Average (µm)
Native skin	n/a	n/a	n/a	40.95 ± 15.02
Day 0	6.66 ± 3.50	4.20 ± 1.54	5.00 ± 1.00	6.23 ± 3.88
Day 3 CON	46.32 ± 16.91	55.75 ± 19.12	7.84 ± 5.19	46.07 ± 16.96
Day 3 HBO	18.62 ± 6.58	43.79 ± 7.58	36.13 ± 8.59	30.79 ± 12.36
Day 5 CON	80.66 ± 21.85	94.59 ± 15.84	29.97 ± 6.17	84.25 ± 17.78
Day 5 HBO	114.88 ± 32.90	97.36 ± 18.37	77.50 ± 11.01	99.06 ± 14.62
Day 9 CON	69.37 ± 17.49	42.40 ± 13.08	77.50 ± 13.02	51.35 ± 18.78
Day 9 HBO	70.11 ± 16.29	57.60 ± 16.04	42.27 ± 11.17	65.20 ± 11.04

Table A35. Summary of the thickness of K16-positive epidermis in the HSE epidermis: Group B

K16	Sample 4 (µm)	Sample 5 (µm)	Sample 6 (µm)	Sample 7 (µm)	Sample 8 (µm)
Native skin	24.20 ± 4.21	26.68 ± 8.56	31.88 ± 7.22	26.82 ± 4.80	32.85 ± 7.90
Day 0	5.37 ± 4.28	12.09 ± 10.18	7.49 ± 6.57	8.45 ± 3.24	6.05 ± 3.55
Day 3 CON	44.95 ± 15.07	44.56 ± 14.76	35.91 ± 5.27	49.55 ± 10.93	55.65 ± 18.42
Day 3 HBO	42.05 ± 10.76	36.92 ± 6.17	37.15 ± 5.29	53.80 ± 18.24	46.59 ± 18.46
Day 5 CON	97.69 ± 21.02	47.77 ± 11.20	64.39 ± 7.10	44.49 ± 10.78	59.88 ± 14.45
Day 5 HBO	97.99 ± 27.64	64.65 ± 16.32	49.45 ± 9.82	57.45 ± 13.74	59.45 ± 12.81
Day 9 CON	81.41 ± 36.61	39.03 ± 8.02	43.07 ± 3.64	42.07 ± 16.18	46.11 ± 16.08
Day 9 HBO	58.82 ± 21.14	34.70 ± 13.48	28.87 ± 6.17	58.24 ± 23.50	56.52 ± 12.74

Table A36. Ontology of differentially expressed genes at day 3

Molecular and Cellular Functions	Significance P-value	Focus Genes
Cell Cycle	3.41E-04 – 4.48E-02	15
Cellular Assembly and Organization	3.41E-04 – 4.88E-02	12
DNA Replication, Recombination, and Repair	3.41E-04 – 4.08E-02	7
Lipid Metabolism	5.65E-04 – 4.48E-02	11
Small Molecule Biochemistry	5.65E-04 – 4.48E-02	18

Table A37. Ontology of differentially expressed genes at day 5

Molecular and Cellular Functions	Significance P-value	Focus Genes
Cellular Movement	1.02E-04 – 4.05E-02	21
Lipid Metabolism	4.66E-04 – 4.38E-02	17
Molecular Transport	4.66E-04 – 4.14E-02	20
Small Molecule Biochemistry	4.66E-04 – 4.38E-02	29
Cellular Growth and Proliferation	4.91E-04 – 3.88E-02	39

Table A38. Ontology of differentially expressed genes at day 9

Molecular and Cellular Functions	Significance P-value	Focus Genes
Lipid Metabolism	7.48E-08 – 2.31E-02	17
Small Molecule Biochemistry	7.48E-08 – 2.31E-02	26
Vitamin and Mineral Metabolism	7.48E-08 – 2.318E-02	8
Drug Metabolism	6.63E-06 – 2.318E-02	11
Cellular Growth and Proliferation	2.91E-05 – 2.31E-02	34

Data presented in these tables contains a range of p-values as each molecular and cellular functions category contains multiple sub-groups and each sub-group has a p-value assigned to it.

Table A39. Top 3 functional networks regulated by HBO treatment in the HSE model at day 3

Network ID	Molecules in network
1	Cancer, gastrointestinal disease, genetic disorder
2	Connective tissue development and function, lipid metabolism, cell signalling
3	Embryonic development, tissue development, cell death

Table A40. Top 3 functional networks regulated by HBO treatment in the HSE model at day 5

Network ID	Molecules in network
1	Dermatological diseases and conditions, genetic disorder, cancer
2	Infection mechanism, nervous system development and function, neurological disease
3	Cell death, lipid metabolism, small molecule biochemistry

Table A41. Top 3 functional networks regulated by HBO treatment in the HSE model at day 9

Network ID	Molecules in network
1	Embryonic development, lipid metabolism, small molecule biochemistry
2	Cellular movement, tumour morphology, behaviour
3	Increased levels of alkaline phosphatise, cell signalling, molecular transport

Table A42. Functional network analysis of genes differentially regulated in response to HBO treatment at day 3

Network ID	Molecules in network	Score	Focus genes
1	ALOX15B, APOBEC3B, Calcineurin protein(s), CREB1, Cytokeratin, DSC1, DSTYK, FBXO32, FKBP1A, FSH, IDO1, IgG, IL1, Immunoglobulin, Insulin, **KLK7**, KRT7, KRT10, KRT13, KRT19, LDL, MAD2L1, NDRG2, NFkB (complex), ORM1/ORM2, P38 MAPK, PDE4C, PLA2G16, PTGS1, RORA, S100A1, SMPD1, TNFRSF9, TYMP, Vegf	54	24
2	Akt, beta-estradiol, CCNT2, CNTNAP2, DLK1, EPB41, ERK1/2, F2RL3, FBXO2, Focal adhesion kinase, Gpcr, GPR19, GPR115, GPR109A, GPRC5A, IL5, IL28A, ITGB1, LCE2B (includes others), LPHN1, MC1R, MC4R, MYC, NDEL1, OSM, P2RY11 (includes others), PKM2, PTGER3, RAN, Rcc1, SPRR3, ZNF14, ZNF17, ZNF91, ZNF230	30	15
3	BCR, BEND7, BEX4, C7orf10, CDC34, CROT, DNAJC1, DNAJC28, DNAJC30, FBXW2, GTF2E1, HNF4A, HSP, HSPE1, IKBKG, KIAA0368, KRT10, LUC7L2, MAP4K4, **MT1H**, NIF3L1, NOD2, PSMB1, PSME3, PSMF1, PTK2, SFXN1, TCF7, TEAD3, TRAF2, TRAF5, TUBB4, UBA5, VGLL1, ZNF646..	22	12

Genes in bold type were deemed as genes of interest and gene expression levels were validated in Chapter 5. The higher the score, the more significant the network was.

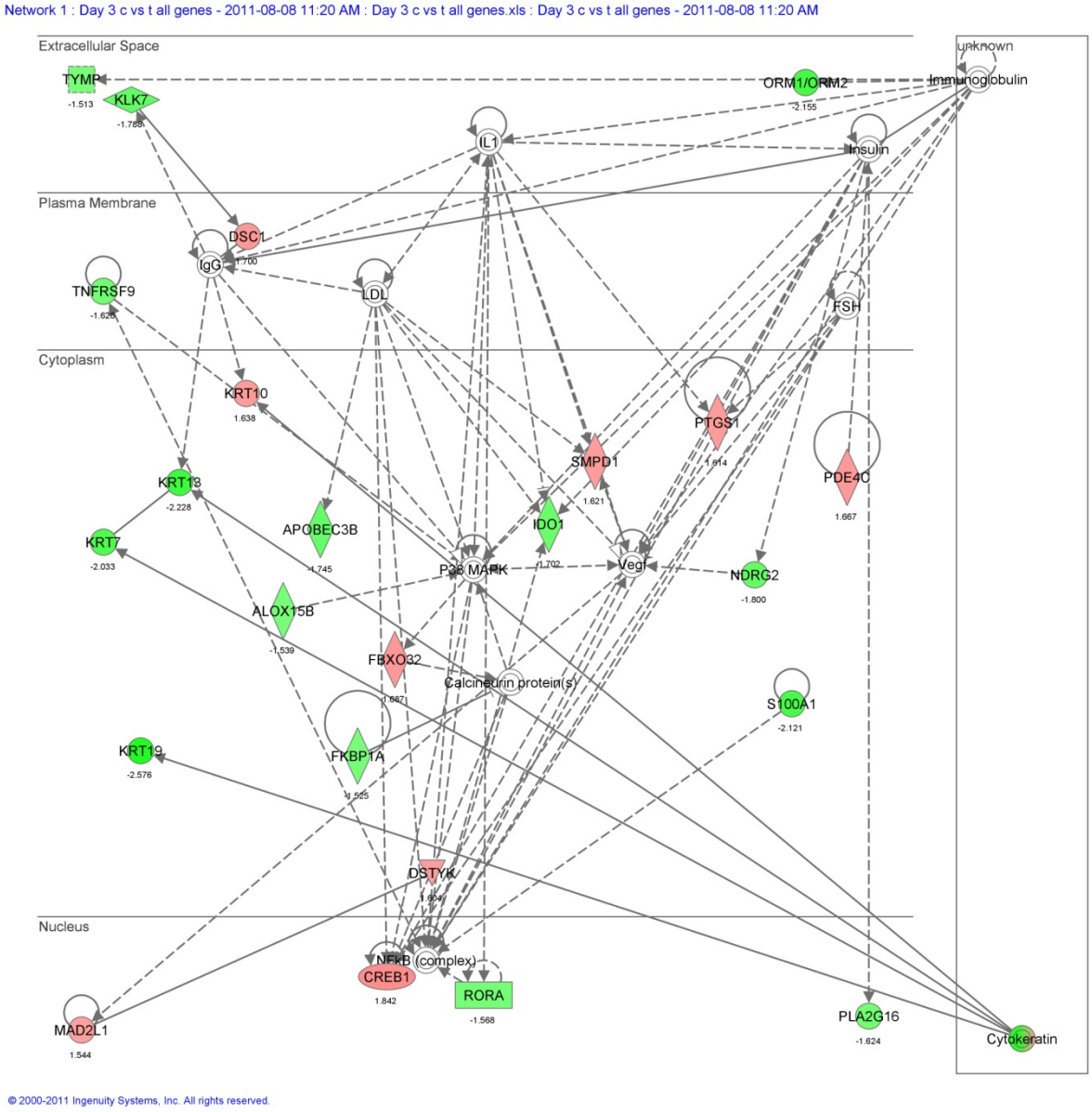

Figure A10. Functional network 1 of genes differentially regulated in response to HBO treatment at day 3

Atop ranking network of significantly associated genes identified to be differentially regulated in response to HBO treatment in the HSE model at day 3. Each of the nodes represents a gene and they are colour – coded to reflect their expression; genes in red were up – regulated, whereas genes in green were down – regulated. The colourless nodes represent genes which were not present in the microarray data, but were added to the network by IPA. The bold line indicates that a gene acts directly on the other gene it was connected to, whereas the dotted line represents a gene indirectly acting on another gene. The gene network was divided into cellular location, including extracellular space, plasma membrane, cytoplasm and nucleus.

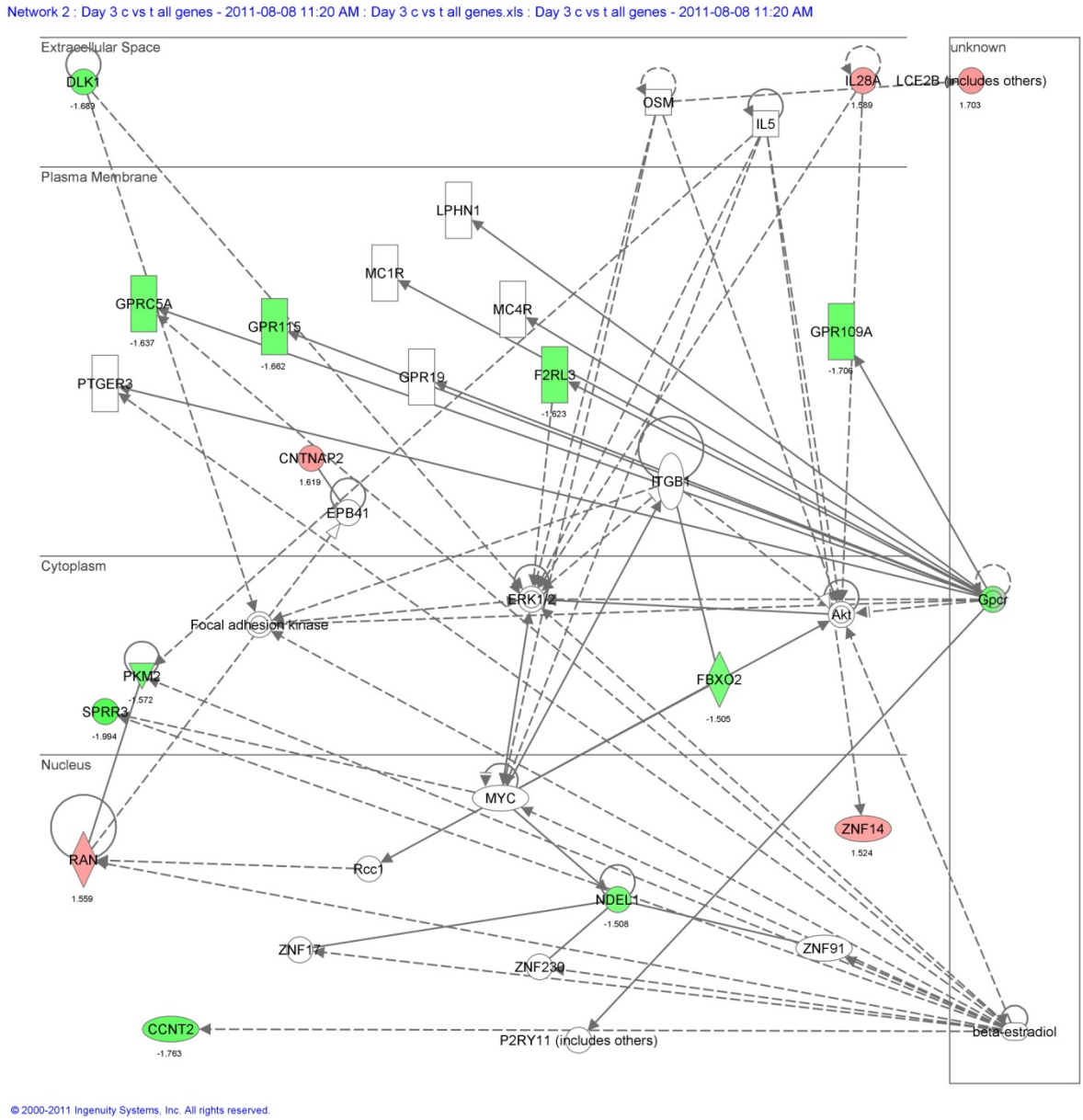

Figure A11. Functional network 2 of genes differentially regulated in response to HBO treatment at day 3

Atop ranking network of significantly associated genes identified to be differentially regulated in response to HBO treatment in the HSE model at day 3. Each of the nodes represents a gene and they are colour – coded to reflect their expression; genes in red were up – regulated, whereas genes in green were down – regulated. The colourless nodes represent genes which were not present in the microarray data, but were added to the network by IPA. The bold line indicates that a gene acts directly on the other gene it was connected to, whereas the dotted line represents a gene indirectly acting on another gene. The gene network was divided into cellular location, including extracellular space, plasma membrane, cytoplasm and nucleus.

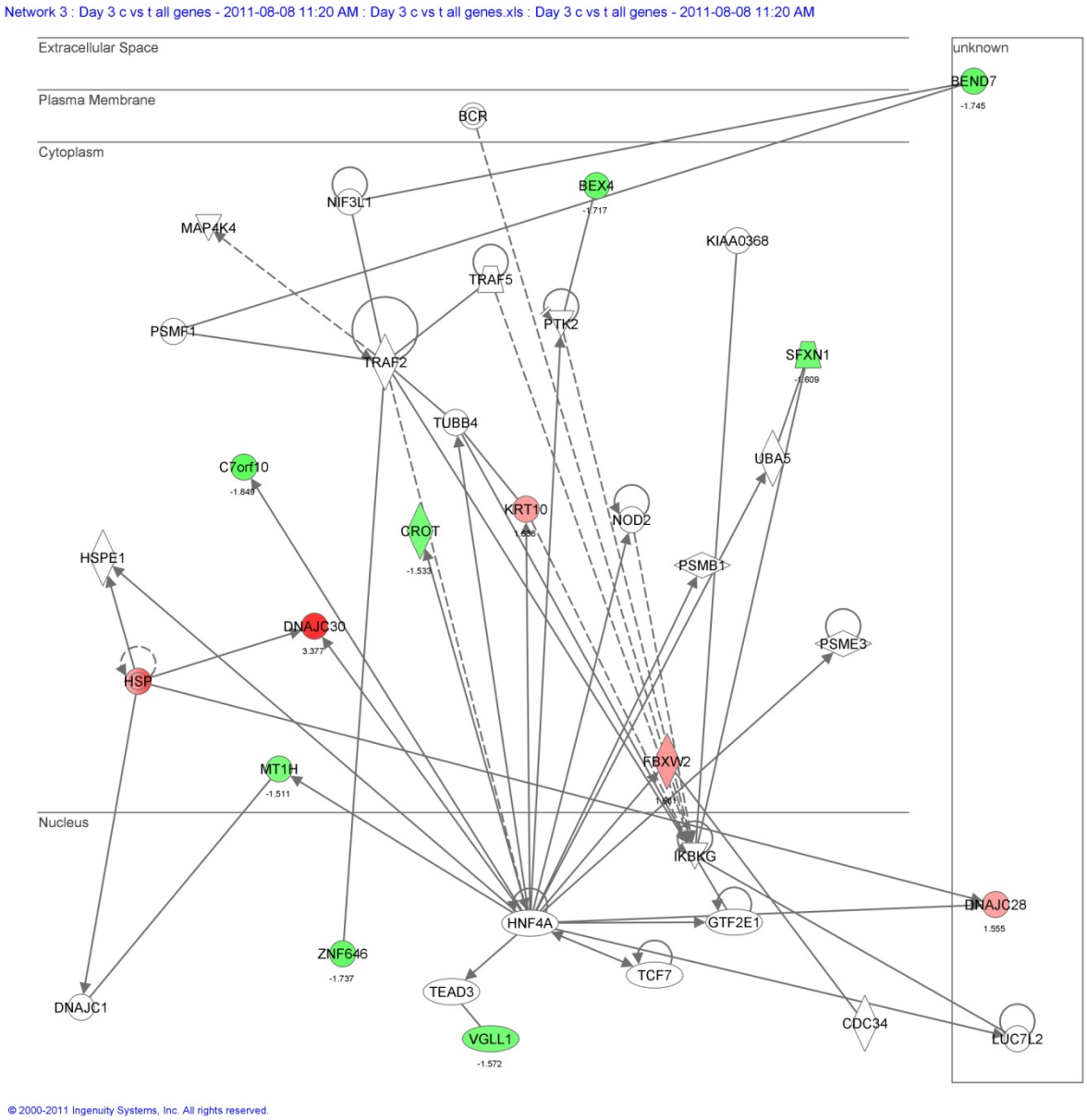

Figure A12. Functional network 3 of genes differentially regulated in response to HBO treatment at day 3

Atop ranking network of significantly associated genes identified to be differentially regulated in response to HBO treatment in the HSE model at day 3. Each of the nodes represents a gene and they are colour – coded to reflect their expression; genes in red were up – regulated, whereas genes in green were down – regulated. The colourless nodes represent genes which were not present in the microarray data, but were added to the network by IPA. The bold line indicates that a gene acts directly on the other gene it was connected to, whereas the dotted line represents a gene indirectly acting on another gene. The gene network was divided into cellular location, including extracellular space, plasma membrane, cytoplasm and nucleus.

Table A43. Functional network analysis of genes differentially regulated in response to HBO treatment at day 5

Network ID	Molecules in network	Score	Focus genes
1	ADAMTS1, ALDH3A1, ATP1B1, CCL20, Cytokeratin, Elastase, FBLN1, HMOX1, HSD17B7, IFN Beta, IgG, IL1, IL1F7, IL1R2, KRT4, KRT13, KRT15, KRT19, LDL, MTTP, NFkB (complex), PCSK5, PNPT1, REG3G, RORA, **S100P**, SERPINA1, SLC7A1, SULT1A1, Tgf beta, TIMP2, TNFRSF9, TRIM16, TXNRD1, VIM	57	27
2	Akt, BIRC3, BTC, CASP14, Caspase, CCNA1, CD63, Cyclin E, DUSP6, ERK1/2, FSH, GAL, hCG, HLA-DRB5, IFI6, IFI27, IGFBP3, IL17RD, IL28A, Insulin, Interferon alpha, Lh, MHC Class II (complex), **KLK7**, MT1H, NADPH oxidase, NDRG2, NFE2L3, PFKFB2, RAPGEF4, Rock, ROCK2, SERPINA3, SLC9A1, Vegf	43	22
3	ANO8, APC, BCL2, BNIP2, BNIPL, C10orf10, CCL1, CCL23, CCR6, COTL1, CTSZ, GM2A, HEXA, Hla-Drb, HPGD, IFI27, IFNG, IL1F7, KIAA1370, KRT15, LAMA3, MCPH1, NNMT, OASL, PNPLA8, PSG4, RARRES1, RNASE1, SERPINA12, SLC35E1, SMARCA4, SOAT1, TIMP4, TNF, ULBP1	28	16

Genes in bold type were deemed as genes of interest and gene expression levels were validated in Chapter 5. The higher the score, the more significant the network was.

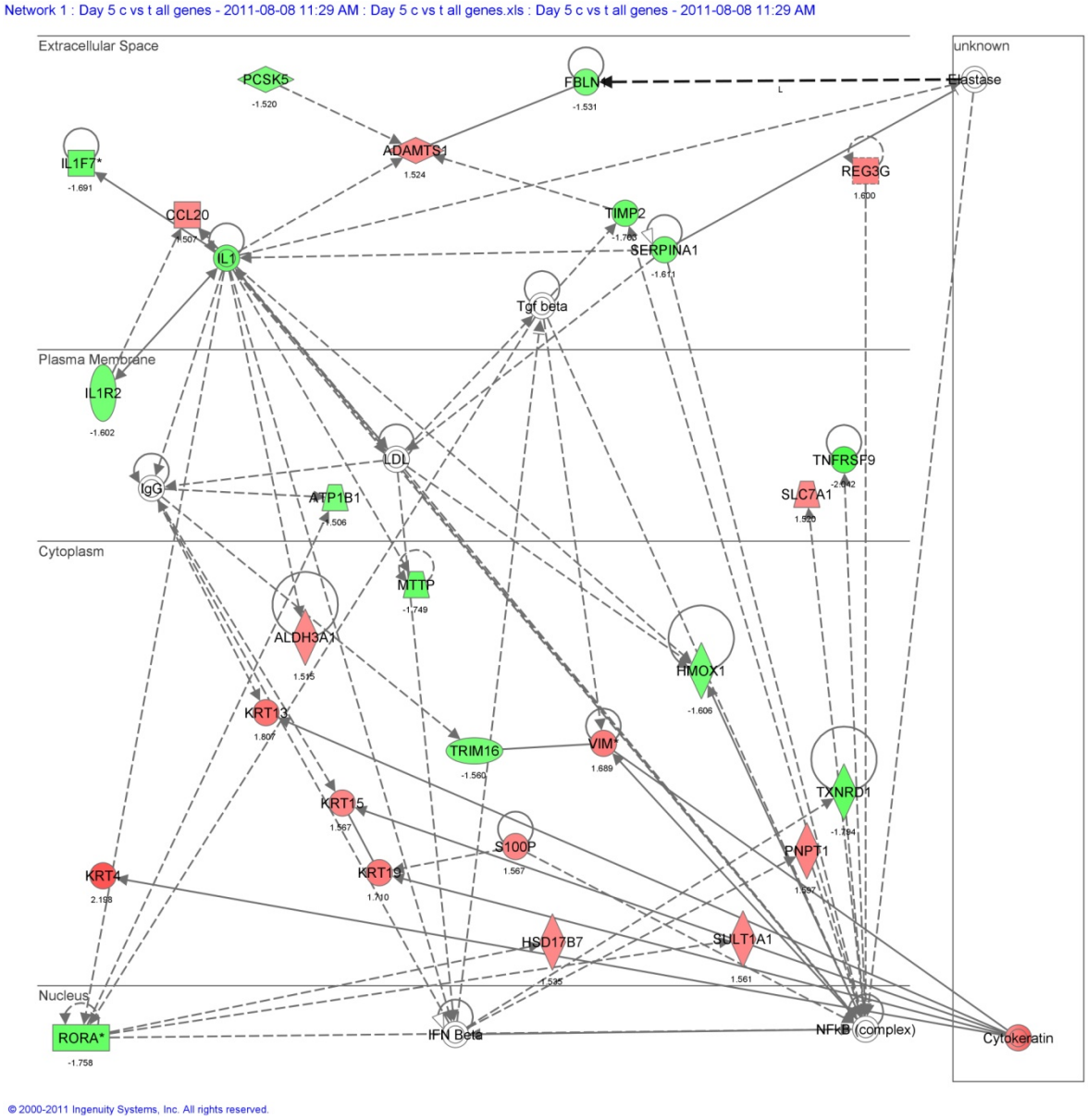

Figure A13. Functional network 1 of genes differentially regulated in response to HBO treatment at day 5

Atop ranking network of significantly associated genes identified to be differentially regulated in response to HBO treatment in the HSE model at day 5. Each of the nodes represents a gene and they are colour – coded to reflect their expression; genes in red were up – regulated, whereas genes in green were down – regulated. The colourless nodes represent genes which were not present in the microarray data, but were added to the network by IPA. The bold line indicates that a gene acts directly on the other gene it was connected to, whereas the dotted line represents a gene indirectly acting on another gene. The gene network was divided into cellular location, including extracellular space, plasma membrane, cytoplasm and nucleus.

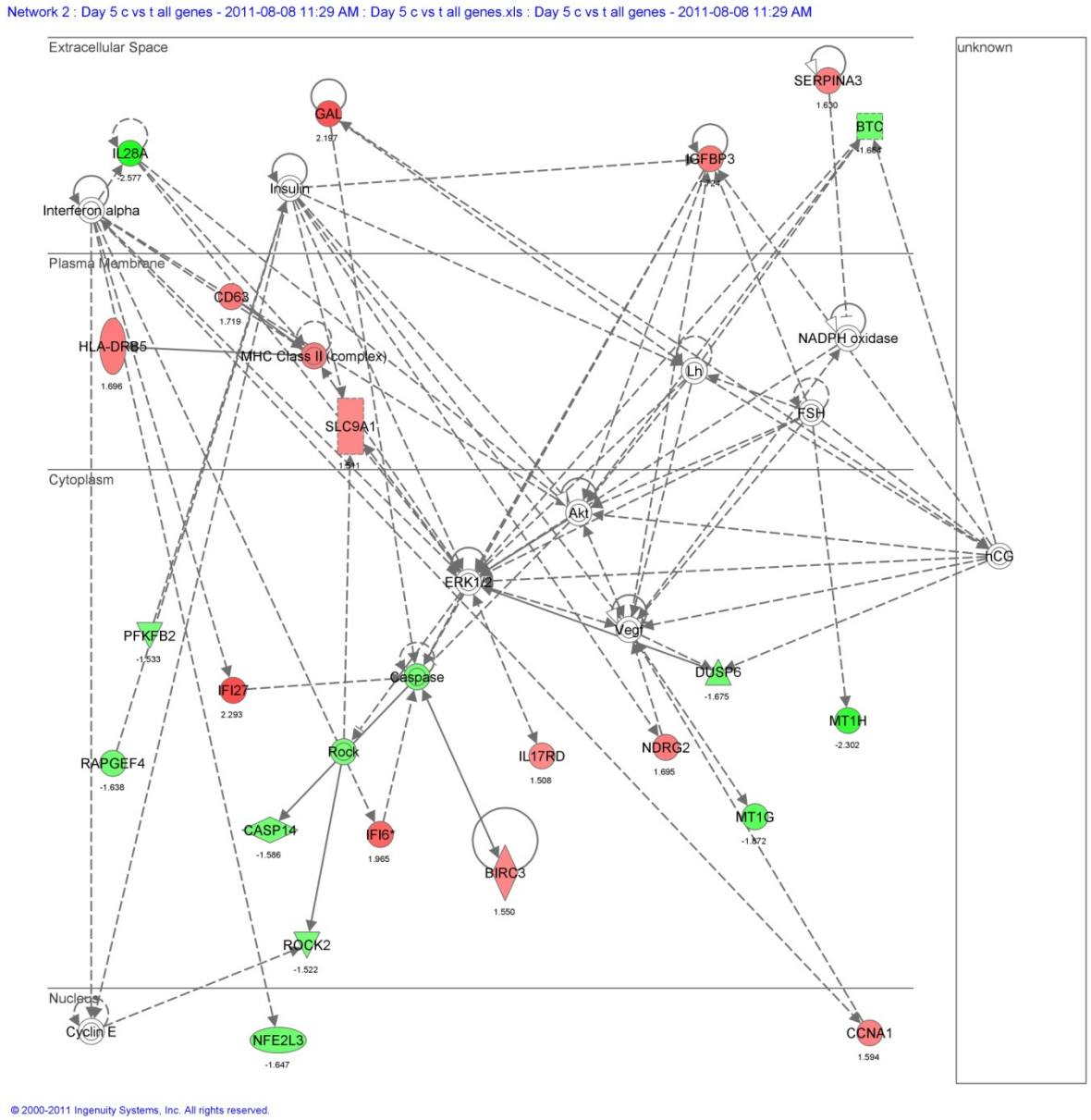

Figure A14. Functional network 2 of genes differentially regulated in response to HBO treatment at day 5

Atop ranking network of significantly associated genes identified to be differentially regulated in response to HBO treatment in the HSE model at day 5. Each of the nodes represents a gene and they are colour – coded to reflect their expression; genes in red were up – regulated, whereas genes in green were down – regulated. The colourless nodes represent genes which were not present in the microarray data, but were added to the network by IPA. The bold line indicates that a gene acts directly on the other gene it was connected to, whereas the dotted line represents a gene indirectly acting on another gene. The gene network was divided into cellular location, including extracellular space, plasma membrane, cytoplasm and nucleus.

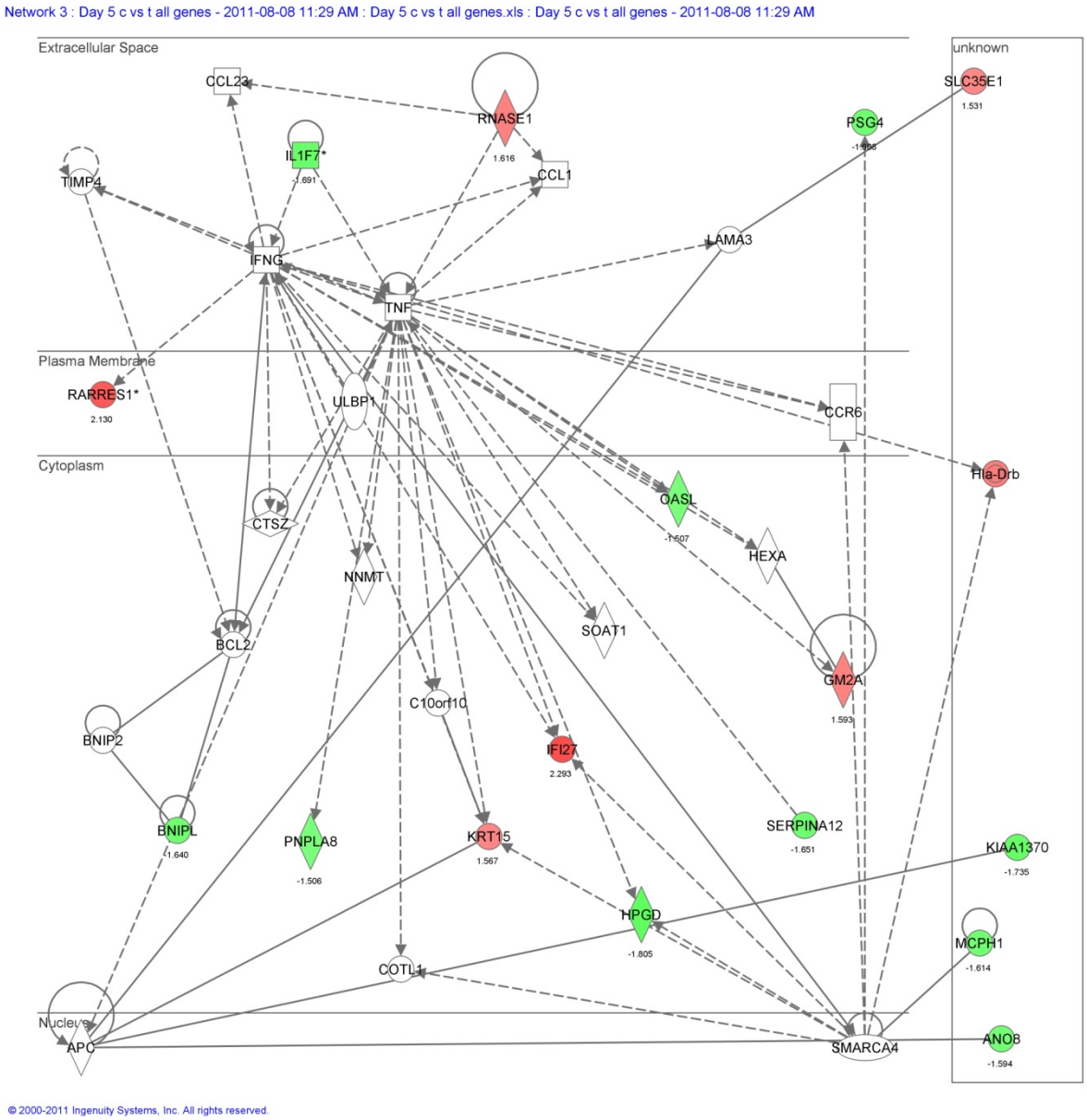

Figure A15. Functional network 3 of genes differentially regulated in response to HBO treatment at day 5

Atop ranking network of significantly associated genes identified to be differentially regulated in response to HBO treatment in the HSE model at day 5. Each of the nodes represents a gene and they are colour – coded to reflect their expression; genes in red were up – regulated, whereas genes in green were down – regulated. The colourless nodes represent genes which were not present in the microarray data, but were added to the network by IPA. The bold line indicates that a gene acts directly on the other gene it was connected to, whereas the dotted line represents a gene indirectly acting on another gene. The gene network was divided into cellular location, including extracellular space, plasma membrane, cytoplasm and nucleus.

Table A44. Functional network analysis of genes differentially regulated in response to HBO treatment at day 9

Network ID	Molecules in network	Score	Focus genes
1	aldehyde dehydrogenase (NAD), ALDH, ALDH1A1, ALDH1A3, ALDH3B2, ALDH4A1, ASNS, CCL20, CD68, CYFIP2, DEFB4A/DEFB4B, E2F7, **EGR1**, FSH, GAL, Growth hormone, GSTM1, hCG, HELLS, IL1R2, Immunoglobulin, **ITGAV**, KLF3, LDL, Lh, MAFF, **KLK7, MT1H**, NAMPT, NFkB (complex), S100A4, SPINK7, TCERG1, TFPI2, Vegf	54	25
2	Actin, Ap1, ARRDC3, ATP6V0B, CASP14, Caspase, CEACAM1 (includes others), CREB1, Cyclin A, DCBLD2, DKK3, ERK1/2, F Actin, GCNT1, IFI27, IFN Beta, IgG, IL1, IL6ST, Insulin, Interferon alpha, KRT13, Mapk, OAS1, P38 MAPK, PDGF BB, Pkc(s), PTGES, Ras homolog, SLC16A6, SLC2A3, THOC4, TMOD3, Ubiquitin, ZBTB16	18	18
3	Acan, AVP, Ca2+, CASP14, CD209, cholecalciferol, CYP27B1, FLG, HAS3, HRNR, KLF10, KRT2, KRT7, MBOAT2, MDH2, NDUFAF4, NMU, NMUR1, NMUR2, OSM, PC, phosphate, PNMT, PRSS22, RAD51C, RAD51L1, RAD51L3, SERPINA3, SERPINB1, SLC2A3, STAT4, TCN1, TGFB1, TNFRSF11B, XRCC2	13	13

Genes in bold type were deemed as genes of interest and gene expression levels were validated in Chapter 5. The higher the score, the more significant the network was.

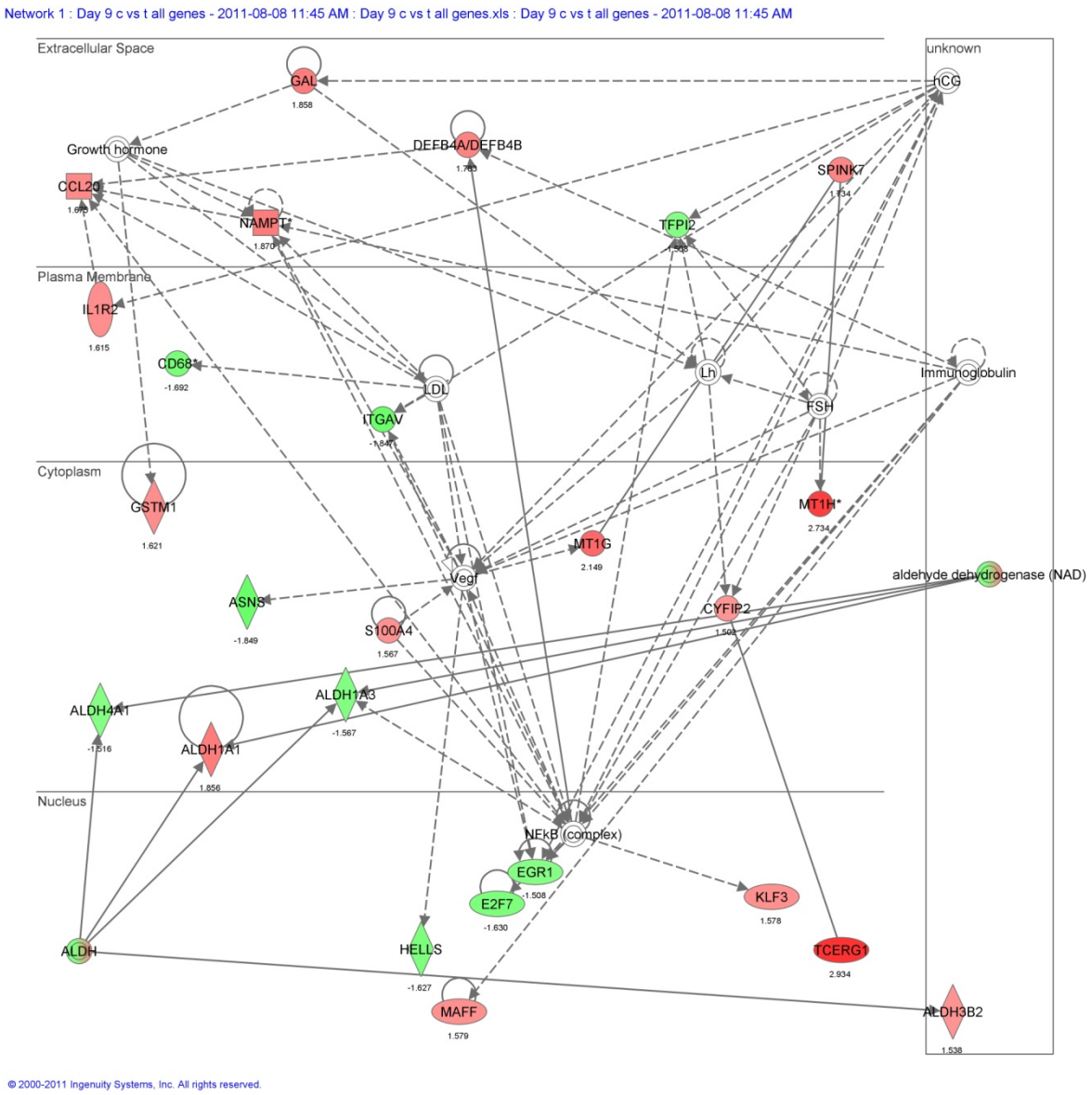

Figure A16. Functional network 1 of genes differentially regulated in response to HBO treatment at day 9

Atop ranking network of significantly associated genes identified to be differentially regulated in response to HBO treatment in the HSE model at day 9. Each of the nodes represents a gene and they are colour – coded to reflect their expression; genes in red were up – regulated, whereas genes in green were down – regulated. The colourless nodes represent genes which were not present in the microarray data, but were added to the network by IPA. The bold line indicates that a gene acts directly on the other gene it was connected to, whereas the dotted line represents a gene indirectly acting on another gene. The gene network was divided into cellular location, including extracellular space, plasma membrane, cytoplasm and nucleus.

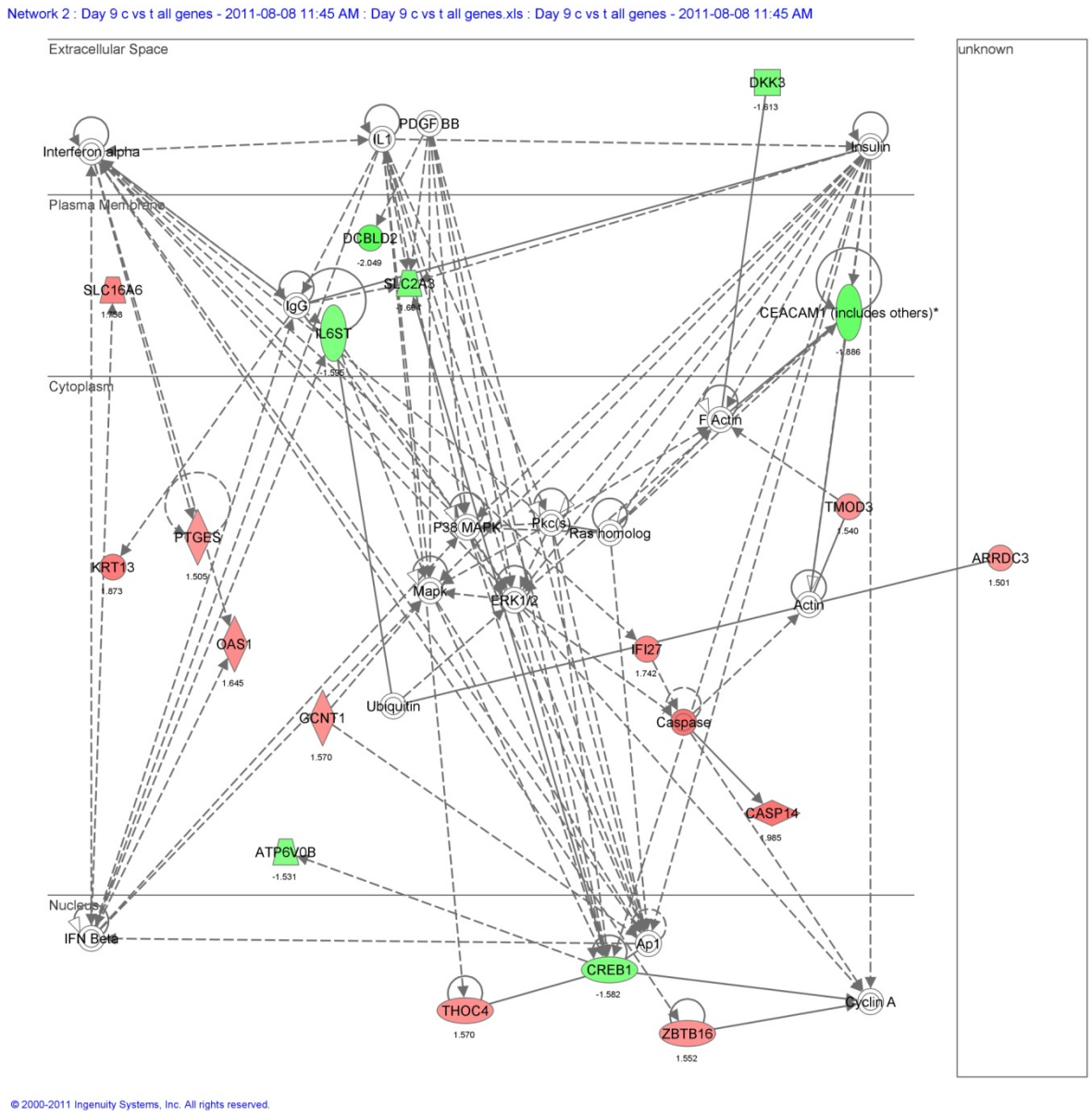

Figure A17. Functional network 2 of genes differentially regulated in response to HBO treatment at day 9

Atop ranking network of significantly associated genes identified to be differentially regulated in response to HBO treatment in the HSE model at day 9. Each of the nodes represents a gene and they are colour – coded to reflect their expression; genes in red were up – regulated, whereas genes in green were down – regulated. The colourless nodes represent genes which were not present in the microarray data, but were added to the network by IPA. The bold line indicates that a gene acts directly on the other gene it was connected to, whereas the dotted line represents a gene indirectly acting on another gene. The gene network was divided into cellular location, including extracellular space, plasma membrane, cytoplasm and nucleus.

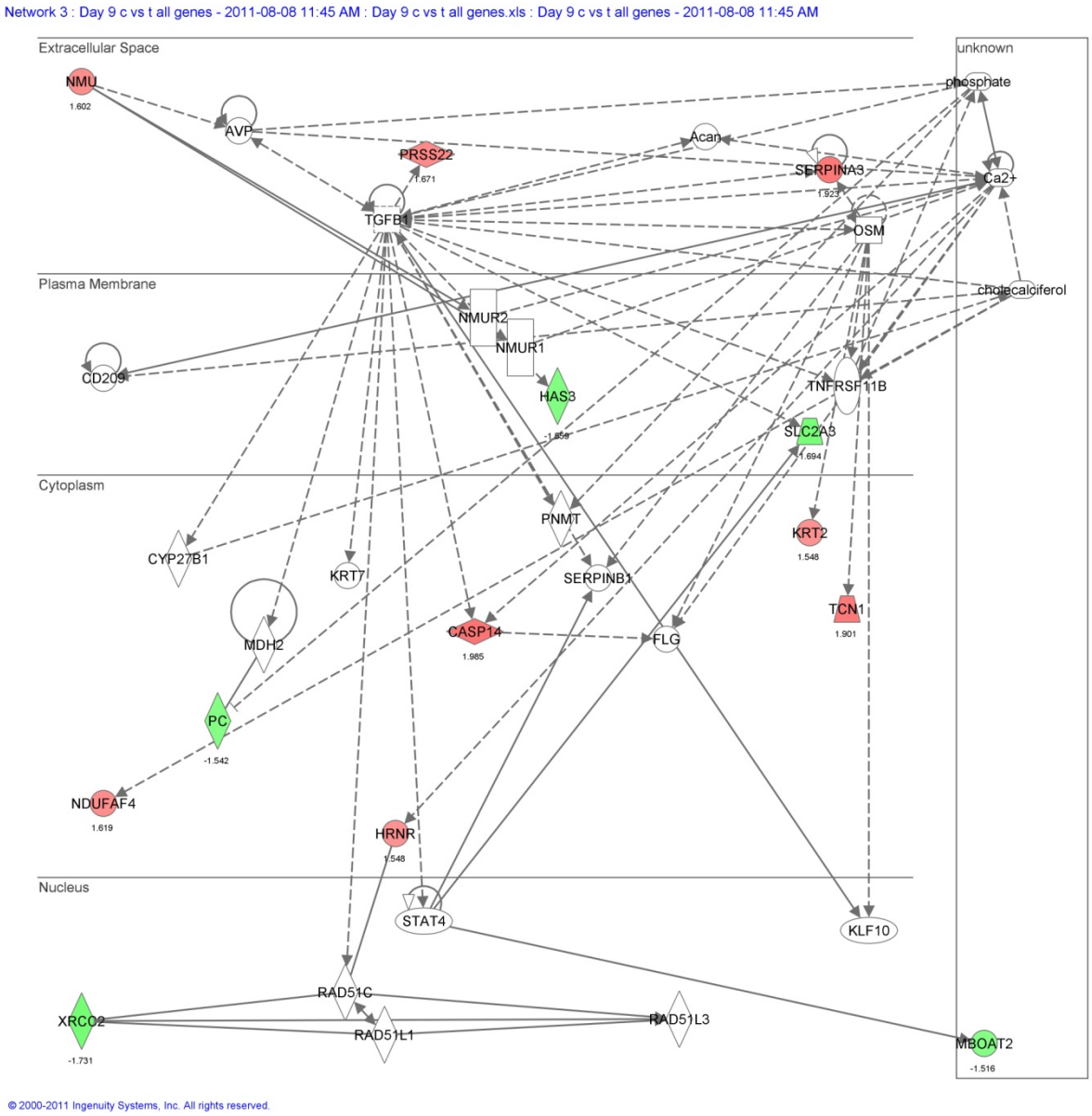

Figure A18. Functional network 3 of genes differentially regulated in response to HBO treatment at day 9

Atop ranking network of significantly associated genes identified to be differentially regulated in response to HBO treatment in the HSE model at day 9. Each of the nodes represents a gene and they are colour – coded to reflect their expression; genes in red were up – regulated, whereas genes in green were down – regulated. The colourless nodes represent genes which were not present in the microarray data, but were added to the network by IPA. The bold line indicates that a gene acts directly on the other gene it was connected to, whereas the dotted line represents a gene indirectly acting on another gene. The gene network was divided into cellular location, including extracellular space, plasma membrane, cytoplasm and nucleus.

Table A45. Summary of MT1G gene expression fold change in HSE models from all patients

MT1G	Day 0	Day 3 Control	Day 3 HBO	Day 5 Control	Day 5 HBO	Day 9 Control	Day 9 HBO
Microarray	1.00	1.82	1.56	2.50	1.34	-6.06	-2.82
Patient 4 HSE	n/a	n/a	n/a	n/a	n/a	n/a	n/a
Patient 5 HSE	1.00 ± 0.00	1.58 ± 0.36	-2.97 ± 0.10	9.00 ± 2.16	130.40 ± 11.83	10.43 ± 0.33	18.03 ± 1.17
Patient 6 HSE	1.00 ± 0.00	101.95 ± 5.83	37.80 ± 2.04	11.25 ± 3.31	124.41 ± 11.24	13.56 ± 3.06	14.42 ± 0.85
Patient 7 HSE	1.00 ± 0.00	146.17 ± 10.72	204.86 ± 15.58	241.11 ± 81.81	72.48 ± 3.50	29.79 ± 2.60	653.68 ± 51.98
Patient 8 HSE	1.00 ± 0.00	-5.19 ± 0.02	79.07 ± 3.35	-4.64 ± 0.13	5.39 ± 2.13	126.03 ± 20.32	4.21 ± 1.40

Table A46. Summary of MT2A gene expression fold change in HSE models from all patients

MT2A	Day 0	Day 3 Control	Day 3 HBO	Day 5 Control	Day 5 HBO	Day 9 Control	Day 9 HBO
Microarray	1.00	1.07	1.10	1.48	1.46	1.90	2.19
Patient 4 HSE	1.00 ± 0.00	1.61 ± 0.28	3.09 ± 0.17	1.07 ± 0.14	1.02 ± 0.04	-1.67 ± 0.07	1.23 ± 0.16
Patient 5 HSE	1.00 ± 0.00	2.61 ± 0.35	2.02 ± 0.03	-1.06 ± 0.22	4.16 ± 0.57	-2.63 ± 0.02	1.08 ± 0.05
Patient 6 HSE	1.00 ± 0.00	-2.34 ± 0.03	-1.94 ± 0.03	-5.15 ± 0.02	-3.01 ± 0.01	-4.88 ± 0.01	-3.27 ± 0.00
Patient 7 HSE	1.00 ± 0.00	-1.38 ± 0.05	-1.22 ± 0.07	-2.48 ± 0.04	-3.67 ± 0.01	-4.79 ± 0.01	-5.39 ± 0.00
Patient 8 HSE	1.00 ± 0.00	-1.11 ± 0.10	-1.21 ± 0.07	-3.66 ± 0.01	-2.84 ± 0.02	-5.01 ± 0.01	-2.37 ± 0.01

Data in the tables represents mean fold change of gene expression (normalised to day 0) ± standard deviation (n = 3).

Table A47. Summary of KLK1 gene expression fold change in HSE models from all patients

KLK1	Day 0	Day 3 Control	Day 3 HBO	Day 5 Control	Day 5 HBO	Day 9 Control	Day 9 HBO
Microarray	1.00	-2.56	-2.58	-4.26	-4.37	-4.47	-3.92
Patient 4	1.00 ± 0.00	3.00 ± 0.25	2.28 ± 0.19	11.79 ± 0.41	3.89 ± 0.17	2.44 ± 0.33	2.67 ± 0.11
Patient 5	1.00 ± 0.00	5.09 ± 0.58	6.34 ± 0.74	3.76 ± 0.15	15.10 ± 2.12	4.58 ± 0.44	3.84 ± 1.09
Patient 6	1.00 ± 0.00	-4.79 ± 0.06	-5.91 ± 0.01	-1.23 ± 0.06	1.83 ± 0.13	-1.89 ± 0.02	1.39 ± 0.17
Patient 7	1.00 ± 0.00	4.11 ± 0.34	3.72 ± 0.28	4.35 ± 1.08	4.11 ± 0.31	5.03 ± 0.15	-1.43 ± 0.04
Patient 8	1.00 ± 0.00	8.94 ± 0.56	3.42 ± 0.52	5.97 ± 0.06	4.10 ± 0.29	4.37 ± 0.65	5.33 ± 0.46

Table A48. Summary of KLK7 gene expression fold change in HSE models from all patients

KLK7	Day 0	Day 3 Control	Day 3 HBO	Day 5 Control	Day 5 HBO	Day 9 Control	Day 9 HBO
Microarray	1.00	-1.86	-3.33	-1.67	-1.91	-1.53	-1.14
Patient 4	1.00 ± 0.00	3.98 ± 0.34	3.50 ± 0.30	5.30 ± 0.71	5.34 ± 1.17	5.18 ± 0.17	-1.53 ± 0.08
Patient 5	1.00 ± 0.00	10.78 ± 1.78	18.24 ± 2.31	4.38 ± 0.52	71.57 ± 8.53	7.74 ± 0.73	9.00 ± 0.88
Patient 6	1.00 ± 0.00	-11.41 ± 0.01	-3.93 ± 0.01	2.29 ± 0.06	2.34 ± 0.31	3.10 ± 0.11	3.85 ± 0.22
Patient 7	1.00 ± 0.00	-1.30 ± 0.05	1.12 ± 0.07	2.99 ± 0.36	2.14 ± 0.18	1.98 ± 0.12	-1.50 ± 0.03
Patient 8	1.00 ± 0.00	3.59 ± 0.47	3.55 ± 0.17	2.51 ± 0.39	1.87 ± 0.09	1.24 ± 0.13	2.44 ± 0.19

Data in the tables represents mean fold change of gene expression (normalised to day 0) ± standard deviation (n = 3).

Table A49. Summary of EGR1 gene expression fold change in HSE models from all patients

EGR1	Day 0	Day 3 Control	Day 3 HBO	Day 5 Control	Day 5 HBO	Day 9 Control	Day 9 HBO
Microarray	1.00	-1.17	1.08	-1.20	-1.13	-1.58	-2.39
Patient 4	1.00 ± 0.00	3.15 ± 0.28	2.71 ± 0.15	1.90 ± 0.32	1.99 ± 0.15	-1.16 ± 0.05	2.13 ± 0.26
Patient 5	1.00 ± 0.00	2.79 ± 0.30	2.47 ± 0.19	1.54 ± 0.13	8.66 ± 1.59	2.19 ± 0.41	3.26 ± 0.46
Patient 6	1.00 ± 0.00	-6.64 ± 0.03	-7.62 ± 0.01	-3.81 ± 0.03	-2.24 ± 0.05	-1.73 ± 0.02	2.31 ± 0.04
Patient 7	1.00 ± 0.00	-1.12 ± 0.03	1.26 ± 0.06	-1.41 ± 0.10	-1.39 ± 0.05	1.51 ± 0.20	2.52 ± 0.42
Patient 8	1.00 ± 0.00	2.72 ± 0.32	2.22 ± 0.25	1.33 ± 0.29	1.60 ± 0.14	1.46 ± 0.51	2.05 ± 0.34

Table A50 Summary of CDCP1 gene expression fold change in HSE models from all patients

CDCP1	Day 0	Day 3 Control	Day 3 HBO	Day 5 Control	Day 5 HBO	Day 9 Control	Day 9 HBO
Microarray	1.00	1.82	1.58	1.31	1.92	2.19	1.37
Patient 4	1.00 ± 0.00	92.90 ± 5.76	94.52 ± 5.97	67.70 ± 2.45	81.04 ± 4.10	53.16 ± 7.28	98.01 ± 8.23
Patient 5	1.00 ± 0.00	1.62 ± 0.11	1.27 ± 0.04	1.04 ± 0.09	3.77 ± 0.45	1.05 ± 0.06	2.23 ± 0.13
Patient 6	1.00 ± 0.00	-12.81 ± 0.01	-12.52 ± 0.01	-6.60 ± 0.01	-1.76 ± 0.03	-1.57 ± 0.03	-1.00 ± 0.06
Patient 7	1.00 ± 0.00	-1.57 ± 0.06	-2.12 ± 0.01	-2.63 ± 0.02	-2.69 ± 0.05	-1.14 ± 0.11	1.67 ± 0.10
Patient 8	1.00 ± 0.00	-1.14 ± 0.11	1.67 ± 0.10	-1.70 ± 0.07	-2.09 ± 0.04	-2.15 ± 0.09	-2.39 ± 0.04

Data in the tables represents mean fold change of gene expression (normalised to day 0) ± standard deviation (n = 3).

Table A51. Summary of EGR3 gene expression fold change in HSE models from all patients

EGR3	Day 0	Day 3 Control	Day 3 HBO	Day 5 Control	Day 5 HBO	Day 9 Control	Day 9 HBO
Microarray	1.00	1.13	-1.08	-1.58	-2.10	-3.51	-3.76
Patient 4	1.00 ± 0.00	6.70 ± 0.55	3.27 ± 0.15	2.61 ± 0.55	3.12 ± 0.70	1.90 ± 0.10	2.70 ± 0.19
Patient 5	1.00 ± 0.00	1.64 ± 0.28	1.88 ± 0.02	2.62 ± 0.18	12.97 ± 0.39	4.16 ± 0.49	8.76 ± 1.05
Patient 6	1.00 ± 0.00	-8.65 ± 0.01	-7.15 ± 0.01	-4.41 ± 0.02	-1.10 ± 0.11	2.39 ± 0.41	1.58 ± 0.06
Patient 7	1.00 ± 0.00	3.36 ± 0.28	1.54 ± 0.06	2.40 ± 0.16	-1.19 ± 0.03	2.43 ± 0.06	3.45 ± 0.09
Patient 8	1.00 ± 0.00	-1.33 ± 0.08	-2.63 ± 0.03	-1.26 ± 0.07	-2.17 ± 0.03	-1.40 ± 0.04	-2.11 ± 0.03

Table A52. Summary of GRHL3 gene expression fold change in HSE models from all patients

GRHL3	Day 0	Day 3 Control	Day 3 HBO	Day 5 Control	Day 5 HBO	Day 9 Control	Day 9 HBO
Microarray	1.00	-1.27	-1.31	-1.93	-2.29	-2.77	-2.74
Patient 4	1.00 ± 0.00	18.61 ± 1.17	21.07 ± 1.57	24.93 ± 3.64	24.98 ± 0.02	20.41 ± 0.30	16.91 ± 0.93
Patient 5	1.00 ± 0.00	11.63 ± 0.30	4.08 ± 2.16	4.75 ± 0.79	44.92 ± 2.25	13.35 ± 1.91	8.89 ± 1.79
Patient 6	1.00 ± 0.00	-16.97 ± 0.01	-11.51 ± 0.01	-1.19 ± 0.10	-2.28 ± 0.10	1.30 ± 0.05	1.33 ± 0.39
Patient 7	1.00 ± 0.00	1.55 ± 0.06	1.22 ± 0.11	1.14 ± 0.29	1.99 ± 0.06	5.68 ± 0.04	5.03 ± 0.38
Patient 8	1.00 ± 0.00	-1.12 ± 0.20	1.01 ± 0.05	1.04 ± 0.06	1.08 ± 0.09	1.04 ± 0.07	2.49 ± 0.27

Data in the tables represents mean fold change of gene expression (normalised to day 0) ± standard deviation (n = 3).

Table A53. Summary of ITGAV gene expression fold change in HSE models from all patients

ITGAV	**Day 0**	**Day 3 Control**	**Day 3 HBO**	**Day 5 Control**	**Day 5 HBO**	**Day 9 Control**	**Day 9 HBO**
Microarray	1.00	1.12	1.12	-1.03	1.18	1.06	-1.74
Patient 4	1.00 ± 0.00	28.84 ± 1.44	16.40 ± 3.33	18.50 ± 1.38	12.44 ± 0.57	16.21 ± 1.42	14.66 ± 0.77
Patient 5	1.00 ± 0.00	3.38 ± 0.14	1.41 ± 0.09	1.31 ± 0.09	8.26 ± 1.52	5.52 ± 0.48	1.49 ± 0.09
Patient 6	1.00 ± 0.00	-11.61 ± 0.02	-12.27 ± 0.00	-3.85 ± 0.07	-2.04 ± 0.06	-2.93 ± 0.05	-2.11 ± 0.07
Patient 7	1.00 ± 0.00	-1.55 ± 0.02	-2.31 ± 0.06	-2.10 ± 0.07	-1.24 ± 0.04	-1.46 ± 0.01	-1.64 ± 0.16
Patient 8	1.00 ± 0.00	2.10 ± 0.28	3.43 ± 0.76	1.30 ± 0.11	1.50 ± 0.13	3.43 ± 0.33	4.55 ± 0.55

Table A54. Summary of S100A8 gene expression fold change in HSE models from all patients

S100A8	**Day 0**	**Day 3 Control**	**Day 3 HBO**	**Day 5 Control**	**Day 5 HBO**	**Day 9 Control**	**Day 9 HBO**
Microarray	n/a	n/a	n/a	n/a	n/a	n/a	n/a
Patient 4	1.00 ± 0.00	3.03 ± 0.49	4.40 ± 0.27	3.76 ± 0.45	2.58 ± 0.14	2.75 ± 0.14	2.63 ± 0.14
Patient 5	1.00 ± 0.00	6.04 ± 0.82	14.38 ± 1.41	2.39 ± 0.15	20.72 ± 0.65	3.98 ± 0.27	3.02 ± 0.26
Patient 6	1.00 ± 0.00	-6.04 ± 0.01	-5.80 ± 0.01	-3.57 ± 0.01	1.02 ± 0.09	-1.51 ± 0.04	1.02 ± 0.14
Patient 7	1.00 ± 0.00	1.18 ± 0.07	1.58 ± 0.10	2.54 ± 0.24	1.54 ± 0.09	1.78 ± 0.15	2.12 ± 0.11
Patient 8	1.00 ± 0.00	3.31 ± 0.29	1.28 ± 0.05	1.21 ± 0.17	2.18 ± 0.29	2.85 ± 0.08	2.50 ± 0.06

Data in the tables represents mean fold change of gene expression (normalised to day 0) ± standard deviation (n = 3).

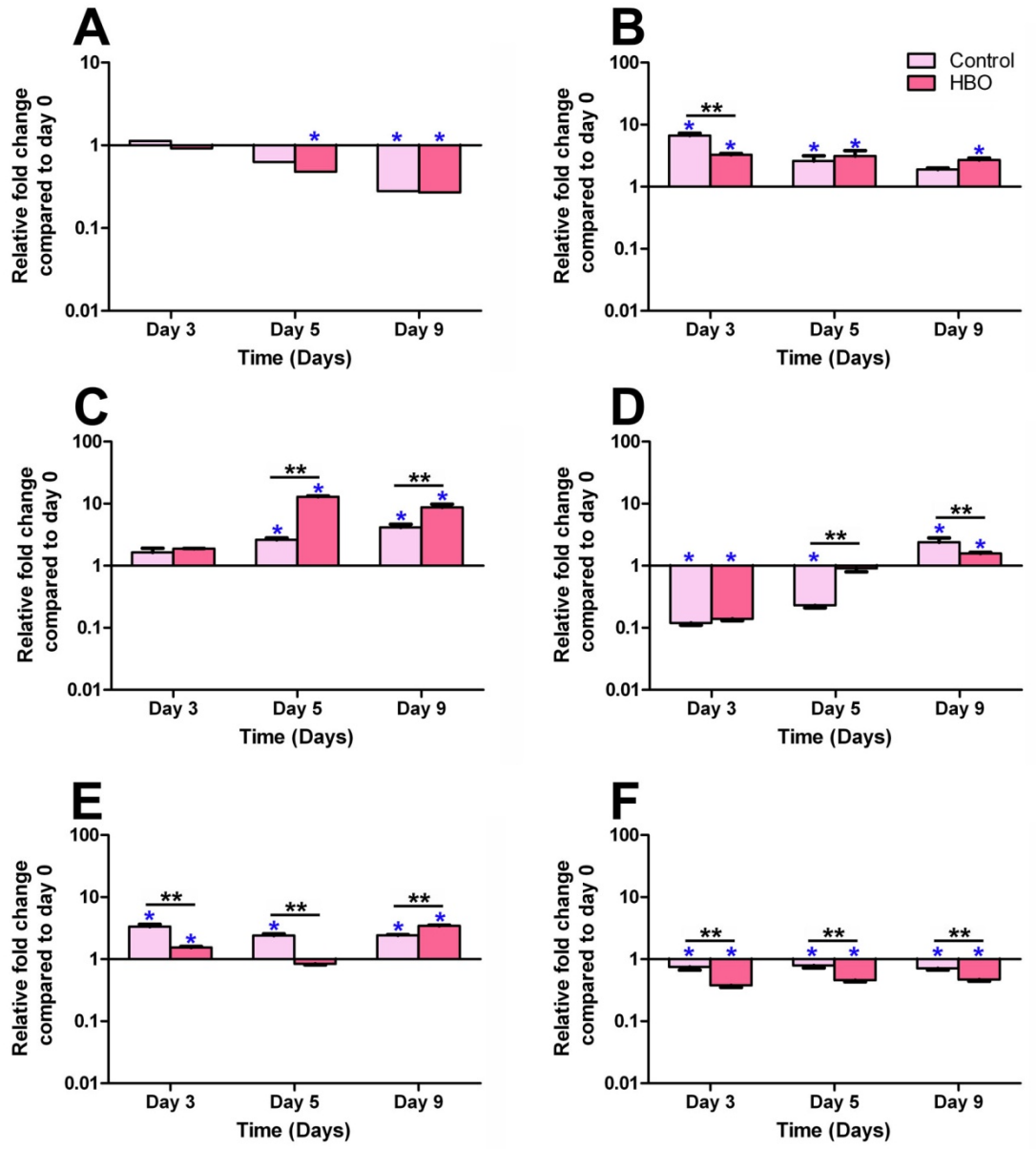

Figure A19. The effect of HBO treatment on *EGR3* gene expression in the HSE model
Gene expression analysis of *EGR3* was performed on total mRNA isolated from the epidermis of the developing HSE. The data was obtained from (**A**) microarray analysis of RNA pooled from group A skin samples. (**B**) *EGR3* qRT-PCR data from HSE models created using sample 4, (**C**) sample 5, (**D**) sample 6, (**E**) sample 7 and (**F**) sample 8. Data was normalised to the day 0 HSE and represents the mean *EGR3* fold change in gene expression ± standard deviation of technical replicates (n = 3). Statistical significance $p < 0.05$ between treatment groups on a given day was represented by **, whereas statistical difference $p < 0.05$ to the day 0 time point was represented by *.

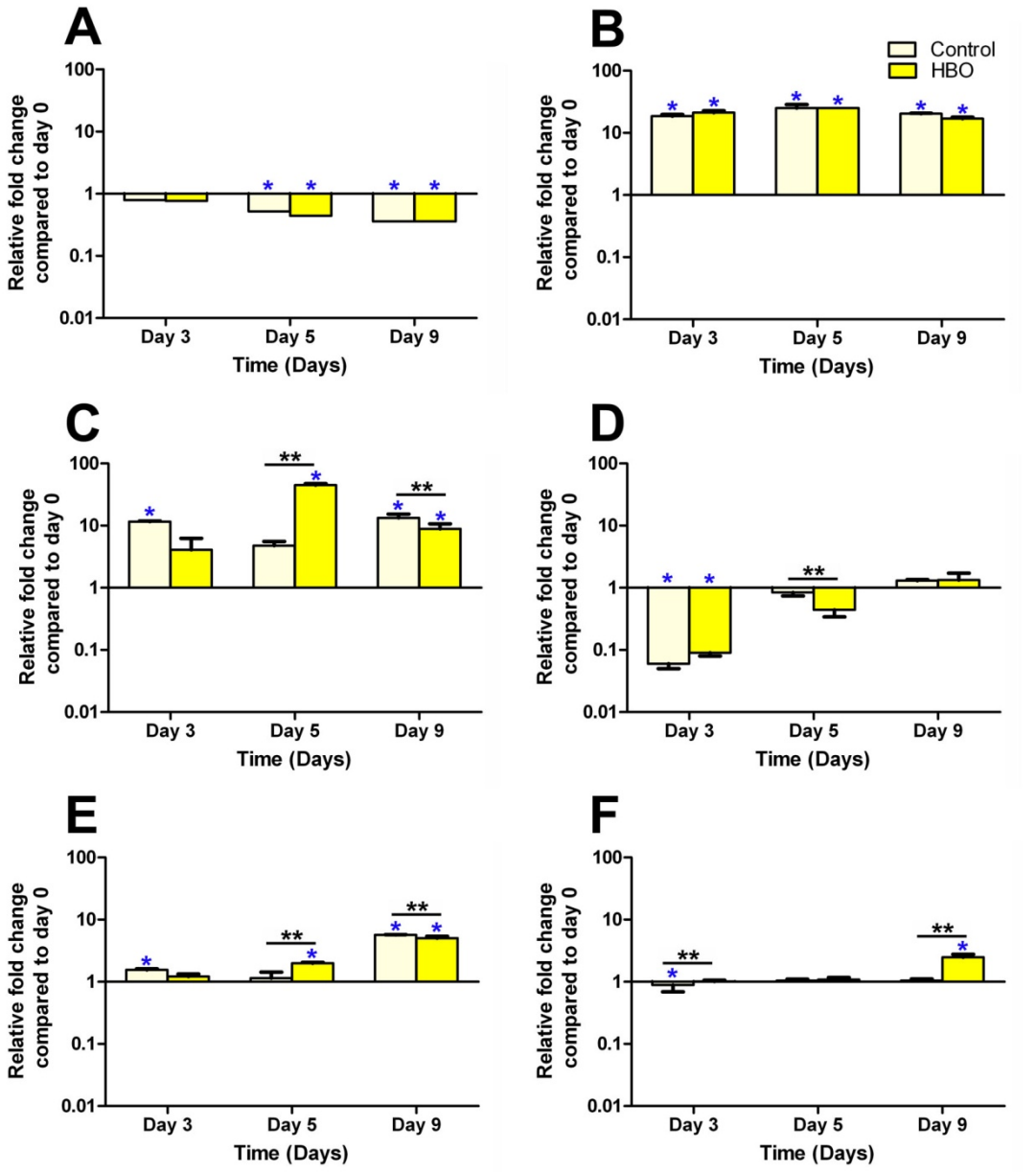

Figure A20. The effect of HBO treatment on *GRHL3* gene expression in the HSE model
Gene expression analysis of *GRHL3* was performed on total mRNA isolated from the epidermis of the developing HSE. The data was obtained from (**A**) microarray analysis of RNA pooled from group A skin samples. (**B**) *GRHL3* qRT-PCR data from HSE models created using sample 4, (**C**) sample 5, (**D**) sample 6, (**E**) sample 7 and (**F**) sample 8. Data was normalised to the day 0 HSE and represents the mean *GRHL3* fold change in gene expression ± standard deviation of technical replicates (n = 3). Statistical significance $p < 0.05$ between treatment groups on a given day was represented by **, whereas statistical difference $p < 0.05$ to the day 0 time point was represented by *.

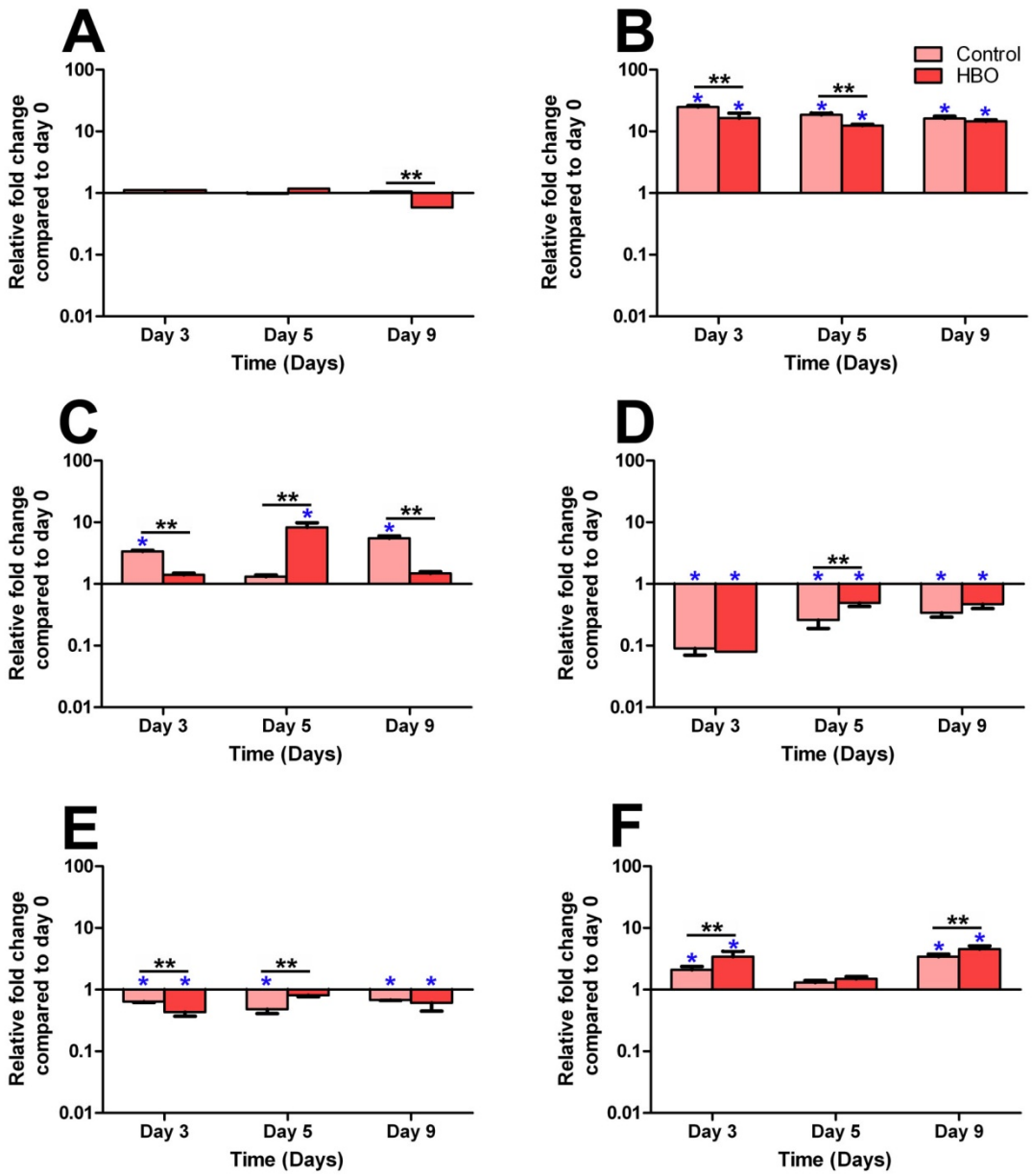

Figure A21. The effect of HBO treatment on *ITGAV* gene expression in the HSE model
Gene expression analysis of *ITGAV* was performed on total mRNA isolated from the epidermis of the developing HSE. The data was obtained from (**A**) microarray analysis of RNA pooled from group A skin samples. (**B**) *ITGAV* qRT-PCR data from HSE models created using sample 4, (**C**) sample 5, (**D**) sample 6, (**E**) sample 7 and (**F**) sample 8. Data was normalised to the day 0 HSE and represents the mean *ITGAV* fold change in gene expression ± standard deviation of technical replicates (n = 3). Statistical significance $p < 0.05$ between treatment groups on a given day was represented by **, whereas statistical difference $p < 0.05$ to the day 0 time point was represented by *.

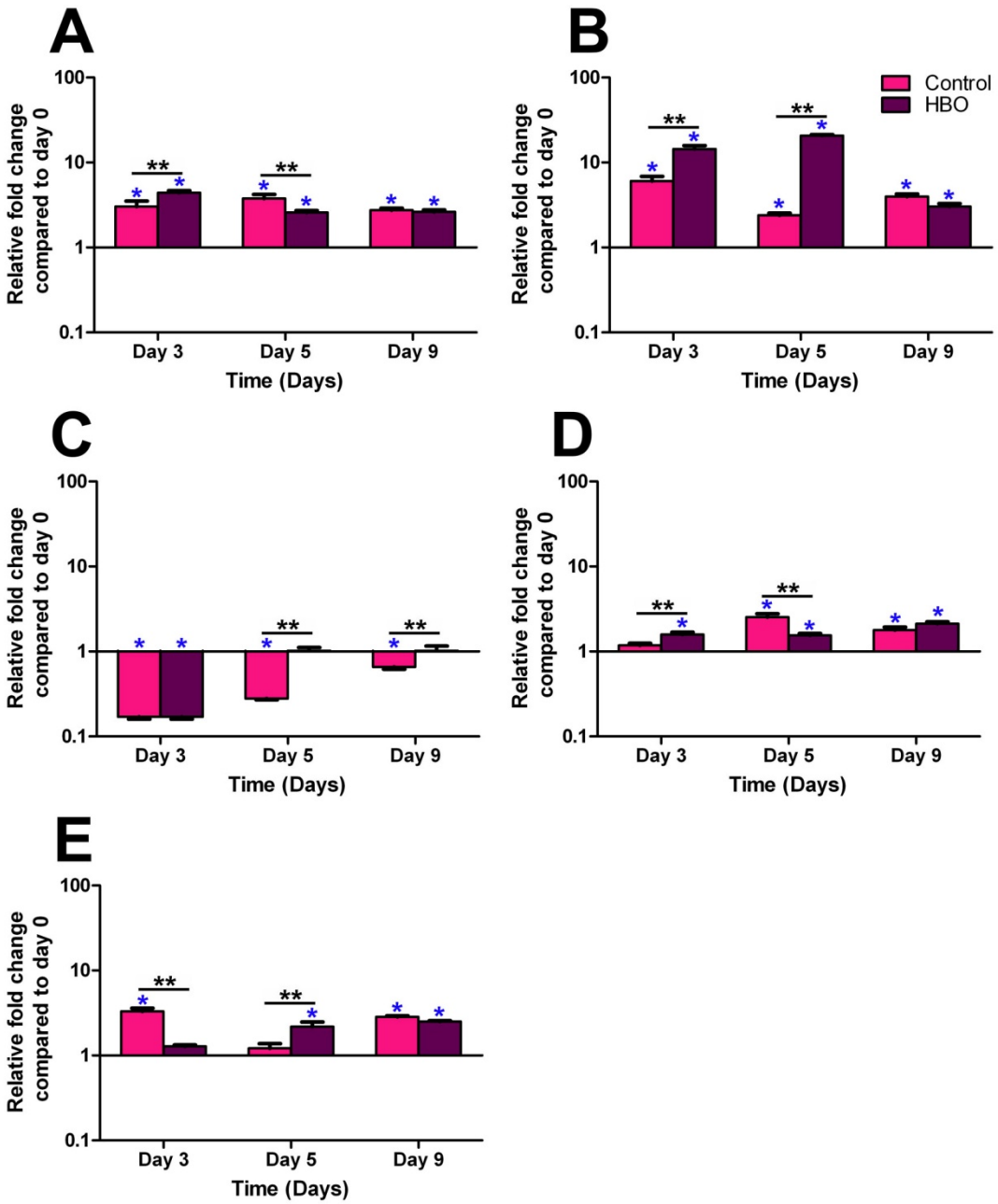

Figure A22. The effect of HBO treatment on *S100A8* gene expression in the HSE model
Gene expression analysis of *S100A8* was performed on total mRNA isolated from the epidermis of the developing HSE. The data was obtained from (**A**) *S100A8* qRT-PCR data from HSE models created using sample 4, (**B**) sample 5, (**C**) sample 6, (**D**) sample 7 and (**E**) sample 8. Data was normalised to the day 0 HSE and represents the mean *S100A8* fold change in gene expression ± standard deviation of technical replicates (n = 3). Statistical significance $p < 0.05$ between treatment groups on a given day was represented by **, whereas statistical difference $p < 0.05$ to the day 0 time point was represented by *.

Table A55. Summary of the thickness of MT - positive epidermis in the HSE epidermis: Group A

MT	Sample 1 (µm)	Sample 2 (µm)	Sample 3 (µm)	Average (µm)
Native skin	n/a	n/a	n/a	39.28 ± 17.27
Day 0	1.79 ± 1.08	4.05 ± 3.07	3.32 ± 4.77	3.05 ± 3.33
Day 3 CON	42.64 ± 7.35	63.96 ± 14.53	32.46 ± 5.23	46.35 ± 16.39
Day 3 HBO	46.64 ± 16.90	56.67 ± 15.30	27.65 ± 5.27	43.65 ± 17.83
Day 5 CON	61.48 ± 15.55	37.25 ± 10.58	49.66 ± 10.12	49.46 ± 15.52
Day 5 HBO	52.62 ± 15.90	42.09 ± 9.94	50.75 ± 10.19	48.49 ± 12.67
Day 9 CON	39.83 ± 8.94	29.45 ± 9.15	43.50 ± 8.53	37.59 ± 10.44
Day 9 HBO	49.37 ± 12.75	46.59 ± 15.18	57.86 ± 13.36	51.27 ± 14.07

Data present in the table represents mean thickness of epidermis immunoreacting positive for MT (µm) ± standard deviation.

Table A56. Summary of the thickness of MT - positive epidermis in the HSE epidermis: Group B

MT	Sample 4 (µm)	Sample 5 (µm)	Sample 6 (µm)	Sample 7 (µm)	Sample 8 (µm)
Native skin	34.55 ± 12.08	25.39 ± 5.28	26.50 ± 6.11	21.61 ± 3.91	26.73 ± 8.23
Day 0	1.95 ± 1.90	6.65 ± 4.84	0.08 ± 0.12	10.13 ± 2.73	11.64 ± 4.23
Day 3 CON	53.20 ± 10.22	42.40 ± 10.85	40.56 ± 5.89	40.72 ± 11.58	45.29 ± 10.75
Day 3 HBO	52.27 ± 13.00	38.08 ± 8.94	34.16 ± 8.00	41.93 ± 7.60	42.33 ± 9.36
Day 5 CON	55.76 ± 15.62	52.54 ± 13.34	56.12 ± 6.94	31.99 ± 12.18	34.76 ± 9.72
Day 5 HBO	53.82 ± 13.22	48.43 ± 14.80	61.40 ± 9.69	36.43 ± 10.11	36.75 ± 10.1
Day 9 CON	53.94 ± 15.40	31.81 ± 9.22	51.90 ± 7.53	23.12 ± 6.69	34.27 ± 6.12
Day 9 HBO	27.75 ± 9.35	50.66 ± 11.82	36.66 ± 12.99	22.12 ± 8.32	35.83 ± 15.18

Data present in the table represents mean thickness of epidermis immunoreacting positive for MT (µm) ± standard deviation.

Table A57. Summary of the thickness of KLK1 - positive epidermis in the HSE epidermis: Group A

KLK1	Sample 1 (µm)	Sample 2 (µm)	Sample 3 (µm)	Average (µm)
Native skin	n/a	n/a	n/a	76.10 ± 24.44
Day 0	4.56 ± 5.38	7.86 ± 4.74	14.45 ± 13.70	9.96 ± 9.13
Day 3 CON	60.16 ± 23.80	86.95 ± 16.81	37.79 ± 7.29	61.63 ± 26.38
Day 3 HBO	60.31 ± 22.97	65.64 ± 20.95	40.64 ± 10.15	55.53 ± 21.13
Day 5 CON	104.36 ± 22.37	113.56 ± 24.26	99.84 ± 20.05	105.92 ± 22.08
Day 5 HBO	122.63 ± 21.79	97.59 ± 22.84	94.16 ± 20.97	104.79 ± 24.60
Day 9 CON	84.99 ± 14.25	41.57 ± 8.44	67.61 ± 17.34	64.72 ± 22.52
Day 9 HBO	75.65 ± 11.40	61.72 ± 13.14	68.54 ± 21.78	68.64 ± 16.44

Data present in the table represents mean thickness of epidermis immunoreacting positive for KLK1 (µm) ± standard deviation.

Table A58. Summary of the thickness of KLK1 - positive epidermis in the HSE epidermis: Group B

KLK1	Sample 4 (µm)	Sample 5 (µm)	Sample 6 (µm)	Sample 7 (µm)	Sample 8 (µm)
Native skin	65.33 ± 15.01	52.73 ± 11.06	57.89 ± 9.76	42.88 ± 5.01	57.73 ± 10.13
Day 0	12.32 ± 10.05	18.10 ± 6.53	11.09 ± 7.79	15.55 ± 3.43	11.68 ± 6.81
Day 3 CON	61.05 ± 15.76	51.00 ± 11.73	55.43 ± 10.35	70.76 ± 12.71	72.66 ± 17.39
Day 3 HBO	64.76 ± 15.42	52.81 ± 9.71	52.06 ± 12.73	80.66 ± 22.67	50.62 ± 10.53
Day 5 CON	105.43 ± 28.04	76.74 ± 20.61	77.28 ± 12.58	60.79 ± 10.99	86.02 ± 24.48
Day 5 HBO	111.82 ± 26.02	68.03 ± 22.98	71.07 ± 25.43	56.54 ± 15.60	76.94 ± 17.01
Day 9 CON	82.27 ± 20.33	52.63 ± 11.61	51.62 ± 6.23	44.63 ± 13.74	57.32 ± 18.57
Day 9 HBO	80.79 ± 25.24	50.97 ± 9.77	51.82 ± 8.56	37.56 ± 16.57	65.28 ± 12.19

Data present in the table represents mean thickness of epidermis immunoreacting positive for KLK1 (µm) ± standard deviation.

Table A59. Summary of the thickness of KLK7 - positive epidermis in the HSE epidermis: Group A

KLK7	Sample 1 (µm)	Sample 2 (µm)	Sample 3 (µm)	Average (µm)
Native skin	n/a	n/a	n/a	30.14 ± 10.55
Day 0	0.09 ± 0.17	0.00 ± 0.00	0.00 ± 0.00	0.03 ± 0.11
Day 3 CON	18.06 ± 8.74	27.46 ± 10.04	14.26 ± 4.18	19.93 ± 9.56
Day 3 HBO	6.44 ± 2.98	17.04 ± 3.40	18.88 ± 4.29	14.12 ± 6.57
Day 5 CON	58.43 ± 12.17	51.81 ± 8.03	40.58 ± 7.12	50.27 ± 11.70
Day 5 HBO	49.85 ± 11.45	58.43 ± 10.98	37.39 ± 8.92	48.56 ± 13.37
Day 9 CON	33.45 ± 8.82	27.53 ± 7.33	39.92 ± 5.81	31.30 ± 7.60
Day 9 HBO	48.95 ± 11.66	26.32 ± 3.23	31.46 ± 7.16	35.58 ± 12.57

Data present in the table represents mean thickness of epidermis immunoreacting positive for KLK7 (µm) ± standard deviation.

Table A60. Summary of the thickness of KLK7 - positive epidermis in the HSE epidermis: Group B

KLK7	Sample 4 (µm)	Sample 5 (µm)	Sample 6 (µm)	Sample 7 (µm)	Sample 8 (µm)
Native skin	17.48 ± 5.71	20.33 ± 4.01	29.56 ± 7.54	20.24 ± 3.04	18.51 ± 3.81
Day 0	0.80 ± 1.35	0.36 ± 0.58	0.00 ± 0.00	0.36 ± 0.62	0.22 ± 0.39
Day 3 CON	5.82 ± 3.15	22.57 ± 3.37	18.03 ± 3.49	25.57 ± 6.45	14.99 ± 4.62
Day 3 HBO	11.82 ± 5.78	20.58 ± 5.15	8.88 ± 3.81	29.08 ± 8.38	17.47 ± 4.92
Day 5 CON	49.72 ± 13.35	33.47 ± 5.91	36.60 ± 4.54	31.38 ± 7.08	35.58 ± 11.60
Day 5 HBO	57.18 ± 18.56	36.91 ± 12.71	25.98 ± 3.20	34.49 ± 8.54	37.21 ± 12.01
Day 9 CON	35.80 ± 10.28	16.55 ± 2.94	25.61 ± 4.86	14.44 ± 6.08	28.66 ± 8.27
Day 9 HBO	20.32 ± 15.82	16.72 ± 4.89	5.24 ± 1.14	12.81 ± 5.87	26.01 ± 8.97

Data present in the table represents mean thickness of epidermis immunoreacting positive for KLK7 (µm) ± standard deviation.

Table A61. Summary of the number of EGR1 positive nuclei in the HSE epidermis: Group A

EGR1	Sample 1 (# nuclei)	Sample 2 (# nuclei)	Sample 3 (# nuclei)	Average (# nuclei)
Native skin	n/a	n/a	n/a	99.79 ± 30.09
Day 0	5.13 ± 2.64	2.75 ± 1.75	2.00 ± 1.31	3.29 ± 2.33
Day 3 CON	66.50 ± 19.10	55.50 ± 15.52	33.25 ± 8.05	51.75 ± 20.09
Day 3 HBO	55.75 ± 16.75	47.13 ± 7.43	27.00 ± 8.33	43.29 ± 16.58
Day 5 CON	58.25 ± 9.77	57.00 ± 11.24	71.00 ± 25.32	62.08 ± 17.45
Day 5 HBO	80.63 ± 31.03	55.00 ± 13.35	59.00 ± 13.03	64.88 ± 23.04
Day 9 CON	60.38 ± 12.24	29.38 ± 5.95	41.63 ± 13.67	43.79 ± 16.82
Day 9 HBO	73.75 ± 34.55	31.63 ± 11.71	49.63 ± 14.24	51.67 ± 27.89

Data present in the table represents mean number of nuclei immunoreacting positive for EGR1 ± standard deviation.

Table A62. Summary of the number of EGR1 positive nuclei in the HSE epidermis: Group B

EGR1	Sample 4 (# nuclei)	Sample 5 (# nuclei)	Sample 6 (# nuclei)	Sample 7 (# nuclei)	Sample 8 (# nuclei)
Native skin	91.63 ± 45.34	109.25 ± 23.30	94.50 ± 9.43	63.25 ± 11.16	114.75 ± 30.05
Day 0	4.50 ± 3.44	12.56 ± 4.43	1.00 ± 0.93	8.38 ± 3.54	6.50 ± 2.13
Day 3 CON	61.38 ± 19.31	51.44 ± 12.03	49.00 ± 13.16	49.13 ± 10.39	70.50 ± 11.42
Day 3 HBO	90.13 ± 18.37	50.63 ± 10.01	55.50 ± 13.65	71.94 ± 14.91	65.50 ± 11.51
Day 5 CON	107.19 ± 15.44	73.94 ± 24.08	61.63 ± 7.95	72.13 ± 15.30	64.38 ± 22.02
Day 5 HBO	110.63 ± 15.51	54.69 ± 9.39	59.75 ± 8.88	56.44 ± 21.65	63.56 ± 18.41
Day 9 CON	125.44 ± 21.63	27.75 ± 4.27	39.38 ± 9.83	36.00 ± 7.59	53.00 ± 18.76
Day 9 HBO	111.19 ± 31.07	27.00 ± 9.22	17.00 ± 10.92	39.38 ± 13.99	48.13 ± 17.81

Data present in the table represents mean number of nuclei immunoreacting positive for EGR1 ± standard deviation.

Table A63. Summary of the thickness of CDCP1 - positive epidermis in the HSE epidermis: Group A

CDCP1	Sample 1 (µm)	Sample 2 (µm)	Sample 3 (µm)	Average (µm)
Native skin	n/a	n/a	n/a	30.50 ± 10.69
Day 0	10.07 ± 55.42	5.92 ± 2.34	5.89 ± 1.43	7.29 ± 3.91
Day 3 CON	22.31 ± 55.48	43.45 ± 8.37	21.10 ± 3.70	28.95 ± 12.02
Day 3 HBO	34.17 ± 514.54	35.33 ± 13.09	21.46 ± 4.81	30.32 ± 12.83
Day 5 CON	38.88 ± 55.48	33.00 ± 6.83	33.98 ± 8.23	35.29 ± 7.13
Day 5 HBO	43.33 ± 59.31	40.08 ± 6.29	39.07 ± 8.51	40.83 ± 7.99
Day 9 CON	37.39 ± 57.40	18.75 ± 3.33	26.31 ± 7.89	27.49 ± 10.01
Day 9 HBO	35.36 ± 11.23	24.78 ± 5.43	28.29 ± 2.40	29.48 ± 8.32

Data present in the table represents mean thickness of epidermis immunoreacting positive for CDCP1 (µm) ± standard deviation.

Table A64. Summary of the thickness of CDCP1 - positive epidermis in the HSE epidermis: Group B

CDCP1	Sample 4 (µm)	Sample 5 (µm)	Sample 6 (µm)	Sample 7 (µm)	Sample 8 (µm)
Native skin	30.18 ± 5.58	27.88 ± 8.82	22.60 ± 2.11	26.17 ± 4.50	30.79 ± 4.03
Day 0	6.50 ± 3.41	15.00 ± 5.79	11.52 ± 7.79	15.07 ± 4.40	11.44 ± 5.78
Day 3 CON	35.03 ± 9.37	25.11 ± 4.90	35.03 ± 8.81	29.88 ± 8.30	29.89 ± 6.93
Day 3 HBO	36.26 ± 7.85	24.71 ± 5.35	28.88 ± 3.55	29.98 ± 10.44	30.25 ± 7.66
Day 5 CON	38.37 ± 8.79	29.20 ± 7.81	25.11 ± 2.70	20.74 ± 5.76	30.29 ± 8.92
Day 5 HBO	35.07 ± 7.29	28.15 ± 5.81	26.50 ± 4.62	19.72 ± 8.00	24.27 ± 7.96
Day 9 CON	30.62 ± 7.20	22.51 ± 4.91	27.87 ± 3.36	21.99 ± 5.59	32.39 ± 10.09
Day 9 HBO	28.24 ± 8.29	35.35 ± 10.79	25.86 ± 4.85	19.41 ± 5.76	23.18 ± 4.66

Data present in the table represents mean thickness of epidermis immunoreacting positive for CDCP1 (µm) ± standard deviation.